Ingo Drummen

Experimental and Numerical Investigation of Nonlinear Wave-Induced Load Effects in Containerships considering Hydroelasticity

Thesis for the degree of philosophiae doctor

Trondheim, June 2008

Norwegian University of
Science and Technology
Faculty of Engineering Science and Technology
Department of Marine Technology

NTNU
Norwegian University of
Science and Technology

NTNU
Norwegian University of Science and Technology

Thesis for the degree of philosophiae doctor

Faculty of Engineering Science and Technology
Department of Marine Technology

©Ingo Drummen

ISBN 978-82-471-1054-6 (printed ver.)
ISBN 978-82-471-1055-3 (electronic ver.)
ISSN 1503-8181

Theses at NTNU, 2008:187

Printed by Tapir Uttrykk

Abstract

It has been known for several decades that ship design loads are influenced by nonlinear and hydroelastic effects. The importance of hydroelastic effects increases with increasing ship size, while nonlinear effects become larger with increasing bow flare and vessel speed. Recently, the design of containerships has rapidly evolved in accordance with these trends. As a result, containerships of novel design are especially sensitive to nonlinear and hydroelastic effects.

This thesis deals with an investigation of nonlinear wave-induced vertical bending moments relevant for ultimate and fatigue limit state design of a containership considering hydroelasticity. The vessel has a length between perpendiculars of 281m. It has a large, flat, overhanging stern, a pronounced bow flare and a large bulb. These features are considered to be representative for novel containerships. The importance of hydroelastic effects was investigated experimentally using a four segment flexible model of the ship. To obtain the design loads numerically, many efforts have been made to develop nonlinear hydroelastic methods. In this thesis the accuracy of one nonlinear hydroelastic strip theory method was investigated by comparing predicted vertical bending moments with the experimental results. Using nonlinear methods or model tests to estimate design loads can be a time consuming task, when many sea states in a long-term analysis need to be considered. This process can be made more efficient by approaches such as response conditioning techniques. The applicability of these techniques was also investigated in this thesis.

In the first part of this work, the experimental and numerical methods used for the investigation are discussed. Uncertainties related to these methods are identified and quantified. The second part of this thesis consists of five papers in which the main contributions of the investigation are presented. Here it is shown that wave-induced vibrations, due to whipping and springing, can cause approximately 40% of the fatigue damage when assuming that the lifetime of the vessel is 20 years and that it spends 2/3 of this time at sea in head seas. It is also shown that slamming loads can increase the vertical bending moments by up to 35% in head waves relevant for design and for realistic speeds. Comparisons between experimental and numerical results showed that the investigated nonlinear hydroelastic strip theory method predicts the vertical bending moments quite well, even in severe sea states. The influence of nonlinear and hydroelastic effects was generally however over-predicted by the method. This is at least partly related to the fact that strip theory over-estimates the vertical force in the bow area of the vessel. Finally, it is shown that response conditioned waves can be used to accurately, within 1% of results in random irregular waves, predict the short-term probability distribution of the midships vertical hogging bending moment in head seas, when slamming is not important or not

accounted for. In this case the method can reduce experimental or numerical simulation times by approximately two orders of magnitude compared to the simulation times required for random irregular waves. When slamming is important and accounted for, response conditioning methods can be used to numerically predict the short-term probability distribution of the midships vertical hogging bending moment with an accuracy of within approximately 5%. Simulation times are then however similar to those required for random irregular waves.

Acknowledgements

This work was carried out under the supervision of Professor Torgeir Moan at the Centre for Ships and Ocean Structures and the Department of Marine Technology at the Norwegian University of Science and Technology in Trondheim, Norway.

The financial support from the Research Council of Norway through CeSOS is gratefully acknowledged. The yard and the owner of the vessel are acknowledged for permitting use of the ship lines, and DNV for providing all the necessary ship data.

First of all I would like to thank Professor Torgeir Moan for the opportunity to learn from him during the past three years, and to do this in the multicultural and multidisciplinary environment of CeSOS.

I would also like to thank Dr. Gaute Storhaug and Dr. MingKang Wu. Particularly Gaute's help and assistance with the design of the model and the first days of model testing I greatly appreciate. The many insights given by MingKang into his program were indispensable. I am very thankful for these and for his guidance in writing papers.

I am also grateful for the help from the staff of MARINTEK, and in particular Bjørn Ola Berge, Dr. Ole Hermundstad and Dr. Ole David Økland.

Furthermore I would like to thank all professors at the Department of Marine Technology for their help whenever I asked for it. For their help and especially their friendship I am also grateful to my fellow PhD students and the postdocs at the Centre for Ships and Ocean Structures and the Department of Marine Technology.

Also Mirek Kaminski and Henk van den Boom deserve thanks for their flexibility towards me regarding time I needed for finishing my thesis, while being employed at MARIN.

Finally, I want to thank Marleen for her tremendous efforts in helping me with my studies. I am particulary grateful for her help during our many evenings spent in the towing tank, the countless proof reads of my papers and of this thesis, and our never ending discussions about my research during dinner.

Thank you!

Contents

Nomenclature

Dots over symbols represent differentiation with respect to time. Bold symbols denote vectors or matrices.

Roman symbols

$\boldsymbol{A}$	Generalised fluid added mass matrix
B	Breadth
$\boldsymbol{B}$	Generalised fluid damping matrix
c	Modal damping
$\boldsymbol{C}$	Modal damping matrix
C_g	Group velocity
E	Modulus of elasticity
EI	Bending stiffness
$\boldsymbol{f}$	Generalised modal excitation force vector
F_n	Froude number
$F_{x;1}$	Horizontal force at the forward quarter length
$F_{x;2}$	Horizontal force at midships
$F_{x;3}$	Horizontal force at the aft quarter length
g	Acceleration due to gravity
H_s	Significant wave height
I	Moment of inertia
I_{55}	Longitudinal moment of inertia
$\boldsymbol{K}$	Modal stiffness matrix
L	Length
L_{pp}	Length between perpendiculars
M	Mass
$\boldsymbol{M}$	Modal mass matrix

M_1	Vertical bending moment at the forward quarter length
M_2	Vertical bending moment at midships
M_3	Vertical bending moment at the aft quarter length
$\boldsymbol{p}$	Modal response vector
$\boldsymbol{R}$	Generalised hydrodynamic restoring matrix
S	Spectral density
t	Time
T_p	Peak period
T_z	Average zero crossing period
U	Forward speed
w	Vertical deflection

Greek symbols

β	Heading angle
γ	Peakedness parameter
ζ	Wave elevation
ζ^a	Wave amplitude
η_1	Surge motion
η_2	Sway motion
η_3	Heave motion
η_4	Roll motion
η_5	Pitch motion
η_6	Yaw motion
θ	Phase angle
Λ	Scale factor
ξ	Damping ratio
ρ	Density
σ	Bending stress
ω	Frequency
ω_e	Frequency of encounter
ω_s	Wet natural frequency of the two node vertical vibration mode

Abbreviations

3QL	Aft quarter length
AP	Aft perpendicular
CFD	Computational fluid dynamics
CIP	Constrained interpolation profile
CoG	Centre of gravity
CRRW	Conditional random response wave
CSR	Common Structural Rules
CSSRC	China Ship and Scientific Research Centre
DNV	Det Norske Veritas
DOF	Degree of freedom
FORM	First order reliability method
FP	Forward perpendicular
IACS	International Association of Classification Societies
ISSC	International Ship and Offshore Structures Congress
ITTC	International Towing Tank Conference
JONSWAP	Joint North Sea Wave Project
LCG	Longitudinal centre of gravity
MLER	Most likely extreme response
MLRW	Most likely response wave
MS	Midships
QL	Forward quarter length
RANS	Reynolds averaged Navier-Stokes
RAO	Response amplitude operator
RIW	Random irregular wave
SPH	Smoothed particle hydrodynamics
std	Standard deviation
VBM	Vertical bending moment
VCG	Vertical centre of gravity
WP	Wave Probe

Chapter 1

Introduction

1.1 Background

1.1.1 General

Traditionally, the wave loads used for the design against ultimate and fatigue failure are found from formulas given in design codes by classification societies, commonly referred to as ship rules. For both the strength and the fatigue assessment, the same formulas may be applied to calculate the wave-induced hull girder bending moments. Initially these formulas were based on experiences with existing ships. Later IACS CSR efforts, however, resulted in a much better basis for them. Common structural rules have so far been developed for bulk carriers and tankers. Even though the basis was improved, the same rule formulas have been maintained and the standard IACS (IACS, 2006) rule vertical bending moments still depend only on the ship length, breadth and block coefficient, and on a wave coefficient. Some classification societies apply correction factors to account for the effects of forward speed and bow flare. Yet, ships with novel features may exceed the rule application limits, as effects like nonlinearities, forward speed or hydroelasticity are not, or not properly, addressed. Moreover, even for ships with characteristics within the application limits, the rule values of the design wave loads might not be optimal for each specific ship.

As an alternative for the design rules, direct load analyses can be performed. The wave loads used for the design are then determined for the specific ship using a theory based computer code. Although this approach is far more time consuming than using rule values, the resulting design loads are more representative for a given vessel. For this direct approach to function properly it is however crucial that current numerical methods describe the loads and load effects accurately. Many model tests have been performed at locations around the world, providing data for the validation of theoretical codes. Some of these tests and validations will be discussed in the next section. Before proceeding with this, three key terms will be defined:

Springing is the steady-state resonant vibration of the two node flexural mode due to continuous wave loading. Linear springing is said to occur when the wave encounter frequency is equal to the natural frequency of the two node flexural mode, nonlinear

springing when it is a multiple of the encounter frequency that equals the two node natural frequency. Springing can also be related to the higher flexible modes. Due the high natural frequencies of these modes, they are, however, not very likely to be excited.

Whipping is the transient elastic vibration of the ship hull girder caused for example by slamming. Because of small damping ratio, the decay of whipping-induced responses is slow. Springing and whipping may therefore be difficult to distinguish when slamming occurs frequently.

Hydroelasticity is defined by Heller and Abramson (1959) as 'the phenomenon involving interactions among inertial, hydrodynamic, and elastic forces'. Bishop and Price (1979) described the term as 'that branch of science which is concerned with the motions of deformable bodies through liquids'. According to Faltinsen (2005), 'hydroelasticity means that the fluid flow and the structural elastic reaction are considered simultaneously and that we have mutual interaction, that is, the elastic vibrations cause a fluid flow with a pressure field and the hydrodynamic loading affects the structural elastic vibrations'. In this thesis the definition by Faltinsen (2005) is used.

1.1.2 Nonlinear Wave-Induced Load Effects

In the 18th ITTC, 23 organisations participated in comparative model experiments using the S175 containership (ITTC, 1987). The seakeeping committee requested measurements of the heave and pitch motions at the centre of gravity and of the vertical accelerations at a location 15% aft of the forward perpendicular. Results were received from 19 organisations in Japan, Brazil, Korea, China, USA, Greece and Poland. O'Dea et al. (1992) observed a rather large scatter in the transfer functions for the heave and pitch motions in head seas in these data. They stated that the scatter appeared to be a function of the wave steepness.

In order to determine the effect of nonlinearities on vertical ship motions, O'Dea et al. (1992) carried out a series of systematic tests using a rigid model, with an L_{pp} of 3.5m, of the S175 ship in the 116m long towing tank of the U.S. Naval Academy Hydrodynamics Laboratory. In their paper they presented the magnitude of the ratio of the amplitude of the first harmonic of the heave and pitch motions and that of the wave elevation, as a function of the wave steepness. This was done for two forward speeds, and three different frequencies around the resonance frequency. O'Dea et al. (1992) showed that the nondimensional amplitudes of the vertical motions decreased with increasing wave steepness and that this decrease was stronger for F_n=0.275 than for F_n=0.200. Another nonlinear effect in the response is the presence of higher order harmonics. The accelerations represent the second derivative of the motions. Therefore, when comparing the second and third harmonic components of the accelerations with those of the motions, the former are respectively four and nine times larger than the latter, and thus the measured accelerations provide a good source for identifying higher harmonics. For the higher waves, O'Dea et al. (1992) found that the second and third harmonics of the accelerations reached approximately 20% and 8%, respectively, of the first harmonic.

Using two 4.5m long (L_{pp}) flexible models of the S175 ship, Watanabe et al. (1989)

investigated the influence of the bow flare on the green water and the asymmetry of the vertical bending moments. One of the models was built using the original body lines, while the other had a modified bow with increased flare above the water line. Tests were carried out in regular and irregular head waves. In their paper they presented first and second harmonics of the vertical bending moments as a function of the wave length. The second harmonic reached up to 25% of the first. They also presented the distribution of sagging and hogging peak values along the ship length. This showed that the hogging and particularly the sagging bending moments were influenced by the shape of the bow flare, and that the degree of asymmetry between the hogging and sagging moments increased with increasing forward speed.

From the above observations it is clear that nonlinear effects can be particularly important for the design loads of ships that combine the requirements of relative high forward speed with large internal volumes and deck area. Such ships, like containerships, generally have considerable flare in the bow and stern areas.

There are many nonlinear wave load calculation methods, ranging from 3D fully nonlinear panel methods to more simple, partial nonlinear strip theories. For the past two decades, significant research efforts have been devoted to the former approaches. An analysis with such a code, however, in general requires long computation time, and results are not consistently better than those from 2D methods (ISSC, 2000). On the other hand, driven by the needs of ship design, some simplified approaches have emerged. Almost all of them are nonlinear modifications of the conventional strip theory (Watanabe and Guedes Soares, 1999; ISSC, 2000). A review of nonlinear wave load calculation methods is given in Section 2.2.

The results obtained by Watanabe et al. (1989) and O'Dea et al. (1992) have widely been used as a database for validating nonlinear codes. Xia et al. (1998) compared these measurements to results from calculations done with the nonlinear hydroelastic time-domain strip theory presented in the same paper. They found that the simulations satisfactorily reproduced the rigid body motions and the vertical sagging and hogging bending moments. No comparison was however made between the measured and the calculated higher harmonics of the response. ISSC (2000) also used the values found by Watanabe et al. (1989) and O'Dea et al. (1992), and compared them with results of partially nonlinear methods, mostly strip theory including the one presented by Xia et al. (1998). All methods used nonlinear restoring and Froude-Krylov forces, some of them incorporated hydroelasticity. They found that most of the methods were fairly well able to predict the variation of the ship motions with the wave steepness. The predicted vertical bending moments were of the same order of magnitude and showed the same trend with respect to degree of bow flare and wave length as the measured values. The calculated higher harmonics of the response on the other hand did not comply very well with the measured ones. Fonseca and Guedes Soares (2002) compared the partially nonlinear time-domain method described by Fonseca and Guedes Soares (1998a,b) with the discussed experimental results. The method evaluated the hydrostatic and Froude-Krylov forces over the instantaneous wetted surface, while radiation and diffraction forces were kept linear. Calculations, from their numerical method, of the vertical motions agreed fairly well with experiments, although the deviation increased with higher Froude numbers. The calculated first harmonic of the vertical bending moments exceeded those of the experiments.

Second and third order effects on the vertical accelerations were reasonably well predicted by the method. The same can be said of the second harmonic of the vertical bending moments.

Other experiments with the S175 ship include those performed by Chen et al. (2001), who did tests in the towing tank at the CSSRC using a self-propelled fully flexible 3.6m long (L_{pp}) model. The goal of their study was to investigate extreme wave loads on a flexible model, with focus on the nonlinearities of the wave-induced loads with respect to the wave height. The obtained data clearly indicated the presence of nonlinear effects in the motions and structural responses. They presented first, second and third harmonics of the midships vertical bending moment. In general, the amplitudes of the higher order components were approximately one order of magnitude smaller than the first order component, and they increased with increasing wave height. Chen et al. (2001) also showed that the amplitude of the vertical bending moment due to the response in the two node flexible mode was approximately 20% of that of the first harmonic in the lower waves, while the two were nearly of the same order of magnitude for the largest wave height.

The most recent tests with the S175 ship were performed at the Laboratory of Ship Dynamics of the El Pardo Model Basin in Madrid. The three segments of the 4.4m long (L_{pp}) wooden model were connected by a rigid steel backbone. The cuts were located at midships and at the forward quarter length. Results obtained with the model in regular head waves were given by Fonseca and Guedes Soares (2004b). Their data clearly showed the effect of nonlinearities on the transfer function (based on the first harmonics of the wave and the response) of the vertical motions and loads. Regarding the illustration of nonlinearities through the presence of higher harmonics in the response, they showed that the amplitude of the second harmonic of the midships vertical bending moment had maximum values that varied between 40% and 60% of the first harmonic amplitude, while for the third harmonic this fraction was around 15%. In the forward section, nonlinear effects were even more pronounced. The authors indicated that the difference between their results for the second order harmonic of the vertical bending moment and those from Watanabe et al. (1989) may be related to the experimental setup. In their study the model was towed and restrained in surge, while the model from Watanabe et al. (1989) was self-propelled and thus free to surge. In the former case the accelerations in the surge direction were higher.

The test results for the vessel in irregular head waves were presented by Fonseca and Guedes Soares (2004a). Three different sea states were tested with significant wave heights of 4.2m, 6.1m and 9.9m. The vertical response of the vessel was given in terms of statistics and short-term probability distributions. It was found that the significant values (defined as the average of the highest 1/3) of the sagging peaks of the midships vertical bending moment were up to approximately 60% higher than the corresponding significant hogging values. The measured statistics were compared to those calculated using the partially nonlinear time-domain method described by Fonseca and Guedes Soares (1998a,b). They concluded that the numerical model was able to capture the nonlinear tendencies of the vertical motions and loads. The probability distributions of the vertical bending moments in the midships and forward section were highly asymmetric, and thus deviated from the Rayleigh distribution. The numerical method was generally quite able to capture this asymmetry between the sagging and the hogging midships bending moments.

Although some of the experiments discussed above were performed with a flexible model, none of the authors, except for Chen et al. (2001), quantified the effect of hull flexibility on the response. In the subsequent two sections the effect of hull flexibility on fatigue damage and extreme response is discussed.

1.1.3 Fatigue Damage due to Wave-Induced Vibrations

In recent years it has been shown that wave-induced vibrations of the vertical two node mode can constitute a considerable part of the fatigue damage in ship hulls. For example, Storhaug et al. (2003) presented results from full scale measurements on board of a 294m long (L_{pp}) iron ore carrier trading in the North Atlantic. A rather extensive measuring system was installed on the vessel, measuring sea states, operational parameters, global ship motions, global hull girder stresses, vertical accelerations and pressure at the bottom of the bow. The measurements were taken during 11 cargo and 11 ballast voyages in the period between July 1999 and May 2000. In ballast condition the wave-induced vibrations caused 62% of the total fatigue damage in deck amidships, while in cargo condition this contribution was 13%. The wave-induced vibrations caused 44% of the total fatigue damage. It should be noted that head seas were mostly encountered in ballast condition, while the carrier experienced following seas in cargo condition.

Storhaug et al. (2003) compared the results from the full scale measurements with those from four nonlinear codes in which the hull was modelled as an elastic beam. One of the methods was a 3D Rankine source method. The nonlinearities taken into account in this code were those due to Froude-Krylov and hydrostatic forces. The other three codes were strip theory methods, of which one was second order and based on a perturbation of the hydrostatic and the hydrodynamic coefficients around the still-water line. The remaining two strip theory methods included amongst others nonlinearities due to Froude-Krylov, hydrostatic, radiation and slamming forces. Storhaug et al. (2003) concluded that the stresses, with frequencies in the wave frequency range, were in satisfactory agreement with the measurements. On the other hand, the trend and response level of the high frequency stresses were not captured by any of the four methods.

Due to the fatigue damage experienced at an early stage of operation, the ship investigated by Storhaug et al. (2003) was repaired and strengthened during the summer of the year 2000. The increased section modulus decreased the stresses in the deck by 32%. A new measuring system was installed on the vessel after strengthening. Data was collected from June 2002 to May 2005. Moe et al. (2005) presented the relative distribution of the fatigue damage in North Atlantic operation. They showed that the wave-induced vibrations caused approximately 50% of the total fatigue damage in deck amidships in ballast condition, in cargo condition this was 18%. The wave-induced vibrations were found to contribute 39% of the total fatigue damage. Comparing these results with those from above shows that the strengthening of the vessel had little effect on the percentage of fatigue damage caused by the wave-induced vibrations.

Storhaug et al. (2006) presented similar results for a 281m long (L_{pp}) vessel which is representative for a large number of Capesize ships. During the period from November 2003 to May 2005, 13308 half hour stress recordings were made. This was done while the vessel traded between Canada and Europe, Brazil and Europe, and South Africa and

Europe. In all cases, the ship traded in ballast condition from Europe and in cargo towards Europe. Storhaug et al. (2006) showed that 56% of the total damage in this period was caused by wave-induced vibrations.

The global vibration of blunt ships is generally dominated by springing, while whipping is the main source of wave-induced vibrations for slender ships, such as containerships (see e.g. Jensen and Dogliani, 1996; Gu and Moan, 2002). Over the past few decades, the dimensions of containerships have steadily increased (see e.g. Payer and Brostella, 2006). Although the development of significantly larger containerships than those in operation today will be limited by aspects such as: a) water depth in ports; b) limiting dimensions of canals and straits on the major world routes, and; c) cargo handling facilities in container terminals, it is expected that the trend of increasing dimensions will continue for the coming years. The larger size of containerships implies an increased flexibility, and a larger natural period of the two node vertical vibration mode (see e.g. Jensen and Dogliani, 1996). As a result the importance of hydroelastic effects associated with whipping and springing is increased (see e.g. Wu and Moan, 2007).

Moe et al. (2005) reported on full scale measurements on a 285m long (L_{pp}), 4000TEU containership. With a flare angle of only 28°, compared to 45° for modern containerships, the vessel is considered to be of relatively old design. Approximately four months of measurements were taken with the vessel trading in the Pacific from USA to China and Japan. In head sea conditions, with a significant wave height of 3m or higher, the vibrations of the lowest flexural modes were responsible for approximately half of the fatigue damage. The relative importance is however dependent on trade. The 56% contribution of the wave-induced vibrations to the fatigue damage presented by Storhaug et al. (2006) was, as discussed above, found from measurements taken with the vessel trading on three different routes. On the route between Canada and Europe, they found that the wave-induced vibrations contributed 57% to the total fatigue damage. For the routes between Brazil and Europe, and South Africa and Europe this was 41% and 73%, respectively. These results are, however, biased due to the lack of winter voyages in these trades. Although the contribution of the wave-induced vibrations to the total damage is particularly high for the vessel trading between South Africa and Europe, the total fatigue damage is insignificant compared to the damage measured in the North Atlantic.

1.1.4 Extreme Responses

Some of today's modern container vessels are trading in the North Atlantic. The unique hull form of these vessels - with a large, flat and overhanging stern, and pronounced bow flare - coupled with high service speeds can cause large ship motions relative to the water surface, resulting in severe slamming impacts. Slamming events increase the hogging as well as the sagging vertical bending moments. Ciappi et al. (2003) investigated the response of a very fast mono hull in rough seas using a segmented model with an elastic backbone. The tests were carried out in the INSEAN towing tank using a model with a length between perpendiculars of 4.28m. The model was tested in regular and irregular head waves. For a sea state corresponding to a significant wave height of 5m and a forward speed of 30kn (F_n=0.44) in full scale, they showed that a whipping event more than doubled both the midships vertical sagging and hogging bending moments. Ciappi

et al. (2003) also compared time series of the experimental and the numerical slamming forces, and found a good agreement in terms of both rise time and maxima. The slamming force was calculated as the sum of integrals of the pressure distribution, which was found using Wagner theory (Wagner, 1932). The relative vertical velocity necessary for this calculation was taken from the measurements. Alternative methods for calculating the slamming force are discussed in Section 2.2.

Takarada et al. (1993) performed tests using a 2.5m long elastic backbone model of a high speed ship with a full scale length between perpendiculars of 200m. The bending rigidity of the aluminum backbone satisfied the similarity law of elasticity at midships. With the model running at F_n=0.1 in a sea state with a full scale significant wave height of 10m and a mean wave period of 8.5s, they found a whipping event that increased the midships hogging and sagging bending moments by approximately 60%.

During a period of four years, extensive research on slamming induced whipping responses of large ships was done at the Marine Technology Centre in Trondheim. In total 80 different bow and stern geometries were tested. Based on these results Zhao et al. (2004) reported that the whipping component of the vertical bending moment in large cruise ships had a magnitude of 30% to 150% of that of the wave component, in extreme wave conditions.

Since containerships in still-water normally operate in hogging condition, any increase in the wave-induced hogging moments has an impact on the design loads for ultimate strength. The most common manner to find these design loads from a direct load evaluation is by means of a long-term description of the response. As the ship response in the most severe sea states is nonlinear, time domain simulations or model tests with long time series are required for this. The analysis therefore becomes both time consuming and expensive. An efficient approach for predicting the nonlinear long-term extreme response is the coefficient of contribution method (see e.g. Baarholm and Moan, 2000), which identifies the most important sea states contributing to the extreme value. Baarholm and Moan (2000) demonstrated that a long-term load analysis for marine structures can be performed by considering only a few short-term sea states, instead of determining responses for all sea states within the scatter diagram. The initial step is to calculate the coefficients of contribution from a linear long-term response analysis. The dominating area in the scatter diagram is then located in the regions where the wave length is approximately equal to the ship length. When nonlinear effects are included, the dominating area does not necessarily coincide with the area found from the linear analysis. Multiple maxima may even occur due to large responses at other periods, e.g. due to slamming, which generally occurs in slightly shorter and steeper waves. Therefore, Baarholm and Moan (2000) described an iterative procedure for finding the coefficients of contribution when nonlinear effects are included.

Although the coefficient of contribution method, and also other methods (see e.g. Section 2.3), can strongly reduce the number of sea states considered in the long-term analysis, finding the short-term probability distributions in the selected sea states is still rather time consuming, especially since the values in the tail of the distribution are of main interest. Based on the methods of Friis-Hansen and Nielsen (1995) and Adegeest et al. (1998), Dietz (2004) proposed the most likely response wave (MLRW) approach, which can be used to efficiently determine the short-term nonlinear probability distribution of a

response. In order to more correctly capture the contribution of transient effects like those of whipping to the probability distribution, Dietz (2004) also developed the conditional random response wave (CRRW) method, which includes a random background wave within the MLRW profile. This is based on the idea of Taylor et al. (1995), who showed how the New Wave (Tromans et al., 1991) can be embedded in a stochastic seaway. Using the nonlinear time domain strip theory code of Xia et al. (1998), Dietz (2004) validated both methods for a Panamax containership. Dietz (2004), however, recommended further analysis with other types of vessels and comparison with results from model tests. Also ISSC (2006) recommended the validation of response conditioning methods with further numerical simulations and experiments before they can be considered as established tools. The fundamental assumption of response conditioning techniques is that the nonlinear response is a correction of the linear response. The range of applicability of these methods therefore particularly needs to be investigated for flexible hull girders, when slamming induced whipping responses are accounted for.

Several simplified methods for finding the design load effects in ships are discussed above. Strip theory methods can be used for efficiently calculating the nonlinear wave loads induced on the ship. The long-term extreme values can be found considering only a few sea states obtained from for example the coefficient of contribution method, and response conditioned waves are a tool for quickly finding the short-term nonlinear probability distributions of the responses in these sea states. Each of these simplifications will introduce uncertainty to the estimated design load effects, and it is important to obtain a good estimate of these uncertainties (e.g. Moan et al., 2006). The values of the uncertainties are crucial to the estimates of the reliability of the vessel.

In their paper, Moan et al. (2006) showed that the long-term (10^{-8}) prediction of the midships vertical bending moment of a containership found from direct calculations using a linear 2D method was approximately 15% higher than the corresponding value obtained using a linear 3D method. Moan et al. (2006) also investigated a bulk carrier, product tanker and a very large crude carrier. For these ships the 2D method gave results which were approximately 20% higher than the 3D values. Comparisons between calculations from several nonlinear strip theory methods and results from model tests are presented in Section 1.1.2.

For the S175 containership, Baarholm and Moan (2000) found that the design bending moment was under-estimated by less than 15% when including only the most contributing sea state, i.e. the sea state with the maximum coefficient of contribution, in the long-term analysis. The coefficient of contribution of this sea state was approximately 10%. When the number of sea states was increased such that the sum of their coefficients of contribution was 50%, the under-estimation was less than 5%. Similar results were obtained for a tanker and a destroyer.

Pastoor (2002) carried out model tests with a frigate in random irregular and MLER waves. An MLER wave is a special case of the MLRW, see Papers 4 and 5. For sea states corresponding to a significant wave height of 2.5m and 4.3m, he showed that the midships vertical sagging bending moments found using response conditioned waves deviated less than approximately 10% from those obtained in random irregular waves. The validation by Dietz (2004) of the MLRW and CRRW methods mentioned above was done for a sea state with a significant wave height of 10m and three different forward speeds,

0m/s, 5m/s and 10m/s, by comparing the results of both methods with brute force results. He compared midships vertical hogging and sagging bending moments at a probability level of 10^{-5}, and showed that moments obtained using the MLRW method deviated less than 10% from those found using brute force. For the CRRW method this was less than 5%. Due to the random background wave in the CRRW the accuracy of this method did not depend on speed, while the accuracy decreased with increasing speed for the MLRW method. The results discussed here were obtained assuming a rigid hull girder. When assuming a flexible hull the accuracy of the response conditioning methods was quite similar, although the accuracy of the predicted hogging moments using the MLRW method decreased somewhat in this case.

1.2 Objectives and Scope of the Present Study

This thesis deals with an experimental and a numerical investigation of nonlinear wave-induced load effects in containerships taking hydroelasticity into account. Both the extreme and fatigue load effects were considered. The experimental results were obtained using a four segment flexible model of a container vessel of newer design. Compared to containerships of older design it is less slender with more bow flare, and has a significantly larger bulb. Moreover, compared to the S175 vessel, it is considerably longer, approximately 60%. The model was tested in head seas in the towing tank at the Marine Technology Centre in Trondheim. Most of the test results were compared with predictions from the hybrid nonlinear hydroelastic strip theory method of Wu and Moan (2005).

The objectives of the study presented in this thesis were to:

A. determine the relative importance of fatigue damage due to wave-induced vibrations of the lowest global flexural modes of a containership of newer design;

B. determine the increase, due to hull flexibility, of the design vertical bending moments of a containership;

C. investigate the application of response conditioned waves for long-term nonlinear analysis, and;

D. determine how accurate the nonlinear hydroelastic strip theory developed by Wu and Moan (2005) is in predicting nonlinear load effects in containerships considering hydroelasticity.

Fig. 1.1 gives an overview of how the objectives relate to the thesis subjects and to the papers. The main contributions of each paper in relation to these objectives are given in Chapter 4.

Chapter 2 briefly deals with some of the theoretical aspects related to the numerical method of Wu and Moan (2005). This chapter also presents the background on extreme and fatigue load effects. In Chapter 3 the model used for the experiments and the considerations regarding its design are described. This chapter furthermore presents the instrumentation, the testing program, the uncertainties and the testing facilities. Chapter 4

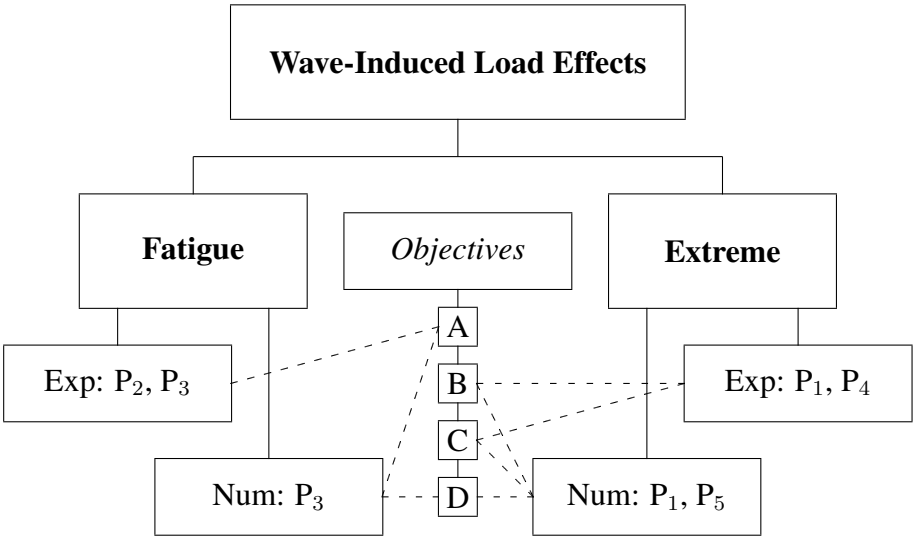

Figure 1.1: Overview of the thesis subjects, objectives and papers (P_i). 'Num' and 'Exp' denote numerical and experimental investigations, respectively.

summarizes each of the five papers, and in the last chapter the conclusions and recommendations are given.

The first of the five papers elaborates on the contribution of higher harmonics to the vertical bending moments in regular waves, when the encounter frequencies of these harmonics are close to the natural frequency of the wet two node vibration mode. The paper also presents the short-term probability distributions of the vertical sagging and hogging bending moments in three severe sea states. With this, the paper illustrates the degree of asymmetry between the sagging and hogging moments, as well as how much these moments are increased due to hull flexibility. The experimental results are compared with numerical predictions in order to show how accurate the above effects are predicted by the nonlinear hydroelastic method of Wu and Moan (2005).

Papers 2 and 3 address the contribution of the wave-induced vibrations to the fatigue damage. The irregular sea states used in the investigation are representative for North Atlantic trade. The fatigue damage was determined using rainflow counting and the Palmgren-Miner linear cumulative damage rule. In order to determine how accurate the numerical method of Wu and Moan (2005) predicts the total damage in general and the damage due to the wave-induced vibrations in particular, estimates from this method are again compared with the experimental results.

The fourth paper compares the short-term probability distribution of the midships vertical hogging moment found from experiments in random irregular waves with the distribution obtained in response conditioned waves, using both MLRWs and CRRWs. The focus is on the sea state contributing most to the midships hogging moment with a mean return period of 10^4 years. A similar comparison is done in Paper 5, based on numerical results. Here the probability distributions of the midships hogging moments in the sea states contributing most to the hogging moment with a mean return period of 20 and 10^4 years are of concern. This paper also deals with a comparison between the experimental

and the numerical results.

1.3 List of Publications

Publications part of this thesis:

Drummen I, Wu MK, Moan T. "Experimental and numerical study of containership responses in severe head seas." *submitted to Marine Structures, under review*.

Drummen I, Storhaug G, Moe E, Moan T (2006). "Experimental and full scale investigation of the importance of fatigue damage due to wave-induced vibration stress in a container vessel." In: *Transactions Royal Institution of Naval Architects, Conference on Design & Operation of Container Ships*. London, UK, pp. 61-74.

Drummen I, Storhaug G, Moan T. "Experimental and numerical investigation of fatigue damage due to wave-induced vibrations in a containership in head seas." *accepted for publication in Journal of Marine Science and Technology*.

Drummen I, Moan T (2007). "Experimental investigation of the application of response conditioned waves for long-term nonlinear analyses." In: *Proceedings 10th International Symposium on Practical Design of Ships and Other Floating Structures*. Houston, US, pp. 322-329.

Drummen I, Wu MK, Moan T. "Numerical and experimental investigation into the application of response conditioned waves for long-term nonlinear analyses." *submitted to Marine Structures, under review*.

Publications outside the scope of this thesis:

Moan T, Shu Z, Drummen I, Amlashi H (2006). "Comparative reliability analysis of ships - considering different ship types and the effect of ship operations on loads." In: *Transactions Society of Naval Architects and Marine Engineers*. Fort Lauderdale, US.

Rodríguez C, Holden C, Perez T, Drummen I, De Almeida Santos Neves M, Fossen TI (2007). " Validation of a container ship model for parametric rolling." In: *Proceedings 10th International Ship Stability Workshop*. Hamburg, Germany.

Chapter 2

Theoretical Background

2.1 Waves

For the design of ships it is important to quantify the wave-induced loads and their effects. Determination of these loads involves the following issues:

- a description of regular and irregular waves;
- hydrodynamic modelling, and;
- structural modelling.

Generally, the instantaneous value of the wave elevation is well characterised by a Gaussian distribution, and according to linear theory the wave elevation may be seen as the superposition of sinusoidal wave components. The wave elevation of a long-crested irregular sea is then given by

$$\zeta(t) = \sum_{n=1}^{N} a_{\zeta;n}[V_n \cos(-\omega_n t) + W_n \sin(-\omega_n t)], \tag{2.1}$$

where N is the number of wave components, V_n and W_n are independent standard normal random variables, ω_n is the frequency of the n^{th} wave component, and t represents time. The coefficients $a_{\zeta;n}$ are found from the wave spectrum, $S_\zeta(\omega)$ as

$$a_{\zeta;n} = \sqrt{S_\zeta(\omega_n)\Delta\omega_n}, \tag{2.2}$$

where $\Delta\omega_n$ is the resolution of the discrete wave frequency. A wave spectrum describes the distribution of the energy in a sea state over the wave frequencies. Recommended spectra from ITTC and ISSC are often used to calculate $S_\zeta(\omega)$. The JONSWAP spectrum and the Pierson-Moskowitz spectrum are most frequently applied. Det Norske Veritas (2000a) defines the spectral density function of the JONSWAP spectrum as

$$S_\zeta(\omega) = \alpha g^2 \omega^{-5} exp\left[-\frac{5}{4}\left(\frac{\omega}{\omega_p}\right)^{-4}\right]\gamma^{exp\left[-0.5\left(\frac{\omega-\omega_p}{\sigma\omega_p}\right)^2\right]}, \tag{2.3}$$

where

$$\begin{aligned} \alpha &= \frac{5}{16}\frac{H_s^2\omega_p^4}{g^2}(1-0.287\ln\gamma), \\ \sigma &= \begin{cases} 0.07 & \text{if} \quad \omega \leq \omega_p \\ 0.09 & \text{if} \quad \omega > \omega_p \end{cases}, \end{aligned}$$

and where ω_p is the peak frequency ($\omega_p = 2\pi/T_p$). For γ equal to one this results in the Pierson-Moskowitz spectrum. The JONSWAP spectrum is representative for developing seas, while the Pierson-Moskowitz spectrum represents fully developed sea states. Both spectra are deep-water spectra. This characterisation of the sea state by constant parameters is only valid when the sea state can be described as a stationary process. In general this description is limited to a time period in the range from half an hour to 10 hours. A common assumption is three hours. During this period the instantaneous value of the wave elevation has zero mean, and a variance equal to $\int_0^\infty S_\zeta(\omega)d\omega$. Assuming that the wave elevation process is also narrow-banded, the probability density function of the maxima, $\hat{\zeta}$, of the wave elevation is given by the Rayleigh distribution, with the following probability density function

$$f(\hat{\zeta}) = \frac{\hat{\zeta}}{m_0}\exp\left(-\frac{\hat{\zeta}^2}{2m_0}\right), \tag{2.4}$$

where m_0 is equal to the variance, σ^2, of the underlying Gaussian distribution, and to the area under the spectral curve. More in general, the k^{th} spectral moment, m_k, is given by

$$m_k = \int_0^\infty \omega^k S_\zeta(\omega)d\omega. \tag{2.5}$$

Assuming that the ship responds to these waves in a linear manner, the response, $R(t)$, can be written as

$$R(t) = \sum_{n=1}^{N} a_{R;n}^e[V_n\cos(-\omega_{e;n}t + \theta_{R;n}^e) + W_n\sin(-\omega_{e;n}t + \theta_{R;n}^e)], \tag{2.6}$$

where $\omega_{e;n}$ is the encounter frequency of the n^{th} component. In head seas the encounter frequency is related to the wave frequency by

$$\omega_e = \omega + \omega^2\frac{U}{g}. \tag{2.7}$$

The coefficient $a_{R;n}^e$ is

$$a_{R;n}^e = \sqrt{S_R^e(\omega_{e;n})\Delta\omega_{e;n}} = \Phi_R^e(\omega_{e;n})\sqrt{S_\zeta^e(\omega_{e;n})\Delta\omega_{e;n}}. \tag{2.8}$$

Here $S_R^e(\omega_e)$ is the response spectrum and $\Delta\omega_{e;n}$ the resolution of the discrete encounter frequency. $\Phi_R^e(\omega_e)$ and $\theta_R^e(\omega_e)$ respectively denote the amplitude and the phase angle information of the transfer function of the response. Furthermore, in Eq. 2.6 is $\theta_{R;n}^e$ equal to $\theta_R^e(\omega_{e,n})$.

Finally, the encountered wave spectrum, $S_\zeta^e(\omega_e)$, is found from the wave spectrum as

$$S_\zeta^e(\omega_e) = S_\zeta(\omega)\frac{d\omega}{d\omega_e}. \tag{2.9}$$

$R(t)$ is also a Gaussian process and is characterised by a zero mean and a variance equal to $\int_0^\infty S_R^e(\omega_e)d\omega_e$. The individual maxima of the response are also Rayleigh distributed, if the process is narrow-banded.

Methods to calculate the linear response are widely available and provide accurate results for situations in which the response is linear or nearly linear. In the introduction it was however mentioned that nonlinear effects can be important for the determination of the loads on ships. In this case the distribution of the individual maxima, $\hat{R}$, is no longer well represented by the Rayleigh distribution. Then other distributions such as, for instance, the Weibull distribution should be used. The probability density function is given by

$$f(\hat{R}) = \frac{\nu}{\mu}\left(\frac{\hat{R}-\delta}{\mu}\right)^{(\nu-1)} \exp\left[-\left(\frac{\hat{R}-\delta}{\mu}\right)^{\nu}\right], \tag{2.10}$$

where μ is the scale parameter, ν the shape parameter and δ the location parameter of the distribution. For $\nu = 2$ and $\delta = 0$, the Rayleigh distribution appears. μ is then equal to $\sqrt{2}$ times the standard deviation of the response. Methods for calculating nonlinear wave-induced loads are less well established than those for calculating linear loads, and are discussed in the following section.

2.2 Methods for Calculating Nonlinear Wave - Induced Loads

2.2.1 General

Ever since it was recognised that nonlinear effects can affect the design loads for certain types of vessels, many efforts have been directed towards methods for calculating nonlinear hydrodynamic loads on ships (e.g. ISSC, 2000). The methods developed basically fall into one of the following two groups:

- 2D nonlinear methods, and;
- 3D nonlinear methods.

In the past two decades, significant research efforts have been devoted to nonlinear 3D time domain hydrodynamic codes, with and without accounting for viscous effects. When assuming potential flow, the nonlinear 3D problem can be efficiently solved using the Green function method (e.g. ISSC, 2006) with various levels of approximation regarding the nonlinear effects (e.g. ITTC, 2005). Often the nonlinearities due to Froude-Krylov and hydrostatic forces are accounted for, while the radiation and diffraction forces are kept linear. Lin and Yue (1991) were the first to include the nonlinear effects due to these last two forces. Fully nonlinear methods based on potential theory are still at a developing stage.

One of the most successful approaches in this area is the mixed Eulerian-Lagrangian method, used for example by Shirakura et al. (2002). Methods based on potential flow can however not adequately deal with highly nonlinear phenomena in which viscous effects are important. In order to solve these problems CFD approaches such as RANS , CIP or SPH have been employed (e.g. Weymouth et al., 2005; Hu and Kashiwagi, 2004; Imas, 2004). A comprehensive review of state-of-the-art developments in 3D nonlinear methods was given by ITTC (2005).

An analysis with a nonlinear 3D code will in general require long computation time. Driven by the needs of ship design, some simplified approaches have emerged. Almost all of them are nonlinear modifications of some kind to the conventional strip theory (e.g. Watanabe and Guedes Soares, 1999; ISSC, 2000). Here there are also various levels of approximation regarding the nonlinear effects. The method proposed by Fonseca and Guedes Soares (1998a,b) is based on time domain strip theory and computes the Froude-Krylov and the hydrostatic forces over the wetted hull surface. The radiation and diffraction forces are kept linear. This method assumes a rigid hull.

As mentioned in the introduction, the larger size of ships implies an increased flexibility, and a larger natural period of the two node vertical vibration mode. As a result the importance of hydroelastic effects associated with whipping and springing is increased. Under such circumstances it is therefore important that these effects are accurately accounted for. The theory for elastic ships is presented in the next section.

2.2.2 Theory for Elastic Ships

In order to represent the flexibility of the hull girder in numerical analyses, the vessel is often modelled as a beam. Several beam theories are adopted; examples are Euler-Bernoulli, Timoshenko or Vlasov beam theory. Bishop and Price (1974) discussed a number of approaches for assessing the structural dynamic effects and concluded that 'modal analysis is likely to offer the best rewards'. The method has been in common use ever since. By employing the dry principal modes of the beam (ship) instead of the wet ones, the simple orthogonality relations may be retained. The global hull deformation is then an aggregate of the dry flexible modes. Generally there is little difference between the shape of the dry and the wet modes of a ship.

When the hull is assumed to be rigid, the displacement of any point on the hull is represented by the six rigid-body modes of motion. The only damping present in the system is then the hydrodynamic damping. For flexible hulls the global flexible modes also have to be taken into account, as mentioned above. The damping in these modes is a result of hydrodynamic and structural damping. The shape, natural frequency and structural damping of the global flexible modes of the model, used in the experimental investigation presented in this thesis, are given in Sections 3.4.3 and 3.4.4.

Using the definition of hydroelasticity by Faltinsen (2005), see Section 1.1.1, it is clear that the approach presented above can be a basis for hydroelastic methods. The first 3D nonlinear hydroelastic theory was presented by Wu et al. (1997). The nonlinearities taken into account in their model were those due to second-order hydrodynamic forces. 3D nonlinear hydroelastic codes are, however, mainly applied for calculating the responses of very large floating structures.

Jensen and Dogliani (1996) presented a nonlinear quadratic strip theory. Their method included nonlinear effects due to changes in added mass, hydrodynamic damping and water line breadth with sectional immersion in waves. Hull flexibility was taken into account using a non-prismatic Timoshenko beam, such that the springing vibration could be determined. Whipping vibrations resulting from slamming loads were not considered. The method presented by Xia et al. (1998) accounted for the nonlinearities due to the Froude-Krylov, the restoring and the radiation forces. They modelled the hull as a linear elastic nonuniform Timoshenko beam. The slamming force was included by using momentum slamming theory. Chen et al. (2006) gave a review of hydroelastic theories for the global response of marine structures.

Wu and Moan (1996) presented a nonlinear hydroelastic simulation method for the prediction of wave-induced vertical motions and loads in ships with large amplitude motions and small hull deformations. In this approach the hull is modelled as a Vlasov beam and the global hull deformations are approximated by an aggregate of flexible modes. The wave-induced ship responses are obtained by modal superposition. The nonlinear effects in the vertical motions and cross-sectional load effects are introduced in the form of a nonlinear vertical excitation force. In this way the relationship between the ship motions or the load effects and the excitation force can remain linear, while the excitation force is no longer linearly related to the incident wave. The total nonlinear excitation force consists of a linear part and a nonlinear modification part. The response is decomposed in the same manner. The linear part is evaluated by using 2D or 2.5D strip theory. The nonlinear modification part is obtained as the convolution of the linear impulse response function and the nonlinear modification force. The nonlinearities considered are the slamming impact force, the nonlinear incident wave force and the nonlinear hydrostatic restoring force.

Wu and Hermundstad (2002) further improved the method of Wu and Moan (1996) by partitioning the global flexible modes into dynamic and quasi-static ones so that the computational time for a nonlinear simulation could be reduced, while the structural dynamic effects were still accounted for. In their paper, Wu and Hermundstad (2002) compared numerical results of the S175 vessel with the experimental values obtained by O'Dea et al. (1992) and Watanabe et al. (1989). They concluded that the agreement between the measured and predicted vertical motions was quite satisfactory. Results from a fully nonlinear 3D method (Lin et al., 1996) were in most cases close to the 2D predictions, and did not consistently exhibit a better agreement with the experimental values. The sagging and hogging bending moments calculated by the 2D code for the vessel in regular and irregular head waves compared very well with the measured ones, although the method tended to under-predict the sagging moments in the fore-part of the vessel.

Although partitioning the global flexible modes into dynamic and quasi-static ones can reduce the computational time, it is still necessary to determine the required number of global flexible modes. This number varies from ship to ship and from response to response and can only be determined by a convergence study, which should then be carried out for each and every response. Furthermore, it should be noted that it sometimes can be very difficult to determine whether convergence is achieved or not. Recently, Wu and Moan (2005) extended the method by Wu and Moan (1996) and Wu and Hermundstad (2002), and presented a hybrid method, WINSIR Hybrid, for calculating the hydroelastic

responses. This method is applied in this thesis, and is discussed in more detail in the next section.

2.2.3 WINSIR Hybrid

The hybrid approach is a combination of the conventional direct load evaluation for a rigid body and the modal superposition for a flexible hull. The dynamic effects, in the lowest few global flexible modes, calculated by modal superposition are added to the responses obtained from the conventional load evaluation, see Paper 1.

The presentation in this section is based on a right-handed coordinate system with its origin in the undisturbed free surface. The positive z-direction is vertically upwards through the centre of gravity and the positive x-direction points to the stern. The generalised equation of motion is written as

$$(\boldsymbol{M}+\boldsymbol{A})\ddot{\boldsymbol{p}}(t)+(\boldsymbol{C}+\boldsymbol{B})\dot{\boldsymbol{p}}(t)+(\boldsymbol{K}+\boldsymbol{R})\boldsymbol{p}(t)=\boldsymbol{f}(t). \tag{2.11}$$

$\boldsymbol{p}(t)$ contains 6+N components, the first six describe the rigid body motions and the rest represent the responses in the flexible modes. $\boldsymbol{A}$, $\boldsymbol{B}$ and $\boldsymbol{R}$ are the generalised fluid added mass, damping and hydrostatic restoring matrices, and $\boldsymbol{M}$, $\boldsymbol{C}$ and $\boldsymbol{K}$ are given as

$$\boldsymbol{M}=\begin{bmatrix}\boldsymbol{M}_R & \boldsymbol{0}\\ \boldsymbol{0} & \boldsymbol{M}_F\end{bmatrix},\quad \boldsymbol{C}=\begin{bmatrix}\boldsymbol{0} & \boldsymbol{0}\\ \boldsymbol{0} & \boldsymbol{C}_F\end{bmatrix},\quad \boldsymbol{K}=\begin{bmatrix}\boldsymbol{K}_R & \boldsymbol{0}\\ \boldsymbol{0} & \boldsymbol{K}_F\end{bmatrix}, \tag{2.12}$$

where $\boldsymbol{M}_R$ and $\boldsymbol{K}_R$ are the modal mass and gravity matrices for the six rigid body motions. The gravity matrix is introduced to account for the instantaneous relative direction of the acceleration of gravity, as the restoring matrix is found by integration of the hydrostatic pressure using the unit normal vector on the mean wetted body surface. $\boldsymbol{M}_F$, $\boldsymbol{C}_F$ and $\boldsymbol{K}_F$ are respectively the modal mass, damping and stiffness matrices related to the flexible modes. The total damping includes the internal structural damping and the linear potential hydrodynamic damping. The influences of viscous effects associated with relative motion (Fonseca and Guedes Soares, 2002) and forward speed on the damping ratio are, however, not or not fully accounted for by WINSIR Hybrid. The total nonlinear excitation force, $\boldsymbol{f}(t)$, consists of a linear part, $\boldsymbol{f}_l(t)$, and a nonlinear modification part, $\boldsymbol{f}_{nm}(t)$

$$\boldsymbol{f}(t)=\boldsymbol{f}_l(t)+\boldsymbol{f}_{nm}(t). \tag{2.13}$$

The k^{th}component of the vector $\boldsymbol{f}_{nm}(t)$ takes the following form:

$$f_{nm,k}(t)=\rho g\int_{bow}^{stern}\delta_{z,k}(x)\{Q(x,t)-Q_0(x,t)+b_0(x)\nu(x,t)\}dx+ \\ -\int_{bow}^{stern}\delta_{z,k}(x)c(x,t)\frac{\partial m(x,t)}{\partial t}\frac{D\nu(x,t)}{Dt}dx, \tag{2.14}$$

where $\delta_{z,k}(x)$ is the vertical displacement of the centroid of a transverse cross section in mode k. For heave and pitch, $\delta_{z,3}$=1 and $\delta_{z,5}$=-x, respectively. $Q(x,t)$ and $Q_0(x,t)$ respectively denote the areas of the instantaneous and mean submerged cross section. $b_0(x)$ is the sectional beam at mean draft. $m(x,t)$ is the high frequency added mass for the instantaneous submerged cross section without pile-up water. $\nu(x,t)$ represents the vertical displacement of the ship hull relative to the wave surface. The incident wave elevation is used to compute the nonlinear modification force. The effect of the radiated and the diffracted wave on this force is not accounted for.

The first integral in Eq. 2.14 is the nonlinear modification of the Froude-Krylov and hydrostatic restoring forces, while the second integral represents the slamming force. The slamming force is neglected during water exit. The effects of pile-up water are included in an approximate manner by a correction factor, $c(x,t)$, which is a function of the tangent to the body plan profile at the point where the wave surface meets the ship hull. The correction factor is based on the investigations of Zhao et al. (1996) for wedges with varying dead rise angles. They presented an approximate approach based on Wagner's solution (Wagner, 1932) and showed that this method gave a reasonable approximation of the total slamming force and the local slamming loads. Hermundstad and Moan (2005) used this generalised Wagner approach to calculate bow flare slamming loads on a Ro-Ro vessel. They showed that the calculated slamming pressures corrected for 3D effects compared well with measured data. The correction factor for the pile-up water used by Wu and Moan (2005) is given as the ratio between the vertical slamming force found using the generalised Wagner method and the one found from momentum slamming without water pile-up. However, in general, 2D slamming calculations give too large forces because the flow in the bow area is not two dimensional. A quantitative estimate of this effect is given in Paper 1.

Concerning nonlinearities, WINSIR Hybrid does not account for the quadratic velocity term in Bernoulli's equation for the fluid pressure. Furthermore, the code only calculates a first order velocity potential. It is thus not able to produce a second order pressure field which, under certain conditions, oscillates with the sum-frequency and does not decay with depth. These two features were accounted for in the second order strip theory presented by Jensen and Dogliani (1996) (see Jensen and Pedersen, 1979), and may cause significant nonlinear springing (e.g. Storhaug, 2007; Vidic-Perunovic, 2005). WINSIR Hybrid does also not take into account the steady wave around the hull due to the forward speed of the model. The effect of the steady wave on the magnitude of the fatigue damage is investigated in a simplified manner in Paper 3.

In order to validate their hybrid method, Wu and Moan (2005) compared vertical bending moment RAOs obtained by the hybrid method with those obtained by a conventional direct response evaluation. For the comparison, use was made of the SL-7 containership. For the hybrid method a flexible hull was used, while a rigid hull was assumed for the conventional approach. Over the relevant frequency range the results obtained by using the hybrid method were very similar to the ones obtained by conventional calculations. Wu and Moan (2005) also compared predictions by their method with experimental results. The tests were conducted at the Netherlands Ship Research Centre TNO. The model was constructed of glass reinforced polyester using a scale of 1:55 and consisted of four rigid segments joined by three five-component strain-gauge balances. The cuts were located at

sections 5, 10 and 15 and were sealed with thin flexible adhesive tape. Experiments were performed in seven wave directions. In each direction, the model was run in seven regular waves. Predicted first harmonics of the nonlinear vertical bending moments were found to be in good agreement with measured ones.

Wu and Hermundstad (2002) and Wu and Moan (2005) showed that their method can, in general, quite accurately predict the vertical bending moments in containerships. No explicit comparison with experimental results has however been made in order to evaluate the accuracy of the method in predicting hydroelastic effects. This issue is investigated in Papers 1, 3 and 5.

2.3 Extreme Load Effects

The most common manner to estimate the lifetime extreme value for a particular ship response from a direct load evaluation is by means of a long-term analysis. The long-term distributions of peaks is obtained by summing short-term probabilities of exceedance in all possible combinations of peak periods, significant wave heights, heading angles and speeds. The long-term probability that a maximum, $\hat{R}$, of the response will be larger than r can be written as

$$Q_{LT}(r) = \int_{H_s} \int_{T_p} \int_{U} \int_{\beta} Q_R(\hat{R} > r|h,t,u,\beta) f_{H_s,T_p,U,\beta}(h,t,u,\beta) \bar{w}\, dh\, dt\, du\, d\beta, \quad (2.15)$$

where $\bar{w}$ is a weight function, which expresses the relative rate of peak responses within each sea state. $f_{H_s,T_p,U,\beta}(h,t,u,\beta)$ is the joint long-term probability distribution function of the significant wave heights, peak periods, forward speeds and heading angles. $Q_R(\hat{R} > r|h,t,u,\beta)$ is the short-term cumulative probability distribution. When using linear theory, the response is Gaussian. Moreover, assuming narrow-banded response $Q_R(\hat{R} > r|h,t,u,\beta)$ may be described by the Rayleigh distribution. The variance of the response is efficiently obtained from the transfer function of the vessel for specific conditions and the wave spectrum, see e.g. Faltinsen (1990) or Farnes (1990).

As stated in the introduction, nonlinearities should be accounted for when determining the design load effects in containerships. In case this is done, the cumulative probability distribution is no longer well described by the Rayleigh distribution and alternative distributions such as the Weibull distribution should be used. Using the latter distribution the short-term probability that a maximum of the response will be larger than r can be written as

$$Q_R(\hat{R} > r|h,t,u,\beta) = \exp\left[-\left(\frac{r-\delta}{\mu}\right)^{\nu}\right]. \quad (2.16)$$

Accurate determination of the parameters in this distribution requires nonlinear simulations or model tests with long time series for each specific condition, particularly because the tail of the distribution is of main interest. Therefore, many simplified methods have been developed. A discussion regarding some of these methods was given by ISSC (2000).

For example, Guedes Soares et al. (2004) estimated the maximum wave-induced vertical bending moment of a fast mono hull, expected to occur during 25 years of operation in the Northern North Sea. For the integration in Eq. 2.15 they assumed that $Q_R(\hat{R} > r|h,t,u,\beta)$ may be described by the Rayleigh distribution. Nonlinear pseudo-transfer functions were, however, used to calculate the variances of the short-term responses, obtained by a nonlinear code (Fonseca and Guedes Soares, 1998a,b). They accounted for the nonlinear effects by using transfer functions calculated in regular waves with a height equal to the significant wave height of the sea state for which the variance had to be obtained. Another alternative is to apply the coefficient of contribution method, as described for instance by Baarholm and Moan (2000). In this method the most important sea states contributing to the extreme value are identified, and considered in the long-term analysis. As mentioned in the introduction, Baarholm and Moan (2000) demonstrated that a long-term load analysis for marine structures can be performed by considering only a few short-term sea states, instead of determining responses for all sea states within the scatter diagram.

Using an inverse FORM, Winterstein et al. (1993) showed how to find the sea states in which a certain response of the structure is exceeded with a given probability. Baarholm and Moan (2001) used the method to identify a set of sea states on the contour line in the (H_s,T_p)-plane. They proposed an approach which uses these sea states for determining the D-year response, i.e. the value of the response with a mean return period of D years. The advantage of this method is that the environmental and the response analysis are uncoupled. Baarholm and Moan (2001) showed that the extreme response obtained using this approach was close to the one determined by Eq. 2.15. This evaluation was, however, only based on responses in the wave frequency range and did not include high frequency effects. Baarholm and Jensen (2004) verified the contour line approach, taking whipping effects into consideration. For the case investigated, it was concluded that the method gave a satisfactory estimate of the long-term extreme value.

In both the coefficient of contribution method and the contour line approach, it is still necessary to find the short-term nonlinear probability distribution of the response in several sea states. This can be done efficiently using the MLRW or the CRRW method. These methods are further described and investigated in Papers 4 and 5.

2.4 Fatigue Load Effects

In a fatigue analysis, the resistance against fatigue damage (crack growth) is represented by an SN-curve

$$N = \frac{a}{S^m}, \tag{2.17}$$

where N is the number of cycles to failure at constant stress range S. a and m are the parameters of the SN-curve. The fatigue damage can be calculated by the Miner-Palmgren linear cumulative damage rule

$$D = \frac{1}{a}\sum_{i=1}^{n} S_i^m, \tag{2.18}$$

where S_i is the stress range at the i^{th} stress cycle. The expected damage, $\bar{D}$, is then found to be

$$\bar{D} = \frac{1}{a} E\left[\sum_{i=1}^{n} S_i^m\right] = \frac{n_0}{a}\bar{S}, \tag{2.19}$$

where n_0 is the mean number of stress cycles, and $\bar{S}$ is

$$\bar{S} = \frac{1}{n_0}\sum_{i=1}^{n} S_i^m = \int_0^\infty S^m f_S(s) dS, \tag{2.20}$$

where $f_S(S)$ is the stress range distribution, if the stress is a stationary process. For a narrow-banded Gaussian random process, $X(t)$, the stress amplitude, $\hat{R}$, follows the Rayleigh distribution

$$f_R(r) = \frac{r}{\sigma_x^2}\exp\left(-\frac{r^2}{2\sigma_x^2}\right). \tag{2.21}$$

Since $S = 2\hat{R}$ for a narrow-banded response, $\bar{S}$ can be written as

$$\bar{S} = \int_0^\infty (2r)^m f_R(r) dr = (2\sqrt{2}\sigma_x)^m \Gamma\left(\frac{m}{2}+1\right), \tag{2.22}$$

where Γ is the gamma function. The expected damage due to $X(t)$ in a period of T seconds is found to be

$$\bar{D} = \frac{\mu_{0,x} T}{a}(2\sqrt{2}\sigma_x)^m \Gamma\left(\frac{m}{2}+1\right), \tag{2.23}$$

where $\mu_{0,x}$ is the mean zero-upcrossing rate of $X(t)$. A similar formula for a bi-linear SN-curve is given in Det Norske Veritas (2003).

If the stress response is broad-banded, the response history needs to be transformed to fatigue cycles by a cycle counting method. In general the so-called rainflow counting method (e.g. Almar-Næss, 1985; Rychlik, 1987) should be applied. In the rainflow counting procedure, all stress ranges counted will form closed hysteresis loops. This method is generally regarded as the best approach for estimating the fatigue damage. The algorithm described by Rychlik (1987) was implemented in a Matlab toolbox at the Centre for Mathematical Sciences at the Lund University in Sweden. A rainflow count needs to be carried out in the time domain. Alternatively, if the response is obtained (efficiently) in the frequency domain, the fatigue damage should preferably also be determined in this domain. It is difficult to develop frequency domain models for fatigue damage which are applicable for processes with various spectra. Jiao and Moan (1990) provided theoretical solutions for Gaussian processes with well-separated bimodal spectra relevant in the situation of combined wave frequency stress and high frequency stress due to springing vibration, and for non-stationary Gaussian processes which are combinations of a stationary low frequency Gaussian process and a high frequency transient component when the high frequency stress is related to whipping vibration.

Based on the theory of Jiao and Moan (1990) for bi-modal processes, Gao and Moan (2007) proposed a frequency domain method for tri-modal Gaussian fatigue damage estimation. Initially the approach was derived for Gaussian processes which were a combi-

nation of three, in frequency well separated, narrow-banded Gaussian components. They however also described how the method can be applied to general broad-band Gaussian processes by dividing the spectrum into three segments. As part of their study they investigated the option of using the narrow-band assumption on broad-band processes. For processes with a Vanmarcke's bandwidth parameter, ε, of less than 0.5, they found that this assumption led to a maximum over-prediction of 30%. ε is defined as

$$\varepsilon = \sqrt{1 - \frac{m_1^2}{m_0 m_2}}, \tag{2.24}$$

where m_0, m_1 and m_2 are the first three moments of the response spectrum (see also Eq. 2.5). As a reference they used extensive time series, simulated with the same spectra, and the rainflow counting algorithm. For ε between 0.5 and 0.85 the proposed trimodal method over-estimated the fatigue damage by 10% to 15%.

Chapter 3

Experimental Methods

3.1 Introduction

As mentioned in the introduction, the dimensions of containerships have increased steadily over the past few decades, and it is expected that this trend will continue for some years to come. The larger size of ships implies an increased flexibility, and an increased importance of hydroelastic effects associated with whipping and springing. Secondly, some of the large container vessels today are trading in harsh environments such as the North Atlantic. Moreover, the unique hull form of these vessels - with a large, flat and overhanging sterns together with pronounced bow flare - coupled with high service speeds introduce nonlinear ship motions and loads that also have a significant impact on the springing and whipping.

Figure 3.1: Picture of the 4400TEU containership. *taken from the internet, website unknown*

The tests presented in this thesis were performed using a model of a 4400TEU containership. With the characteristics as described above, the vessel is considered representative

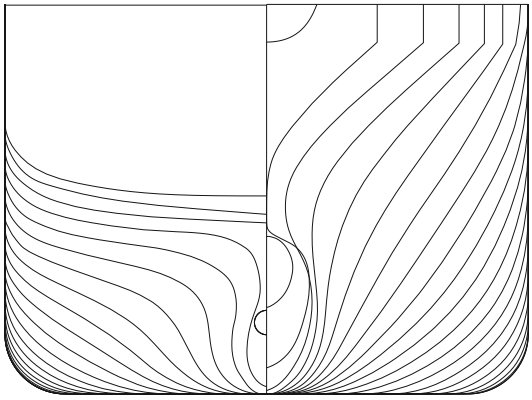

Figure 3.2: Body plan of the vessel.

for containerships of newer design. Fig. 3.1 shows a picture of the ship, and the body plan is shown in Fig. 3.2. A three dimensional illustration of the vessel is given in Fig. 3.8. The vessel was built in 2003 and operates in a trade between Canada, The UK, Germany and France. The main particulars are given in Table 3.1.

When it was decided that model tests would be performed using this vessel, DNV also instrumented the vessel for full scale measurements. The purpose of this was amongst others to determine the importance of hull flexibility for fatigue damage and wave-induced extreme loading. At the beginning of 2007 the first results from these measurements became available. Based on these results, Storhaug and Moe (2007) described the additional fatigue damage resulting from wave-induced vibrations.

Table 3.1: Main particulars of the full scale vessel.

Main particular	
Length overall	294.01m
Length between perpendiculars	280.98m
Beam	32.26m
Design draft	10.78m
Maximum service speed	23kn

3.2 Description of the Model

An important issue in ship model testing is the scale factor. One aspect of concern in this decision is tank wall interference. When the model is towed through the water it generates its own wave system, due to both diffracted and radiated waves. These waves will reach the tank wall and will be reflected. If the speed of the model is low, they will influence its response. Since it is generally difficult to completely eliminate tank wall interference in a towing tank, the criterion to be met was that no interference should occur for full scale speeds above 15kn. With realistic wave conditions and a tank breadth of 10.5m, the model should not be longer than approximately 7m to meet this criterion. The scale factor should therefore be larger than approximately 40.

One of the objectives of the model tests was to determine the importance of wave-induced vibrations for fatigue damage. The model should therefore not be too small, since the tail of the wave spectrum, i.e. the part that can excite the two node vibration mode, will then become unreliable for realistic sea states. The aim was to have waves of sufficient quality that can excite the two node mode through the sum frequencies. Waves of good quality are characterised by maintaining their height and period along the length of the tank. Based on experience with a sister vessel, the wet natural frequency of the first flexible mode was estimated to be 4rad/s. Assuming a full scale speed of 25kn, waves with a period of 6.9s will have an encounter frequency of 2rad/s. In head seas the wave frequency and the frequency of encounter are related according to Eq. 2.7. A 'realistic' height for a regular wave with a period of 7s would be approximately 2m. Using a model scale of 1:45, this wave will have a height of 0.044m and a period of 1.04s in the tank. Based on results from Storhaug (2007) it was decided that the quality of this regular wave along the tank would be sufficient for the planned experiments. The scale factor was thus chosen to be 45.

Ships in operation will be subject to gravity forces and frictional forces. During model testing the balance between inertial, viscous and gravitational forces should be the same as for the full scale case. Froude's and Reynold's laws should thus both be fulfilled. For a model substantially smaller than the full scale vessel this is generally not possible. Thus, it was considered that for ships in waves the viscous forces are smaller than the inertial forces (Newman, 1977), and so fulfillment of Froude's law should be preferred over Reynold's. As a result, Froude scaling was used as scaling law (see Appendix A). This implies that the dynamic similarity requirement is applied to the ratio between inertia and gravity forces.

Using a scale factor of 45 leads to a model with a length between perpendiculars of 6.24m, see Table 3.2. A rough form of the model hull was first made by pasting several layers of divinycell foam on top of each other. Subsequently, the hull was cut using an automated system. The movements of the machine were determined from an electronic file containing the hull lines. The hull was made water tight by a number of coatings. Plywood was used internally to increase local strength. In order to initiate turbulence in the boundary layer, a thin wire was glued around a section in the bow area of the model.

Another important decision in ship model design regards the mass distribution. Fig. 3.3 shows the distribution based on information from the loading manual of the vessel. This condition corresponds to a draft of 11.75m and zero trim. The chosen draft is approximately one meter more than the design draft. This means that, compared to the design draft, springing effects will be less important while whipping effects will be increased. The draft, trim and displacement of the model in this condition are also given in Table 3.2.

In order to include the hydroelastic effect in the experiments, the model was made flexible. Currently, two main types of flexible models are being used:

- fully flexible models, and;
- flexible segmented models.

Fully flexible models are basically a better representation of reality. There are however drawbacks. The most important ones are the costs and the difficulties in building a model

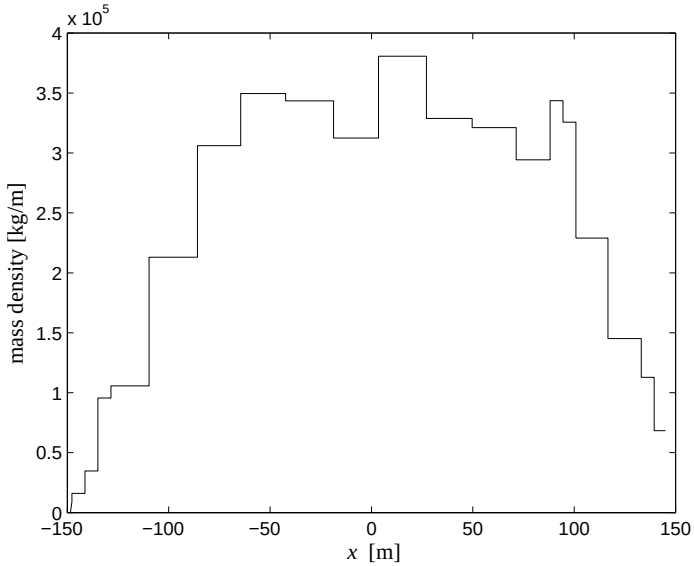

Figure 3.3: Objective mass distribution (i.e. according to the loading manual of the 4400TEU vessel). The longitudinal coordinate is relative to midships, and positive in the aft direction.

which accurately reproduces the flexibility of the full scale ship, yet with sufficient transverse stiffness to resist the loads experienced during testing. A thorough review of the use of fully flexible models at the CSSRC was given by Wu et al. (2003).

Table 3.2: Main particulars of the model.

Main Particulars	
Length overall	6.53m
Length between perpendiculars	6.24m
Beam	0.72m
Draft	0.26m
Displacement	841.2kg
Trim	0.0m
Longitudinal centre of gravity	-0.09m

Two different alternatives of flexible segmented models exist, backbone models and spring models. The main advantages of the former method are that the elastic backbone ensures a continuous stiffness distribution and that the strains are easily measured by strain gauges glued on to the beam (see e.g. Ciappi et al., 2003). The models used by Økland (2002) and Storhaug (2007) comprised segments connected by rotational springs. The latter used springs with an adjustable stiffness. In this way it became straightforward to obtain correct scaling of the first flexible mode. Therefore a flexible segmented spring model was used for the tests described in this thesis. A drawback of this approach is, however, that the number of locations where the forces can be measured is limited.

Økland et al. (2003) gave a numerical assessment of the spring model approach for the measurement of whipping responses. They concluded that global bending moments were relatively well modelled by a two segment model, although the results were sensitive to

the location of the cut. In the case of slamming events against flat parts of the model, they stated that three or four segment models should be used. As whipping also was an important aspect of the present tests, it was decided that a four segment test model would be well suited. This means that the model consisted of four rigid segments connected by three elastic rotational springs. The model could thus mimic the first three global flexible vertical modes of the full scale vessel.

Originally, the three cuts were planned at the location of the quarter lengths and the midship section. However, for the design of the aluminum frames (which will be discussed below) a slightly different location of the midships section was accidently used. This resulted in cuts that were located 0.13m (i.e. $0.02L_{pp}$) forward of the quarter lengths and the midship section of the vessel. This shift will influence the flexible mode shapes of the model, and thus the vertical bending moments found from the measurements. The numerical method described in Section 2.2.3 was used to quantify this effect. The code inputs were the mass distribution from Fig. 3.3 and a stiffness distribution that represented the segmented character of the model, see Section 3.4.4. As expected, the rigid body bending moments were not affected by the shift. The resonance peak of the two node vibration mode was somewhat increased (less than 1%) as a result of the displaced cuts. Thus, from this point of view, the slight difference in location was irrelevant.

Fig. 3.4 shows a sketch of the four segment model. The neutral line of the model was assumed at the same relative height above the baseline as is the case for the full scale vessel. The latter was found using Nauticus Hull (Det Norske Veritas, 2000b). The three cuts each consisted of two parts. One part was made up by the rotational spring system, which consisted of a spring at the top and a hinge at the neutral line. The second part of each cut contained the instrumentation necessary for measuring the vertical and horizontal forces at these locations, see also Section 3.3. Using this system it was not possible to measure the forces at the same longitudinal locations as those of the springs, which is considered an additional disadvantage. In Appendix C, the effect of measuring the forces in front of, instead of *at*, the quarter length and midships sections is quantified.

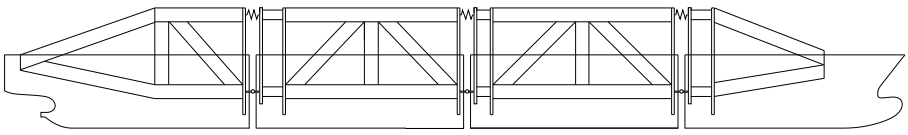

Figure 3.4: Sketch of the four segment model.

Each hinge consisted of a steel plate with a width of 30mm and a thickness of 10mm. In order to create the actual hinge, the thickness was locally decreased to 3mm, see Fig. 3.5. The physical gaps between the segments were 10mm wide, which ensured that the segments would not collide during testing. The gaps were sealed with a rubber membrane attached to the outside of the hull. This membrane stretched during testing, forming small ripples in the membrane which locally disturbed the flow field. The introduced error is however considered to be small. The membranes also led to additional damping. Ciappi et al. (2003) quantified this effect for the modal damping of the first three global flexible modes of a segmented model of a fast mono hull. The effect is strongly dependent on the material used and its thickness. Since the main concern was the total damping of the

model, the effect of the membranes on the damping was not investigated. The damping ratios of the three flexible modes of the model are presented in Section 3.4.3. The damping presented in this section is the total damping and thus also includes the effect of the membranes.

The springs were designed such that the stiffness could easily be adjusted. Each spring consisted of two rigid and two flexible bearings, as shown in Fig. 3.5.

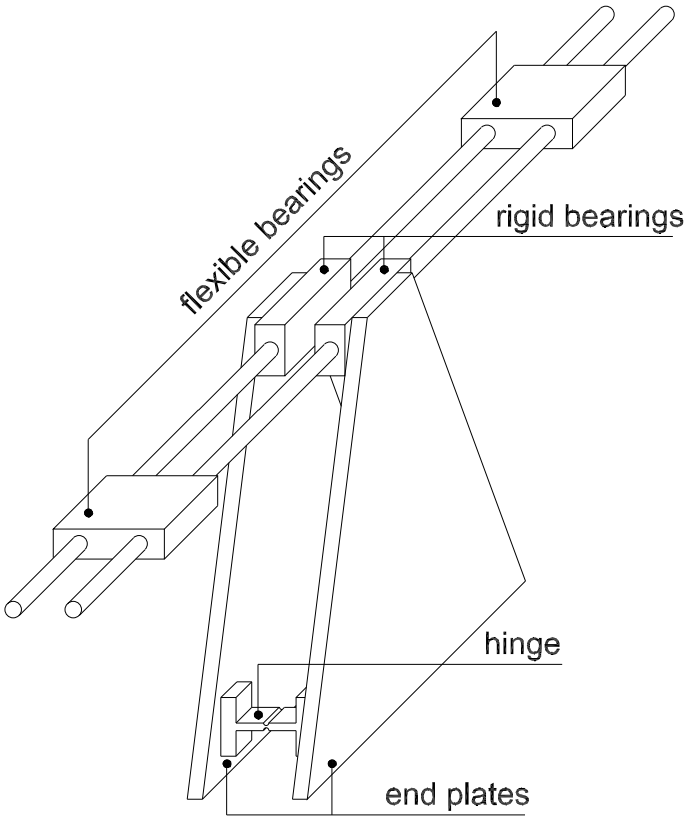

Figure 3.5: Sketch of the spring system.

The rigid bearings were connected to the end plates. They had a thickness of 40mm and each held one spring beam in position. These beams had a diameter of 22mm and were connected by the two 40mm thick flexible bearings, one at port and one at starboard side. By moving the flexible bearing in and out, the stiffness of the spring could be adjusted. The horizontal distance between the rigid bearings was chosen 20mm to ensure that they would not collide during testing. Construction drawings and pictures of the springs are shown in Appendices B.1 and B.2. Because the model would also be tested in extreme conditions, the distance between the hinges and the springs was chosen to be quite large in order to reduce the forces in the springs. The vertical distance between the hinges and the centre of the springs was 0.56m. In order for the damping of the model to be as linear as possible, the spring beams and bearings were made of steel. The end plates were constructed of aluminum. Compared to the spring design used by Storhaug (2007), the present design provided a more natural transfer of the forces, where the end plates connecting the frames to the spring systems basically did not take part in transfer of the loads through the model.

The four segments were made rigid by mounting an aluminum frame on each segment. These were designed such that the natural frequencies of the total frame did not interfere with frequencies of interest. The dry natural frequencies of the first three flexible modes were therefore estimated from the mass as well as the stiffness distribution of the full scale vessel using a simple finite element code. The mass distribution was the one presented in Fig. 3.3. The stiffness was determined from the construction drawings using the program Nauticus Hull (Det Norske Veritas, 2000b) and is shown in Fig. 3.6. The dry natural frequencies are given in Table 3.3.

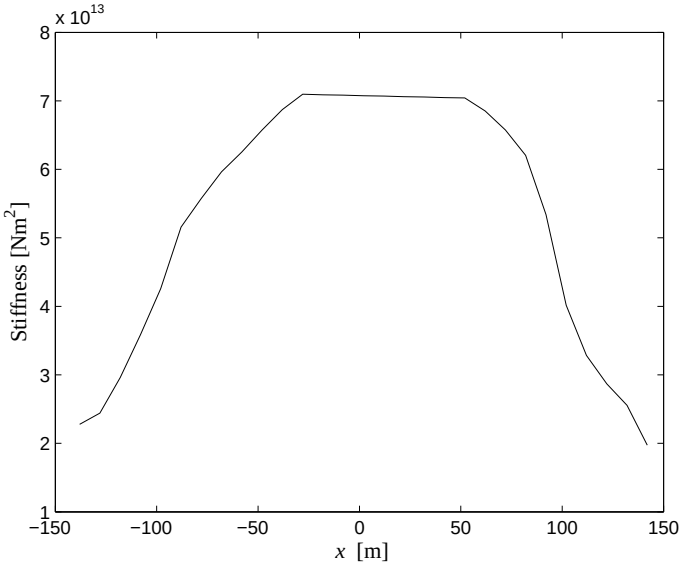

Figure 3.6: Stiffness distribution of the vessel.

The dry natural frequencies were used together with the dry mode shapes, also found from the finite element code, as input to the numerical method discussed in Section 2.2.3. This led to a wet natural frequency of the first flexible mode of approximately 3.5rad/s. At realistic vessel speeds, the length of the wave that will excite this mode is approximately 10 times the distance between the cross sections in the geometry file. For the second mode this length is approximately four times the distance between the cross sections, which does not lead to an accurate description of the incident wave. With that particular geometry file it was thus not possible to find the wet natural frequency of the second and third flexible modes. It was however noticed that the ratio between the dry and wet natural frequency of the first flexural mode was approximately equal to $\sqrt{2}$, which implies that the generalised fluid added mass is approximately equal to the modal mass. This is a well-known rule of thumb, which can be used to estimate the wet natural frequency of the three and four node vibration mode. This seems reasonable because the added mass for the two node mode should be close to the infinite frequency added mass, and thus change little for higher frequencies. The results are given in Table 3.3. The aluminum frames were thus designed to have a lowest natural frequency higher than 15.5rad/s. Construction drawings of the frames are shown in Appendix B.1. The frames were connected to the hull using glass fiber reinforced glue.

The model was towed through the tank by a carriage. The connection between the two was made at the front and aft of the model and consisted of two pieces of rope with

Table 3.3: Natural frequencies of the first three flexible modes of the full scale vessel, in rad/s. The dry natural frequencies were obtained using a simple finite element code. The wet natural frequency of the two node mode was found using the numerical method discussed in Section 2.2.3. The remaining two natural frequencies were estimated using the rule of thumb that the ratio between the dry and the wet natural frequency is $\sqrt{2}$.

	Two node mode	Three node mode	Four node mode
Dry	5.0	12.3	21.9
Wet	3.5	8.7	15.5

a spring in the middle, with a combined length of about 4m. A more detailed description, illustrated with a picture of the model, is given in Section 3.8. The stiffness of the springs was chosen to be 250N/m in order to have a sufficiently low surge natural frequency, which did not interfere with other frequencies. The pre-tension in the springs was approximately 150N. This flexibility introduced an additional restoring force in the sway, heave, pitch and yaw motions. Since only the vertical motions of the model were of interest, the additional restoring forces in sway and yaw were irrelevant. Regarding the additional restoring force in heave, a simple calculation showed that its magnitude was approximately 0.2% of that of the hydrodynamic restoring force. For the pitch restoring moment this was 1%. Thus, these additional restoring forces were negligible compared to the hydrodynamic ones.

3.3 Instrumentation and Data Acquisition

In order to measure hydrodynamic loads and load effects, the model was equipped with instruments measuring:

- horizontal and vertical forces;
- vertical accelerations;
- pressures;
- relative motions;
- rigid body motions, and;
- towing forces.

In total approximately 50 channels were used. Two video cameras were employed, one recording the fore-part of the model and one the aft part. Both quarter lengths were instrumented with three force transducers, denoted as '3 DOF force transducers' in Appendix B.3. Two of the force transducers were located at the height of the neutral line, while the third was located above it, at the height of the spring. The locations are also shown in Appendix B.1. All three transducers measured the vertical force, while the one at the top also recorded the horizontal force. By summing the three measured vertical forces, the shear force in the cut could be calculated. In the midships cut only the horizontal force at

the top was measured. In all three cuts, the vertical bending moment, M, was found from the measured horizontal force, F_x, simply as

$$M = F_x h, \tag{3.1}$$

where h is the vertical distance between the hinge and the force transducer. In this calculation it was assumed that the axial force (i.e. the horizontal force at the neutral line) in the model was negligible. From full scale measurements on the vessel presented by Storhaug and Moe (2007), it can however be seen that this is not necessarily the case. The stress from the axial force had the same period as the wave frequency part of the vertical bending stress, and the two were approximately in phase. The vertical bending moments found using Eq. 3.1 can therefore be up to 10% too high. Therefore, for future tests it is recommended that the axial force is also measured.

The vertical accelerations were measured at the bow and stern as well as in each cut. Pressure cells from Kulite Semiconductor Products recorded the pressures at several places in the fore body of the model. Two slamming panels that measured forces were installed at the port side of the bow (see Fig. B.8) and three at the port side of the flat stern. Wave probes attached to the model at the forward and aft perpendicular captured the relative motion between the model and the water at these locations. At three intermediate locations the relative motions were measured using capacitive strips. These strips are convenient in use and do not disturb the flow field around the model. They can however only be used when the wall of the model is vertical or nearly vertical. The rigid body motions were measured using an optical system with which the six degrees of freedom of a so-called NyPos-tree were recorded using two cameras. These motions were transformed to motions of the centre of gravity of the model. The NyPos-tree was placed on Segment III and did not measure the relative motion due to the flexibility between this segment and the other ones. The numbering of the segments is as shown in Fig. B.1. The longitudinal centre of gravity of the model was also located in Segment III. The measurements of the motions of the CoG, which are of main interest, were thus not effected by the flexibility. The forces in the springs used for the towing of the model as well as the speed of the carriage were also measured. An overview of the exact location of all sensors is given in Appendix B.3.

Wave probes were used to measure the waves in the towing tank. Wave probe one (WP1) was located approximately 5m in front of the wave maker. The remaining wave probes were located on the towing carriage, see Fig. 3.7, with Wave probe two approximately 5m in front of the model. The wave measured here was the most relevant one for describing the wave quality in front of the model. The disturbance of the measured wave elevation by the model is discussed in Paper 1. Wave probes three, six and seven were located parallel to the forward perpendicular, the longitudinal centre of gravity and the aft perpendicular, respectively. In order to accurately determine the wave elevation as a function of space in the forward part of the model, two additional wave probes were placed between WP3 and WP6. A fine resolution in the wave elevation as a function of space was helpful during tests with the model in response conditioned waves, see Section 3.6. In order to minimise the disturbance from one wave probe on another, they were placed in a zigzag formation.

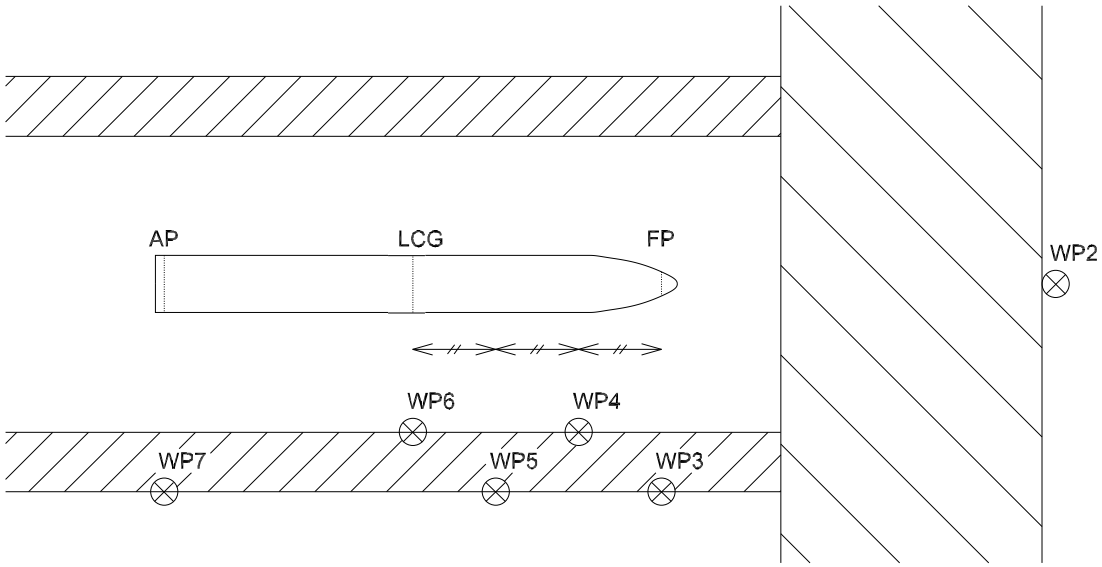

Figure 3.7: Location of the wave probes.

Each wave probe consisted of two vertical steel wires separated by approximately 2cm. The wave height was deduced from the resistance of a current through the wires. It should be noted that this type of wave measuring equipment disturbs the wave profile. Yet the disturbance was considered insignificant compared to the height of the waves. Another issue was the run up of water in front of the wave probes fixed to the carriage. From runs in calm water it was deduced that this run up was very local and had a maximum height of approximately 5mm. Moreover, the mean value of the measured wave elevation was generally filtered.

Slamming forces and pressures were sampled at 4800Hz and low pass filtered at 1000Hz using a Butterworth filter. All other instrumentation was sampled at 200Hz with a 100Hz Butterworth filter. The NyPos-tree sent information on its location 25 times per second. The motions of the CoG of the model were therefore sampled at 25Hz.

The instrumentation used during the experiments had already been used in earlier projects, and the obtained results indicated they were trustworthy. Furthermore, all sensors were calibrated before mounting. A few critical sensors were also calibrated after mounting. The calibration of these and of the wave probes is discussed in Section 3.5. The ranges of the sensors were determined from preliminary calculations using the numerical method described in Section 2.2.3. The zeros of the experimental responses were taken with the model in static equilibrium in still-water, without forward speed. Zero settings were performed regularly in order to reduce the effect of drifting.

Because the model would be tested in severe conditions, it was covered by a plastic sheet. It was made sure that there was no water accumulation on the cover. The plastic was applied such that it would not influence the damping or stiffness of the model. Near the cuts the model was therefore not completely covered by the plastic. It could thus not be avoided that some water entered the model during the tests. It has been verified though that for each run in severe conditions only a limited amount of water came into the model,

and seven pumps were installed to pump it out again.

3.4 Model Parameters

3.4.1 General

Two sets of experiments were performed using the same model. The parameters of the model were very similar in both tests and are therefore presented only once. In the following, the mass distribution of the mass of the model as well as the natural frequency, damping and shape of its global flexural modes are discussed.

3.4.2 Mass Distribution

After the model was instrumented, weights were placed in the model in order to obtain the correct mass and mass distribution, see Table 3.2 and Fig. 3.3. The total mass was correct, but it was not possible to obtain its correct distribution, due to the relatively large mass in the springs. Even without additional weights, the mass density near the springs was larger than that of Fig. 3.3. From this viewpoint the design of the spring system was not satisfactory. On the other hand, Ciappi et al. (2003) used a segmented model in combination with the elastic backbone technique and experienced the same problem. It should be noted that even though the mass distribution was not as desired, it has been possible to obtain the desired location of the longitudinal centre of gravity and the moment of inertia in pitch.

The measured inertial properties of the model are given in Table 3.4. The x-coordinates are relative to the midships section, positive aft. The y-position is given relative to the centre line and is positive in the starboard direction. The z-position is relative to the baseline and positive in the upward direction, see Fig. 3.8.

Table 3.4: Measured inertial properties of the model. The numbering of the segments is as shown in Fig. B.1.

Description	Segm. I	Segm. II	Segm. III	Segm. IV	Model
M [kg]	82.1	277.9	327.9	153.3	841.2
LCG [m]	-2.26	-0.89	0.54	2.13	0.09
VCG [m]	0.44	0.25	0.23	0.35	0.28
I_{55} [kgm^2]	491.0	351.7	122.1	717.7	1682.4

The mass, M, was measured by lifting the model or the segment with a crane. Between the crane and the carrying ropes a weighing scale was attached. This was a digital system with an inherent precision error of $\pm$0.1kg, which is very small compared to the mass of the segments and the model as can be seen from Table 3.4. The weighing scale was calibrated regularly and therefore the bias error is considered small.

The longitudinal and vertical position of the centre of gravity as well as the longitudinal moment of inertia, I_{55}, of each segment and of the model were determined through pendulum tests using a cradle. The use of the cradle at the Marine Technology Centre

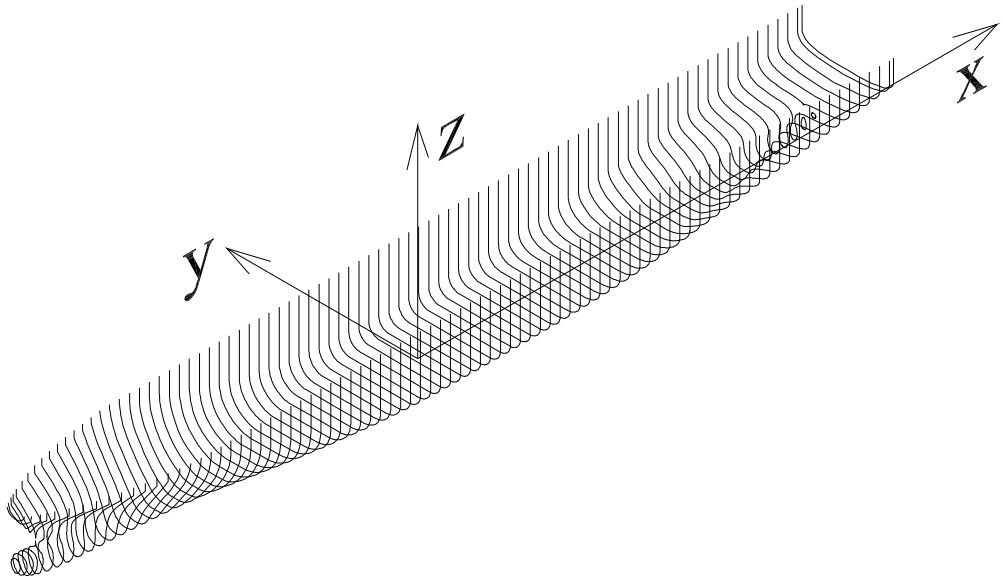

Figure 3.8: Three dimensional illustration of the vessel and the coordinate system.

was described by Storhaug (2007). The LCGs were determined by placing the part on the cradle and balancing it on even keel. The LCG was then measured using a measuring tape. The main uncertainty in this measurement was whether or not the cradle was exactly horizontal, in other words, whether the LCG was at the same longitudinal location as the centre point of rotation of the cradle. Therefore the maximum error in the LCGs was estimated at $\pm$0.005m.

The vertical centres of gravity were found from measurements taken during the pendulum tests. In order to investigate the errors, the maximum error in all the input terms for the calculations was identified. By looking at 'worst case scenarios', a maximum error of $\pm$0.01m was found for the VCG of the model. For Segment I, which was the lightest segment, this was $\pm$0.1m. Although this is quite large, it is emphasised that this is a 'worst case' value, and that the true error is most likely smaller. Furthermore, the analysis showed that a large part of the error is related to the uncertainty in the oscillation periods. These were measured using a crystal clock, with an accuracy of one millisecond. Although this is very accurate, the oscillation period may be slightly influenced by external disturbances. If the mass of the segment is small compared to that of the cradle, there is little difference between oscillation periods with and without the segment in the cradle. Slight uncertainties in the oscillation periods can then lead to relatively large uncertainties in the prediction of the VCG. Therefore, the oscillation periods were determined as the mean of six different measurements for which in each case 10 to 20 oscillations were recorded. Combining the VCGs of the four segments, weighted by their mass, also provides an estimate of the VCG of the model. This results in a value of 0.28m, which is equal to the value in Table 3.4. The fact that both estimates agree gives confidence that the VCGs were determined with sufficient accuracy.

The maximum error in the longitudinal moment of inertia of the model was estimated in the same way as the one in the VCG, and was approximately $\pm$20kgm^2. The longi-

tudinal moments of inertia of the four segments found directly from the pendulum tests refer to the segments' CoG. The ones presented in Table 3.4 on the other hand refer to the CoG of the total model. The main contribution to this moment of inertia, and also to the error in its measurement, comes from the transformation of the moment of inertia from the segments' CoG to that of the model. This transformation involves the product of the mass of the segment and the square of the distance between the CoG of the segment and that of the model. The maximum total error in the longitudinal moment of inertia of each segment was also approximately $\pm 20\text{kgm}^2$.

The measured distribution of the mass is given in Fig. 3.9 and compared with the (objective) mass distributions in Fig. 3.3. The values are given for model scale. The measured mass distribution is relevant for comparison of experimental and numerical results. Fig. 3.9 shows that the mass was irregularly distributed. This was the result of the heavy springs as well as of the fact that the additional mass could not be placed close to the cuts. The inertial properties of the four segments and of the model as a whole, found from this mass distribution, compare well with those given in Table 3.4. The comparison between the vertical bending moments calculated with the numerical method described in Section 2.2.3 using the measured mass distribution and the objective one as input is given in Appendix C. Here it is shown that the peaks of the rigid body vertical bending moment RAOs for the measured mass distribution are up to approximately 7% higher than those for the objective distribution.

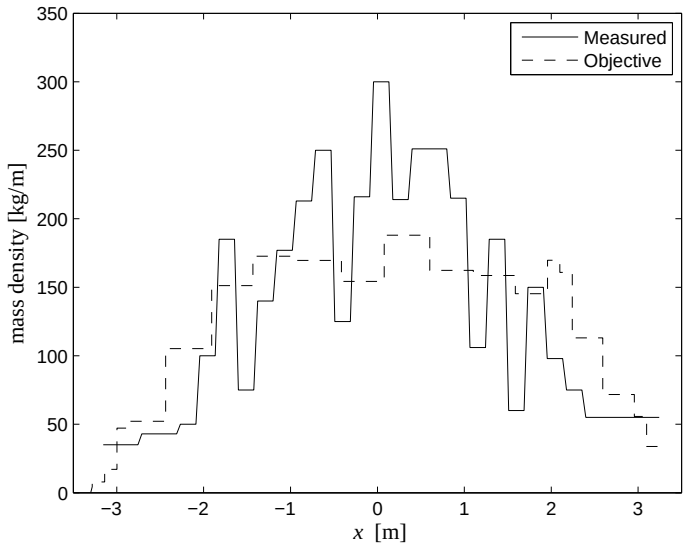

Figure 3.9: Measured mass distribution compared with the objective one (Fig. 3.3) based on the loading manual of the vessel.

3.4.3 Natural Frequency and Damping

As mentioned in Section 3.2, the springs were designed such that the stiffness could easily be modified by moving the flexible bearings. For the tests the stiffness of the three springs was chosen to be equal, and tuned to give the correct Froude scaled wet natural frequency of the first flexible mode of 23.5rad/s ($23.5 = 3.5 \cdot \sqrt{45}$, see Table 3.3 and Appendix A),

which was determined from decay tests in still-water. The flexible modes were excited by an impulse force. The natural frequencies were then found from the peaks in the absolute values of the Fourier transformed time series of the measured horizontal force at midships. The stiffness necessary for the desired natural frequency of the first flexible mode was found after a couple of iterations. By adjusting the springs, such that the natural frequency was correctly scaled, structural similitude and thus Eq. A.13 were satisfied.

The resulting natural frequencies for the three flexible modes are shown in Table 3.5. The results are presented in terms of the mean values and 95% confidence limits of the mean values, based on several decay tests during several testing days.

Table 3.5: Mean and 95% confidence interval of the mean natural frequencies of the flexible modes, in water in rad/s.

Two node mode	Three node mode	Four node mode
23.57 ± 0.04	55.28 ± 0.21	86.10 ± 0.40

Since the stiffness of the springs was adjusted to give the correct natural frequency of the two node mode, the first natural frequency of the flexible model was obviously close to the Froude scaled value from Table 3.5. No adjustments were made to obtain the wet natural frequency of the other two modes. These were however still quite close to the scaled values from Table 3.5, 58rad/s and 104rad/s respectively. This implies that the chosen constant stiffness was quite representative for the actual stiffness of the full scale vessel shown in Fig. 3.6.

The same measurements were used to determine the damping ratio of the flexible modes in water. An example of a time series of the horizontal force at midship after application of an impulse force is given in Fig. 3.10. In this case the impulse force was applied at the forward perpendicular at time $t \approx 23.5$s. From the spectral density function, $S_{F_{x;2}}(\omega)$, given in the same figure, it is clear that all three modes were excited by the impulse.

In order to determine the damping ratio of the three different modes, the signal was filtered. The boundaries for the filter were chosen such that the natural frequency of the mode under consideration was approximately in the middle of the interval and such that the influence of other modes was removed. Fig. 3.11 presents the data of Fig. 3.10 after being band passed filtered around the natural frequency of the first flexible mode.

The damping ratio was determined using two methods. The first was the free-vibration decay method. The damping was then obtained from the ratio of two peaks, separated by m cycles

$$\xi = \frac{1}{2\pi m} \ln \frac{\hat{F}^n_{x;2}}{\hat{F}^{n+m}_{x;2}}, \tag{3.2}$$

where $\hat{F}^n_{x;2}$ is the n^{th} peak in the time series of $F_{x;2}(t)$. Application of this method to each peak in Fig. 3.11 resulted in the damping ratio shown in Fig. 3.12 when $m = 10$. The damping ratio is plotted as a function of the equivalent horizontal force time derivative.

The damping ratio was also determined by fitting the following envelope process to the positive peak process, $\hat{F}_{x;2}$, of $F_{x;2}$

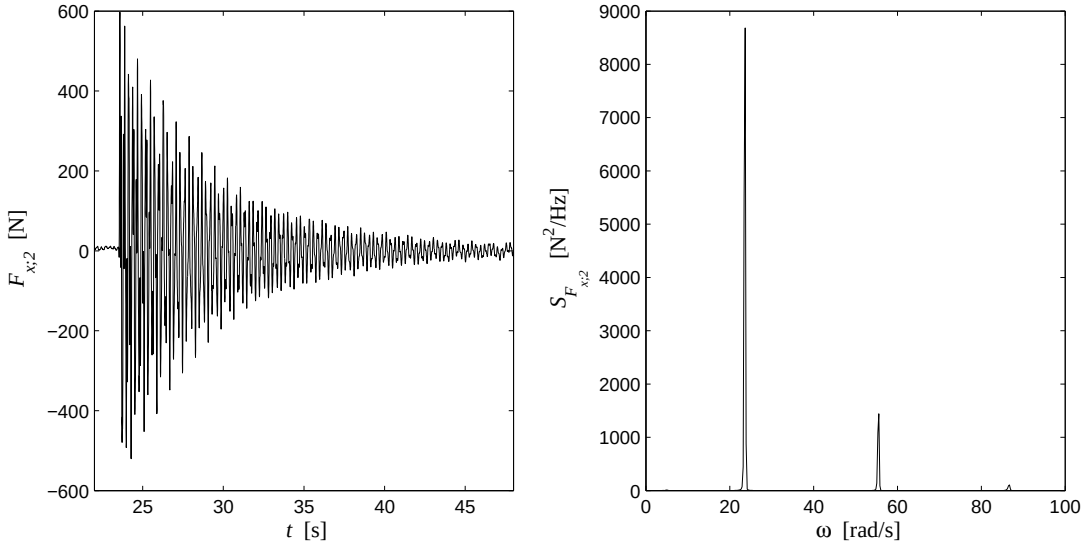

Figure 3.10: Time series of the midships horizontal force after application of an impulse force (left) and its spectral density function (right).

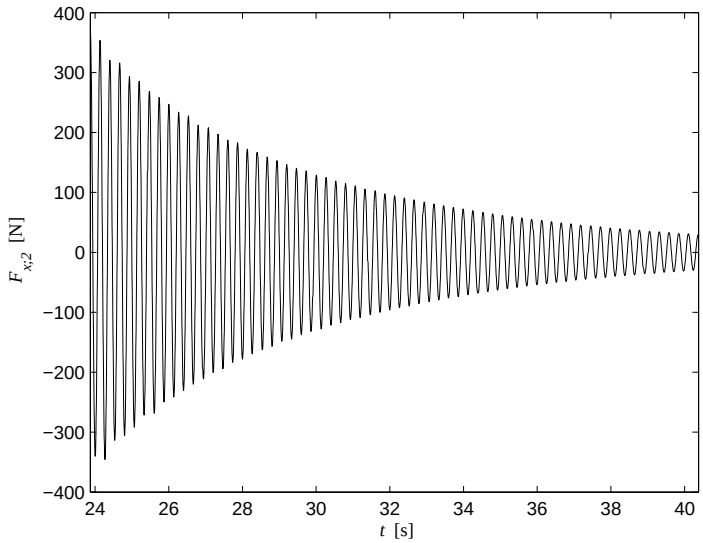

Figure 3.11: Time series of Fig. 3.10 band passed filtered around the natural frequency of the two node mode.

$$\hat{F}_{x;2}(t) = Ae^{-\xi\omega_0(t-t_0)} \quad \forall \quad t \geq t_0, \tag{3.3}$$

where ω_0, A and ξ are determined from the least square curve fit, and t_0 is the time instant at which the impulse force was applied. Using this method for the signal presented in Fig. 3.11 leads to Fig. 3.13. The figure shows the decaying time series of the filtered midships horizontal force in combination with the fitted envelope process.

Similar calculations were done for the other two flexible modes. The results obtained by the various tests are presented in Table 3.6. The table gives the mean and 95% confidence interval of the mean damping ratios of the different modes determined by the two

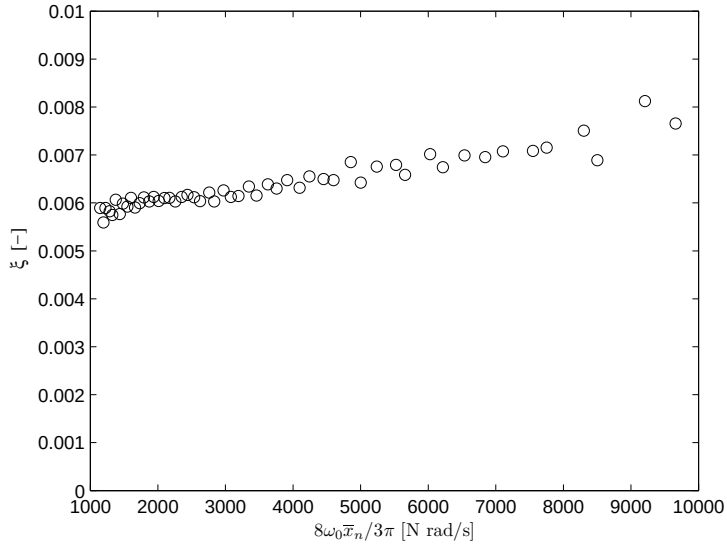

Figure 3.12: Damping ratios obtained by the free-vibration decay method. $\overline{x}_n$ denotes the average value of the two peaks used for finding the damping ratio and ω_0 is the natural frequency of the mode under consideration, in this case the two node mode.

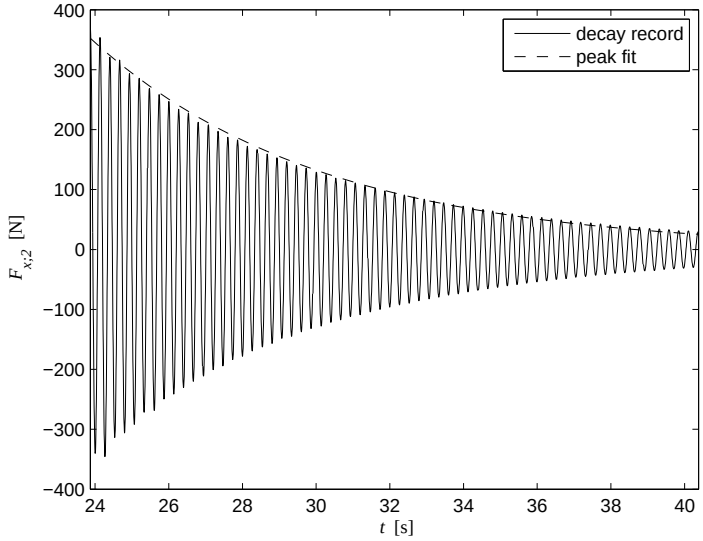

Figure 3.13: Example of the envelope fitting method.

methods. The values in the table are the results of several decay tests across several testing days.

Table 3.6 shows that the damping ratios determined by the two methods are fairly similar. In all cases the mean damping ratio of one method is within the 95% confidence interval of the other, and the borders of these intervals are between 6% and 13% of the mean value. One aspect of importance for the width of the intervals is the slight nonlinear character of the damping. As can be seen from Fig. 3.12, the damping ratio is somewhat dependent on the amplitude of the vibration. Furthermore, Fig. 3.13 shows that the fit is initially slightly higher than the peak values, while it is somewhat lower in the second

half of the time trace. Additional damping at higher responses due to stern slamming is believed to have been one of the reasons for this nonlinear behaviour. Also small imperfections in the construction of the springs led to nonlinear damping. The nonlinearity was however small. This is in agreement with full scale estimates performed by Storhaug et al. (2003) and Storhaug and Moan (2006), who indicated linear to weakly nonlinear damping for large ocean going vessels. Therefore, from the point of view of damping, the design of the structural system was very satisfactory.

Table 3.6: Mean and 95% confidence interval of the mean damping ratios of the flexible modes, in water in %.

	Two node mode	Three node mode	Four node mode
Eq. 3.2	0.62 ± 0.04	0.31 ± 0.03	0.44 ± 0.05
Eq. 3.3	0.65 ± 0.05	0.34 ± 0.03	0.47 ± 0.06

The damping was also determined in air. For this purpose, the model was hung in ropes at the locations of the nodes of the two node vertical vibration mode. It is believed that in this way reasonably good estimates are found for the natural frequency and damping ratio of at least the first flexible mode. From these tests a dry natural frequency of 32.4rad/s and a dry structural damping ratio equal to 0.2% were found. It was noticed that the ratio between the dry and wet natural frequencies was approximately $\sqrt{2}$, as could be expected. The other two flexible modes were too much influenced by the ropes, and thus the method did not give useful results for these modes. The shape of the two node vibration is shown in Fig. 3.18 in the next section.

The results presented above show that the damping of the two node mode was dominated by hydrodynamic damping. The fact that during the decay tests no waves were generated with a frequency higher than the natural frequency of the first flexible mode, implied that the potential hydrodynamic damping for the three and four node modes was negligible. Furthermore, the viscous damping is very small for vertical ship motions (see e.g. Salvesen et al., 1970). Therefore, for the three and four node mode, it was assumed that the structural damping in water was equal to the total damping given in Table 3.6, approximately 0.32 and 0.45 respectively.

The damping ratio of a mode is defined as the ratio between the modal damping, c, and the critical modal damping

$$\xi = \frac{c}{2k/\omega_0}, \tag{3.4}$$

where k represents the modal stiffness and ω_0 is the natural frequency of the mode. Therefore, in order to determine the dry structural damping ratio, the difference between the dry and the wet natural frequencies for the first flexible mode should be accounted for by

$$\xi_d = \xi_w \frac{\omega_{0;d}}{\omega_{0;w}}, \tag{3.5}$$

where the subscripts d and w denote dry and wet respectively. The dry natural frequencies of the three and four node vibration modes were unknown. Therefore, following the reasoning given in Section 3.2, the ratio between the dry and the wet natural frequencies

was taken to be $\sqrt{2}$. This resulted in dry structural damping ratios of 0.45 and 0.64 for the three and four node mode respectively.

There are some uncertainties related to the measurements of the dry structural damping ratio of the two node flexural mode. The effect of these uncertainties on the response is illustrated in Fig. 3.14. For the sea states investigated in Paper 3, this figure shows the ratios of the standard deviation stresses found from nonlinear time domain simulations using a dry structural damping ratio of 0.4% and 0.2%. A damping ratio of 0.4% was investigated as it can be considered as an upper limit for the structural damping found from the decay tests in air.

The damping ratios of the first flexible mode presented in Table 3.6 are significantly lower than those found in Paper 2 and by Storhaug and Moe (2007) from full scale measurements on containerships. The damping ratio found by full scale measurements was influenced by the cargo system, container racks, etc. Therefore, a structural damping ratio of 1.0% was also studied. The Fig. 3.14 shows that an increase of the damping ratio by 0.8 percentage point, i.e. a factor of five in this case, reduced the stresses by less than 5%. The effect was similar in all three cuts and is therefore only presented for the midships section.

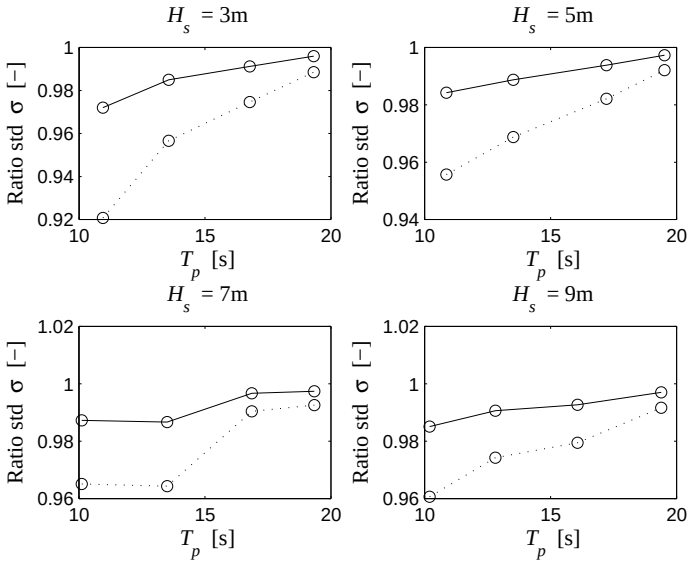

Figure 3.14: Ratio of the standard deviation of the midships bending stresses, found using nonlinear time domain simulations with two different structural damping ratios. The fully drawn line gives the ratio for a structural damping of 0.4% and of 0.2%, and the dotted line for 1.0% and 0.2 %.

A similar investigation was done for the maximum midships hogging and sagging bending moments in these half hour sea states. The time series of the wave elevation was identical for all three investigated damping ratios. Increasing the dry structural damping from 0.2% to 0.4% decreased the midships sagging and hogging moments by up to 3% and up to 5% respectively. With an increase from 0.2% to 1.0%, these values are 9% and 12%.

3.4.4 Mode Shapes

The mode shapes of the three flexible modes of the model were found from accelerations measured during the decay tests. One accelerometer was placed close to the FP, and one close to the AP. The three other accelerometers were placed near the physical cuts of the model. The exact locations are given in Appendix B.3. In order to determine the mode shapes the relative amplitudes of the vertical displacements along the length of the model as well as their relative phases should be known. Because only relative amplitudes were of interest, the procedure described in Paper 1 could be used to determine the amplitude and phase information of the time series of the five accelerometers. It was verified numerically that the error introduced to the relative amplitudes by the exponential terms in the decaying signals was small. The word 'amplitude' in this section denotes an average amplitude of the decaying signal. The notation used here is similar to that in Paper 1. The amplitude of the vertical acceleration, $\ddot{w}$, was found as

$$\hat{\ddot{w}} = \frac{2}{N} \max_j \left[\left\{ \sum_{k=1}^{N} \ddot{w}_k \sin(\Omega_j t_k) \right\}^2 + \left\{ \sum_{k=1}^{N} \ddot{w}_k \cos(\Omega_j t_k) \right\}^2 \right]^{1/2}, \tag{3.6}$$

where Ω_j is the j^{th} component of the vector $\mathbf{\Omega}$

$$\mathbf{\Omega} = [\omega_m, \ \omega_m + \Delta\Omega, \ \omega_m + 2\Delta\Omega, \ \ldots \ \omega_{m+2}]^T, \tag{3.7}$$

and ω_{m+1} is the preliminary natural frequency of the mode under consideration identified from a standard Fourier transformation of the signal. ω_m and ω_{m+2} are the frequencies to the left and to the right of ω_{m+1}, respectively. The value of j for which Eq. 3.6 achieved its maximum, is denoted as l. The amplitude of the vertical deflection was then found from

$$\hat{w} = \frac{\hat{\ddot{w}}}{\Omega_l^2}, \tag{3.8}$$

Here Ω_l is the natural frequency of the mode found from a locally refined Fourier series analysis. This last step was strictly speaking not necessary because it did not change the normalised value of the amplitude, as the same natural frequency was found from each accelerometer. The corresponding phase angle, θ, is given by

$$\theta = \arctan \left(\frac{\sum_{k=1}^{N} \ddot{w}_k \cos(\Omega_l t)}{\sum_{k=1}^{N} \ddot{w}_k \sin(\Omega_l t)} \right), \tag{3.9}$$

where it should be noted that θ is equal to $\pi/2$ if the denominator is zero and that θ should be increased by π if the denominator is smaller than zero. The mode shapes are given in Figs. 3.15$\sim$3.17. These figures present the mean results of several decay tests over several days. For all decay tests the impulse force was applied at the forward perpendicular. The vertical bars indicate the 95% confidence intervals of the mean values. Part of this uncertainty was related to the small error in the approach described in Paper 1, as discussed above.

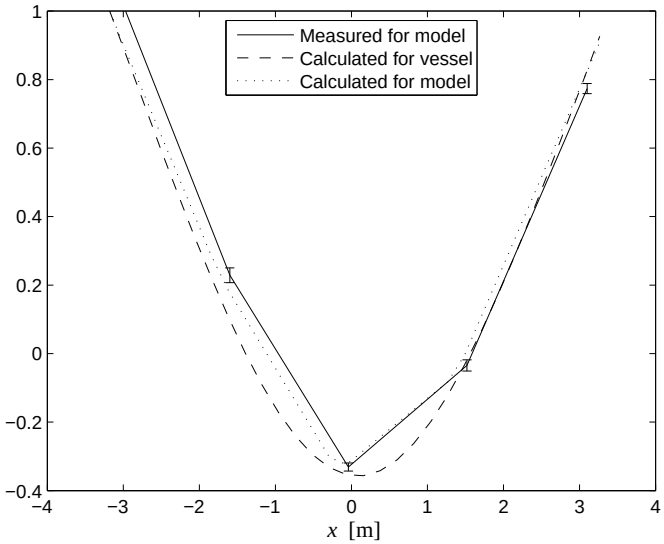

Figure 3.15: Normalised mode shapes of the two node vertical vibration mode. 'Calculated for vessel' refers to the wet mode for the objective (full scale) mass distribution and a continuous stiffness distribution. 'Calculated for model' refers to the wet mode for the measured mass distribution and a segmented stiffness distribution.

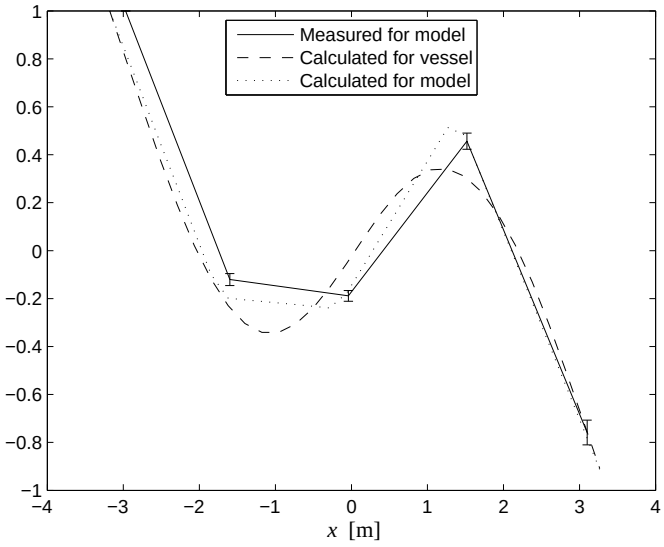

Figure 3.16: Normalised mode shapes of the three node vertical vibration mode. 'Calculated for vessel' refers to the wet mode for the objective (full scale) mass distribution and a continuous stiffness distribution. 'Calculated for model' refers to the wet mode for the measured mass distribution and a segmented stiffness distribution.

For comparison, the figures include the calculated wet modes found using a simple finite element code. The stiffness distribution from Fig. 3.6 and the mass distribution from Fig. 3.3 were used as input. Actually, the latter was multiplied by two to account for the effect of added mass. Sections 3.2 and 3.4.3 show that this is a reasonable assumption. These mode shapes are denoted 'Calculated for vessel' in the figure. The term 'vessel' is

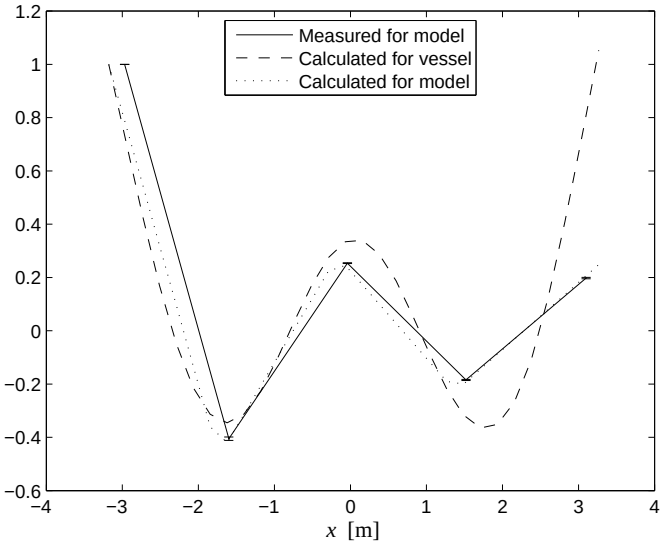

Figure 3.17: Normalised mode shapes of the four node vertical vibration mode. 'Calculated for vessel' refers to the wet mode for the objective (full scale) mass distribution and a continuous stiffness distribution. 'Calculated for model' refers to the wet mode for the measured mass distribution and a segmented stiffness distribution.

used because this case is representative for the full scale vessel. The figures show that the first three mode shapes of the vessel were well represented by the four segment flexible model.

In order to reduce the uncertainties in comparing measurements with calculations, it is better to use mode shapes that are based on the measured mass distribution (Fig. 3.9) and a segmented stiffness distribution. The latter was found by increasing the modulus of elasticity in the rigid parts of the model, and decreasing it close to the springs. The stiffness in the spring parts were chosen such that the product of E and I was constant for each of the three springs, and the wet natural frequency of the two node mode matched the one from Table 3.5. The continuous and segmented stiffness distributions are shown in Table 3.7. The distributions are given in terms of full scale values, as these were used as input to the finite element code. The wet mode shapes, calculated with this code using the measured mass distribution (also multiplied by two to account for the effect of added mass) and the segmented stiffness distribution, are shown in Figs. 3.15$\sim$3.17 and are denoted as 'Calculated for model'. The effect of using a segmented stiffness distribution instead of a continuous one on the vertical bending moment RAOs is quantified in Appendix C. Here it is shown that the rigid body RAOs do not differ for a segmented or continuous distribution of the stiffness, and that the natural frequency of the two node vibration mode occurs for a slightly higher frequency for the continuous stiffness than for the segmented one.

The mode shapes given above are all wet modes. The shape of the two node vertical mode in air in ropes is presented in Fig. 3.18. This figure shows that the calculated and the measured mode shapes compare fairly well. However, considering the good agreement between the wet two node mode shapes (Fig. 3.15), it is clear that the ropes influenced the vibration. As a result of this influence, both the damping and the natural frequency are

Table 3.7: Continuous and segmented stiffness distributions in terms of full scale values. The locations of the cuts in the model are indicated by bold 'x' values.

x	Continuous		Segmented	
	E [N/m^2]	I [m^4]	E [N/m^2]	I [m^4]
-143m : -133m	$210{\cdot}10^9$	108	$210{\cdot}10^{15}$	108
-133m : -123m	$210{\cdot}10^9$	116	$210{\cdot}10^{15}$	116
-123m : -113m	$210{\cdot}10^9$	141	$210{\cdot}10^{15}$	141
-113m : -103m	$210{\cdot}10^9$	171	$210{\cdot}10^{15}$	171
-103m : -93m	$210{\cdot}10^9$	203	$210{\cdot}10^{15}$	203
-93m : -83m	$210{\cdot}10^9$	246	$210{\cdot}10^{15}$	246
-83m : -73m	$210{\cdot}10^9$	266	$35{\cdot}10^9$	266
-73m : -63m	$210{\cdot}10^9$	284	$210{\cdot}10^{15}$	284
-63m : -53m	$210{\cdot}10^9$	298	$210{\cdot}10^{15}$	298
-53m : -43m	$210{\cdot}10^9$	313	$210{\cdot}10^{15}$	313
-43m : -33m	$210{\cdot}10^9$	327	$210{\cdot}10^{15}$	327
-33m : -23m	$210{\cdot}10^9$	338	$210{\cdot}10^{15}$	338
-23m : -13m	$210{\cdot}10^9$	338	$210{\cdot}10^{15}$	338
-13m : -3m	$210{\cdot}10^9$	337	$28{\cdot}10^9$	337
-3m : 7m	$210{\cdot}10^9$	337	$210{\cdot}10^{15}$	337
7m : 17m	$210{\cdot}10^9$	337	$210{\cdot}10^{15}$	337
17m : 27m	$210{\cdot}10^9$	336	$210{\cdot}10^{15}$	336
27m : 37m	$210{\cdot}10^9$	336	$210{\cdot}10^{15}$	336
37m : 47m	$210{\cdot}10^9$	336	$210{\cdot}10^{15}$	336
47m : 57m	$210{\cdot}10^9$	335	$210{\cdot}10^{15}$	335
57m : 67m	$210{\cdot}10^9$	326	$29{\cdot}10^9$	326
67m : 77m	$210{\cdot}10^9$	313	$210{\cdot}10^{15}$	319
77m : 87m	$210{\cdot}10^9$	295	$210{\cdot}10^{15}$	295
87m : 97m	$210{\cdot}10^9$	254	$210{\cdot}10^{15}$	254
97m : 107m	$210{\cdot}10^9$	191	$210{\cdot}10^{15}$	191
107m : 117m	$210{\cdot}10^9$	156	$210{\cdot}10^{15}$	156
117m : 127m	$210{\cdot}10^9$	137	$210{\cdot}10^{15}$	137
127m : 137m	$210{\cdot}10^9$	122	$210{\cdot}10^{15}$	122
137m : 147m	$210{\cdot}10^9$	94	$210{\cdot}10^{15}$	94

increased. However, the fact that, as mentioned in the previous section, the ratio between the dry and the wet natural frequencies is approximately $\sqrt{2}$ as could be expected, gives confidence that at least for the natural frequency this influence was small.

The accelerations were not measured during the decay tests in air. Contrary to the wet modes, the dry mode was therefore determined from the measured horizontal forces in the three cuts. A similar method as outlined above was used in order to determine the relative amplitudes. It was verified, however, that the difference between mode shapes determined from measured accelerations and measured horizontal forces is small, as expected.

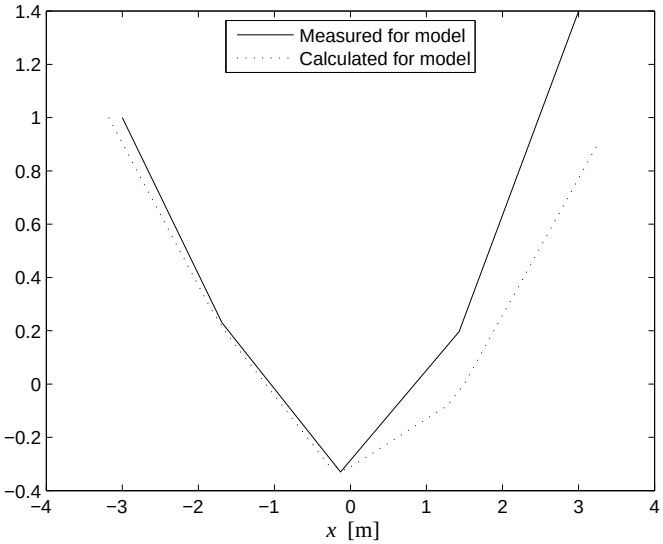

Figure 3.18: Normalised dry mode shapes of the two node vertical vibration mode. 'Calculated for model' refers to the dry mode for the measured mass distribution and a segmented stiffness distribution.

3.5 Calibration

3.5.1 General

All sensors were calibrated before mounting. These calibrations were performed by a stepwise increase and subsequent decrease of the load on the sensor. The used calibration factor was then found by fitting a straight line through the measured points using the least square method. This approach did however not provide any uncertainty measure relating to the calibration factor. Uncertainties in the calibration factors represent bias errors in the measurements (see Section 3.7). Therefore, after the initial calibration, the most important sensors were re-calibrated.

3.5.2 Force Transducers

The force transducers measuring the horizontal force at the top of each cut were re-calibrated after mounting. In order to do this the model was placed on supports such that the spring, in the cut with the transducer under investigation, could freely rotate. A mass, m_1, was then placed at a distance, a, from the transducer. The applied mass was subsequently stepwise increased, and then decreased again. Fig. 3.19 presents a step in the calibration procedure for the transducer in the forward cut. Using the obtained results, the calibration factor was determined from a least square fit. This procedure was repeated six times for all three transducers. The results are presented in Figs. 3.20∼3.22. The applied mass was transformed to a horizontal force on the sensor, F_{app}, see Eqs. 3.1 and 3.10. The absolute value of the calibration factor should therefore be equal to one.

$$F_{app} = \frac{ag\sum_i m_i}{h} \tag{3.10}$$

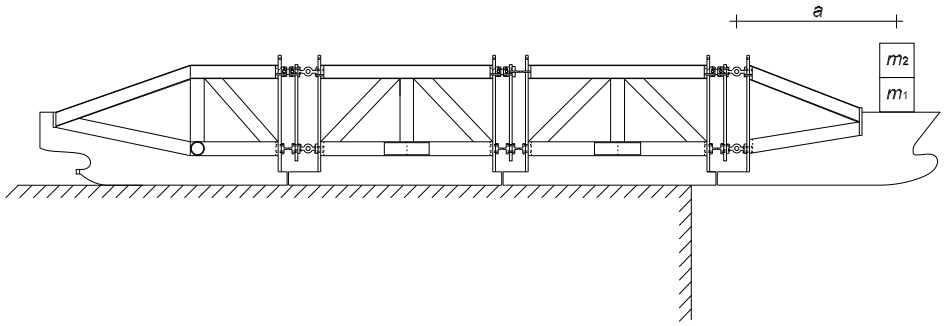

Figure 3.19: Step in the calibration procedure for the force transducer in the top of the forward cut.

The measured points reflect the linear relation between the applied and measured force well, and the six fitted lines almost coincide. The mean of the measured calibration factors together with their 95% confidence intervals are shown in Table 3.8. The table shows that the absolute values of the calibration factors are indeed close to one; the maximum deviation is approximately 3%. This deviation is at least partly attributed to uncertainties during the calibration after mounting. The calibration of sensors after mounting was less controlled than the one before mounting. The masses of the weights used for the calibration after mounting were known very accurately. The distance from the weights to the sensor was determined using a measuring tape. The main problem lay in determining the exact begin and end point of the measurement, as the location where the force was measured within the sensor, and that of the force resulting from the applied mass were somewhat uncertain. The latter is related to the shape of the frame and model, which did not allow for placing the masses as nicely on the top of each other as shown in Fig. 3.19.

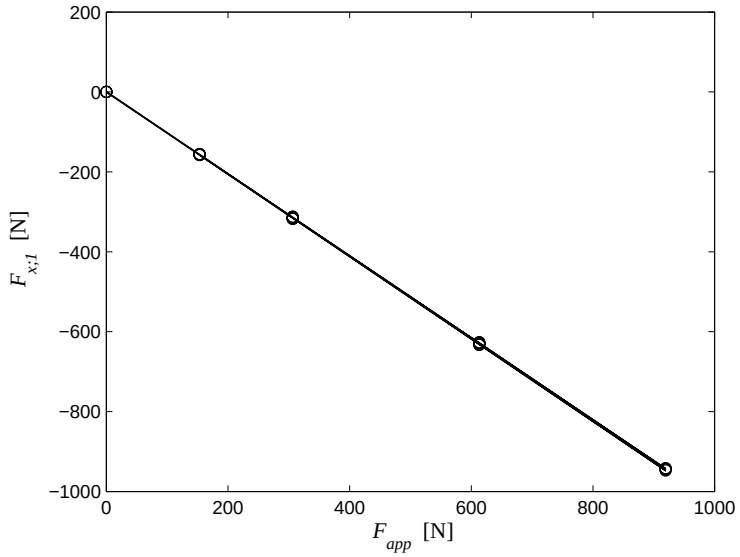

Figure 3.20: Calibration of the horizontal force transducer at QL. Force transducer in tension.

Table 3.8 furthermore shows that the confidence interval is very small, less than 1.5%

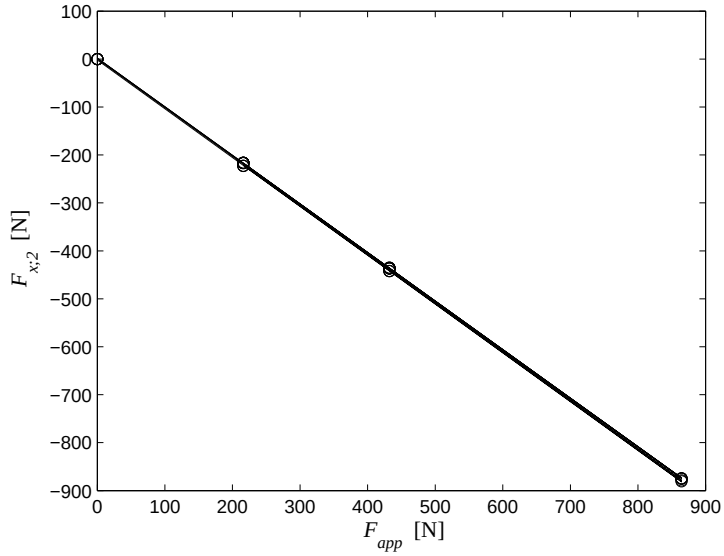

Figure 3.21: Calibration of the horizontal force transducer at MS. Force transducer in tension.

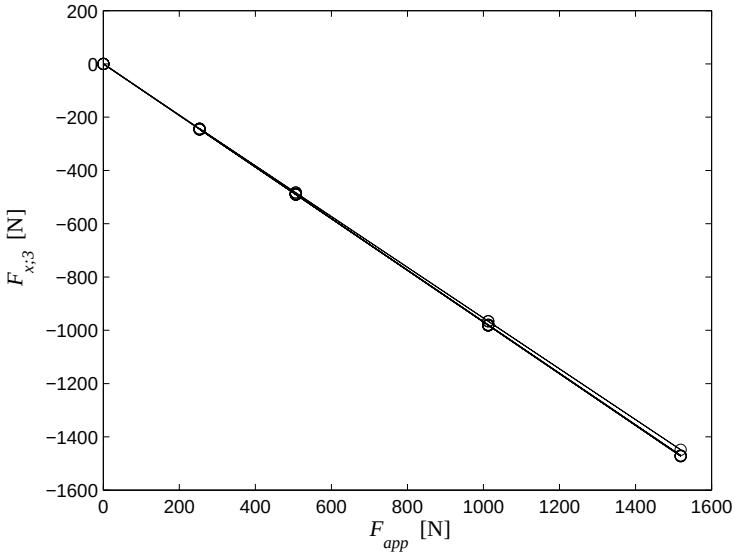

Figure 3.22: Calibration of the horizontal force transducer at 3QL. Force transducer in tension.

of the mean value. This means that the error made by performing the calibration before mounting only once was very small. The initial calibration factors were therefore not changed.

Table 3.8: Mean and 95% confidence interval of the mean calibration factors of the transducers measuring the horizontal forces.

QL	MS	3QL	MS (upward)
-1.027±0.003	-1.014±0.002	-0.966±0.007	0.968±0.033

The calibrations described above were performed by placing a mass at a certain distance from the sensor, which is then in tension. The procedure was repeated applying a

force in the upward direction using a crane. Between the crane and the rope used for the lifting, a weighing scale was attached. Section 3.4.2 discusses the error of this weighing scale. The calibration was done twice, the results are given in Fig. 3.23 and Table 3.8. The force range for the calibration in compression was larger than for the one in tension. The measurements, however, still follow a straight line. Compared to the calibration in tension, the uncertainty in these measurements is slightly larger due to the width of the rope used to lift the model, which was approximately 15cm. Similar results were obtained for the forward and aft cut. These are, however, not presented here.

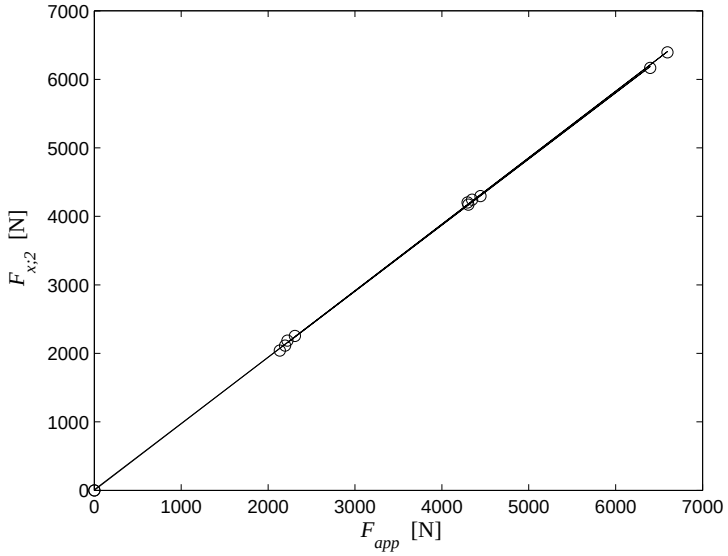

Figure 3.23: Calibration of the horizontal force transducer at MS. Force transducer in compression.

3.5.3 Wave Probes

As mentioned before, according to Storhaug (2007) there was some discrepancy between the requested and the measured wave in the towing tank at the Marine Technology Centre, and wave probes had to be used to measure the actual waves. To determine the bias error due to uncertainties in the calibration factor, one wave probe was calibrated in a similar manner as described in the previous section. The wave probe was lowered step by step into still-water, and subsequently lifted again using the same steps. This was repeated five times, each time determining the calibration factor. The results are presented in Fig. 3.24.

This figure shows that the linear fits of the five calibrations agree very well. The mean calibration factor was 0.973 with a 95% confidence interval of 0.011. So the uncertainty in the calibration factor was small. Yet the deviation of the mean from 1.000 was almost 3%. Calibration of wave probes should be done with consideration of the waves to be measured. For instance, if a probe will only measure small waves, it is not necessary to calibrate it over its full range. As the wave probes are not perfect, the calibration factor will vary somewhat with the calibration range. The re-calibration was performed on a wave probe which was calibrated for measuring waves in another project. Therefore, the 3% difference might have been caused by differences in calibration range. Another aspect

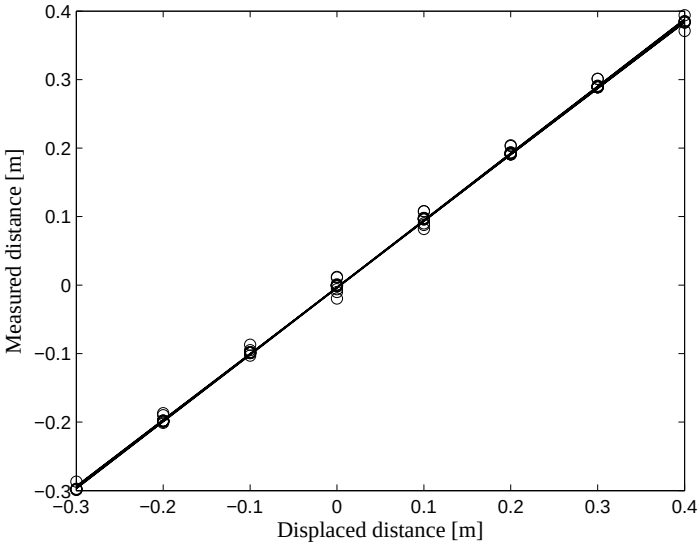

Figure 3.24: Calibration of a wave probe.

is that the probe was not 100% vertical. If the wave probe during the re-calibration was slightly rotated around the vertical axis with respect to the initial calibration, this would also have contributed to the 3% difference. In any case, the goal of this exercise was to determine the uncertainty in the calibration factor, which is shown here to be small.

3.6 Test Program

Two sets of experiments were performed for this thesis. The main goal of the first set was to investigate the influence of wave-induced vibrations on fatigue damage. In order to study the nonlinear and hydroelastic effects on the vertical bending moments, the model was also run in regular and irregular waves of varying severity. Finally, some pilot tests in response conditioned waves were performed. The goal of the second test set was to investigate the application of response conditioned waves for long-term response analysis. The test program is described in more detail below, starting with the first set of tests.

The influence of wave-induced vibrations on fatigue damage was studied by running the model in 16 sea states representative for the North Atlantic and relevant for fatigue damage. The parameters of these sea states, as well as the vessel speeds, are given in Paper 3. In order to identify the response amplitude operators of the vertical motions and load effects of the model, a large number of tests in regular waves were performed, with a minimum full scale wave height of 4m. Details of this part of the test program are presented in Paper 1. This paper also gives the parameters of three irregular sea states which were run with the purpose to excite whipping, and thus had peak periods that approximately coincided with the period of maximum relative motion. In order to excite linear, second and third order springing the model was tested at forward speed in regular waves of which the encounter frequency was approximately

$$\omega_e \approx \frac{\omega_s}{i}, \qquad i = 1, 2, 3. \tag{3.11}$$

The relationship between the wave frequency and the encounter frequency in head waves is given by Eq. 2.7. The tests for second and third order springing (i=2 and i=3 respectively) were performed using the full scale maximum service speed of 23kn. By testing several waves that approximately satisfied Eq. 3.11, the true resonance frequencies were iteratively found. Subsequently, two irregular sea states were tested with these frequencies as the peak frequencies. For linear springing (i=1), the chosen speed was 25kn such that, compared to 23kn forward speed, waves with a slightly lower frequency would excite the first flexible mode. The quality of small waves in the tank increased with decreasing frequency.

As mentioned above, as part of the first set of experiments, some pilot tests of the model in response conditioned waves were performed. These results were however prone to large uncertainties and were not publishable. This was partly related to the fact that the waves produced by the wave maker did not repeat very well. Another aspect causing problems were the difficulties involved in timing. The model should be at a certain location at a certain time. Both were decided on upfront, and partly determined the wave produced by the wave maker. Part of the problem was that it could not be determined whether or not the timing was correct. Between the first and the second testing periods, the facilities at the Marine Technology Centre in Trondheim were improved. Advanced methods were implemented for operation of the wave maker and the towing carriage. These are discussed in Section 3.8. It was also verified that the waves repeated very well after the improvements.

With the improvements made to the operating system in the towing tank, the model could be tested in response conditioned waves in a controlled manner during the second testing period. It was possible to determine whether the model hit the wave at the desired location and time instant, and how the response was influenced by this location. Approximately two of the five testing days were used for this type of investigations. Some details about the experimental use of response conditioned waves are given in Appendix D. Results from tests in the conditioned waves were compared to those from random irregular wave tests for the same sea state. A more detailed overview of the program for the second test period is given in Paper 4.

The profile of the conditioned waves was found using the transfer function of the midships vertical bending moment of the vessel at a 5kn forward speed. Results from the first testing series gave a transfer function of the model only for waves with a height of 16m. As the response in these waves was strongly affected by nonlinearities and the frequency range was very narrow, these results could not be used for the calculation of the conditioned wave profiles. It was however noted that the experimental transfer function agreed very well with the calculated one, for a forward speed of 23kn and 4m wave height (Paper 1). Therefore, the transfer function for a forward speed of 5kn found from the same numerical code (Section 2.2.3) was used as a basis for the calculations of the response conditioned wave profiles. In order to investigate whether the experimental and numerical transfer functions at 5kn compared equally well as those at 23kn, a 5kn transfer function was determined during the second test period. In a trade-off between measuring accuracy and the desire to have experimental results as close to linear as possible, the transfer function was determined using waves with a height of 2m.

An important part of the test program during both sets of tests was to repeat tests with

nominally identical conditions, such that the uncertainties in the measurements could be quantified. A more detailed discussion of the uncertainties is given in the next section.

3.7 Uncertainties

Uncertainty analysis of experimental results is important as it provides information on the quality of the obtained results. Drawing conclusions based on experimental results without quantifying the uncertainties can lead to significant errors. A test outcome is only one example of the range of possible outcomes of the experiment. It is thus vital to know the uncertainties and to try to quantify them, particularly as experimental results are often regarded as the 'true' results when comparing them with predictions from computer codes.

A number of uncertainties that affected the experimental results are listed below. Whenever relevant, it is indicated where the effect of this uncertainty is further discussed.

- In order to include hull flexibility, a segmented test model was used. This leads to a segmented distribution of the stiffness, which is continuous for the full scale vessel. See Section 3.4.
- A model was used which was only able to mimic the first three global flexible modes of the full scale vessel. See Section 3.4.4 and Paper 3.
- The physical cuts in the model were located $0.02L_{pp}$ forward of the quarter lengths and the midships section. See Section 3.2 and Papers 1 and 3.
- All three springs had equal stiffness which was tuned to give the correct Froude scaled natural frequency of the first flexural mode of the full scale vessel. The natural frequencies of the second and third flexural modes of the model were respectively 5% and 17% lower than those of the vessel. See Section 3.4.3.
- The damping of the two node vertical mode of the model was smaller than that obtained from full scale measurements on containerships. See Section 3.4.3 and Papers 1 and 3.
- The dry natural frequency and damping of the two node mode of the model was found by hanging it in ropes at the location of the nodes. See Section 3.4.3 and Paper 3.
- The calibration factors of the force transducers and the wave probes were determined by only one stepwise increase and subsequent decrease of the load on the sensor. See Section 3.5.
- For the sensors placed in the model, the calibration factors were determined under ideal conditions. See Section 3.5.
- The zeros of the sensors drifted. See Section 3.3 and below.

- The mass distribution of the model was not the desired one from the loading manual of the ship. See Section 3.4.2 and Paper 1.
- The model was connected to the carriage by springs, which introduced additional stiffness for some of the rigid body motions as well as a low frequency surge motion. See Section 3.2.
- The axial force in the model was not measured. The obtained vertical bending moments might therefore be approximately 10% too high. See Section 3.3 and Papers 1 and 3.
- The wave which was requested to appear in the towing tank deviated from the measured wave. See Papers 3, 4 and 5.
- The wave radiated and diffracted by the model influenced the measured incident wave. See Paper 1.
- Particularly at higher forward speeds, water ran up in front of the wave probes fixed to the carriage. See Section 3.3.
- The wave probes influenced the wave profile. See Section 3.3.
- Near the wave maker, the track over which the carriage ran was slightly inclined. This influence was small, as low frequencies were generally filtered from the time series of the wave elevations and those of the vertical motions.
- During the tests in severe conditions water came into the model. See Section 3.3.
- Some of the water that entered the model in the forward cut could not be pumped out, and slightly influenced the trim.
- Wall interference occurred at full scale forward speeds lower than approximately 15kn.
- The steady responses of the model at 5kn and 15kn full scale forward speed were small, and thus easily influenced by external factors. See Paper 1.
- Wave disturbances from previous runs, dampers and reflection at the beach and the wave maker influenced the wave produced by the wave maker.
- Sea states were generally only run for a full scale duration of 30 to 45 minutes. This introduces statistical uncertainties in the obtained quantities such as the standard deviation. See Paper 3.
- The wave frequency part of the bending moments was obtained by high pass filtering of the original time series at a frequency below the natural frequency of the two node mode. In this way not only hull flexibility was filtered, but also some of the higher order nonlinear effects. See Paper 1.

Also Storhaug (2007), who performed tests at the same facilities, gave a list of uncertainties relating to the tests he performed. Where possible, these were removed for the tests presented here and are thus not mentioned in the list above.

ITTC (2006) provided a methodology for estimating the uncertainties. This was partly based on the theory described e.g. by Coleman and Steele (1989). The method considers the total error to be composed of two distinct parts, a systematic or bias error, which is constant during experiments, and a precision error, which contributes to the scatter of the results. From a practical point of view, the precision error can be estimated to a reasonable degree of accuracy by repeating the tests. The bias error on the other hand is difficult to determine, particularly in large and expensive laboratories like a towing tank. As it was not possible to carry out a complete uncertainty analysis using the methodology from ITTC (2006), an estimate of the precision error and a short discussion of the bias error are given below.

One measure for the precision error is the 95% confidence interval of the mean value of repeated runs. Consider a run which is repeated and analysed such that N values of the quantity X_i are obtained. The 95% confidence interval of the mean value is then given by

$$\bar{X} \pm k\frac{\sigma_x}{\sqrt{N}}, \tag{3.12}$$

where $\bar{X}$ and σ_x represent the mean and the unbiased standard deviation of the N measured values X_i. If N is finite, k is found from the Student's t-distribution function with $N-1$ degrees of freedom. In order to determine the precision error of the experimental results, many of the runs were performed six times, N=6. k is then approximately equal to 2.5. For this value of k, the width of the 95% confidence interval, normalised by the mean value, is approximately equal to twice the coefficient of variation, as the square root of six is approximately equal to 2.5. Most of the experimental results are presented in the appended five papers. Wherever possible, the precision error was estimated. For example, Paper 1 shows that the width of the 95% confidence interval of the vertical responses in regular waves was on average approximately 5% of the mean. For the response conditioned waves, the value was less than 5%, as can be concluded from Paper 4.

Many of the uncertainties discussed in the list above led to a bias in the experimental results. In some cases this bias could be reduced, e.g. by calibrating all sensors and by regularly performing zero setting, although it should be noted that not all runs were preceded by zero setting, due to time limitations. Whenever possible the influence of the bias on the results are indicated, as shown above. Also mentioned above is that it can be very expensive and time consuming to quantify this bias experimentally. The numerical method discussed in Section 2.2.3 was therefore occasionally also used for this purpose.

3.8 Experimental Facilities

The experiments were performed in the towing tank at the Marine Technology Centre in Trondheim, Norway. The tank consists of two parts, one part is 175m long, 10.5m wide and 5.6m deep, the other one is equally wide but with a length of 85m and a depth of 10m. The layout of the tank is shown in Fig. 3.25. The two parts can be separated by

a dock gate. For the tests presented here, the separation was removed and the two parts were used as one tank of 260m length.

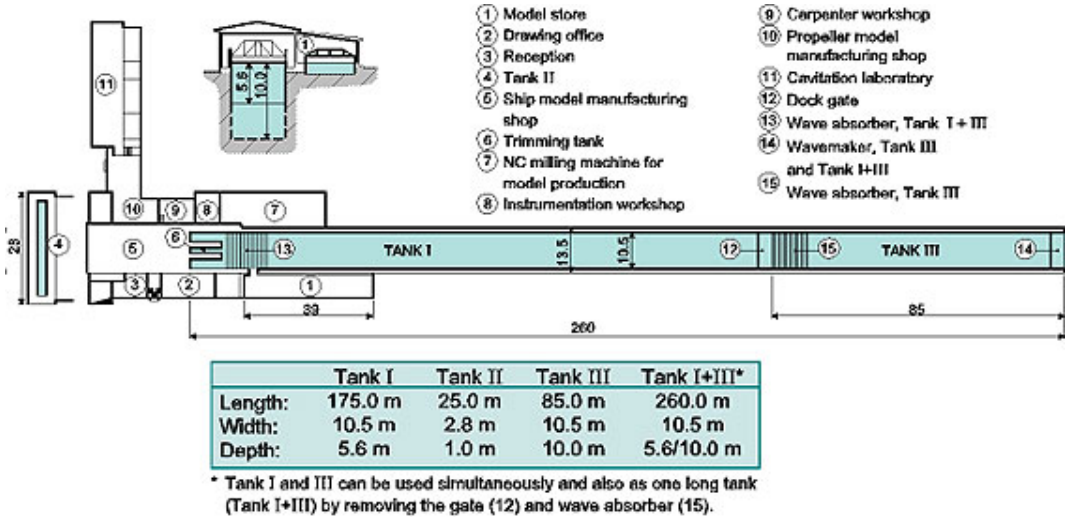

	Tank I	Tank II	Tank III	Tank I+III*
Length:	175.0 m	25.0 m	85.0 m	260.0 m
Width:	10.5 m	2.8 m	10.5 m	10.5 m
Depth:	5.6 m	1.0 m	10.0 m	5.6/10.0 m

* Tank I and III can be used simultaneously and also as one long tank (Tank I+III) by removing the gate (12) and wave absorber (15).

Figure 3.25: Layout of the towing tank at the Marine Technology Centre in Trondheim. *taken from www.sintef.no/content/page1____1132.aspx*

The double flap wave maker in the tank is able to produce both regular and irregular waves with a period of approximately 0.8s to 5s and a maximum wave height of about 0.9m. For the model scale used in this investigation, the full scale values are 5.4s, 33.5s and 40.5m respectively. In order to damp the fluid motion in the tank, dampers can be placed along the walls at the water surface. These are floating perforated plastic discs with a diameter of about 15cm. They are kept in place by an iron string running through the centre of each disc, and along both tank walls from 90m in front of the wave maker to the end of the tank. When the dampers are not in use, they are pulled under water. A wave beach at the end of the tank reduced the reflection of waves.

The model was towed through the tank, as mentioned in Section 3.2, by a carriage running over a track on both sides of the tank. A picture of the model, carriage and towing tank is given in Fig. 3.26. The connection between the model and the carriage was made at the front and aft of the vessel. Each connection consisted of two pieces of rope with a spring in the middle, and had a total length of about 4m. By looking carefully at the lower left corner of the picture the connection of the rope to the front part of the vessel can be seen. The rope above this connection was used to reduce the surge motions of the model during the acceleration period. Using this setup meant that the model was basically free to move in all six rigid body motions. The influence of the restoring forces introduced by the springs on the heave and pitch motions is discussed in Section 3.2.

From the picture it can furthermore be seen that all cables were collected and connected to the top of the towing carriage. A separate connection between the cables and the carriage was made using a spring. In this way the cables were held up without influencing the motions of the model, even when these were large.

As mentioned in Section 3.6, the facilities were improved between the first and the second testing period. A new operating system made it possible for the towing carriage

Figure 3.26: Picture of the model under the carriage in the towing tank.

to be positioned very accurately using a digital positioning system. The towing carriage and the wave maker could now also be started simultaneously. It was verified that both the acceleration period and distance of the towing carriage repeated very well. This was tested by accelerating the carriage three times from 0m/s to 0.383m/s and in all cases starting the measurements and the carriage simultaneously. Fig. 3.27 shows the result of this investigation. It took approximately 3s for the carriage to begin moving after pressing start, and the requested speed was reached after about 5.1s for all three cases. During this period the covered distance was 0.43m, 0.44m and 0.47m for run 1, 2 and 3 respectively.

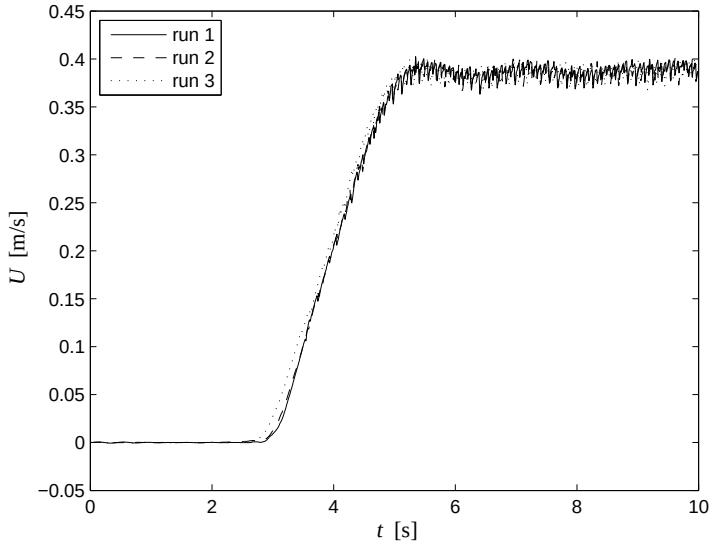

Figure 3.27: Speed of the carriage during acceleration from 0m/s to 0.383m/s, for three different runs.

Chapter 4

Summary and Main Contributions of the Papers

In this chapter each paper is summarised and the main contributions are emphasised, with reference to the four objectives given in Section 1.2. The results can typically be divided into two categories:

- insight into the physical behaviour of the model and the full scale vessel, and;
- insight into, and improvement of, experimental methods.

Paper 1: Experimental and numerical study of containership responses in severe head seas

For Paper 1, the experimental results in regular waves were used to calculate the response amplitude operators (RAOs) of several vertical ship responses, for 5kn and 23kn forward speed. For both speeds the rigid body RAOs of the heave and pitch motions are given, as well as the RAOs of the bending moments amidships and at the forward and aft quarter lengths. The paper also presents higher order RAOs of the vertical bending moments. For 23kn forward speed, $4\omega_e \approx \omega_s$ for waves with encounter frequencies of around the rigid body resonance frequencies. Therefore, the 4^{th} order RAOs at this speed are presented. The n^{th} order RAO is defined as the ratio of the amplitudes of the n^{th} harmonic of the response and of the first harmonic of the wave elevation. For 5kn, n=6 because at this forward speed, $6\omega_e \approx \omega_s$ for waves with encounter frequencies of around the rigid body resonance frequencies. The investigation shows that the amplitudes of the fourth and sixth harmonics of the bending moment have maximum values between 25% and 50% of that of the first harmonic.

The peak periods of the sea states which were investigated, were chosen close to the period of maximum relative motion. The significant wave heights were 8m, 10m and 12m. The vertical bending moments measured in these sea states are presented in terms of exceedance plots. These show that hull flexibility can increase the vertical bending moments by up to 35%. Comparisons of moments found experimentally with results from the nonlinear hydroelastic strip theory method of Wu and Moan (2005) show that

the method slightly over-predicts the effect of nonlinearities on the rigid body moments in the aft body. The method also tends to over-predict the increase of the moments due to hull flexibility. In general however, numerical and experimental results compare reasonably well.

The main contributions of this paper are:

- that hull flexibility is shown to increase the vertical bending moments in the hull of a containership of newer design by up to 35% for realistic speeds in head sea states relevant for design (Objective B);
- that predictions of the vertical bending moments in severe head seas using the nonlinear hydroelastic strip theory method of Wu and Moan (2005) are shown to compare reasonably well with experimental results (Objective D), although
- the increase of the vertical bending moments due to hull flexibility is shown to be over-predicted by the method (Objective D);
- that the relatively large mass, in the designed spring system, is shown to complicate achieving the desired mass distribution of the model.

Paper 2: Experimental and full scale investigation of the importance of fatigue damage due to wave-induced vibration stress in a container vessel

The second paper deals with an experimental and full scale investigation of the importance of fatigue damage due to wave-induced vibrations. The experimental results were based on 16 sea states with significant wave heights between 3m and 9m. These sea states are representative for the North Atlantic. Using interpolation the results were extended to 49 sea states. The fatigue damage was determined using rainflow counting and the Palmgren-Miner linear cumulative damage rule. Assuming that the lifetime of the vessel is 20 years and that it spends 2/3 of this time at sea in head seas, it is found that the wave-induced vibrations cause 37% of the fatigue damage for a deck detail amidships. These results are compared with full scale measurements on a similar container vessel, but of older design. This vessel has an overall length of 294m, is more slender with less bow flare and has a bulb which is significantly smaller than the vessel for which the model tests were performed. The measurements were carried out between April and June in 2002 and between January and April in 2005. For the former period the contribution of the wave-induced vibrations to the fatigue damage was 39%, while it was 46% in the latter period. Damping ratios were estimated based on the model test results as well as on the full scale measurements. The comparison between these two results shows that the damping ratio of the two node vertical vibration found from full scale measurements is significantly higher than the one obtained during the model tests. This could be related to damping originating from the containers and the lashing system.

The main contributions of this paper are:

- that wave-induced vibrations are shown to cause 37% of the fatigue damage in the midships section of a containership of newer design operating in head waves (Objective A);
- that the damping ratio of the first global flexible mode of the model is shown to have been significantly lower than the values found from full scale measurements on containerships.

Paper 3: Experimental and numerical investigation of fatigue damage due to wave-induced vibrations in a containership in head seas

Paper 3 presents similar experimental results as the second paper, yet the results include values for the fatigue damage in the forward and aft quarter lengths as well. The contribution of the wave-induced vibrations to the total damage is approximately the same for all three cases, although it slightly increases from forward to aft. The difference between the damping ratio found during the model tests and the one obtained from full scale measurements is more thoroughly discussed in this paper. Using the numerical method of Wu and Moan (2005), the effect of the damping on the contribution of the wave-induced vibrations was investigated. From this it is found that using a structural damping ratio of 1.0% instead of 0.2% decreases the above mentioned contribution of 37% to 27%. The paper also presents a comparison between experimental and numerical results, which shows that the numerical method over-predicts the fatigue damage by 50%. This is mainly due to an over-estimation of the wave-induced vibrations. The reason for this is partly attributed to 3D effects which are not included in the 2D slamming calculation, and partly to an over-prediction of the springing contribution. Furthermore, the numerical method does not account for the steady wave around the hull due to forward speed. Using a simplified approach it is shown that by including this wave in the numerical simulations, the calculated damage resulting from wave-induced vibrations can be reduced significantly.

The main contributions of this paper are:

- that wave-induced vibrations are shown to cause approximately 40% of the fatigue damage in a containership of newer design operating in head waves (Objective A);
- that the wave frequency stress and damage is shown to be quite accurately predicted by the nonlinear hydroelastic strip theory method of Wu and Moan (2005) for the investigated head sea states (Objective D);
- that the high frequency stress and damage is shown to be over-predicted by the numerical method of Wu and Moan (2005) in almost all the investigated sea states (Objective D);
- that for the presented purpose a model which can mimic the first three global flexible modes of the full scale vessel is shown to be sufficient, and;

- that the high frequency fatigue damage is numerically shown to decrease by approximately 35% as a result of an increase in the structural damping ratio from 0.2% to 1.0%. For the total fatigue damage the decrease is about 15%.

Paper 4: Experimental investigation of the application of response conditioned waves for long-term nonlinear analyses

This paper deals with an experimental study of the application of response conditioned waves for long-term nonlinear analyses of extreme responses. Both the most likely response wave method and a simplified conditional random response wave method were investigated, see also the summary of Paper 5. Using results from a linear long-term analysis, the coefficient of contribution method (Baarholm and Moan, 2000) was applied together with the nonlinear numerical method of Wu and Moan (2005). Thus, the five sea states contributing most to the nonlinear midships vertical hogging bending moment with a mean return period of 10^4 years were found, assuming that the vessel operated in head seas at 5kn. These five sea states were investigated experimentally. The rigid body hogging moment found from the long-term analysis based on this investigation is roughly twice the 20 years ship rule value, and is increased by approximately 20% when hull flexibility is accounted for. The paper also presents a comparison between the short-term probability distributions of the midships hogging moment found from experiments in random irregular and in response conditioned waves. This comparison was carried out for the sea state most contributing to the hogging moment with a mean return period of 10^4 years, and shows that results from the response conditioning techniques agree well with random irregular wave results as long as the hull is assumed to be rigid. For a flexible hull, results of response conditioned waves are approximately 15% lower than those of random irregular waves in the case where severe slamming occurs.

The main contributions of this paper are:

- that hull flexibility is experimentally shown to increase the vertical hogging bending moments in the hull of a containership of newer design by approximately 20% when operating in head seas with a forward speed of 5kn (Objective B);
- that the short-term probability distributions, obtained using response conditioning techniques, of the midships vertical hogging bending moments of a containership operating in head seas at 5kn forward speed are experimentally shown to agree well with the distribution obtained using random irregular waves, when the hull is rigid (Objective C);
- that midships vertical hogging bending moments found using response conditioned waves are experimentally shown to be approximately 15% lower than those obtained in corresponding random irregular head waves in the case severe slamming occurs and hull flexibility is accounted for (Objective C);
- that it is shown that tests with response conditioned waves and a model with forward speed can only be carried out successfully if the operating system present in the

towing tank allows for accurately positioning the towing carriage and starting the wave maker at a given time before or after starting the carriage, and;

- that the repeatability of tests in response conditioned waves with a model with forward speed in the towing tank at the Marine Technology Centre in Trondheim is shown to have been very good when using such an operating system.

Paper 5: Numerical and experimental investigation into the application of response conditioned waves for long-term nonlinear analyses

In this paper the application of response conditioned waves for long-term nonlinear analyses of extreme responses was investigated numerically, using the nonlinear hydroelastic strip theory method of Wu and Moan (2005). The response conditioned results were obtained using the most likely response wave (MLRW) method, a full conditional random response wave (CRRW) analysis, as described by Dietz (2004) and Dietz et al. (2004), and a simplified CRRW analysis. In the latter method median values of a limited number of simulations were used. The probability distributions of the midships vertical hogging bending moment in the sea states contributing most to the hogging moment with a mean return period of 20 years and 10^4 years were investigated. As also shown in Paper 4, the MLRW method can be used very efficiently to accurately determine the nonlinear short-term probability distribution for rigid hulls in head waves, but the method is not reliable for flexible hulls when slamming induced whipping responses are accounted for. On the other hand, a full CRRW analysis gives accurate results for flexible hulls, compared to those obtained in random irregular waves without any conditioning. The high computational efficiency of the MLRW method is, however, to a large effect lost when background waves are introduced in the CRRW approach. For the flexible hull, responses obtained from the simplified CRRW analysis are approximately 15% to 25% lower than those found in random irregular waves. The paper also presents a comparison between the time series of the measured and the calculated midships bending moments due to the same MLRW. This shows an almost perfect agreement when the hull is rigid. For the flexible hull, the maximum hogging bending moment obtained using the numerical method is approximately 30% higher than the one found during the experiments. This is at least partly attributed to the fact that 3D effects are not accounted for in the 2D slamming force calculation.

The main contributions of this paper are:

- that short-term probability distributions, obtained using response conditioning techniques, of the midships vertical hogging bending moments of a containership operating in head seas at 5kn forward speed are numerically shown to agree well with the distribution obtained using random irregular waves, when the hull is rigid (Objective C);

- that it is shown for flexible hulls that using the MLRW method in combination with a correction factor, as proposed by Dietz (2004), can lead to unreliable results (Objective C);

- that vertical bending moments obtained numerically from a full CRRW analysis are shown to agree very well with those found in random irregular head waves, even for the flexible hull (Objective C);
- that vertical hogging bending moments in the flexible hull obtained from a simplified CRRW analysis, based on median values of a limited number of runs, are shown to be 15% to 25% lower than those found in random irregular head waves, for exceedance probabilities relevant for design (Objective C);
- that the time series of the midships vertical bending moment calculated as a response to an MLRW, using the method of Wu and Moan (2005), is shown to be in almost perfect agreement with the measured one, when the hull is rigid (Objective D);
- that the maximum hogging bending moment in the flexible hull obtained as a response to an MLRW, using the numerical method, is shown to be approximately 30% higher than the one found during the experiments (Objective D), and;
- that it is shown to be practically impossible to experimentally carry out a full CRRW analysis.

Chapter 5

Conclusions and Recommendations for Future Work

5.1 General

This thesis deals with an experimental and a numerical study of fatigue and extreme load effects in a modern containership with a length between perpendiculars, L_{pp}, of 281m. A 1:45 scale, four segment, flexible model was designed and applied in the tests. These were performed in the towing tank at the Marine Technology Centre in Trondheim, Norway. All tests were carried out in head sea conditions. Numerical results were obtained using the nonlinear hybrid hydroelastic strip theory method developed by Wu and Moan (2005).

Three categories of conclusions can be drawn from the investigations. Conclusions regarding the experimental methods are stated in Section 5.2. The majority of the conclusions that could be drawn from the experimental and numerical results are discussed in the five appended papers. Sections 5.3 and 5.4 only describe the main conclusions regarding the objectives stated in Section 1.2, and some of the overall conclusions. The recommendations are given in the same three groups.

5.2 Experimental Methods

For this PhD study the author performed two sets of experiments. As the author had no previous relevant experience with experiments, the first set of tests was quite challenging. The planning as well as the performance of the experiments strongly depended on help from more experienced people. From this point of view, the second set was more satisfactory. It is recommended that people without previous testing experience use one round of testing dedicated to becoming familiar with the whole process.

As mentioned above, the model which was built for these test purposes had a scale of 1:45, and thus a length between perpendiculars of 6.24m. The draft of the model was 0.26m (11.75m full scale) with no trim. The model therefore had a displacement of 841.2kg. The scale factor was chosen such as to satisfy criteria of wall interference and wave quality. However, also from an operational point of view, the length and mass of the model proved to be satisfactory.

In order to include the hydroelastic effect in the experiments, the model was made of four rigid segments connected by three rotational springs. The cuts were located 0.13m (i.e. $0.02L_{pp}$) forward of the quarter lengths and the midships section. Aluminum frames designed by the author were mounted on the four segments in order to make them rigid. It was made sure that the natural frequencies of the total frame did not interfere with the frequencies of interest. As mentioned above, the four segments were connected by three rotational springs.

For the purpose of the tests for this PhD study, a new rotational spring system was designed. This design was very satisfactory from the point of view that the damping of the model in still-water was close to linear. The natural frequency of the model could also be adjusted very easily using this system. Thus, the correct Froude scaled natural frequency could be obtained in a quite straightforward manner, as discussed below. The mass of the system was however relatively large and has its centre of gravity at a significant distance above the neutral line of the model (Fig. B.1). As a result it was not possible to obtain the desired mass distribution according to the loading manual. If this spring system is used in future tests due account should be given to its mass and the location of the mass' centre of gravity.

The first three global vertical flexible mode shapes of the full scale vessel were well represented by the segmented model. Also the natural frequencies of the three modes were in good agreement with those calculated for the full scale vessel, even though the stiffness of the springs was chosen equal and tuned to give the correct Froude scaled natural frequency of the first flexible mode only. The lowest natural frequency of the frame, or any part of it, was higher than the natural frequency of the third flexural mode.

The damping ratio of the two node vibration mode of the model was significantly lower than similar values found from full scale measurements on containerships. The damping ratio obtained by full scale measurements was influenced by the cargo system, container racks, etc. These influences on the damping ratio should be investigated. Hence, further study is necessary, particularly because the methods to estimate damping under in-service conditions are prone to large uncertainties. For future tests it is, furthermore, advised to tune the damping of the model to be equal to the full scale damping.

In order to determine the vertical bending moments from the measurements, it was assumed that the axial force of the model was zero. This is however not necessarily the case, and can lead to over-estimates of the bending moments by approximately 10%. For future tests with a similar model setup it is therefore recommended to measure this force and investigate its influence on the vertical bending moments.

The model was towed through the tank by a carriage. The connection between the two was made at the front and aft of the model and consisted of two pieces of rope with a spring in the middle. This flexibility introduced an additional restoring force in the vertical motions of the model. The additional force in heave was approximately 0.2% of that of the hydrodynamic restoring force. For the pitch restoring moment this was 1%. Thus, using the setup described here, these additional restoring forces were negligible compared to the hydrodynamic ones.

For most of the experimental results an estimate of the precision error was found by repeating some of the tests. From this study it was concluded that runs repeated well. In general the obtained results had a coefficient of variation of approximately 3% or less.

A large part of the bias error was removed by calibrating all sensors and by regularly performing zero setting. Estimates of the bias error in the calibration factor of the most important sensors indicated that this error was small.

Finally, it was found that tests with response conditioned waves require an advanced operating system of the carriage and the wave maker in the towing tank. In particular it is necessary that the carriage can be accurately positioned and that the wave maker can be started at any given time before or after starting the carriage.

5.3 Experimental Results

Regarding Objective A, the model tests showed that the fatigue damage due to wave-induced vibrations made up approximately 40% of the total damage. The main contribution to the high frequency damage came from the two node vibration mode, while vibration in the other two modes contributed less than 5% to the total damage. The damage in the forward cut was negligible compared to that in the midships section, while the damage in the aft cut was about 25% of the latter value. The fatigue analysis also showed that the largest contribution to fatigue occurred in sea states with a peak period of around 14s and a significant wave height of 5m for the midships section and the aft quarter length, and 7m for the forward quarter length.

From the model tests it was furthermore found that, depending on forward speed, hull flexibility increased the vertical bending moments by up to 35% in irregular sea states relevant for ship design. Although sagging moments were most influenced by the flexibility of the hull, the hogging moments were also significantly increased. Since containerships in still-water normally are in a hogging condition, any increase in wave-induced hogging moments has an impact on design load effects. Regarding this it was also found that a change in speed had more effect on the vertical bending moment of a flexible hull than on that of a rigid hull.

With respect to Objective C it was found experimentally for 5kn full scale forward speed that, in case the hull was assumed to be rigid, the most likely response wave (MLRW) method could be used very efficiently for accurately, within 1% of results in random irregular waves (RIWs), predicting the nonlinear short-term probability distribution of the midships vertical hogging moment. It only took four runs, each with a duration of one to two minutes. In case of a flexible hull, the agreement between results from RIWs and the MLRW method was less. In the sea state that contributed most to the extreme hogging vertical bending moment with a mean return period of 10 000 years, the hogging moments obtained using the MLRW method were up to approximately 15% lower than those found from RIWs. This is because the fundamental assumption of the response conditioning techniques, that the nonlinear response is a correction of the linear response, is less valid when whipping responses are important and accounted for.

A full conditional random response wave (CRRW) analysis as described by Dietz (2004) or Dietz et al. (2004) requires several hundreds or even thousands of runs, and is therefore very expensive and time consuming to perform. A complete experimental analysis is thus generally not possible. As a compromise between the MLRW method and a full CRRW analysis, 10 CRRWs were run for four different response levels. The median values of the 10 midships hogging moments for each response level were compared with

results from RIWs. This showed an agreement quite similar to that discussed above for the MLRW method. For flexible hulls, the simplified CRRW method is however more reliable than the MLRW method, as discussed in the next section.

The response conditioned waves measured in the tank differed from the requested ones. This was partly related to the fact that the transformation, of the response conditioned wave profile from the target location to that of the wave maker, was done using Airy wave theory. Due to the steepness of the wave it was affected by nonlinear wave interactions during its propagation from the wave maker to the model. As Objective C was basically to compare the short-term probability distribution obtained from random irregular waves with the one found using response conditioned waves, this disagreement was no issue. However, if the actual value of the response is of interest the difference is important. In these cases, the transformation of the wave profile from the target location to that of the wave maker should be done using nonlinear techniques such as those described for example by Clauss et al. (2004).

5.4 Numerical Results

For design purposes, the midship vertical bending moment in the ship hull is of main interest. It was found that the numerical method presented by Wu and Moan (2005), even in severe conditions, accurately predicted the midships bending moments when the vessel was assumed to be rigid. The bending moments resulting from whipping vibrations were also described quite well, taking into account that, for the present case, the impact forces from 2D slamming calculations should be reduced by approximately 20% to account for 3D effects. The method can under these conditions confidently be used for the prediction of extreme load effects in containerships of newer design.

The springing vibrations on the other hand were less well predicted. This was at least partly attributed to the fact that several damping mechanisms were not accounted for by the method. As a result, the additional fatigue damage due to wave-induced vibrations was strongly over-estimated by the method. More work, therefore, needs to be done to improve the high frequency load modelling. This includes amongst others identifying and quantifying the sources of damping of the vibrations, and verification of the excitation sources of the high frequency response.

In order to achieve Objective C the response conditioned wave methods were implemented in the strip theory code developed by Wu and Moan (2005). Using the code it was also numerically found that the MLRW method could very efficiently be used to accurately determine the nonlinear short-term probability distribution of the midships vertical bending moment for rigid hulls, but not for flexible ones. This was shown for the sea states most contributing to the hogging moment with mean return periods of 20 years and 10 000 years. It was furthermore found that using the MLRW method in combination with a correction factor, as proposed by Dietz (2004), led to unreliable results because the complete probability distribution obtained with this method was based on different scalings of the same wave profile.

Numerically it was possible to carry out a full CRRW analysis. The vertical bending moments obtained from this analysis agreed very well with those found in RIWs, even for the flexible hull. The required simulation time for finding the short-term probability

distributions from a full CRRW analysis was, however, of the same order of magnitude as the time needed for a conventional analysis in RIWs.

The simplified CRRW analysis was also carried out numerically, and was based on 26 simulations for each of the eight response levels. Hogging moments in the flexible hull obtained from this approach were 15% to 25% lower than those found in RIWs for exceedance probabilities relevant for design. Contrary to the MLRW method, this method depends on more than one wave profile. The method is thus more reliable, and therefore, for flexible hulls, recommended in combination with the correction factor proposed by Dietz (2004).

References

Adegeest L, Braathen A, Løseth R (1998). "Use of non-linear sea-loads simulations in design of ships." In: *Proceedings 7th International Symposium on Practical Design of Ships and Other Floating Structures.* The Hague, The Netherlands, pp. 53–58.

Almar-Næss A (1985). *Fatigue Handbook: Offshore Steel Structures.* Trondheim: Tapir.

Baarholm GS, Jensen JJ (2004). "Influence of whipping on long-term vertical bending moment." *Journal of Ship Research* 28 (4): 261–272.

Baarholm GS, Moan T (2000). "Estimation of nonlinear long-term extremes of hull girder loads in ships." *Marine Structures* 13 (6): 495–516.

Baarholm GS, Moan T (2001). "Application of contour line method to estimate extreme ship hull loads considering operational restrictions." *Journal of Ship Research* 45: 288–240.

Bishop R, Price W (1974). "On modal analysis of ship strength." In: *Proceedings Royal Society of London. Series A, Mathematical and Physical Sciences.* Vol. 341. pp. 121–134.

Bishop R, Price W (1979). *Hydroelasticity of Ships.* Cambridge: Cambridge University Press.

Chen RZ, Du SX, Wu YS, Lin JR, Hu JJ, Yue YL (2001). "Experiment on extreme wave loads of a flexible ship model." In: *Proceedings 8th International Symposium on Practical Design of Ships and Other Floating Structures.* Shanghai, China, pp. 871–878.

Chen XJ, Wu YS, Cui WC, Jensen JJ (2006). "Review of hydroelasticity theories for global response of marine structures." *Ocean Engineering* 33: 439–457.

Ciappi E, Dessi D, Maiani R (2003). "Slamming and whipping response analysis of a fast monohull via segmented model tests." In: *Proceedings Hydroelasticity in Marine Technology.* Oxford, UK, pp. 143–153.

Clauss GF, Henning J, Schmittner CE, Kühnlein WL (2004). "Non-linear calculations of tailored wave trains for experimental investigations of extreme structure behavior." In: *Proceedings 23rd International Conference on Offshore Mechanics and Arctic Engineering.* Vancouver, Canada.

Coleman HW, Steele WG (1989). *Experimentation and Uncertainty Analysis for Engineers.* New York: Wiley.

Det Norske Veritas (2000a). *Classification Note 30.5: Environmental Conditions and Environmental Loads.* Oslo, Norway.

Det Norske Veritas (2000b). *Nauticus Hull User Manual.* Oslo, Norway.

Det Norske Veritas (2003). *Classification Note 30.7: Fatigue Assessment of Ship Structures.* Oslo, Norway.

Dietz JS (2004). *Application of conditional waves as critical wave episodes for extreme loads on marine structures.* PhD thesis, Dept. Mechanical Engineering, Technical University of Denmark, Lyngby, Denmark.

Dietz JS, Friis-Hansen P, Jensen JJ (2004). "Design wave episodes for extreme value ship responses." In: *Proceedings 9th International Symposium on Practical Design of Ships and Other Floating Structures.* Luebeck-Travemuende, Germany.

Faltinsen O (1990). *Sea Loads on Ships and Offshore Structures.* Cambridge: Cambridge University Press.

Faltinsen O (2005). *Hydrodynamics of High-Speed Marine Vessels.* Cambridge: Cambridge University Press.

Farnes KA (1990). *Long-term statistics of response in non-linear marine structures.* PhD thesis, Dept. of Marine Technology, Norwegian University of Science and Technology, Trondheim, Norway.

Fonseca N, Guedes Soares C (1998a). "Non-linear wave induced responses of ships in irregular seas." In: *Proceedings 17th International Conference on Offshore Mechanics and Arctic Engineering.* Lisbon, Portugal.

Fonseca N, Guedes Soares C (1998b). "Time-domain analysis of large-amplitude vertical ship motions and wave loads." *Journal of Ship Research* 42 (2): 139–153.

Fonseca N, Guedes Soares C (2002). "Comparison of numerical and experimental results of nonlinear wave-induced vertical ship motions and loads." *Journal of Marine Science and Technology* 6: 193–204.

Fonseca N, Guedes Soares C (2004a). "Experimental investigation of the nonlinear effects on the statistics of vertical motions and loads of a containership in irregular waves." *Journal of Ship Research* 48 (2): 148–167.

Fonseca N, Guedes Soares C (2004b). "Experimental investigation of the nonlinear effects on the vertical motions and loads of a containership in regular waves." *Journal of Ship Research* 48 (2): 118–147.

Friis-Hansen P, Nielsen LP (1995). "On the new wave model for the kinematics of large ocean waves." In: *Proceedings 14th International Conference on Offshore Mechanics and Arctic Engineering.* Copenhagen, Denmark, pp. 17–24.

Gao Z, Moan T (2007). "Fatigue damage estimation of wide-band stationary Gaussian processes using a trimodal spectral formulation." *accepted for publication in International Journal of Fatigue.*

Gu X, Moan T (2002). "Long-term fatigue damage of ship structures under nonlinear wave loads." *Marine Technology* 39 (2): 95–104.

Guedes Soares C, Fonseca N, Pascoal R (2004). "Long term prediction of non-linear vertical bending moments on a fast monohull." *Applied Ocean Research* 26: 288–297.

Heller S, Abramson HN (1959). "Hydroelasticity: A new naval science." *Journal of American Society of Naval Engineers* 71 (2): 205–209.

Hermundstad OA, Moan T (2005). "Numerical and experimental analysis of bow flare slamming on a ro-ro vessel in regular oblique waves." *Journal of Marine Science and Technology* 10: 105–102.

Hu C, Kashiwagi M (2004). "A CIP-based method for numerical simulations of violent free-surface flows." *Journal of Marine Science and Technology* 9: 143–157.

IACS (2006). *UR S.11: Longitudinal Strength Standard.*

Imas L (2004). "Evaluation of the SPH method for hydrodynamics; single and multiphase flows." In: *Proceedings 25th Symposium on Naval Hydrodynamics.* St. John's, Canada.

ISSC (2000). "Report of special task committee VI.1: Extreme hull girder loading." In: *Proceedings 14th International Ship and Offshore Structures Congress.* Nagasaki, Japan, pp. 263–320.

ISSC (2006). "Report of committee I.2: Loads." In: *Proceedings 16th International Ship and Offshore Structures Congress.* Southampton, UK, pp. 85–173.

ITTC (1987). "ITTC seakeeping committee report." In: *Proceedings 18th International Towing Tank Conference.* Kobe, Japan.

ITTC (2005). "ITTC seakeeping committee report." In: *Proceedings 24th International Towing Tank Conference.* Edinburgh, Scotland.

ITTC (2006). *Recommended Procedures and Guidelines: Testing and Extrapolation methods,* Section 7.5-02.

Jensen JJ, Dogliani M (1996). "Wave-induced ship hull vibrations in stochastic seaways." *Marine Structures* 9: 353–387.

Jensen JJ, Pedersen PT (1979). "Wave-induced bending moments in ships - a quadratic theory." In: *Transactions Royal Institution of Naval Architects.* pp. 151–165.

Jiao G, Moan T (1990). "Probabilistic analysis of fatigue due to Gaussian load processes." *Probabilistic Engineering Mechanics* 5: 76–82.

Lin W, Meinhold M, Salvesen N, Yue D (1996). "Large-amplitude motions and wave loads for ship design." In: *Proceedings 20th Symposium on Naval Hydrodynamics.* Santa Barbara, US, pp. 205–226.

Lin W, Yue D (1991). "Numerical solutions for large-amplitude ship motions in the time domain." In: *Proceedings 18th Symposium on Naval Hydrodynamics.* Ann Arbor, US, pp. 41–66.

Moan T, Shu Z, Drummen I, Amlashi H (2006). "Comparative reliability analysis of ships - considering different ship types and the effect of ship operations on loads." In: *Transactions Society of Naval Architects and Marine Engineers.* Fort Lauderdale, US.

Moe E, Holtsmark G, Storhaug G (2005). "Full scale measurements of the wave induced hull girder vibrations of an ore carrier trading in the North Atlantic." In: *Transactions Royal Institution of Naval Architects, Conference on Design & Operation of Bulk Carriers.* London, UK.

Newman J (1977). *Marine Hydrodynamics.* Cambridge, Massachusetts: The MIT Press.

O'Dea J, Powers E, Zselecsky J (1992). "Experimental determination of nonlinearities in vertical plane ship motions." In: *Proceedings 19th Symposium on Navel Hydrodynamics.* Seoul, Korea, pp. 73–91.

Økland OD (2002). *Numerical and experimental investigation of whipping in twin hull vessels exposed to severe wet deck slamming.* PhD thesis, Dept. of Marine Technology, Norwegian University of Science and Technology, Trondheim, Norway.

Økland OD, Zhao R, Moan T (2003). "Numerical assessment of segmented test model approach for measurements of whipping responses." In: *Proceedings 7th International Conference on Fast Sea Transportation.* Ischia, Italy, pp. 87–94.

Pastoor LW (2000). *Experimental Generation of Response Conditioned Waves (MLER method).* Delft University of Technology, Ship Hydromechanics Laboratory, Report No.1244.

Pastoor LW (2002). *On the assessment of nonlinear ship motions and loads.* PhD thesis, Ship Hydromechanics Laboratory, Faculty of Design Engineering and Production, Delft University of Technology, Delft, The Netherlands.

Payer HG, Brostella R (2006). "The Panama Canal expansion and the Panamax vessels of the future." In: *Transactions Society of Naval Architects and Marine Engineers.* Fort Lauderdale, US.

Rychlik I (1987). "A new definition of the Rainflow cycle counting method." *International Journal of Fatigue* 9 (2): 119–121.

Salvesen N, Tuch E, Faltinsen OM (1970). "Ship motions and sea loads." In: *Transactions Society of Naval Architects and Marine Engineers.* pp. 250–287.

Shirakura Y, Tanizawa K, Naito S (2002). "Development of 3-D fully nonlinear numerical wave tank - 2nd report: Waves around sphere and speroid with and without forward speed." *Journal of Kansai Society of Naval Architects of Japan* 238: 131–146.

Storhaug G (2007). *Experimental investigation of wave induced vibrations increasing fatigue damage in ships.* PhD thesis, Dept. of Marine Technology, Norwegian University of Science and Technology, Trondheim, Norway.

Storhaug G, Moan T (2006). "Springing/whipping response of a large ocean-going vessel - investigated by an experimental method." In: *Proceedings Hydroelasticity in Marine Technology.* Wuxi, China.

Storhaug G, Moe E (2007). "Measurements of wave induced vibrations onboard a large container vessel operating in harsh environment." In: *Proceedings 10th International Symposium on Practical Design of Ships and Other Floating Structures.* Houston, US, pp. 64–72.

Storhaug G, Moe E, Holtsmark G (2006). "Measurements of wave induced hull girder vibrations of an ore carrier in different trades." In: *Proceedings 25th International Conference on Offshore Mechanics and Arctic Engineering.* Hamburg, Germany.

Storhaug G, Vidic-Perunovic J, Rüdinger F, Holtsmark G, Helmers JB, Gu X (2003). "Springing/whipping response of a large ocean going vessel - a comparison between numerical simulations and full scale measurements." In: *Proceedings Hydroelasticity in Marine Technology.* Oxford, UK, pp. 117–129.

Takarada N, Sumi Y, Iwahashi Y, Okamoto T, Kawai H (1993). "R&D of a displacement-type high speed ship." In: *Proceedings 2nd International Conference on Fast Sea Transportation,* Volume 1. Yokohama, Japan, pp. 351–359.

Taylor PH, Jonathan P, Harland LA (1995). "Time domain simulations of jack-up dynamics with the extremes of a Gaussian process." In: *Proceedings 14th International Conference on Offshore Mechanics and Arctic Engineering.* Copenhagen, Denmark, pp. 313–319.

Tromans PS, Anaturk AR, Hagemeijer P (1991). "A new model for the kinematics of large ocean waves - application as a design wave." In: *Proceedings 1st International Offshore and Polar Engineering Conference.* UK, pp. 64–71.

Vidic-Perunovic J (2005). *Springing response due to bidirectional wave excitation.* PhD thesis, Dept. Mechanical Engineering, Technical University of Denmark, Lyngby, Denmark.

Wagner H (1932). "Über stoss-und gleitvergänge an der oberfläche von flüssigkeiten." *Angew. Math. Mech.* 12: 201–215.

Watanabe I, Guedes Soares C (1999). "Comparative study on the time-domain analysis of non-linear ship motions and loads." *Marine Structures* 12 (2): 153–170.

Watanabe I, Ueno M, Sawada H (1989). "Effects of bow flare shape on wave loads of a container ship." *Journal of the Society of Naval Architects of Japan* 166: 259–266.

Weymouth GD, Wilson RV, Stern F (2005). "RANS computational fluid dynamics predictions of pitch and heave ship motions in head seas." *Journal of Ship Research* 49 (2): 80–97.

Winterstein S, Ude T, Cornell C, Bjerager P, Haver S (1993). "Environmental parameters for extreme response: Inverse form with omission factors." In: *Proceedings International Conference on Structural Safety and Reliability.* Innsbruck, Austria, pp. 551–557.

Wu MK, Hermundstad OA (2002). "Time-domain simulation of wave-induced nonlinear motions and loads and its applications in ship design." *Marine Structures* 15 (6): 561–597.

Wu MK, Moan T (1996). "Linear and nonlinear hydroelastic analysis of high-speed vessels." *Journal of Ship Research* 40 (2): 149–163.

Wu MK, Moan T (2005). "Efficient calculation of wave-induced ship responses considering structural dynamic effects." *Applied Ocean Research* 21 (2): 81–96.

Wu MK, Moan T (2007). "Sensitivity of extreme hydroelastic load effects to changes in ship hull stiffness and structural damping." *Ocean Engineering* 32: 1745–1756.

Wu YS, Chen RZ, Lin JR (2003). "Experimental technique of hydroelastic ship model." In: *Proceedings Hydroelasticity in Marine Technology.* Oxford, UK, pp. 131–142.

Wu YS, Hisaaki M, Takeshi K (1997). "The second order hydrodynamic actions on a flexible body (Part I)." *Journal of Institute of Industrial Science,* University of Tokyo 49 (4): 8–19.

Xia J, Wang Z, Jensen JJ (1998). "Non-linear wave loads and ship responses by a time-domain strip theory." *Marine Structures* 11: 101–123.

Zhao R, Faltinsen OM, Aarnes JV (1996). "Water entry of arbitrary two-dimensional sections with and without flow seperation." In: *Proceedings 21th Symposium on Naval Hydrodynamics.* Trondheim, Norway, pp. 408–423.

Zhao R, Økland OD, Hoff JR, Aarsnes JV (2004). "Bowflare and stern slamming induced whipping of large ships." In: *Proceedings 6th International Conference on Hydrodynamics.* Perth, Australia, pp. 167–172.

Appendix A

Scaling Laws

Physical models are used to represent a full scale system as accurately as possible at a smaller scale. In order to determine the properties of the model, scaling laws are necessary to ensure similar behaviour in model and full scale. In this thesis, Froude scaling was the basic scaling law. It is based on a dynamic similarity of the ratio between inertia and gravity forces. The Froude number, F_n, is defined by

$$F_n = \frac{U}{\sqrt{Lg}}. \tag{A.1}$$

Using also geometrical similarity with scale factor $\Lambda = L_f/L_m$, the equality in Froude number gives

$$U_m = U_f\sqrt{\frac{L_m}{L_f}} = \frac{U_f}{\sqrt{\Lambda}}. \tag{A.2}$$

The subscripts 'f' and 'm' denote full and model scale respectively. From these basic rules, the scaling between other physical parameters can be derived from a dimensional analysis. The frequency and the time are both scaled using $\sqrt{\Lambda}$

$$\omega_f = \omega_m/\sqrt{\Lambda}, \tag{A.3}$$

$$t_f = t_m\sqrt{\Lambda}. \tag{A.4}$$

The translatory motions and the wave elevation are found from geometrical similarity and are simply scaled by Λ

$$\eta_{i,f} = \eta_{i,m}\Lambda, \qquad i = 1, 2, 3, \tag{A.5}$$

$$\zeta_f = \zeta_m\Lambda. \tag{A.6}$$

The angular motions are not scaled. From this as well as from Eqs. A.4 and A.5 it is deduced that the translatory and angular velocities are scaled as

$$\dot{\eta}_{i,f} = \dot{\eta}_{i,m}\sqrt{\Lambda}, \qquad i = 1, 2, 3, \tag{A.7}$$

$$\dot{\eta}_{i,f} = \dot{\eta}_{i,m}/\sqrt{\Lambda}, \qquad i = 4, 5, 6. \tag{A.8}$$

By combining these results again with Eq. A.4 it is found that the translatory accelerations are not scaled, and that the angular accelerations are scaled according to

$$\ddot{\eta}_{i,f} = \ddot{\eta}_{i,m}/\Lambda, \qquad i = 4, 5, 6. \tag{A.9}$$

The pressure, p, on the hull of the model is proportional to the density of the fluid. The same is therefore true for the forces, F, and moments, M. The quantities are scaled as

$$p_f = p_m \frac{\rho_f}{\rho_m} \Lambda, \tag{A.10}$$

$$F_f = F_m \frac{\rho_f}{\rho_m} \Lambda^3, \tag{A.11}$$

$$M_f = M_m \frac{\rho_f}{\rho_m} \Lambda^4. \tag{A.12}$$

Next to geometrical and dynamical similitude, an elastic model should also satisfy structural similitude. This implies that the strains in model scale should be equal to those in full scale. From this condition it is found that the bending stiffness should be scaled according to

$$EI_f = EI_m \frac{\rho_f}{\rho_m} \Lambda^5. \tag{A.13}$$

Appendix B

Construction Drawings, Pictures and Instrumentation

B.1 Construction Drawings

The construction drawings used to construct the frames and the spring systems are shown in this appendix. Fig. B.1 shows the top view of the model, as well as a longitudinal cross section taken at the centre line. The figure also shows a horizontal cross section taken at 267mm above the base line. The positions of the force transducers in the three cuts are shown as well. Distances are given in mm, and the position of midships is indicated by MS. There are five cross sections indicated in the figure, A-A$\sim$E-E. These cross sections are shown in Figs. B.2$\sim$B.6. Distances in these figures are given in mm. The spring systems were made of steel, while the frames, and the end-plates, were made of aluminum.

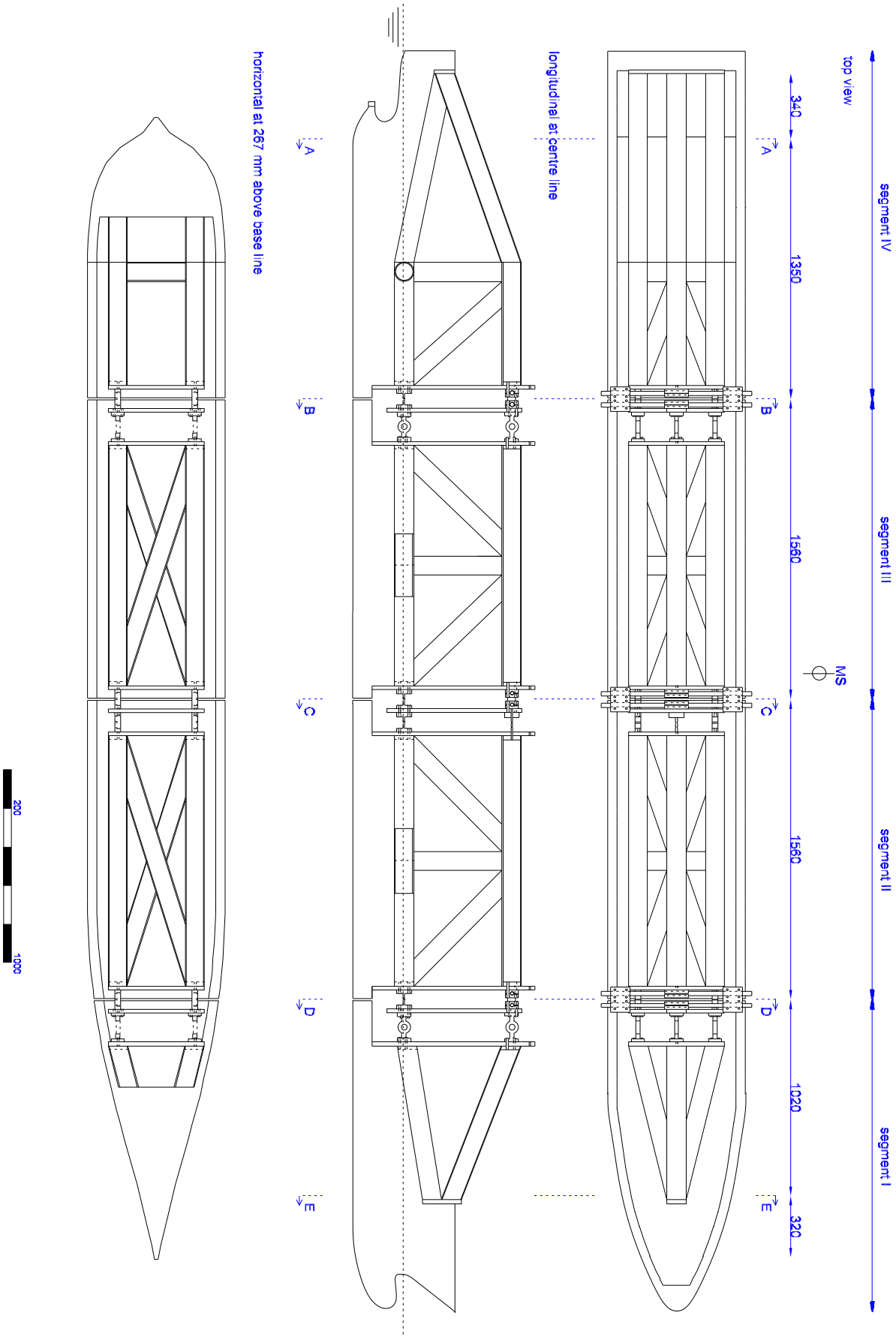

Figure B.1: Construction drawing and overview of the cross sections.

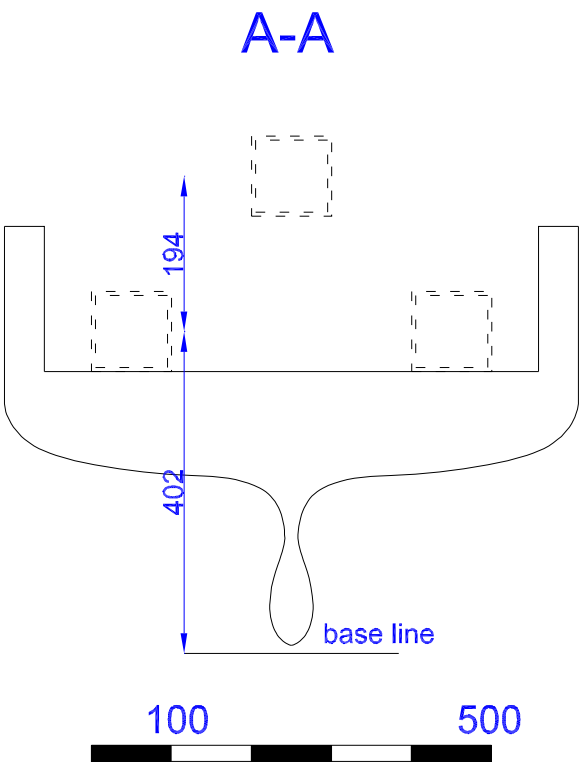

Figure B.2: Cross section A-A.

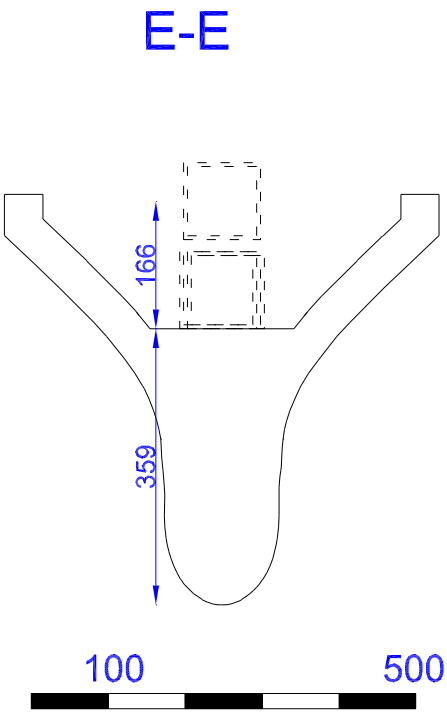

Figure B.3: Cross section E-E.

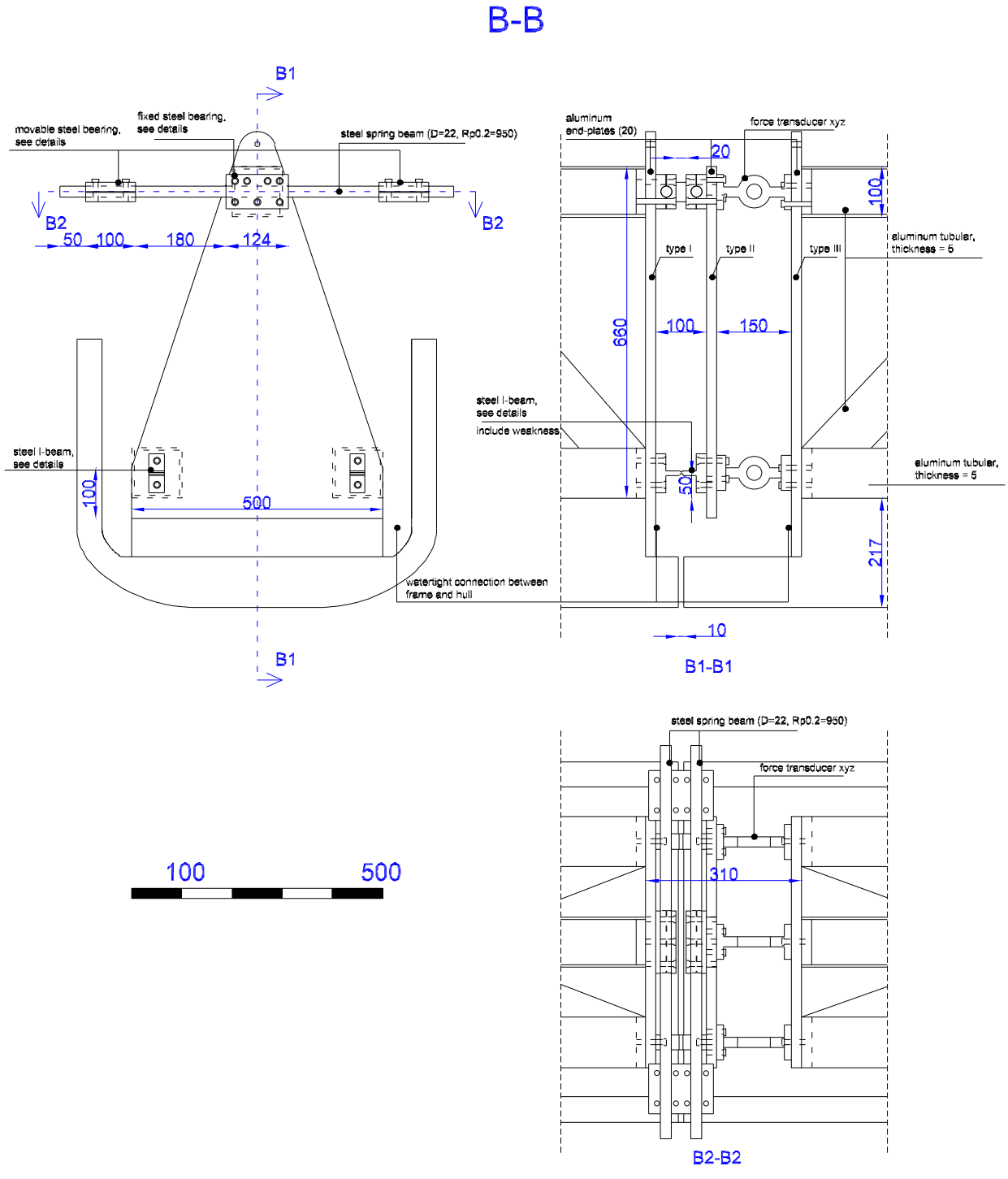

Figure B.4: Cross section B-B.

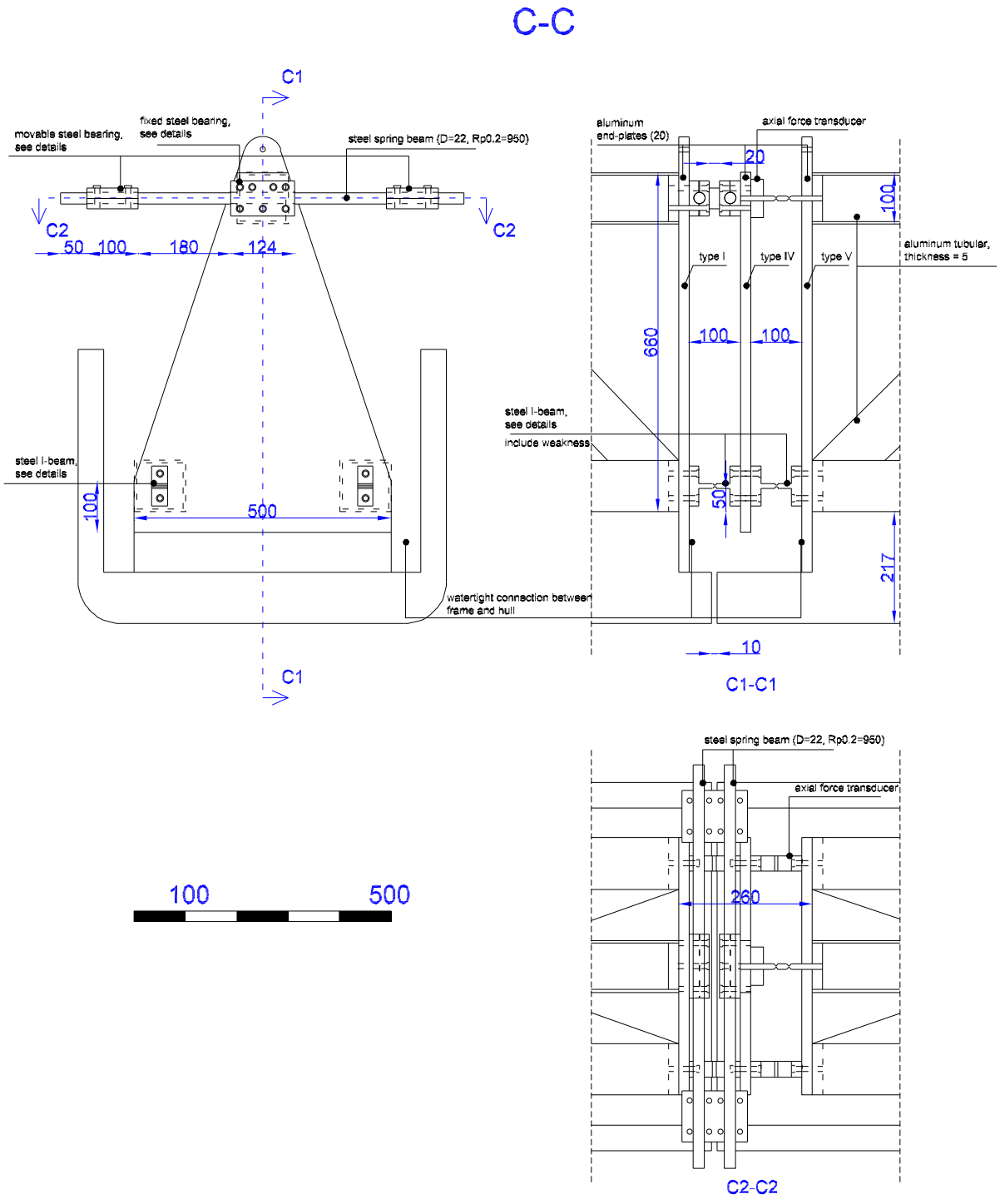

Figure B.5: Cross section C-C.

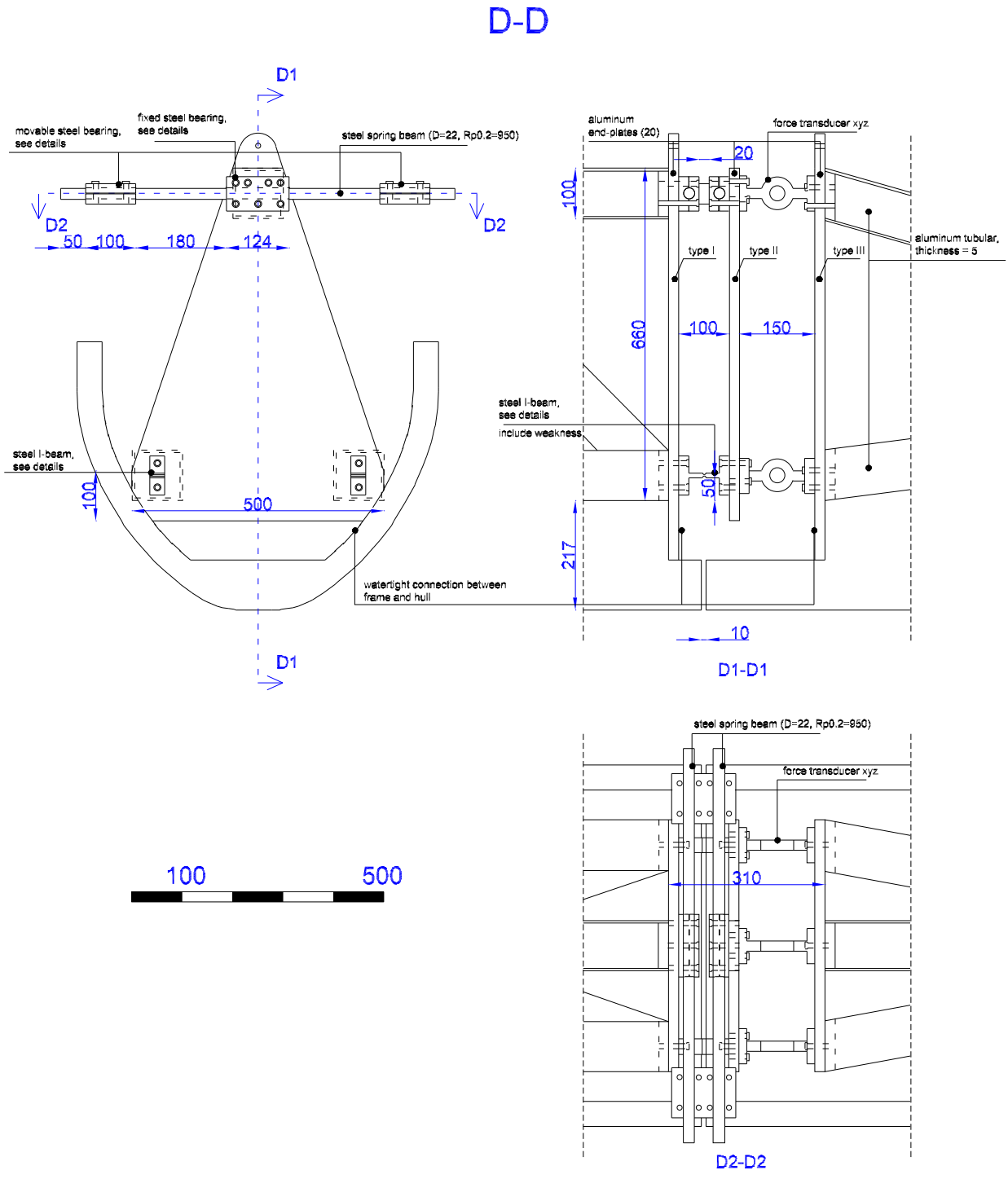

Figure B.6: Cross section D-D.

B.2 Pictures of the Model

Fig. B.7 shows a picture of the complete model. Separate pictures of the four segments are given in Figs. B.8∼B.11. Note that the model was made rigid in these figures as the two end plates on both sides of the cuts were connected by a steel beam. After the model was transferred into the water, these beams where removed. In Fig. B.10 part of the NyPos-tree is shown.

Figure B.7: Picture of the model.

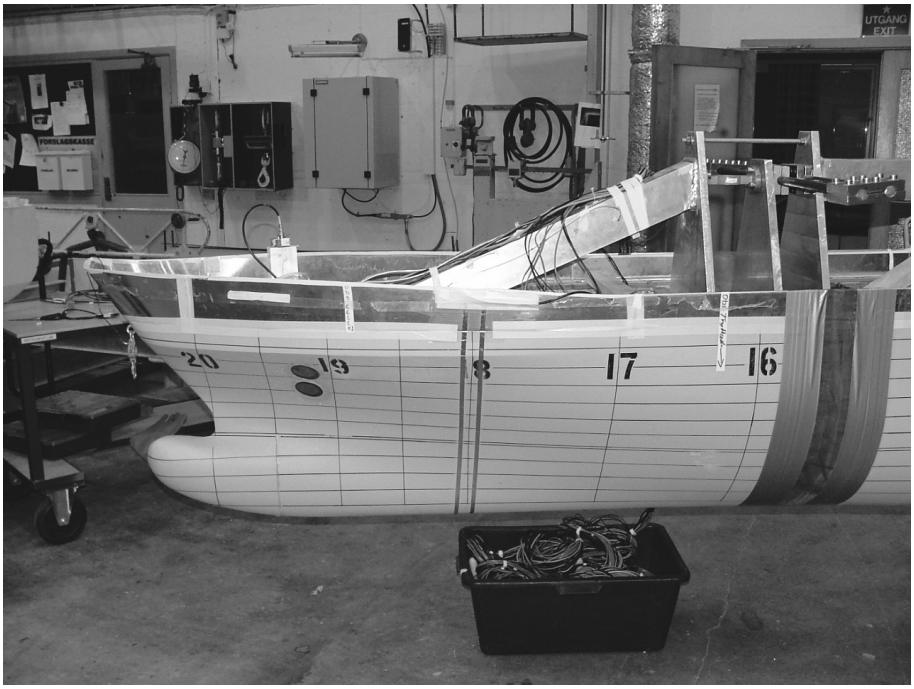

Figure B.8: Picture of Segment I.

Figure B.9: Picture of Segment II.

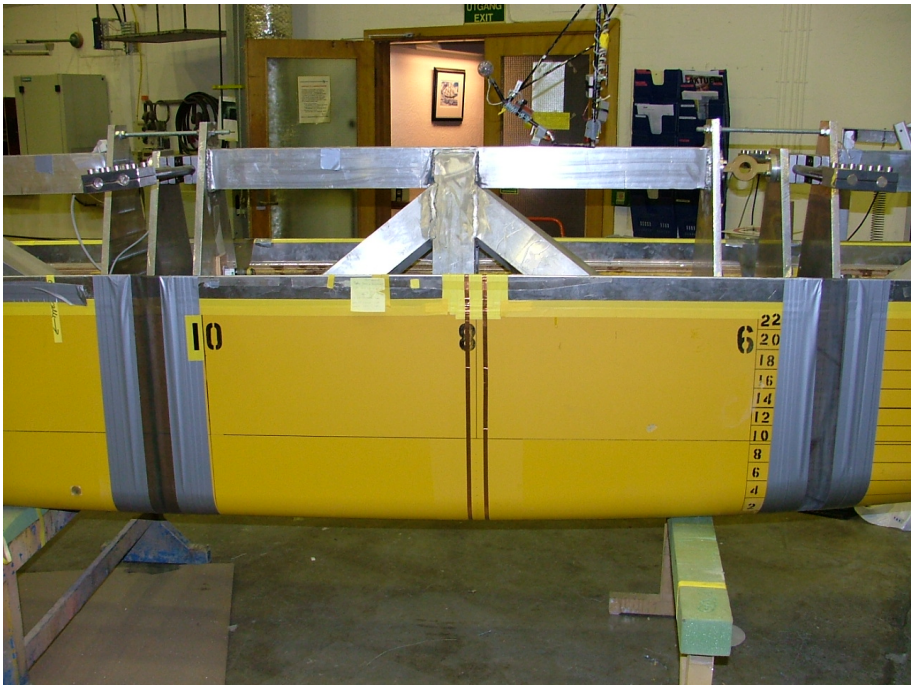

Figure B.10: Picture of Segment III.

Figure B.11: Picture of Segment IV.

B.3 Location of the Instrumentation

The location and mass of the instruments is given in Table B.1. The x-coordinates of the instrumentation were measured relative to the midships section, positive aft. The y-position is positive in starboard direction and given relative to the centre line. The z-position is given relative to the baseline and is positive in the upward direction.

Table B.1: Location of the instrumentation.

Component	x[m]	y[m]	z[m]	Mass[kg]	Measuring
force transducer	-0.22	0	0.82	0.93	horizontal force at midships
3 DOF force transducer	-1.84	0	0.83	0.68	horizontal and vertical forces at forward cut
3 DOF force transducer	-1.84	0.20	0.26	0.68	vertical force at forward cut
3 DOF force transducer	-1.84	-0.20	0.26	0.68	vertical force at forward cut
3 DOF force transducer	1.28	0	0.82	0.68	horizontal and vertical forces at aft cut
3 DOF force transducer	1.28	0.20	0.25	0.68	vertical force at aft cut
3 DOF force transducer	1.28	-0.20	0.25	0.68	vertical force at aft cut
accelerometer	-2.97	0	0.58	0.18	vertical accelerations
accelerometer	-1.60	0	0.56	0.18	vertical accelerations
accelerometer	-0.04	0	0.57	0.18	vertical accelerations
accelerometer	1.52	0	0.57	0.18	vertical accelerations
accelerometer	3.10	0	0.60	0.18	vertical accelerations
slamming panel	-2.88	0.17	0.42	4.00	slamming force
slamming panel	-2.87	0.12	0.37	4.00	slamming force
slamming panel	3.06	0.10	0.25	4.00	slamming force
slamming panel	3.17	0.09	0.21	4.00	slamming force
slamming panel	3.17	0.23	0.28	4.00	slamming force
pressure cell	-3.26	0	0.46	0.10	pressure
pressure cell	-2.77	0	0	0.10	pressure
pressure cell	-1.96	0	0	0.10	pressure
pressure cell	-0.35	0	0	0.10	pressure
pressure cell	-0.36	0.36	0.08	0.10	pressure

Table B.1: Location of the instrumentation, continued.

Component	x[m]	y[m]	z[m]	Mass[kg]	Measuring
force ring	-3.28	0	0.48	0.15	forward towing force
force ring	3.23	0	0.48	0.15	aft towing force
NyPos	0.87	0	0.88	0.68	rigid body motions
relative motion strip	-2.50	-	-	-	relative motion
relative motion strip	-0.94	-	-	-	relative motion
relative motion strip	0.63	-	-	-	relative motion
relative motion wave probe	-2.98	-	-	0.16	relative motion
relative motion wave probe	3.12	-	-	0.17	relative motion

Appendix C

Uncertainties in the Vertical Bending Moments

In this appendix the following three uncertainties are assessed:

- the effect of the location of the cuts;
- the effect of the mass distribution, and;
- the effect of the stiffness distribution.

The physical cuts in the model were located $0.02L_{pp}$ forward of the quarter lengths and the midships section (see Section 3.2). Furthermore, the horizontal forces were measured $0.016L_{pp}$ forward of the physical cut, and thus $0.036L_{pp}$ forward of the quarter lengths and the midships section. The bending moments derived from the measured horizontal forces (Eq. 3.1) are however still referred to as moments for the midships section and the quarter length sections. The notations QL, MS and 3QL are used. The difference in locations between the true quarter lengths and midships sections and those where the horizontal forces were measured (the actual locations) is shown in Table C.1.

Table C.1: Locations of the true and the actual quarter length and midships sections.

	True			Actual		
	QL	MS	3QL	QL	MS	3QL
x [m]	-70.25	0.00	70.25	-80.78	-10.53	59.72

In order to see the effect of this difference in location, as well as that of using the measured mass distribution instead of the objective one (according to the loading manual), several vertical bending moment RAOs for a forward speed of 23kn were calculated. The results are given in Figs. C.1∼C.3. For sake of clarity, the peak values of the vertical bending moments for the rigid and the flexible hull are also given in Table C.2. From the figures and tables it can be concluded that, for the true locations, the rigid body vertical bending moments for the measured mass distribution are up to approximately 7% higher than those for the objective distribution. For the latter distribution, moving from the actual to the true location, on the other hand, increases the QL rigid body vertical bending

moment by 50%, and decreases the 3QL moment by approximately 20%. The midships bending moment is hardly effected by the change.

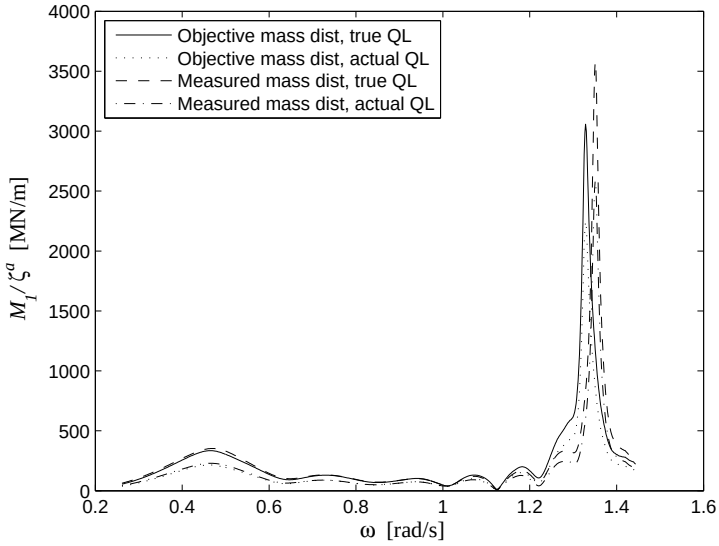

Figure C.1: Dependence of the 23kn QL VBM RAO on the mass distribution and the location of the cut.

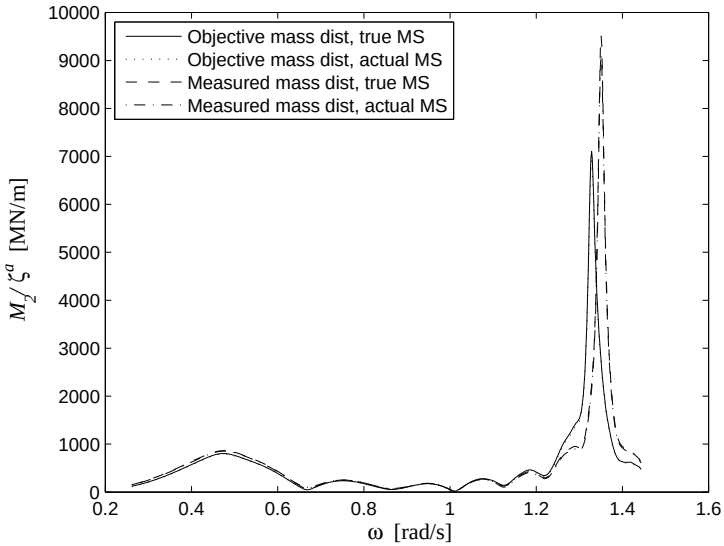

Figure C.2: Dependence of the 23kn MS VBM RAO on the mass distribution and the location of the cut.

It should be noted that the force, due to the hydrodynamic pressure acting on the whole rigid segment, is measured by the force transducers (see Fig. C.4). From this point of view, the measured horizontal forces are representative for the location of the physical cuts. For the inertia force due to the mass of the model on the other hand, $0.016L_{pp}$ forward of the physical cut is a more representative location. The differences presented in Figs. C.1∼C.3 and Table C.2 can thus be considered as an upper limit.

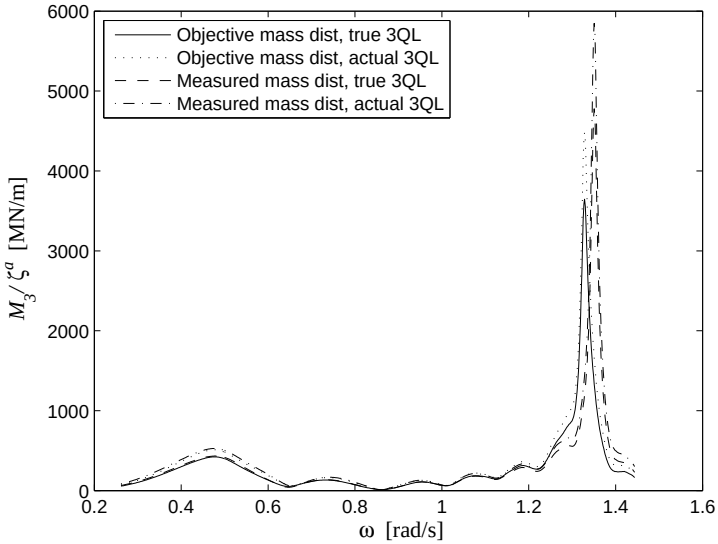

Figure C.3: Dependence of the 23kn 3QL VBM RAO on the mass distribution and the location of the cut.

Table C.2: Peaks of the VBM RAOs, values are given in MNm/m for the rigid and the flexible hull.

	Rigid			Flexible		
	M_1	M_2	M_3	M_1	M_2	M_3
Objective mass distribution, true location	336	808	424	3059	7104	3647
Objective mass distribution, actual location	216	797	513	2247	6916	4483
Measured mass distribution, true location	354	867	434	3579	9511	4779
Measured mass distribution, actual location	230	857	528	2586	9132	5847

1) objective mass distribution refers to the mass distribution according to the loading manual
2) measured mass distribution refers to the mass distribution of the actual model
3) true location refers to the true quarter length and midships sections
4) actual location refers to the sections where the horizontal forces were actually measured

The influence of using a segmented instead of a continuous stiffness distribution (Table 3.7) on the bending moments is given in Figs. C.5∼C.7. The measured mass distribution (Fig. 3.9) was used as input for the calculations. The figures show, as expected, that the rigid body vertical bending moments are independent of the stiffness distribution. The resonance peak for the continuous stiffness occurs for a slightly higher frequency and is approximately 10% lower than the peak for the segmented stiffness distribution.

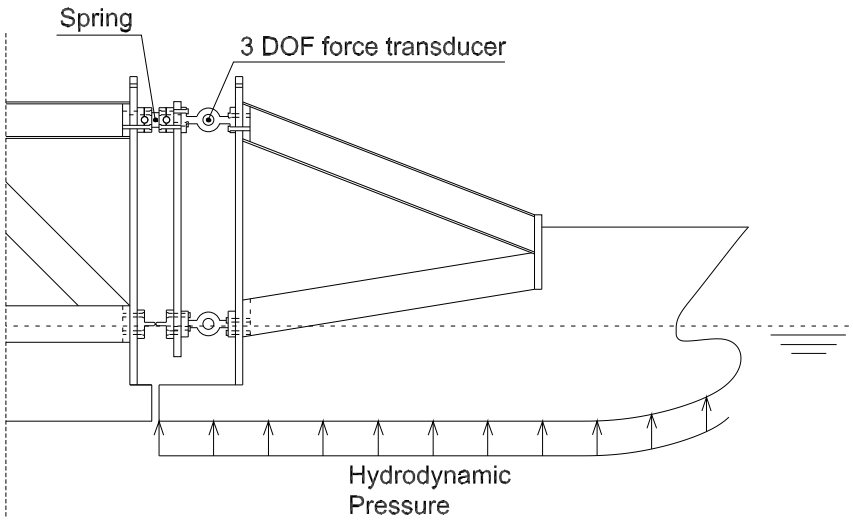

Figure C.4: Illustration of the hydrodynamic pressure acting on one of the segments.

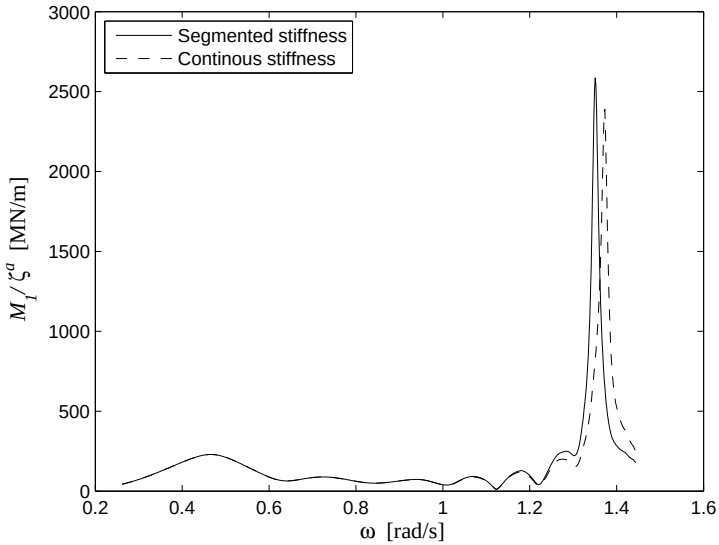

Figure C.5: Dependence of the 23kn QL VBM RAO on the stiffness distribution.

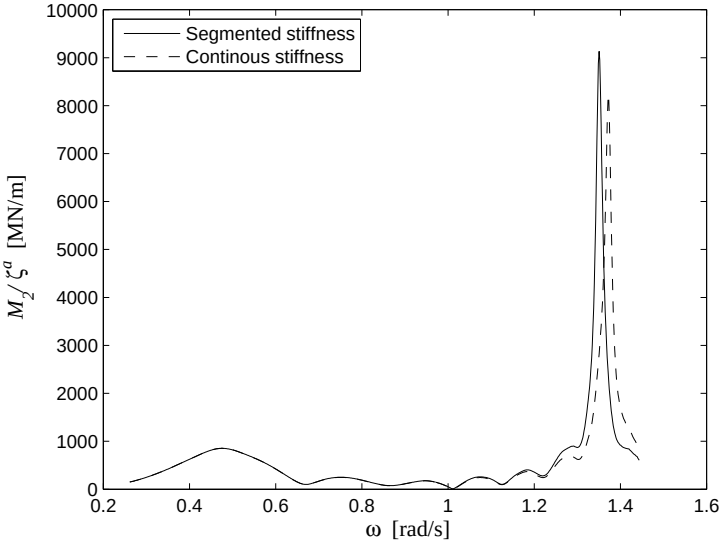

Figure C.6: Dependence of the 23kn MS VBM RAO on the stiffness distribution.

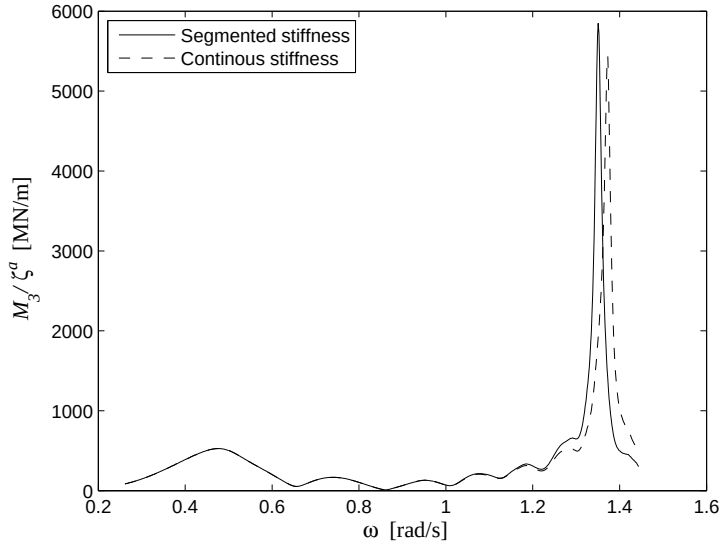

Figure C.7: Dependence of the 23kn 3QL VBM RAO on the stiffness distribution.

Appendix D

Details of Tests with Response Conditioned Waves

Using response conditioned waves experimentally in combination with a model with forward speed is a challenging task. The model should be at a specific location at a particular time. Both location and time were determined before the experiments were carried out, and the response conditioned wave profiles were determined accordingly. The theory of the response conditioned waves method is given in Paper 5. Pastoor (2002) performed experiments in most likely extreme response (MLER) waves (Adegeest et al., 1998). In order to overcome the difficulties described above, a program controlling the speed of the carriage and incorporating a simultaneous start of the wave maker was developed. Before each run, the carriage was placed at the location where the MLER event would occur (30m in front of the wave maker). The carriage was then driven backwards while the computer measured the distance. The control program used this distance to accurately drive the carriage up to the MLER location and arrive there at the correct time instant. Some of the details of his tests are described by Pastoor (2000). This approach however assumes that the MLER location is exactly known. Although this is theoretically true, in practice this location may vary somewhat. The waves used by Pastoor (2002) were fairly low, and thus well described by linear wave theory. When the waves are higher, group velocities differ from linear predictions, and discrepancies between the wave in the tank and the one calculated from linear theory increase.

Therefore a method was needed to confirm that the model was at the correct location at the desired time. One possibility was to determine this from the analysis of the wave probes on the carriage. This is however difficult. If the model was at the correct location at the desired time, the measured wave elevation should in principle be approximately equal to the theoretical wave profile. The measured profile was however disturbed by the model and influenced by nonlinear interactions. Moreover, in general the wave does not have a maximum at the time and location of the extreme event.

It was found that the best way to determine if the model was at the correct place at the correct time was by analysis of the low pass filtered (1.87Hz full scale) signal of the midships horizontal force of the model. The response conditioning methods used in this thesis are based on the fact that all components of the response are in phase when the extreme event occurs (see Paper 5). Therefore, if the location is not correct the response

will have a lower value than if it is correct. Strictly speaking this is only true for the linear response. Using the numerical method described in Section 2.2.3 it was however determined that this is also true for the nonlinear rigid body response.

The time delay between the starting of the wave maker and the arrival of the wave at the desired location was used to determine the starting point of the carriage. Starting from this location, the model was then run into the response conditioned wave. The response of interest was the maximum midships horizontal force measured during the run. The result from repeating the above and moving the starting point each time somewhat closer to or further from the wave maker is shown in Fig. D.1.

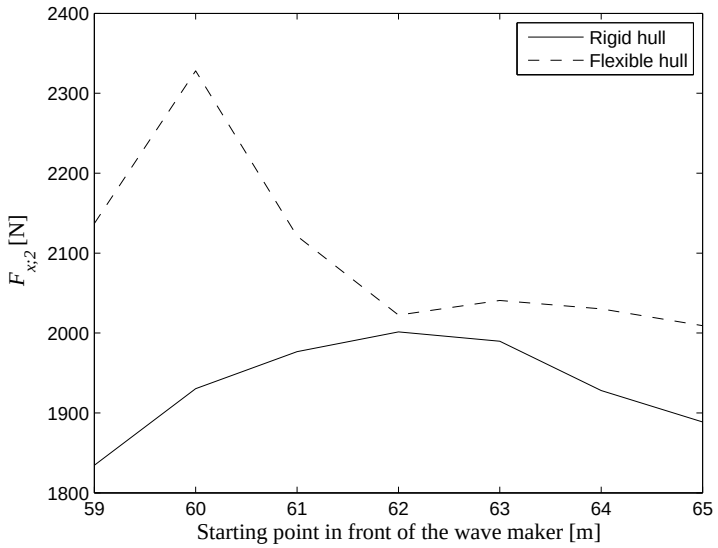

Figure D.1: Measured midships horizontal force as a function of the starting point of the carriage in front of the wave maker.

The location where the extreme response should occur was chosen at 30m in front of the wave maker. As the wave propagates through the tank, the nonlinear interactions influencing the wave profile increase with increasing distance. So the location of 30m was chosen such that it would be as close as possible to the wave maker without any risk of running into it. The time delay between the starting of the wave maker and the arrival of the wave at the desired location was chosen to be 90s. In this way the shortest waves were approximately at 50m in front of the wave maker when the extreme response occurred, and it was made sure that all wave components were present in the response conditioned wave at the desired time and location. The group velocity of waves in deep water is

$$C_g = 0.5\frac{g}{\omega}. \tag{D.1}$$

The deep water assumption holds for all but the longest components of the response conditioned waves. By considering the time delay of 90s and the acceleration period of the carriage (Section 3.8) it was found that the carriage should start 62m in front of the wave maker in order to be at 30m after 90s when the full scale speed is 5kn. Fig. D.1 shows that starting from this location indeed leads to the largest response, and that the force gradually reduces towards both ends. This means that when starting from 62m the model

is at the correct location at the desired time. The unfiltered response had its maximum when the starting point was 60m in front of the wave maker. This indicates that the flexible response does not correlate well with the rigid one, and thus also not with the linear one. The figure furthermore shows that the rigid body response is fairly insensitive to the starting position. A deviation of about 1m decreases the force by approximately 1%. The flexible response is more sensitive. The example given in Fig. D.1 is for one of the lowest waves tested and agreed well with linear predictions. Still, the maximum height of this wave in the tank was approximately 0.5m. For higher waves the procedure was similar, although the starting location was in general found to differ from the linear prediction.

The fact that the variation of the response with the starting point is relatively small means that the uncertainty as a result of timing imperfections is also small, at least for the rigid body response. Therefore it might seem that, for this case, the advanced measures for operating the carriage and the wave maker described in Section 3.8 or by Pastoor (2002) are not necessary. Although this is true to some extent, without advanced facilities it becomes difficult to produce graphs like the one in Fig. D.1, and thus to prove that the found response is the correct one.

Appendix E

Papers

Paper 1:
Experimental and numerical study of containership responses in severe head seas

Paper 2:
Experimental and full scale investigation of the importance of fatigue damage due to wave-induced vibration stress in a container vessel

Paper 3:
Experimental and numerical investigation of fatigue damage due to wave-induced vibrations in a containership in head seas

Paper 4:
Experimental investigation of the application of response conditioned waves for long-term nonlinear analyses

Paper 5:
Numerical and experimental investigation into the application of response conditioned waves for long-term nonlinear analyses

Paper 1

Experimental and numerical study of containership responses in severe head seas

Ingo Drummen, MingKang Wu and Torgeir Moan

submitted to Marine Structures, under review

Experimental and numerical study of containership responses in severe head seas

Ingo Drummen [a,b,*] MingKang Wu [a,c] Torgeir Moan [a,b]

[a] *Centre for Ships and Ocean Structures*
Norwegian University of Science and Technology
Otto Nielsens veg 10, NO-7491 Trondheim, Norway

[b] *Department of Marine Technology*
Norwegian University of Science and Technology
Otto Nielsens veg 10, NO-7491 Trondheim, Norway

[c] *Norwegian Marine Technology Research Institute, POB 4125 Valentinlyst, NO-7450 Trondheim, Norway*

Abstract

An accurate determination of the global load effects in a ship is vital for the design of the vessel. This paper addresses an experimental and numerical study of containership responses in severe head seas. Experimental results were obtained using a flexible model of a containership of newer design. The experiments showed that, taking hull flexibility into account, the fourth and sixth harmonic of the vertical bending moments had a maximum value of between 25% and 50% of the first harmonic. We also demonstrated that hull flexibility can increase the vertical bending moment by up to 35% in sea states relevant for design. Comparisons of vertical bending moments found experimentally with results from a nonlinear hydroelastic strip theory method showed that the effect of nonlinearities on the rigid body vertical bending moments was slightly over-predicted in the aft body. The method also tends to over-predict the increase of the bending moments due to hull flexibility. In general however, the numerical results compared reasonably well with the experimental ones.

Key words: nonlinear, hydroelastic, vertical response, experiments, strip theory, containership

* Corresponding author. Tel.: +47 73 59 55 00; fax: +47 73 59 55 28.
E-mail address: drummen@ntnu.no (I. Drummen).

Preprint submitted to Elsevier

Nomenclature

B	Breadth of the vessel
g	Acceleration of gravity
H	Wave height
H_s	Significant wave height
L	Length (between perpendiculars) of the vessel
M_1	Vertical bending moment at the forward quarter length
M_2	Vertical bending moment amidships
M_3	Vertical bending moment at the aft quarter length
$M_{1;r}$	Rigid body vertical bending moment at the forward quarter length
$M_{2;r}$	Rigid body vertical bending moment amidships
$M_{3;r}$	Rigid body vertical bending moment at the aft quarter length
T	Period
T_p	Peak period
U	Vessel speed

γ	Peakedness parameter
ζ^a	Amplitude of the first harmonic of the wave elevation
η_3	Heave motion at the centre of gravity
η_5	Pitch motion at the centre of gravity
ρ	Mass density of salt water
ω_e	Frequency of encounter
ω_s	Wet natural frequency of the two node mode
QL	Forward quarter length
MS	Midships
3QL	Aft quarter length

The superscript (n) denotes the n^{th} harmonic.

1 Introduction

An accurate determination of the global load effects on a ship is vital for the design of the vessel. The rules issued by classification societies are convenient, but are restricted to ships of conventional design. Over the past few decades, the dimensions of containerships have increased steadily. And it is expected that this trend will continue. An increased size implies an increased flexibility, which leads to significant hydroelastic effects such as whipping and springing. Secondly, some of today's container vessels are trading in harsh environments such as the North Atlantic and therefore the incident waves are severe. Moreover, the unique hull form of these vessels - large, flat and overhanging stern, and pronounced bow flare - coupled with high service speeds can cause large ship motions relative to the water surface, which result in severe slamming impacts. For the design of these ships, the rule values do not apply and direct calculations are necessary. The chosen calculation method should then reflect the structural dynamic effect as well as the nonlinearities in an accurate manner.

Watanabe and Guedes Soares [1] performed a benchmark study by comparing predictions of different nonlinear time-domain computer codes for determining the vertical wave-induced bending moment in a containership in waves of different steepness. Most of the methods investigated were based on strip theory formulations applied to either a rigid body or a flexible hull. They showed that the results were consistent with the linear estimates in the lower wave height region. However, the agreement among the calculated values became poor in the higher wave region when the elastic behaviour of the hull played a significant role. They recommended to make comparisons with experimental data in order to decide whether nonlinear programs are reliable tools for predicting the wave-induced load effects on ships. ISSC [2] presented a comparison between measured and calculated wave bending moments. In this comparison several nonlinear strip theory methods were used. Their general conclusion was that although the methods may give results with sufficient engineering accuracy, the calculated higher harmonics of the response did not comply very well with the measured values. This indicates that the modelling of the nonlinear effects does not represent the real physics consistently. Further validation of the methods is therefore necessary.

Several persons have performed experiments using a model of the ITTC S-175 vessel. Watanabe et al. [3] investigated the influence of the bow flare on the green water and the asymmetry of the vertical bending moment. As part of their work they presented second harmonics of the vertical bending moment as a function of the wave length. O'Dea et al. [4] conducted experiments using a rigid model of the S-175 vessel with the objective of identifying nonlinear effects on the vertical motions and verifying if these responses may

be represented by a third order Volterra functional series. Higher order spectral analysis was carried out, and it was possible to identify the presence of nonlinear components in the vertical motions and accelerations. It was also concluded that the third order Volterra model is a good approximation of the measured responses and that cubic effects are important and even dominate the responses at the high frequency range.

The most recent model tests, performed with a rigid model of the S-175 vessel, were presented in [5] and [6]. The second harmonic of the vertical motions, and the second and third harmonics of the vertical loads were presented in [5]. The second harmonic of the midships vertical bending moment had maximum values that varied between 40% and 60% of the first harmonic amplitudes. The third harmonics reached values of around 15% of the first harmonics. In the light of the results from O'Dea et al. [4], it should be noted that cubic effects appear in the first and third harmonics, while square effects only appear in the second harmonic. Regarding nonlinear characteristics Fonseca and Guedes Soares [6] only compared the asymmetry in positive and negative peaks, which is mainly influenced by square effects. They compared their results with a nonlinear numerical strip theory method. The nonlinearities included Froude-Krylov forces, hydrostatic forces and green water forces. By comparing experimental and numerical results in terms of significant and mean values, they concluded that the numerical method was able to capture the nonlinear tendencies of the experimental vertical motions and loads.

The S-175 vessel is however a container vessel of older design. With a length between perpendiculars of 175m the vessel is considered relatively short. Moreover, due to a less pronounced flare, nonlinear effects in the bow area are less significant than for container vessels of modern design. From the published work discussed above, it is clear that only the first, second and third harmonics have been investigated. This might be sufficient when assuming a rigid hull. However, when considering hull flexibility, higher harmonics than third might become important, because they coincide with the natural frequency of the vertical two node vibration mode. In this paper we will present experimental results of vertical ship responses, obtained with a four segment flexible model of a container vessel of newer design. The model was tested in the towing tank at the Marine Technology Centre in Trondheim in head seas. For the vertical motions only the first harmonics are presented. The first harmonics as well as the higher harmonics, which can excite the two node vertical vibration, are presented for the vertical bending moments. Results from these tests were compared with predictions from a hybrid nonlinear hydroelastic strip theory method of Wu and Moan [7].

2 Theoretical background

For the past two decades, significant research efforts have been devoted to nonlinear 3D time domain hydrodynamic codes. An analysis with one of these codes will in general however require long computation time. On the other hand, driven by the needs of ship design, some simplified approaches have emerged. Almost all of them are nonlinear modifications of some kind to the conventional strip theory, see e.g. [1] or [2]. As one effort in this direction Wu and Moan [8] presented a nonlinear hydroelastic simulation method for the prediction of wave-induced vertical motions and loads in ships with large amplitude motions and small hull deformations. The global hull deformation is approximated by an aggregate of flexible modes, and the wave-induced ship responses are obtained by modal superposition. The nonlinear effects in the vertical motions and cross-sectional load effects are introduced in the form of a nonlinear vertical excitation force. In this way the relationship between the ship motions or the load effects and the excitation force can remain linear, while the latter is no longer linearly related to the incident wave. The total nonlinear excitation force, $f(t)$, consists of a linear part, $f_l(t)$, and a nonlinear modification part, $f_{nm}(t)$:

$$f(t) = f_l(t) + f_{nm}(t) \tag{1}$$

Similarly the response is decomposed. The linear part is evaluated by using 2D or 2.5D strip theory. The nonlinear modification part is obtained as the convolution of the linear impulse response function and the nonlinear modification force. The nonlinearities considered are the slamming impact force, the nonlinear incident wave force and the nonlinear hydrostatic restoring force. The slamming force is determined from momentum considerations and is neglected during water exit. According to Zhao et al. [9] the slamming loads calculated using the principle of conservation of momentum and the exact body boundary condition are lower than those obtained from a fully nonlinear numerical method because the effects of local water rise-up are generally neglected.

Wu and Hermundstad [10] further improved the method of Wu and Moan [8] by partitioning the global flexible modes into dynamic and quasi-static ones so that the computational time for a nonlinear simulation could be reduced, while the structural dynamic effects were still accounted for. Partitioning of the global flexible modes into dynamic modes and quasi-static ones can reduce the computation time. However, the total number of global flexible modes required varies from ship to ship and from response to response. It can only be determined by a convergence study, which should be carried out for each and every response. Furthermore, it should be noted that it sometimes can be very difficult to know whether convergence is achieved or not.

Recently, Wu and Moan [7] presented an alternative, hybrid, method for calculating the hydroelastic responses. This is a combination of the conventional direct load evaluation for a rigid body and the modal superposition for a flexible hull. It still accounts for the dynamic effect in the lowest few global flexible modes, but no longer evaluates the quasi-static responses in the higher global flexible modes. In the modal superposition approach, any time domain hydroelastic response $r(t)$, such as the bending moment, is expressed as an aggregate of dynamic flexible responses $p_i^d(t)$,

$$r(t) = \sum_{i=7}^{\infty} c_i p_i^d(t) \tag{2}$$

where $i = 1..6$ represent the rigid body motions and c_i are the modal coefficients. If the global structural dynamic effect is absent or insignificant in any of the flexible modes, the dynamic modal responses reduce to quasi-static ones, $p_i^q(t)$, and

$$r(t) = \sum_{i=7}^{\infty} c_i p^q i(t) \tag{3}$$

is equivalent to that obtained by the conventional direct response evaluation, familiar to naval architects. Since the global structural dynamic effect, if any, is only present in the lowest few flexible modes, the hydroelastic response can be approximated adequately by:

$$r(t) = \sum_{i=7}^{m+6} c_i p_i^d(t) + \sum_{j=m+7}^{\infty} c_j p_j^q(t) = \sum_{i=7}^{m+6} c_i [p_i^d(t) - p_i^q(t)] + r^{rb}(t) \tag{4}$$

where $r^{rb}(t)$ is the response calculated by the conventional direct load evaluation approach and m is the number of global flexible modes for which the dynamic effect is taken into account. In this way the need to calculate many modal responses is eliminated. This hybrid method has been implemented into WINSIR Hybrid, which is the computer code used in this paper.

Wu and Moan [7] also improved the description of the slamming force compared to Wu and Moan [8], by including the effects of pile-up water. These effects are included approximately by a correction factor, which is a function of the tangent to the body plan profile at the point where the wave surface meets the ship hull. The correction factor is based on the investigations of Zhao et al. [9] for wedges with varying dead rise angles. They presented an approximate approach based on Wagner's [11] solution and showed that this method gave a reasonable approximation of the total slamming force and the local slamming loads. Hermundstad and Moan [12] used this generalised Wagner approach

to calculate bow flare slamming loads on a Ro-Ro vessel. They showed that the calculated slamming pressures corrected for 3D effects compared well with measured data. The correction factor for the pile-up water used by Wu and Moan [7] is given as the ratio between the vertical slamming force found using the generalised Wagner method and the one found from momentum slamming without water pile-up.

However, in general, two dimensional slamming calculations give too high forces because the flow in the bow area is not two dimensional. A quantitative estimate of this effect is given in the uncertainty analysis.

3 Experimental setup

The model tests were performed in the towing tank at the Marine Technology Centre in Trondheim. The tank is 260m long, 10.5m wide and between 5.6m and 10m deep. The double flap wave maker is able to produce both regular and irregular waves. The model was built based on a container vessel with an overall length of 294m. It has a large, flat, overhanging stern and a pronounced bowflare. With these characteristics, it is considered to be representative for modern container vessels. The main particulars are given in Table 1. The scale of the model was 1:45, resulting in a length between perpendiculars of 6.24m. The body plan of the vessel is shown in Fig. 1. In order to include the hydroelastic effect in the experiments, the model was made of four rigid segments connected by three springs. The cuts were located 0.13m (i.e. $0.02L_{pp}$) forward of the quarter lengths and the midships section. In this paper, the forward, midships and aft cut will be denoted as QL-cut, MS-cut and 3QL-cut respectively.

Rigid body motions were measured using an optical system. Axial force transducers were placed in the three cuts above the neutral axis of the model. The axial forces are then a measure for the vertical bending moments in these cuts. From full scale measurements on the present vessel presented by Storhaug and Moe [13], it can be seen that the stress from the axial force at the neutral line had the same period as the wave frequency part of the vertical bending stress and that the two were approximately in phase. This means that the vertical bending moments presented in this paper can be up to 10% too high. This is however more likely to be an issue for the irregular wave results, than for the regular wave results. More detailed information about the experimental setup can be found in [14] and [15].

The mass distribution used in the experiments is given in Fig. 2. We attempted to model one of the mass distributions from the loading manual of the vessel. However, it was not possible to obtain this mass distribution in the model due

to the high mass of the springs. The mass distribution used in the experiments was characterised by lumped masses around the springs. This means that the vertical bending moments, determined by the numerical method, in the forward and aft cut were sensitive to the exact location. This sensitivity is quantified in the subsequent uncertainty analysis.

The model was tested in head regular and irregular waves, as this wave heading usually is the most severe condition with respect to the vertical response, see e.g. [10]. The test program for the regular waves is given in Table 2. In determining which waves to investigate wave frequencies were used rather than wave periods. The maximum value of the midships vertical bending moment RAO was expected to occur for a wave frequency approximately equal to 0.49rad/s. In order to experimentally confirm this location, waves were run with frequencies slightly higher and lower than 0.49rad/s, e.g. 0.48rad/s and 0.50rad/s. This explains the somewhat arbitrarily looking wave periods considered. At a speed of 23kn, the vessel was tested in waves with heights of 4m and 8m. With a speed of 5kn the main tests were performed for wave heights of 2m and 16m, but for T=12.72s, wave heights between 6m and 24m were also tested. For higher waves it was iteratively found that the peak value in the vertical bending moment RAO occurs for waves with a period of 12.72s. The test program for the irregular waves is shown in Table 3. The peak periods were chosen such that they approximately coincided with the period of maximum relative motion. For each sea state, depending on the speed, two or three runs were conducted in waves that were realisations of the same spectrum. The realisation period was short enough to avoid repeating wave trains. The combination of the runs resulted in a full scale duration between 45 and 60 minutes for each sea state.

The motions are represented in a coordinate system fixed in the centre of gravity of the model, with the z-axis in the vertical upward direction. The x-axis is along the longitudinal direction of the model and pointing to the stern. The y-axis is pointing towards the starboard direction. Heave motion and the wave elevation are thus positive upwards, while pitch is positive when the bow goes up.

4 Experimental and numerical results

4.1 General

This section deals with the experimental data obtained, their analysis and the comparison with the numerical results. The zeros of the experimental responses were taken with the model in static equilibrium in still-water. In this

paper, the harmonics of the response, $r(t)$, will be particular discussed. In general $r(t)$ can always be expressed as an infinite sum of harmonic components:

$$r(t) = r^{(0)} + r^{(1)} \sin(\omega_e t + \varepsilon_1) + \sum_{n=2}^{\infty} r^{(n)} \sin(n\omega_e t + \varepsilon_n) \tag{5}$$

where ω_e, t and ε_n represent the encounter frequency, time and phase angle, respectively. The superscript (0) and (1) denote mean and first harmonic. The superscript (n) denotes the n^{th} harmonic. Furthermore, the heave and pitch response of the vessel will be denoted as $\eta_3(t)$ and $\eta_5(t)$ respectively. $M_1(t)$, $M_2(t)$ and $M_3(t)$ will denote the vertical bending moments in the forward cut, midships cut and aft cut respectively.

As the damping ratio is important for hydroelastic responses, the measurements of the damping ratio will be dealt with first. Subsequently, the still-water results and the results from the vessel in waves will be presented.

4.2 Damping ratio

In order to determine the damping ratio in water for the two, three and four node vertical vibration modes, decay tests were performed. The natural vertical vibration modes were excited by an impulse force. This method will in general give vibration in all eigenmodes. For the determination of the damping ratio, measurements of the axial force transducer at midships were used. The damping ratio was determined using two methods. The first method was the free-vibration decay method. In the second method an envelope process was fitted to the positive peak values. The results obtained by the various tests are presented in Table 4. The table gives the mean and 95% confidence interval of the mean damping ratios of the different modes as determined by the two methods of estimation.

The damping was also determined in air by using the same methods. From these tests a dry natural frequency of 4.8rad/s and a dry (structural) damping ratio of 0.2% were found for the two node vibration mode. This method did not give useful results for the damping ratios of the three and four node modes. Based on the observation that, during the decay tests, no waves were generated with a frequency higher than the natural frequency of the two node vibration mode, it was assumed that the structural damping ratios of the three and four node modes were approximately equal to 0.45% and 0.64% respectively. More details about this estimation can be found in [15].

4.3 Still-water results

Preliminary tests were carried out with the model advancing in still-water at a forward speed of 5kn, 15kn and 23kn. The objective was to measure the steady responses without waves, i.e. the responses due to the steady flow. The results are given Table 5. Note that the values in the table are mean values, found by averaging the results of several runs. By comparing the values in this table with those in Figs. 21∼29, it is seen that for exceedance probabilities below 10^{-1}, the still-water vertical bending moments are more than an order of magnitude smaller than the dynamic moments.

At a forward speed of 23kn, the coefficient of variation of the three vertical bending moments was quite small, less than 0.02. For the heave and especially the pitch motion this coefficient was larger, 0.09 and 0.35 respectively. The reason why the variation in the measured pitch response was so large is related to the fact that the measured values were very small. The measured difference in draft between the fore and aft part of the vessel was around 10mm. This means that these measurements were easily influenced by external factors. This problem was even more pronounced for 15kn and especially for 5kn. Although the problem was mainly an issue for the heave and pitch motion, at 5kn the problem also arose for the vertical bending moments. The vertical bending moments however show a clear trend, which is very little affected by the problem. The trend for heave and pitch on the other hand is not clear from the table, because almost all the measurements were influenced by the problem. The values in the table which have a large uncertainty due to this problem are indicated by an asterisks.

It should be noted however that if the still-water responses are too small to be measured accurately, they are also negligible compared to the wave-induced responses for even the smallest waves tested.

4.4 Regular wave results

4.4.1 General

In this section, the response of the vessel in regular waves will be presented. A common way to present these results is a response amplitude operator (RAO) defined as the ratio between the response amplitude and the wave amplitude as a function of the wave frequency. Strictly speaking, RAOs, and more generally transfer functions, can only be used in relation with linear systems. In this paper the first order RAO, or simply RAO, is defined as the ratio of the amplitude of the first harmonic of the response and that of the wave elevation. More in general, the n^{th} order RAO is defined as the ratio of the amplitude of

the n^{th} harmonic of the response and that of the first harmonic of the wave elevation. Contrary to a proper RAO, an RAO for a nonlinear system should include a specification of wave height in order to be uniquely defined.

The first order RAOs presented in this paper do not include the effect of hull flexibility and are therefore referred to as rigid body RAOs, or simply RAOs. These will be given for the two vertical motions, heave and pitch, as well as for the vertical bending moments in the three cuts. The higher order RAOs on the other hand are related to the hydroelastic response of the vessel and are given only for the bending moments in the three cuts. However, first the method for determining the amplitudes of the RAOs is described.

Independent of whether the response is found experimentally or numerically, the time series of the response, $x(t)$, is sampled at N equally spaced points with a distance Δt apart. The sampling times are then given as $t_{k+1} = k\Delta t$, thus:

$$x_{k+1} = x(k\Delta t) \qquad k = 0..N-1$$

The amplitude, $\hat{x}$, of the response can be found in the frequency domain by taking the maximum of the modulus of the Fourier transformed response.

$$\hat{x} = \frac{2}{N} \max_k |X_{k+1}| \qquad k = 0..N-1 \tag{6}$$

where X_k is the k^{th} component of $\boldsymbol{X}$, the Fourier transform of the discrete response $\boldsymbol{x}$, which is generally given for:

$$\omega_{k+1} = k\frac{2\pi}{N\Delta t} \qquad k = 0..N-1$$

The value of k where the maximum of the modulus of the Fourier transformed response is found is denoted as m. The exact form of Eq. 6 depends on the definition of the fast Fourier transformation used.

The amplitude of the wave can be found using the same method. The value of the RAO at a certain frequency is subsequently found by dividing the response amplitude by the wave amplitude. The signal of the wave probe in front of the towing carriage was used for finding the wave amplitude, as this is the most relevant for describing the wave quality in front of the model. For a full scale forward speed of 5kn, the wave measured by this probe might include the radiated and diffracted waves. Due to the shape of the vessel, with a sharp bow, this effect is considered small. Moreover, the comparison of the wave measured in front of the wave maker with the one measured in front of the towing carriage was similar for 5kn and 23kn forward speed. At 23kn

the radiated and diffracted waves propagate too slow to influence the wave measurements in front of the towing carriage.

The method presented here is quite common for finding first order RAOs. This method works well, even for short time series, because in general first order RAOs are quite smooth with respect to the wave frequency. The fact however that RAOs are predicted accurately does not imply that the method is also able to accurately predict the wave or response amplitude separately in case of short time series, which have relatively poor frequency resolution. For the first order RAOs this causes no problem. However, for higher order response the limited resolution becomes quite relevant. For the higher order RAOs the wave and response amplitudes were therefore found from:

$$\hat{x} = \frac{2}{N} \max_j \left[\left\{ \sum_{k=1}^{N} x_k \sin(\Omega_j t_k) \right\}^2 + \left\{ \sum_{k=1}^{N} x_k \cos(\Omega_j t_k) \right\}^2 \right]^{1/2} \tag{7}$$

where Ω_j is the j^{th} component of the vector $\mathbf{\Omega}$:

$$\mathbf{\Omega} = [\omega_m, \quad \omega_m + \Delta\Omega, \quad \omega_m + 2\Delta\Omega, \quad ... \quad \omega_{m+2}]^T \tag{8}$$

In this way the standard FFT resolution can locally be improved in an efficient manner, which results in a more accurate estimate of the amplitude.

4.4.2 Rigid body response

The heave and pitch RAOs for a forward speed of 23kn are presented in Figs. 3 and 4. The figures show the RAOs found using the numerical method as well as determined from experimental results. The experiments were performed using regular waves with a height of 4m and 8m. Results from both cases are given in the figures, and are denoted as 'Experiments 4m' and 'Experiments 8m', respectively. The calculated RAOs are given for the linear and the nonlinear cases. The nonlinear RAOs were found by running time domain simulations using several regular waves, with wave heights of 4m and 8m. In the figures these results are denoted as 'Nonlinear 4m' and 'Nonlinear 8m'. Using the latter method, and thus including nonlinearities, gives a better comparison with the experimental results. Each experimental value presented in these figures, and those to come, is based on results from a single run. In the figures ζ^a denotes the amplitude of the first harmonic of the wave elevation and k the wave number. By comparing experimental results with simulated ones in Fig. 3, it can be seen that the numerical method is not able to predict the hump around 0.5 rad/s. In general however the trend is reasonably well predicted. Fig. 4 shows that the RAO for the pitch motion is predicted very accurately. Calculated results in Figs. 3 and 4 show that nonlinearities are only important

at frequencies with large relative motion. In this area, the values of the RAOs are slightly reduced as the wave height increases. From the two wave heights investigated here experimentally, this effect could not be confirmed. It was however observed by Fonseca and Guedes Soares [5] in their test results.

Figs. 5∼7 show the RAOs of the vertical bending moments in the three cuts. The RAOs are first order, and are thus found from the ratio of the amplitude of the first harmonic of the vertical bending moment and that of the wave elevation. From Fig. 5 it is clearly seen that nonlinearities in the vertical bending moment are quite important in the forward part of the vessel. Since the nonlinearities in the first harmonic of the response can only be caused by odd order nonlinear effects, they are most likely related to the cubic effects. The measured nonlinear effects are captured by the numerical method. Both the experimental results as well as the numerical results show that nonlinearities increase the value of the RAO. The nonlinear behaviour in the bow area may be explained by the fact that the bow segment of the ship is the one that has the largest flare and the largest relative motion at the same time. When the ship sides are vertical, the vertical force is approximately linear with the relative motion between the hull and the waves. When there is a bow flare, the vertical force becomes nonlinear.

Fig. 6 reveals that the odd order nonlinear effects are smaller in the midships area of the vessel than in the forepart. This is believed to be due to the fact that the vessel has a long mid section with vertical walls. The figure also shows that the midships vertical bending moment is predicted very accurately by the numerical method. This could however be related to a balance between an over-prediction due to the 2D assumption and an under-estimation of the forward speed effects, see also Fig. 11.

As indicated by Fig. 7, the vertical bending moment in the aft cut of the vessel is less accurately predicted. The numerical method over-predicts the maximum vertical bending moment in this cut by approximately 15%. The influence of odd order nonlinear effects on the vertical bending moments amidships and in the aft cut are predicted quite well.

Figs. 8 and 9 present the heave and pitch RAOs for a forward speed of 5kn. The experimental results are obtained using regular waves with a wave height of 16m, 'Experiments 16m', as well as for a mixture of wave heights, r26 to r29 in Table 2. The latter are denoted as 'Experiments 6m∼24m'. Fig. 8 shows that the measurements compare well with the calculated results, even though the frequency range is quite narrow. This range was chosen so narrow, because the main goal was to capture the peak response in the midships vertical bending moment. The calculated results indicate that the nonlinearities tend to reduce the heave motion, in this case particularly in the range between 0.45rad/s

and 0.65rad/s. Calculated results in Fig. 9 are also in good agreement with measurements, although it looks like the measurements are somewhat shifted to the left compared to the calculations. This shift between experimental and numerical results was not observed in Fig. 4. It is believed to be related to the fact that the numerical method calculates the added mass for the mean wetted body surface, which leads to an under-prediction of the added mass in waves with a wave height of 16m.

The RAOs of the vertical bending moments are shown in Figs. 10∼12. These figures also include experimental results found using regular waves with a wave height of 2m. Results from these tests are considered as linear. The values for the outermost frequencies for this wave height are based on results from a single run. The other values represent the average of six different runs at each frequency. The experimental results for wave heights of 6m and higher show quite some scatter. A large part of the observed scatter in the figures is due to results obtained for different wave heights, 'Experiments 6m∼24m'. The influence of nonlinearities on the RAOs of the vertical bending moments increases with increasing wave height. The reason for the scatter in the results at 16m wave height is believed to be related to the severe nature of these waves for the present vessel. Differences in results from repeated runs in severe waves are expected to be larger than those in moderate waves. This is because effects like green water on deck start playing a roll.

Fig. 10 shows that the peak value predicted by linear theory is close to the maximum found from experiments in waves with 2m height. Linear theory is however not able to predict the second peak seen for the experimental results. Comparing Fig. 10 with Fig. 5 it seems that the nonlinearities, as expected, are even more important in higher waves. Further, the predicted degree of nonlinearities agrees well with measurements.

Fig. 11 shows that nonlinear effects are clearly present in the vertical bending moment amidships for the higher waves. These are related to the fact that the forepart of the model emerges completely from the water. Linear predictions from the numerical method of the peak value seem to slightly over-estimate the measured peak value in the vertical bending moment RAO in waves of 2m height. Again, the predicted degree of nonlinearities agrees well with measurements. For the aft cut (Fig. 12), the method over-predicts the linear vertical bending moment by approximately 10% to 15%. Also here, the predicted degree of nonlinearities agrees well with measurements.

From the results presented in this section it is seen that nonlinear effects tend to decrease the amplitude of the first harmonic of the vertical motions, while they increase those of the vertical bending moments. For the latter this was observed on the measured results as well as the calculated ones. For the motions, the effect could only be confirmed from numerical results. The effect

of nonlinearities on the heave motion was found to be greater than that on the pitch motion.

4.4.3 Nonlinear hydroelastic response

Fig. 13 shows the peaks of several higher order RAOs of the midships vertical bending moment for a forward speed of 23kn. The results were found using the numerical method. For each peak in the n^{th} order RAO $n\omega_e \approx \omega_s$, where ω_e is the encounter frequency and ω_s is the wet natural frequency of the two node vertical vibration mode. There are two distinct contributions to these higher order RAOs. The first contribution comes from nonlinear rigid body effects, the second comes from slamming.

In Figs. 14∼16, the case for $n = 4$ is compared with experimental results. At a forward speed of 23kn, $4\omega_e \approx \omega_s$ for waves with encounter frequencies around the rigid body resonance frequencies. The three figures look quite similar. By comparing the experimental results with those in Figs. 5∼7 it can be seen that the peak values of the fourth order RAOs for regular waves with a wave height of 4m are approximately 25% of the peak values of the rigid body vertical bending moments. For 8m waves this increases to 50%. For waves of approximately the same height, Fonseca and Guedes Soares [5] found a maximum value of the second order RAO of approximately 50% of the first order RAO.

For waves with a wave height of 4m it seems that the numerical method under-predicts the peak of the nonlinear hydroelastic response by approximately 70%. In the case of a wave height of 8m this is only 25%. This could indicate that the fourth order nonlinear effects are under-estimated by the method, while the sixth or higher even order nonlinear effects are over-predicted.

Figs. 14∼16 clearly show that the peak values of the measured results occur for different frequencies than for the calculated results. In the former case the peak occurs approximately at a frequency of 0.51rad/s, while it is 0.54rad/s in the latter case. This shift is the result of a difference in the natural frequency of the two node vertical vibration. Therefore, the calculations for waves with an 8m wave height were repeated using lower stiffness, i.e. 95%, 90% and 85% of the original stiffness. In the figures, these cases are denoted as 0.95EI, 0.90EI and 0.85EI respectively. The stiffness was modified because this is more straightforward than modifying the mass, even though the actual problem might be related to the added mass. From the results it can be seen that 85% of the original stiffness gives a natural frequency quite close to the natural frequency determined experimentally. This change does however hardly influence the calculated peak values.

It can also be seen that the predicted resonance peak is more narrow than the

measured one. This is true for results from waves with a wave height of 4m as well as 8m. One reason for this is related to the fact that the wave energy, which should only occur at one specific frequency for regular waves, spreads somewhat to neighbouring frequencies during the experiments. This does not happen in a numerical method based on linear wave theory.

It should be noted that the wave, measured in the towing tank, was generally different from the requested wave. The measured wave height during the run which gave the largest value for the 8m case in Figs. 14∼16 was not 8m, but 8.45m. This difference is particularly relevant for the higher order response, assuming that the fourth harmonic of the response is dominated by fourth order effects, the former will be increased by approximately 25% due to a 6% increase in wave height. Using a wave height of 8.45m a new peak value was calculated. Table 6 compares the value of this new peak with the peak value found by using a wave height of 8m. The comparison was done using the original stiffness distribution. From the table it can be seen that an increase in wave height of 45cm increases the peak response by approximately 22% in this case. Even though this increase brings the experimental and the numerical values closer to each other, numerical results are still lower than measured results, by approximately 20%.

Fig. 17 is similar to Fig. 13, but is given for a forward speed of 5kn. For this speed, the comparison between numerical and experimental results was done for $n = 6$, see Figs. 18∼20. At 5kn, $6\omega_e \approx \omega_s$ for waves with encounter frequencies around the rigid body resonance frequencies. The figures compare the results for waves with a wave height of 16m. The experimental peak value found in the first of these figures is approximately 25% of the peak value in Fig. 10. On the other hand, the peak value of the sixth order vertical bending moment RAO for the midships and aft section are approximately 50% of that of the rigid body vertical bending moment RAO. This means that the amplitude of the sixth harmonic reaches values of up to half of those of the first harmonic.

From Figs. 18∼20 it can furthermore be seen that the predicted values are considerably higher than the measured values. The fact that the predicted values are lower for 5kn and higher for 23kn (Figs. 14∼16) rules out that difference between calculations and measurements is related to structural damping. The shift in peak frequency is again noticeable. Therefore two modified stiffnesses were used, 95% and 90% of the original stiffness. From the figures it can be seen that there is a considerable drop in the peak value when moving from the original stiffness to 95% of this stiffness. This is a result from the so-called hump-hollow behaviour of the response at higher frequencies.

For a forward speed of 5kn, 95% of the original stiffness compares best with the

experimental values. For this modified stiffness, the numerical and experimental peak values are quite close. The fact that 85% of the original stiffness gives best results at 23kn, while 95% is more favourable at 5kn could be explained by a difference in added mass between the two cases. Because the numerical method calculates the added mass for the mean wetted surface, the method is not able to predict the change in added mass between the two cases.

4.5 Irregular wave results

The fourth and sixth harmonics described above are fully developed steady state resonances. This situation will not materialise in an irregular wave condition. On the other hand, there may simultaneously be several higher harmonics exciting springing. Sea states with irregular waves considered during the experiments are given in Table 3. The peak periods were chosen close to the resonance period for relative motion, in order to maximally excite whipping. The measured vertical bending moments are presented in this section in the form of exceendance plots. Figs. 21∼23 give the short-term cumulative probability distributions for the forward cut in the three different sea states. The figures show both the experimental and the numerical results. Moreover, all figures consist of two plots, the left plot gives the probability distribution for the flexible hull, while the right plot shows the probability distribution assuming a rigid hull. The latter was found from the low-pass filtered time history of the measured and calculated vertical bending moment. The cut-off frequency (2.55rad/s) was determined such that the high frequency vibration was eliminated from the filtered signal. Using this procedure will also filter some of the higher order effects. However, this is mainly relevant for fourth order effects and higher, and therefore considered of little influence. At a speed of 15kn the peak frequency of the encountered wave spectrum is approximately 0.7rad/s, multiplied by three this becomes 2.1rad/s, which is lower than the cut-off frequency. The probability distributions are given for sagging (sag) as well as hogging (hog). For the numerical case, the linear results were also included. The small difference between the Rayleigh distributions for the flexible and the rigid hull is due to linear springing. For the presentation of the results in this section, the steady response due to the forward speed was subtracted from the total response. Furthermore, $M_{i;r}$ denotes the rigid body vertical bending moment in cut i.

The experimental results show that the sagging bending moments are larger than the hogging bending moments, by up to 30% to 40%. This is the case for the rigid as well as for the flexible hull. The difference between sagging and hogging is the result of even order nonlinear effects and is similar in all three sea states. Depending on the sea state, the vertical bending moment is increased by between 10% and 25% due to hull flexibility. This is based on an

exceedance probability of 10^{-2}. The increase in the hogging bending moment is slightly smaller than that in the sagging bending moment.

The comparison of the experimental results with numerical results shows that the predicted asymmetry between sagging and hogging agrees well with the measured one. In the higher response range of Fig. 21, the predicted response is approximately 20% lower than the response found from experiments. This under-prediction is less in Fig. 22. Fig. 23 shows that except for the rigid body hogging bending moment all short term distributions are predicted very accurately.

Figs. 24∼26 show the short-term probability distributions of the midships vertical bending moment. Experimental results in Fig. 24 indicate that even order nonlinear effects have little influence on the vertical bending moment amidships of the rigid hull, as there is almost no asymmetry between hogging and sagging. A possible reason is that a relatively large part of the vessel has nearly vertical walls. The reason that there is more asymmetry in the other two sea states is partly related to the higher significant wave height. Another reason might be the difference in speed, which affects the encounter frequency. In sea state i1, the vertical bending moment is increased by almost 35% due to hull flexibility, while this value lies between 15% and 30% in the second and third sea state. The fact that hull flexibility increases the vertical bending moment most in the lowest sea state is due to the higher forward speed, and thus more severe slamming events.

When comparing these results with the numerical ones, it is seen that the lack of asymmetry in the experimental vertical bending moment of the rigid hull in sea state i1 (Fig. 24) is not reflected by the numerical method. This could be related to the fact that strip theory tends to over-predict the vertical force near the ends of the vessel, where the geometry is most nonlinear. Consequently, the calculated linear rigid body bending moments compare well with those found experimentally, which is in agreement with Fig. 6. Generally, less asymmetry was found in the measured vertical bending moments than in the calculated ones. However, the nonlinear rigid body vertical moments are well predicted in sea states i2 and i3 (Figs. 25 and 26). Furthermore, the calculated influence of hull flexibility is in reasonable agreement with that from the model tests, but it is increasingly over-predicted with increasing wave height.

The short-term probability distributions of the vertical bending moment in the aft cut are given in Figs. 27∼29. The figures show that the asymmetry between sagging and hogging has increased compared to the midships section. The vertical bending moment in the aft quarter length is over-predicted in the lowest sea state, and increasingly over-predicted in the two higher sea states. This is in agreement with Figs. 7 and 12 where the vertical bending moments in the aft cut are also over-predicted.

The results presented above show that linear vertical bending moment in all cuts in sea state i1 is approximately equal to that in sea state i2. The effect of the decrease in speed from 15kn to 8kn is therefore balanced by that of an increase in significant wave height. The same is not true for the nonlinear results as well as for the experimental ones. The absolute value of the vertical bending moments as well as the asymmetry between them is higher for sea state i2 than i1. The effect of a higher vessel speed in sea state i1 compared to i2 therefore increases the nonlinearities in the vertical bending moments for the rigid hull less than these are decreased by the lower significant wave height. On the other hand, the increase of the moments due to hull flexibility is larger in sea state i1 than in i2.

In general the rigid body vertical bending moments in the forward and midships cuts are predicted quite accurately. In the aft cut, the calculated vertical bending moment is higher than the measured one. This is believed to be the result of an over-prediction of the linear vertical bending moment, see Figs. 7 and 12. From these figures a difference between experiments and calculations of approximately 15% is found. If the numerical results from Fig. 29 are divided by 1.15 as shown in Fig. 30 the measured and the calculated values compare quite well. The contribution of hull flexibility is still overestimated by the numerical method. This is at least partly related to the fact that 2D slamming calculations tend to over-predict the vertical impact force in the bow area of the vessel. The main contribution to the slamming force comes from that area.

In the numerical method, the first three global flexible modes were accounted for. In the model tests, the dynamic effects of the first three flexible modes were observed for the moment in the forward section. However, the dynamic effects of the third mode were absent in the measured bending moments in the midship and aft sections, see Fig. 31.

5 Uncertainties

The uncertainty analysis of the experimental results is important as it provides information on the quality of the results. It was not possible to carry out a complete uncertainty analysis of the experimental data, because many of the error sources could not be explicitly addressed.

There are two distinct types of errors, bias errors, which are constant within an experiment, and precision errors, which contribute to the scatter of the data within an experiment. Because some of the test runs were repeated, it was possible to obtain information on the level of dispersion of the experimental results. For a forward speed of 5kn regular waves were run with a wave height

of 2m. This height was chosen to have results which were as close as possible to linear results, without having problems with small absolute values as indicated in the section on still-water loads. The vertical bending moment RAOs for these cases were found from runs at seven different periods. Five of these runs, r14...r18, were repeated five times.

Table 7 presents the mean value of the ratio of the amplitude of the first harmonic of the vertical bending moments and that of the measured wave elevation, as well as the 95% confidence interval of the mean value resulting from these tests. The table also shows the confidence interval of the same ratio found in regular waves with H=4m, T=12.35s and U=23kn as well as in regular waves with H=12m, T=12.72s and U=5kn, these intervals are based on four repetitions. From the table it can be seen that the confidence interval is less than 10% of the mean value for all cases, and generally is less than 5%.

For these last two waves, i.e. r2 and r27, Table 8 gives the confidence interval of the ratio of the amplitude of the fourth and sixth harmonic of the vertical bending moment and that of the first harmonic of the measured wave, respectively. Here the confidence interval is less than 15% of the mean value. For the same waves, Table 9 shows the mean value and the 95% confidence interval of the mean value of the heave and pitch motions.

In general, two dimensional slamming calculations give too high forces because the flow in the bow area is not two dimensional. A rough estimate of the 3D effect can be obtained based on results from Scolan and Korobkin [16]. Among others, they studied the problem of an elliptic paraboloid entering initially calm water at constant velocity, and present an exact analytical solution to the three dimensional Wagner problem. In order to check the applicability of the strip theory and give an estimate of the implied error, they also derived the vertical hydrodynamic force using strip theory. This derivation uses the solution of the plane problem of the parabolic contour entry given by Wagner [11]. The forward part of the water line contours of the present vessel may be regarded as one half of an ellipse. The results from Scolan and Korobkin [16] were used for four different water line contours, at 8m, 12m, 16m and 20m above the base line. From this it was found that the 2D slamming force is roughly 20% larger than the 3D force.

As mentioned in the section on the experimental setup, the mass distribution used during the experiments was also used in the calculations. The measurements of the mass distribution are however somewhat uncertain, particularly near the three spring where the mass is large and irregular. Because the vertical bending moments were measured and predicted close to these springs, they are very sensitive to the exact mass distribution around the springs. Table 10 shows how the calculated peak values of the linear RAOs of the vertical bending moments change when the cross sections where the moments are cal-

culated are moved 3.51m (one section or $0.0125L$) forward or aft of the base location. The moment in the forward quarter length changes by 18% as a results of this move, at the aft quarter length this is 6% and at midships it is less than 1%. Therefore, in comparing predicted vertical bending moments with measurement ones there will be some uncertainty related to the mass distribution. The uncertainty in the mass distribution can be considered as a bias error. More sources of uncertainty concerning the experimental results are discussed in [15].

6 Conclusions

This paper deals with an experimental and numerical investigation into the vertical response of a modern containership (L_{pp}=281m) with different forward speeds in severe head regular and irregular waves. A 1:45 four segment flexible model was used for the tests. Numerical results were obtained using a nonlinear 2D hydroelastic hybrid method developed by Wu and Moan [7]. Several conclusions can be reached based on the results of this investigation. Points (1) to (4) relate to the experimental results, while the last two points concern the comparison with the numerical method.

(1) The nonlinear effects on the vertical bending moment are more significant in the forward section than in the midships and aft sections, and they tend to increase the bending moment amplitudes in regular waves. Both in regular and irregular waves, the sagging bending moments are larger than the hogging ones. This is in line with the findings of Fonseca and Guedes Soares for a rigid hull [5; 6].
(2) When the flexibility of the containership is taken into account, the amplitude of the fourth and sixth harmonics of the vertical bending moments have a maximum value of between 25% and 50% of that of the first harmonic. This implies that the vertical bending moments of the flexible containership can not be accurately described by a third order Volterra functional series, which was used by O'Dea et al. [4] in their study of the S-175 containership modelled as a rigid body.
(3) Hull flexibility can increase the vertical bending moments by up to 35% in irregular sea states relevant for ship design. Although sagging moments are most influenced by the hull flexibility, the hogging moments are also significantly increased. Since containerships in still-water normally are in a hogging condition, any increase in wave-induced hogging moments will have an impact on design load effects.
(4) A change in speed has more effect on the vertical bending moments of a flexible hull than on those of a rigid hull.
(5) The peak values of the linear vertical bending moment RAOs calculated by the numerical method at 5kn are up to 15% higher than results from

model tests in regular waves with 2m wave height. Compared to this, the measured vertical bending moments with 4m regular wave height and 23kn ship speed are in better agreement with the predictions. This is most likely related to a balance between an over-prediction due to the 2D assumption and an under-estimate of the forward speed effect.

(6) The nonlinear effects on the vertical bending moments in the midships and aft cross sections are slightly over-predicted by the numerical method in irregular waves when the ship is modelled as a rigid body. However, the over-prediction is decreased with increasing significant wave height. The increase of the vertical bending moments due to hull flexibility is also over-predicted in those two sections, especially for the higher sea states. This might be attributed to the fact that the 3D effects are not accounted for in the 2D slamming force calculation. It was estimated that the impact forces from 2D slamming calculations should be reduced by 20% to account for 3D effects. In general, the numerical predictions compare reasonably well to the model test results.

Acknowledgements

The authors acknowledge the financial support from the Research Council of Norway through CeSOS. Moreover, the yard and the owner of the vessel are acknowledged for permitting use of the ship lines. DNV deserves thanks for providing all the necessary ship data. Parts of the contents of this paper were discussed with Prof. Odd M. Faltinsen who offered valuable comments.

References

[1] Watanabe I, Guedes Soares C, Comparative study on the time-domain analysis of non-linear ship motions and loads, Marine Structures 12 (2) (1999) 153–170.

[2] ISSC, Report of special task committee vi.1: Extreme hull girder loading, in: Proceedings 14th International Ship and Offshore Structures Congress, Japan, 2000, pp. 263–320.

[3] Watanabe I, Ueno M, Sawada H, Effects of bow flare shape on wave loads of a container ship, Journal of the Society of Naval Architects of Japan 166 (1989) 259–266.

[4] O'Dea J, Powers E, Zselecsky J, Experimental determination of nonlinearities in vertical plane ship motions, in: Proceedings 19th Symposium on Navel Hydrodynamics, Korea, 1992.

[5] Fonseca N, Guedes Soares C, Experimental investigation of the nonlinear

effects on the vertical motions and loads of a containership in regular waves, Journal of Ship Research 48 (2) (2004) 118–147.
[6] Fonseca N, Guedes Soares C, Experimental investigation of the nonlinear effects on the statistics of vertical motions and loads of a containership in irregular waves, Journal of Ship Research 48 (2) (2004) 148–167.
[7] Wu MK, Moan T, Efficient calculation of wave-induced ships responses considering structural dynamic effects, Applied Ocean Research 21 (2) (2005) 81–96.
[8] Wu MK, Moan T, Linear and nonlinear hydroelastic analysis of high-speed vessels, Journal of Ship Research 40 (2) (1996) 149–163.
[9] Zhao R, Faltinsen OM, Aarnes JV, Water entry of arbitrary two-dimensional sections with and without flow seperation, in: Proceedings 21th Symposium on Naval Hydrodynamics, 1996.
[10] Wu MK, Hermundstad OA, Time-domain simulation of wave-induced noninear motions and loads and its applications in ship design, Marine Structures 15 (6) (2002) 561–597.
[11] Wagner H, Über stoss-und gleitvergänge an der oberfläche von flüssigkeiten, Angew. Math. Mech. 12 (1932) 201–215.
[12] Hermundstad OA, Moan T, Numerical and experimental analysis of bow flare slamming on a ro-ro vessel in regular oblique waves, Journal of Marine Science and Technology 10 (2005) 105–102.
[13] Storhaug G, Moe E, Measurements of wave induced vibrations onboard a large container vessel operating in harsh environment, in: Proceedings of the 10th International Symposium on Practical Design of Ships and Other Floating Structures, US, submitted, 2007.
[14] Drummen I, Storhaug G, Moan T, Experimental and numerical investigation of fatigue damage in a containership in head seas, in prep.
[15] Drummen I, Experimental and numerical investigation of nonlinear wave-induced load effects in containerships considering hydroelasticity, Ph.D. thesis, in prep (2007).
[16] Scolan Y, Korobkin A, Three-dimensional theory of water impact. Part 1. Inverse Wagner problem, Journal of Fluid Mechanics 440 (2001) 293–326.

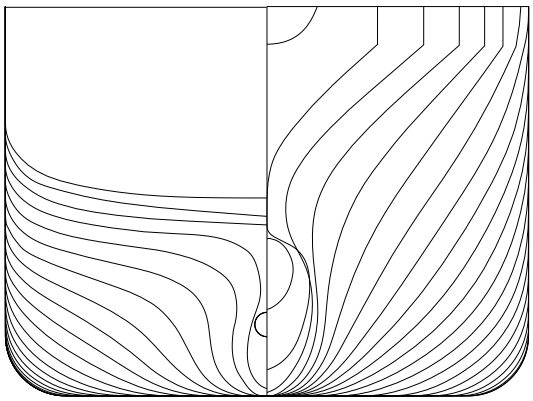

Fig. 1. Body plan.

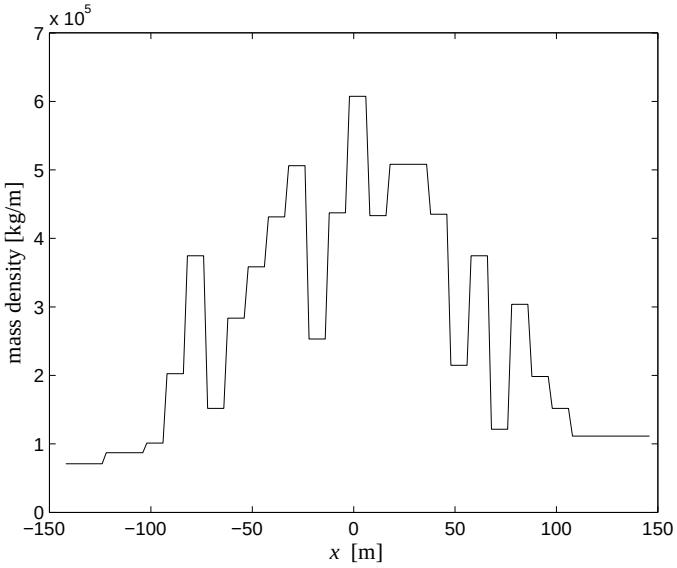

Fig. 2. Mass distribution used during the experiments, scaled to full scale values.

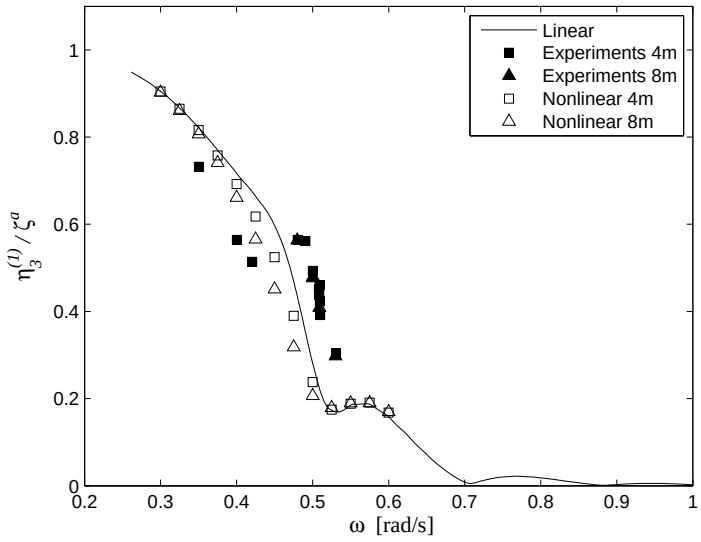

Fig. 3. Heave RAO for U=23kn, based on the first harmonics of both the heave motion and the wave elevation.

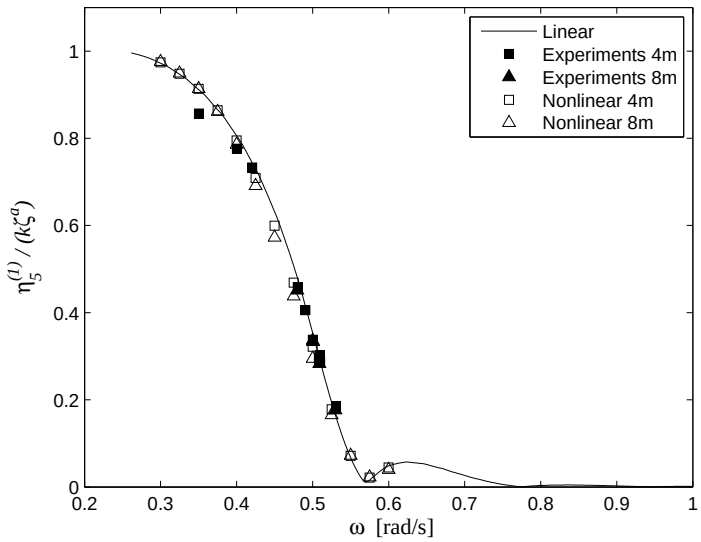

Fig. 4. Pitch RAO for U=23kn, based on the first harmonics of both the pitch motion and the wave elevation.

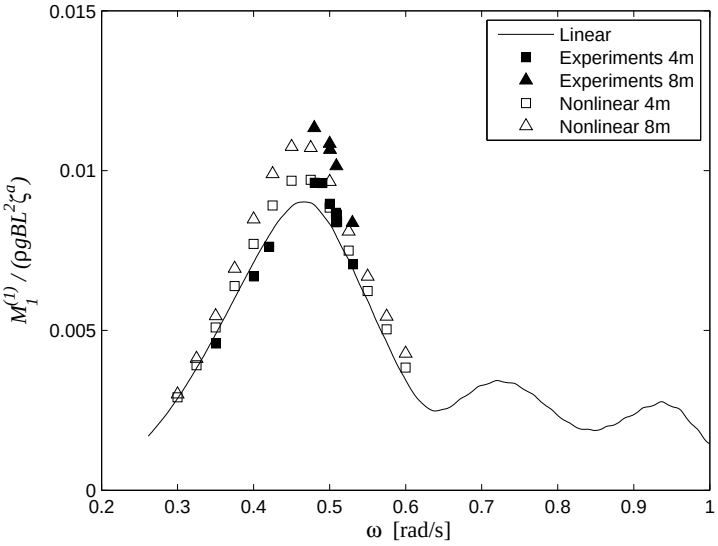

Fig. 5. QL vertical bending moment RAO for U=23kn, based on the first harmonics of both the vertical bending moment and the wave elevation.

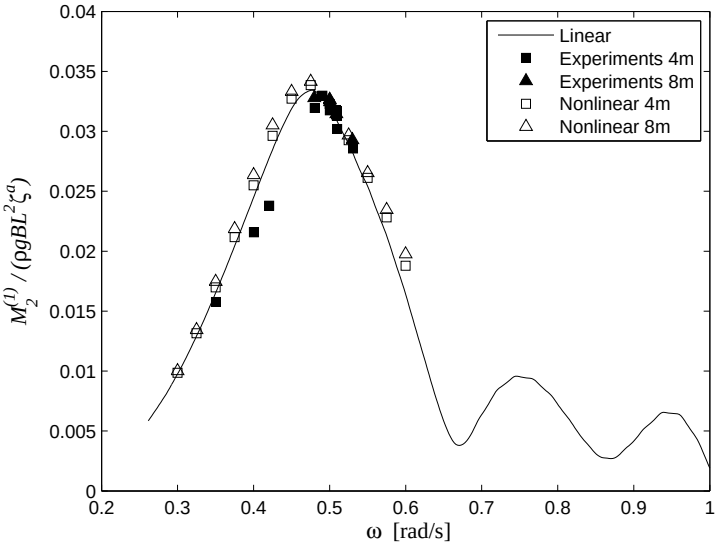

Fig. 6. MS vertical bending moment RAO for U=23kn, based on the first harmonics of both the vertical bending moment and the wave elevation.

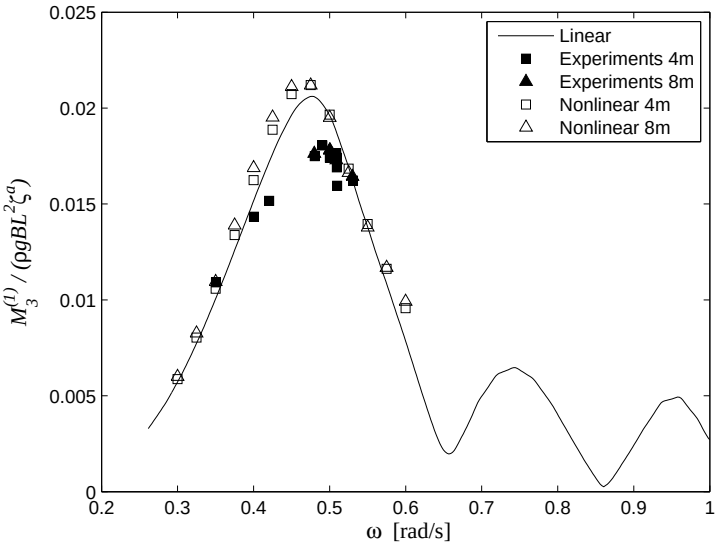

Fig. 7. 3QL vertical bending moment RAO for U=23kn, based on the first harmonics of both the vertical bending moment and the wave elevation.

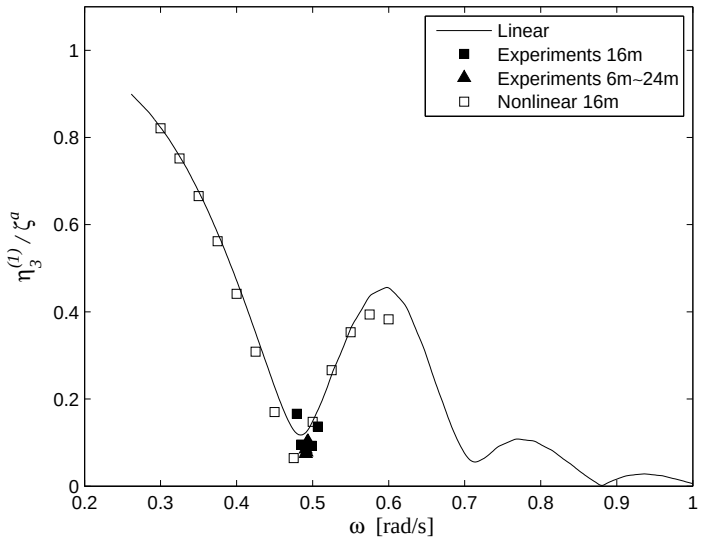

Fig. 8. Heave RAO for U=5kn, based on the first harmonics of both the heave motion and the wave elevation.

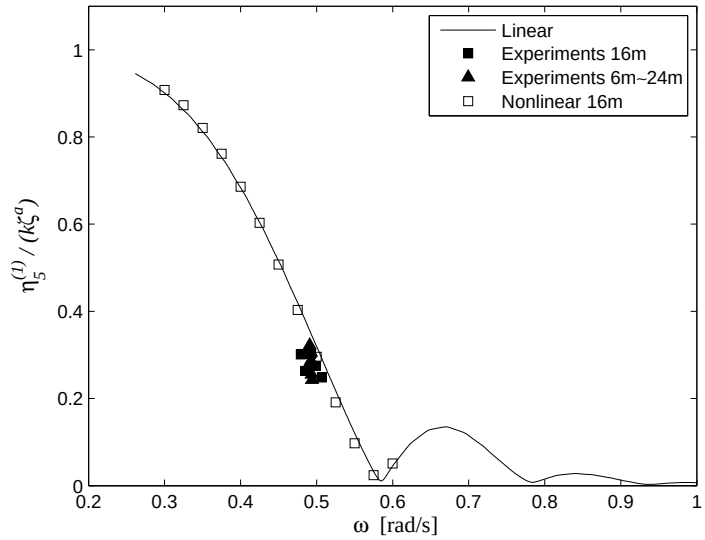

Fig. 9. Pitch RAO for U=5kn, based on the first harmonics of both the pitch motion and the wave elevation.

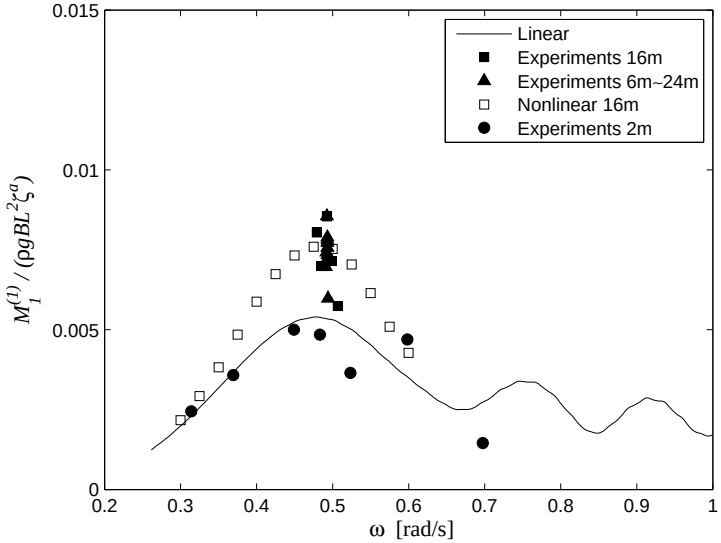

Fig. 10. QL vertical bending moment RAO for U=5kn, based on the first harmonics of both the vertical bending moment and the wave elevation.

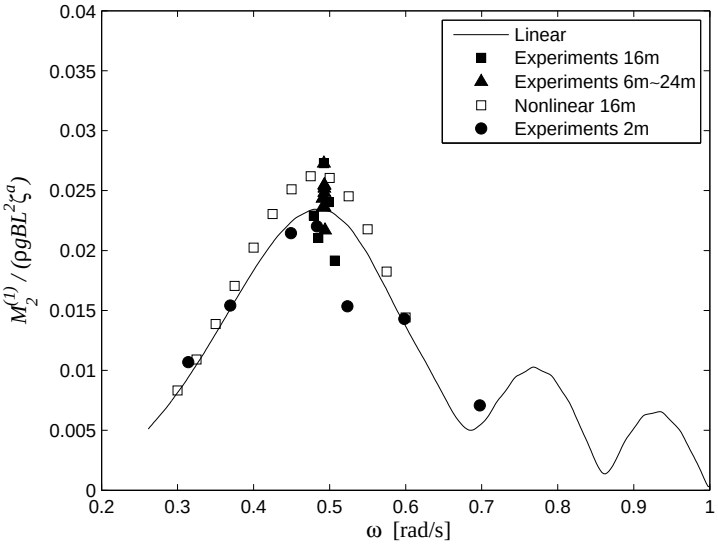

Fig. 11. MS vertical bending moment RAO for U=5kn, based on the first harmonics of both the vertical bending moment and the wave elevation.

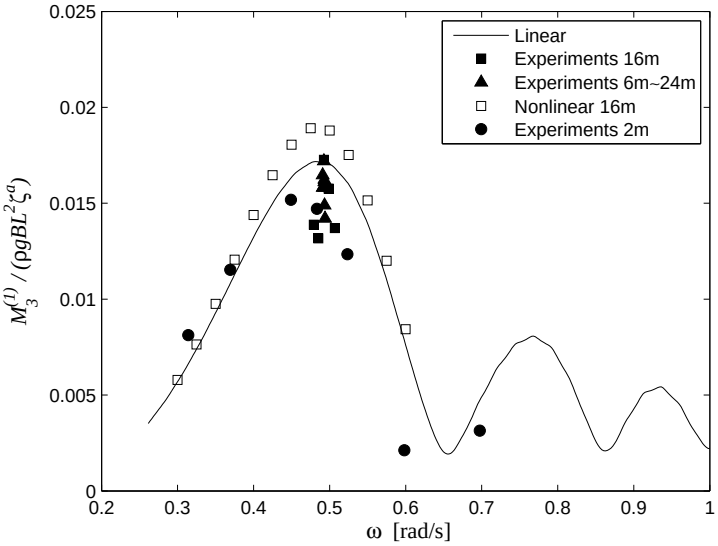

Fig. 12. 3QL vertical bending moment RAO for U=5kn, based on the first harmonics of both the vertical bending moment and the wave elevation.

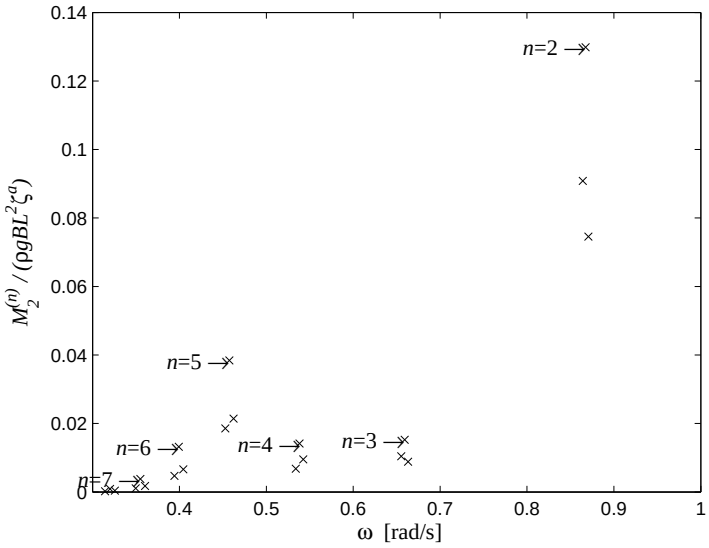

Fig. 13. Numerical estimates of peaks of the n^{th} order midships vertical bending moment RAO for U=23kn. For each n^{th} order RAO $n\omega_e \approx \omega_s$.

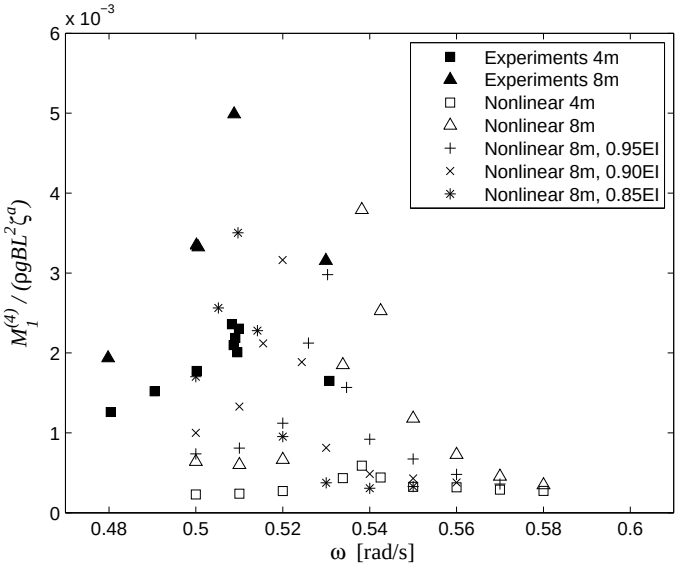

Fig. 14. QL 4^{th} order vertical bending moment RAO for U=23kn. 0.95EI, 0.90EI and 0.85EI means that 95%, 90% and 85% of the original stiffness, respectively, has been used in the numerical calculations.

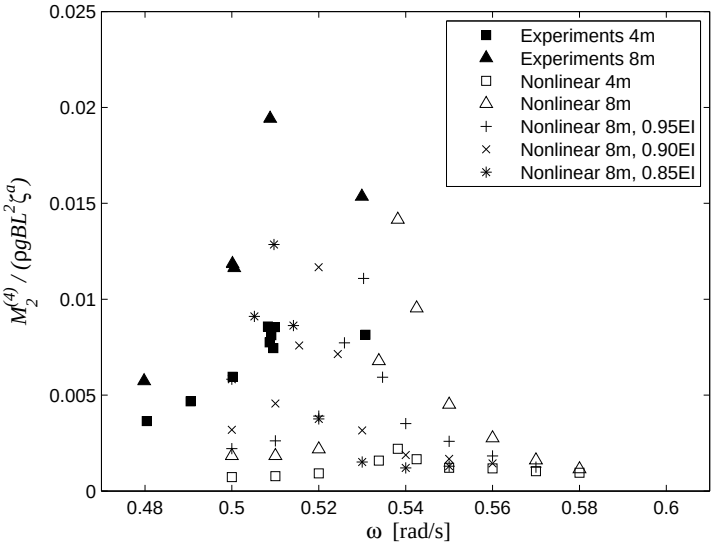

Fig. 15. MS 4^{th} order vertical bending moment RAO for U=23kn. 0.95EI, 0.90EI and 0.85EI means that 95%, 90% and 85% of the original stiffness, respectively, has been used in the numerical calculations.

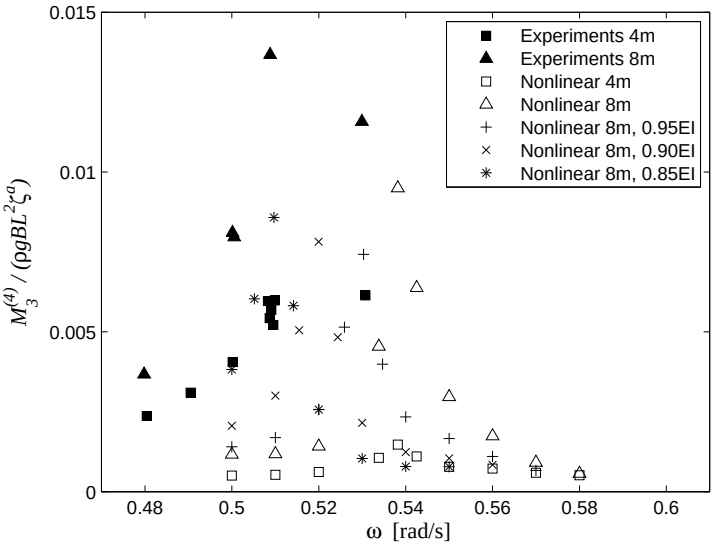

Fig. 16. 3QL 4^{th} order vertical bending moment RAO for U=23kn. 0.95EI, 0.90EI and 0.85EI means that 95%, 90% and 85% of the original stiffness, respectively, has been used in the numerical calculations.

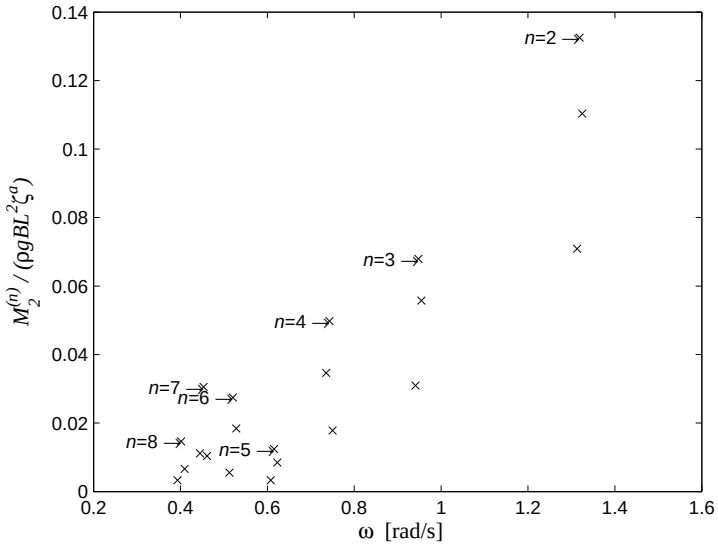

Fig. 17. Numerical estimates of peaks of the n^{th} order midships vertical bending moment RAO for U=5kn. For each n^{th} order RAO $n\omega_e \approx \omega_s$.

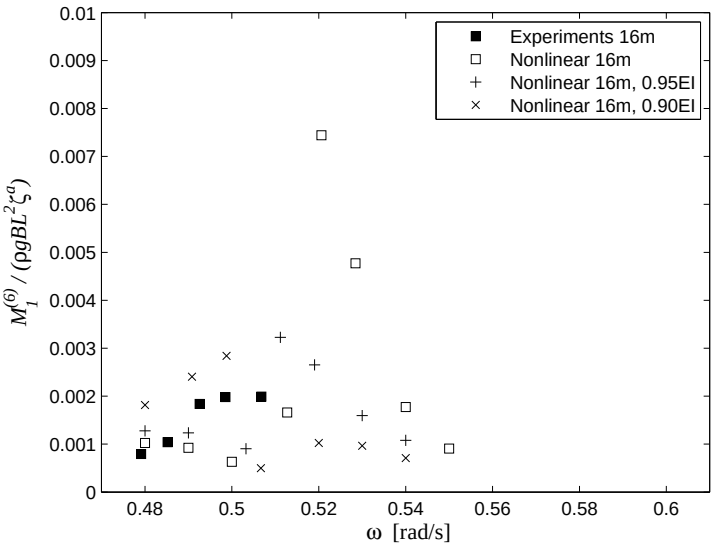

Fig. 18. QL 6^{th} order vertical bending moment RAO for U=5kn. 0.95EI and 0.90EI means that 95% and 90% of the original stiffness, respectively, has been used in the numerical calculations.

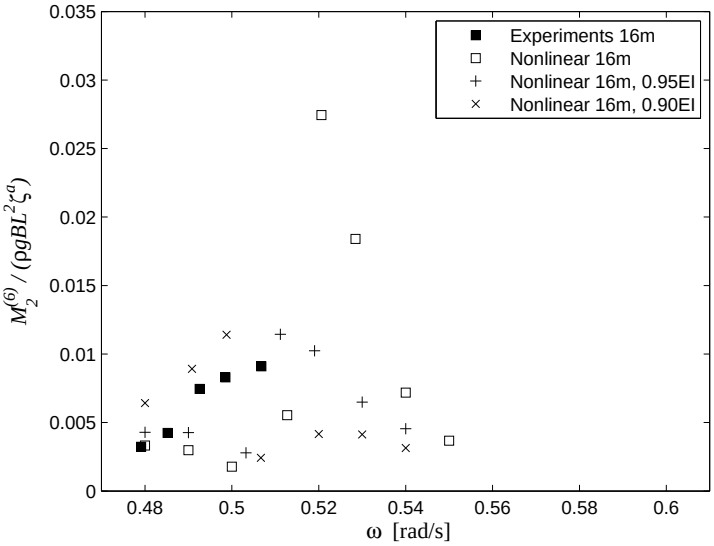

Fig. 19. MS 6^{th} order vertical bending moment RAO for U=5kn. 0.95EI and 0.90EI means that 95% and 90% of the original stiffness, respectively, has been used in the numerical calculations.

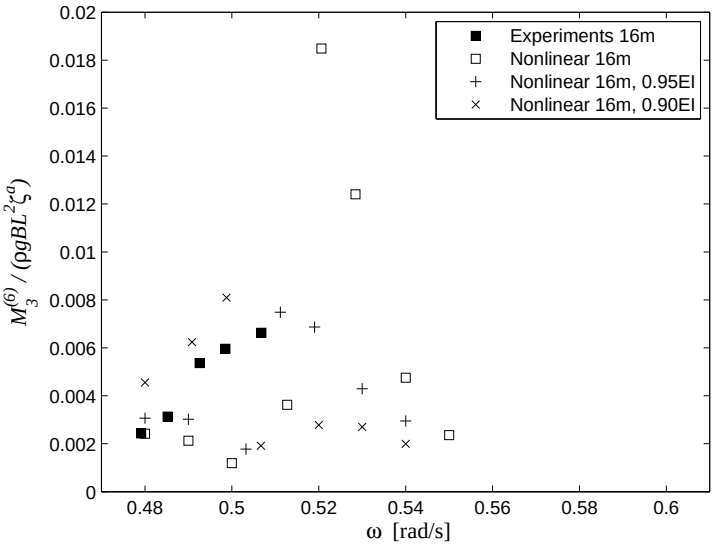

Fig. 20. 3QL 6^{th} order vertical bending moment RAO for U=5kn. 0.95EI and 0.90EI means that 95% and 90% of the original stiffness, respectively, has been used in the numerical calculations.

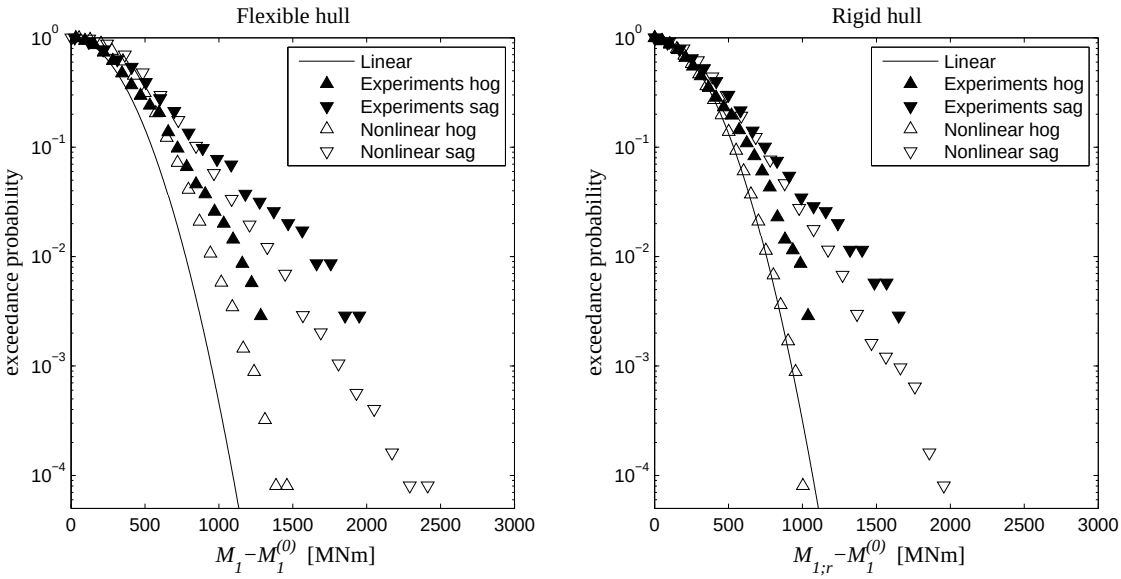

Fig. 21. Probablility distribution of the QL vertical bending moment, H_s=8m, T_p=12.57s, γ=1 and U=15kn.

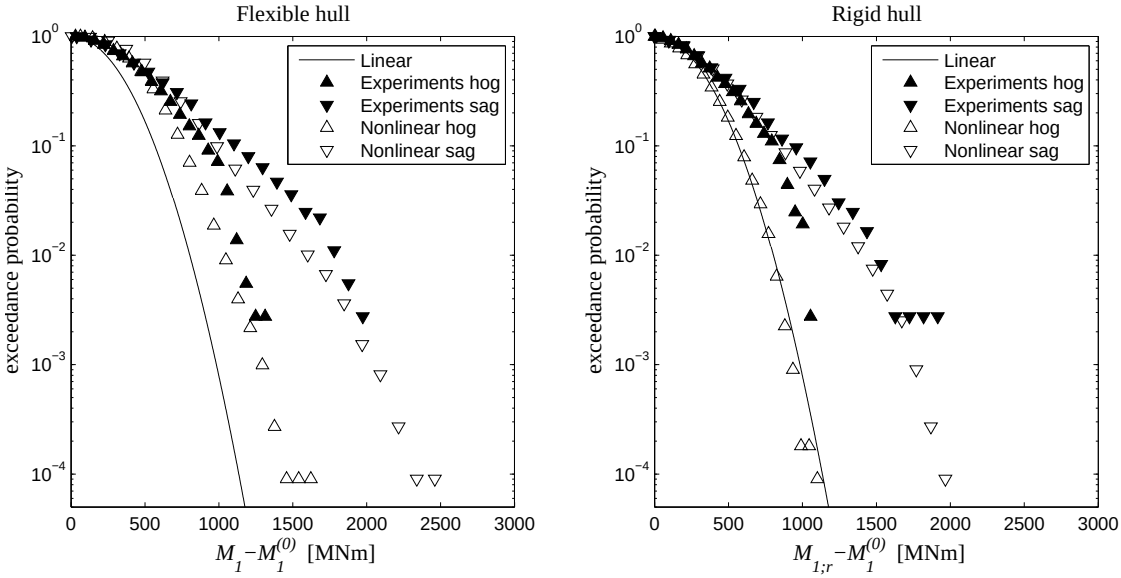

Fig. 22. Probablility distribution of the QL vertical bending moment, H_s=10m, T_p=12.35s, γ=1 and U=8kn.

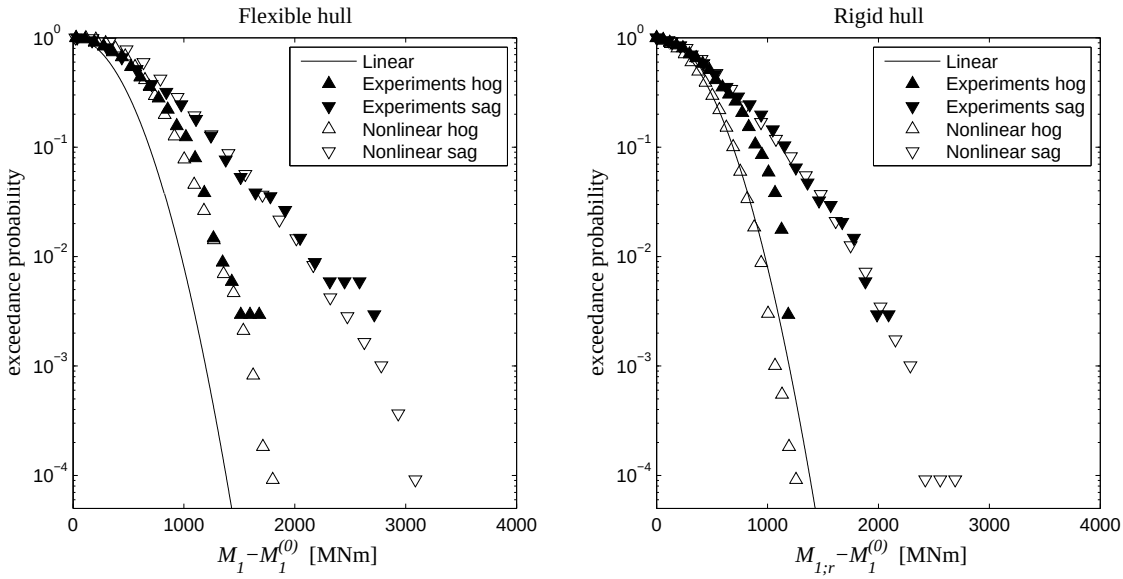

Fig. 23. Probablility distribution of the QL vertical bending moment, H_s=12m, T_p=12.57s, γ=1 and U=8kn.

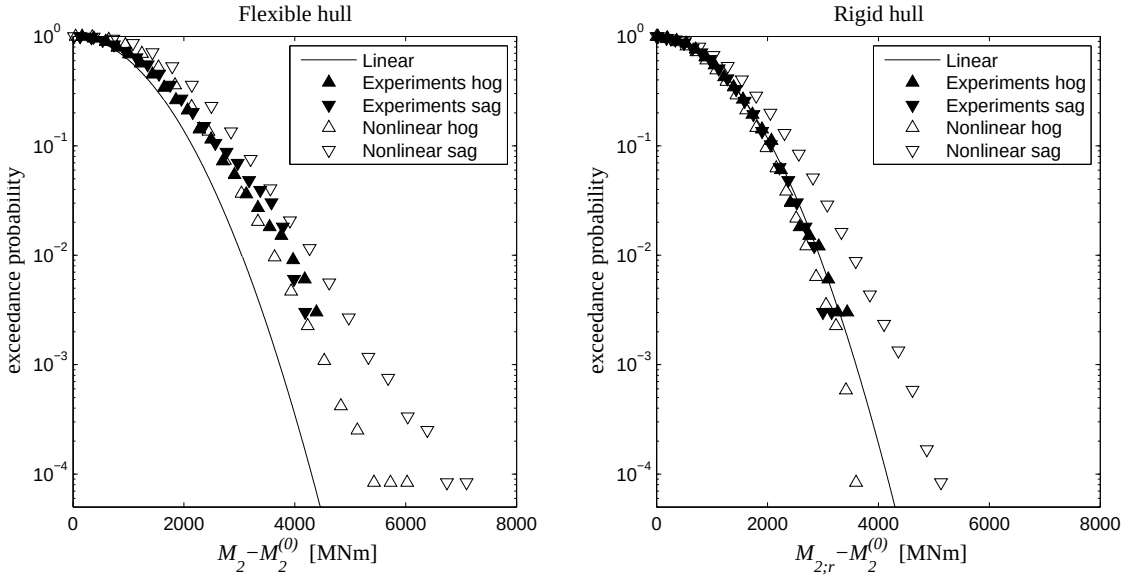

Fig. 24. Probablility distribution of the MS vertical bending moment, H_s=8m, T_p=12.57s, γ=1 and U=15kn.

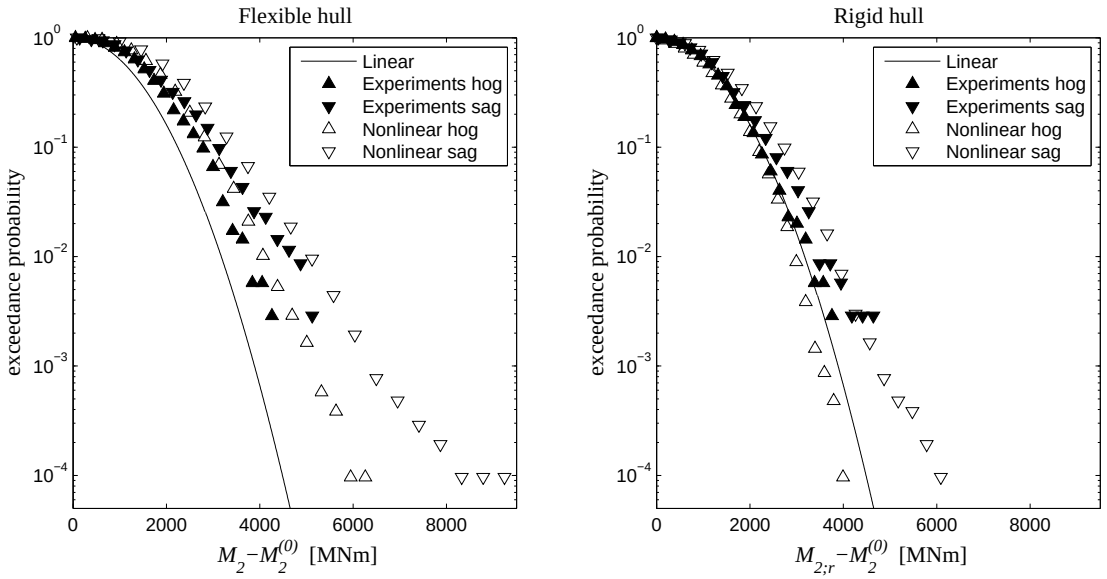

Fig. 25. Probablility distribution of the MS vertical bending moment, H_s=10m, T_p=12.35s, γ=1 and U=8kn.

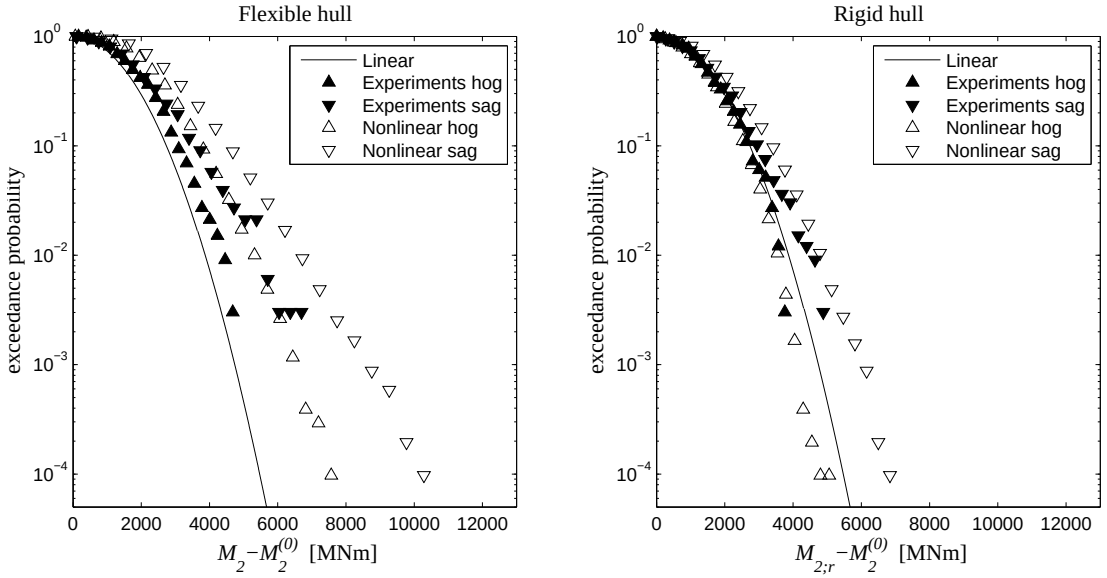

Fig. 26. Probablility distribution of the MS vertical bending moment, H_s=12m, T_p=12.57s, γ=1 and U=8kn.

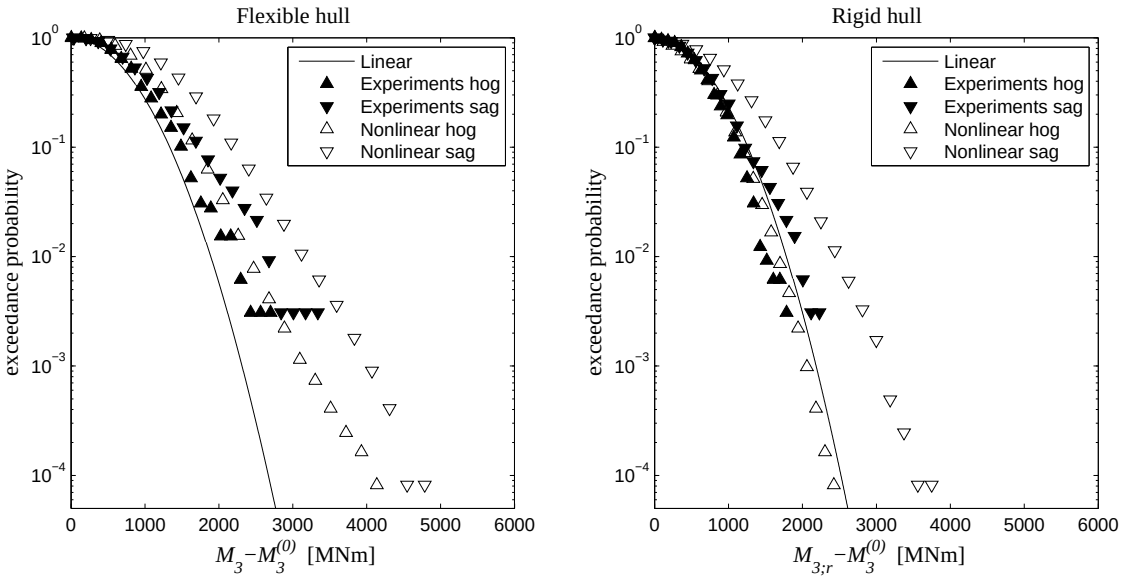

Fig. 27. Probablility distribution of the 3QL vertical bending moment, H_s=8m, T_p=12.57s, γ=1 and U=15kn.

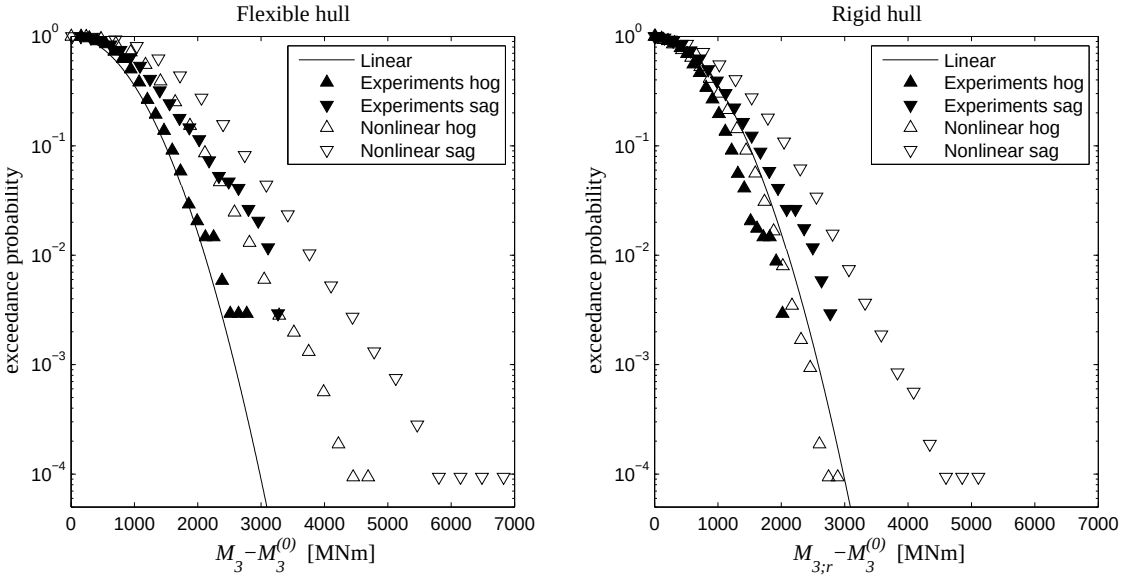

Fig. 28. Probablility distribution of the 3QL vertical bending moment, H_s=10m, T_p=12.35s, γ=1 and U=8kn.

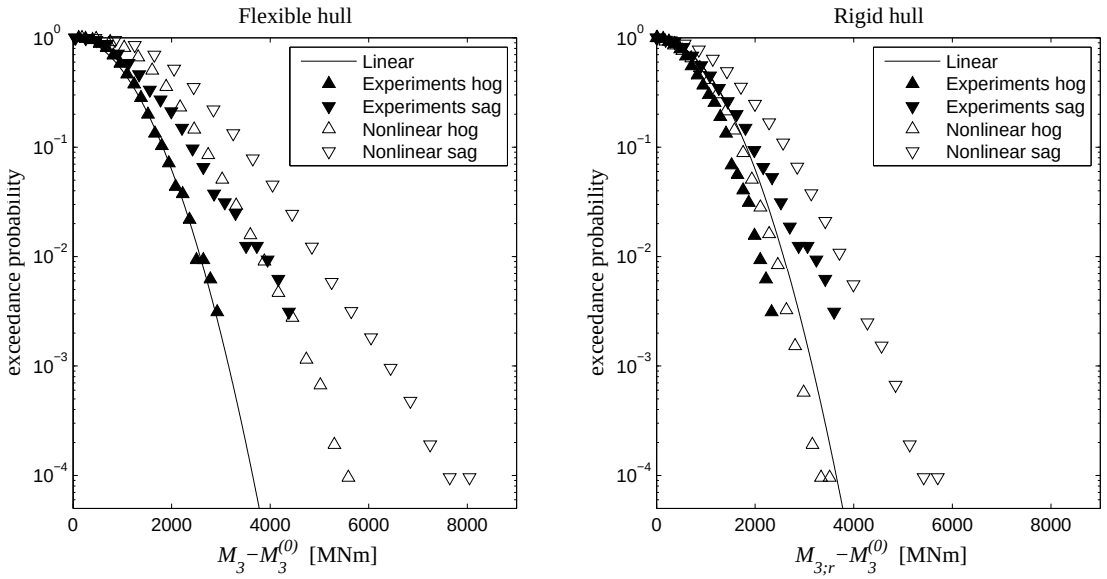

Fig. 29. Probablility distribution of the 3QL vertical bending moment, H_s=12m, T_p=12.57s, γ=1 and U=8kn.

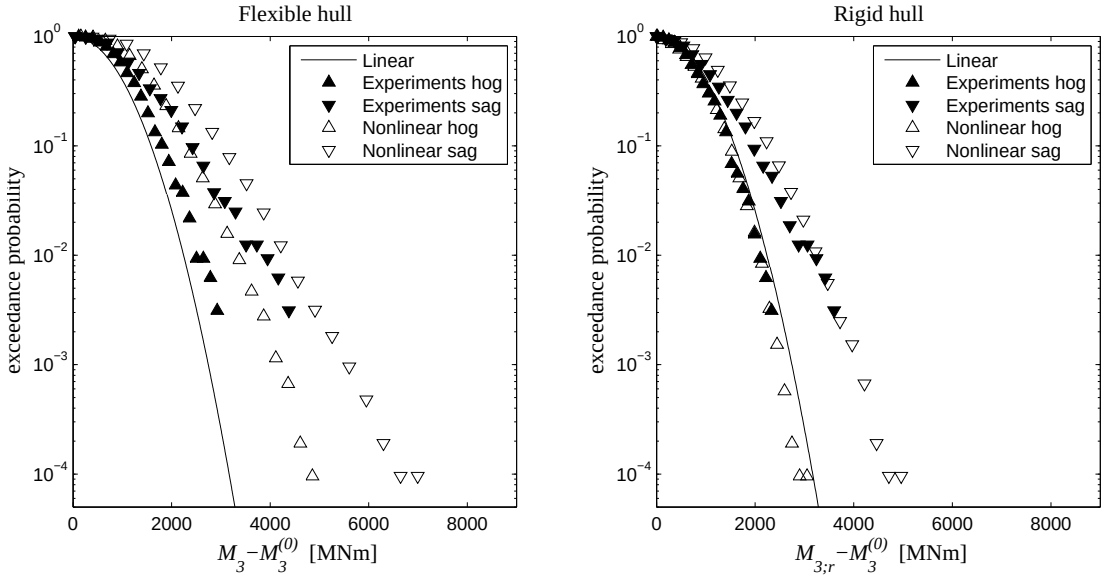

Fig. 30. Probablility distribution of the 3QL vertical bending moment, H_s=12m, T_p=12.57s, γ=1 and U=8kn. Numerical results are divided by 1.15.

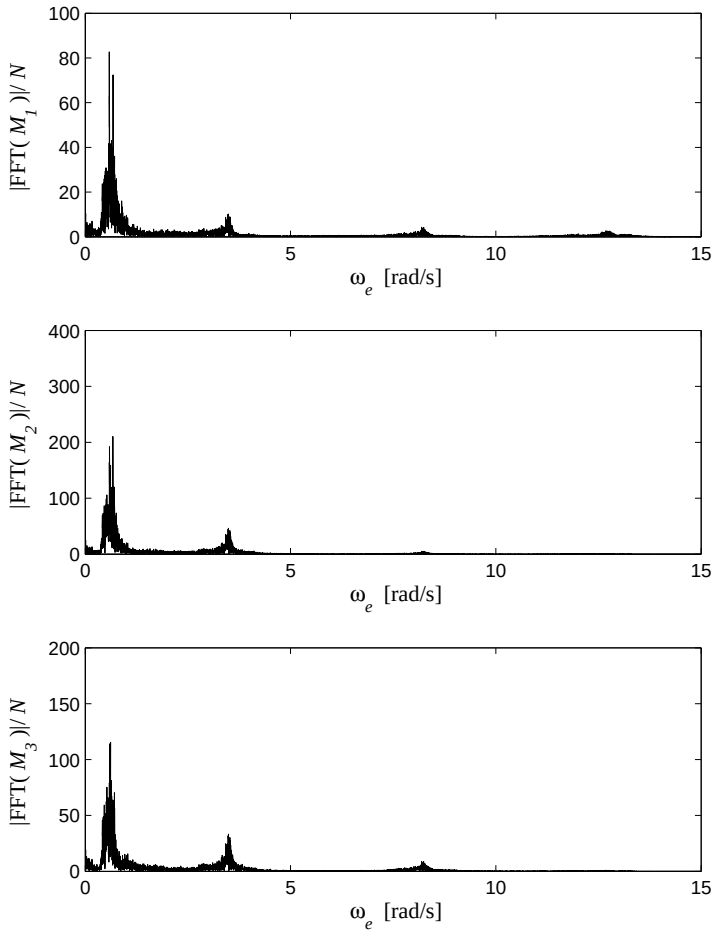

Fig. 31. Absolute value of the fast Fourier transform of the vertical bending moment in the three different cuts for sea state i3, normalised by the number of data points N.

Table 1
Main particulars of the full scale vessel

Main particular	
Length overall	294.01m
Length between perpendiculars	280.98m
Beam	32.26m
Draft design	10.78m
Draft used in model tests	11.75m
Trim used in model tests	0.0m
Displacement (draft = 11.75m)	76656ton
Block coefficient	0.71
Maximum Service Speed	23kn
Natural freq. 2 node vibration	3.51rad/s

Table 2
Test program for regular waves

Wave denotation	H [m]	T [s]	U [kn]		H [m]	T [s]	U [kn]
r1	4	11.86	23	r16	2	13	5
r2	4	12.35	23	r17	2	14	5
r3	4	12.57	23	r18	2	17	5
r4	4	12.82	23	r19	2	20	5
r5	4	13.09	23	r20	16	11.86	5
r6	4	14.96	23	r21	16	12.35	5
r7	4	15.71	23	r22	16	12.57	5
r8	4	17.95	23	r23	16	12.72	5
r9	8	11.86	23	r24	16	12.90	5
r10	8	12.35	23	r25	16	13.09	5
r11	8	12.57	23	r26	6	12.72	5
r12	8	13.09	23	r27	12	12.72	5
r13	2	9	5	r28	20	12.72	5
r14	2	10.50	5	r29	24	12.72	5
r15	2	12	5				

Table 3
Test program for irregular waves

Sea state	H_s [m]	T_p [s]	γ	U [kn]
i1	8	12.57	1	15
i2	10	12.35	1	8
i3	12	12.57	1	8

Table 4
Mean and 95% confidence interval of the mean damping ratios of the first three vertical vibration modes, in water in%. Method 1 refers to the free-vibration decay method, Method 2 to the envelope fitting method

	Two node	Three node	Four node
Method 1	0.62 ± 0.04	0.31 ± 0.03	0.44 ± 0.05
Method 2	0.65 ± 0.05	0.34 ± 0.03	0.47 ± 0.06

Table 5
Still-water results of the vertical responses

	$M_1^{(0)}$ [MNm]	$M_2^{(0)}$ [MNm]	$M_3^{(0)}$ [MNm]	$\eta_3^{(0)}$ [m]	$\eta_5^{(0)}$ [deg]
5kn	-2*	-8*	-12*	0.07*	0.06*
15kn	-21	-76	-126	-0.023*	0.04*
23kn	-64	-151	-269	-0.35	-0.11*

*) the measured value is prone to relative large uncertainties due to the fact that the absolute value is small, and hence easily influenced by external factors

Table 6
Uncertainty in values of the peak of the fourth order vertical bending moment RAOs due to difference between the measured and the requested wave heights. The values are given for the original stiffness distribution

$2\zeta^a$ [m]	$M_1^{(4)}/\zeta^a$ [MNm/m]	$M_2^{(4)}/\zeta^a$ [MNm/m]	$M_3^{(4)}/\zeta^a$ [MNm/m]
8	97	363	243
8.45	119	446	299

Table 7
Mean value and 95% confidence interval of the mean value of the ratio of the amplitude of the first harmonic of the vertical bending moment and that of the wave elevation

Wave	H [m]	T [s]	U [kn]	$M_1^{(1)}/\zeta^a$ [MNm/m]	$M_2^{(1)}/\zeta^a$ [MNm/m]	$M_3^{(1)}/\zeta^a$ [MNm/m]
r2	4	11.86	23	219 ± 4	801 ± 20	438 ± 22
r14	2	10.50	5	120 ± 5	366 ± 10	54 ± 3
r15	2	12	5	93 ± 1	393 ± 8	316 ± 8
r16	2	13	5	124 ± 1	564 ± 4	377 ± 3
r17	2	14	5	128 ± 2	549 ± 15	389 ± 10
r18	2	17	5	92 ± 1	395 ± 9	295 ± 7
r27	12	12.72	5	196 ± 7	638 ± 25	405 ± 17

Table 8
Mean value and 95% confidence interval of the mean value of the ratio of the amplitude of the fourth and sixth harmonic of the vertical bending moments and that of the first harmonic of the wave elevation. Fourth for r2 and sixth for r27

Wave	H [m]	T [s]	U [kn]	$M_1^{(4/6)}/\zeta^a$ [MNm/m]	$M_2^{(4/6)}/\zeta^a$ [MNm/m]	$M_3^{(4/6)}/\zeta^a$ [MNm/m]
r2	4	11.86	23	56 ± 5	207 ± 8	145 ± 11
r27	12	12.72	5	31 ± 1	127 ± 2	92 ± 2

Table 9
Mean value and 95% confidence interval of the mean value of the ratio of the amplitude of the first harmonic of the heave and pitch motion and that of the wave elevation

Wave	H [m]	T [s]	U [kn]	$\eta_3^{(1)}/\zeta^a$ [m/m]	$\eta_5^{(1)}/\zeta^a$ [deg/m]
r2	4	11.86	23	0.43 ± 0.03	0.45 ± 0.01
r27	12	12.72	5	0.10 ± 0.004	0.39 ± 0.02

Table 10
Sensitivity of the peak value of the linear rigid body 23kn vertical bending moment RAO to the location of the cut

Cross section used for calculations	$M_1^{(1)}/\zeta^a$ [MNm/m]	$M_2^{(1)}/\zeta^a$ [MNm/m]	$M_3^{(1)}/\zeta^a$ [MNm/m]
base case	231	856	528
3.51m forward of base case	190	847	559
3.51m aft of base case	272	863	497

Paper 2

Experimental and full scale investigation of the importance of fatigue damage due to wave-induced vibration stress in a container vessel

Ingo Drummen, Gaute Storhaug and Torgeir Moan

Transactions Royal Institution of Naval Architects, Conference on Design & Operation of Container Ships. London, UK, pp. 61-74, 2006

Is not included due to copyright

Paper 3

Experimental and numerical investigation of fatigue damage due to wave-induced vibrations in a containership in head seas

Ingo Drummen, Gaute Storhaug and Torgeir Moan

accepted for publication in Journal of Marine Science and Technology

Experimental and Numerical Investigation of Fatigue Damage due to Wave-Induced Vibrations in a Containership in Head Seas

Ingo Drummen, Gaute Storhaug and Torgeir Moan

Abstract Fatigue cracks have been known to occur in welded ships for several decades. For large ocean going ships wave-induced vibrations can, depending on trade and design, cause up to 50% of the fatigue damage. The vibrations may be due to springing and whipping effects. In this paper, we address the fatigue damage caused by wave-induced vibrations in a containership of newer design trading in the North Atlantic. The fatigue damage was obtained both experimentally and numerically. The experimental results were found from tests performed with a flexible model of the ship, while the numerical predictions were done using a nonlinear hydroelastic strip theory. The measurements showed that the wave-induced vibrations contributed approximately 40% to the total fatigue damage. The numerical method predicted the wave frequency damage well, but was found to over-estimate the total fatigue damage by 50%. This is mainly due to an over-prediction of the wave-induced vibrations. The discrepancy is partly related to 3D effects which are not included in the 2D slamming calculation, and partly to an over-prediction of the springing contribution. Moreover, the numerical method does not account for the steady wave due to forward speed. By using a simplified approach we show that the high frequency damage can be significantly reduced by including the steady wave for the relevant vessel, implying better agreement with the experimental results.

Key words Fatigue damage · hydroelastic · experiments · strip theory · containership

Introduction

Towards the end of 2005, the world fleet of fully cellular containerships consisted of 3500 vessels, with a combined capacity of 8 million TEU[1]. As there is almost no limit to the type of commodities that can be transported in a container, the containership market has grown faster than world trade and the economy in general. In order to meet the demand, the dimensions of containerships have increased steadily over the past few decades. Although the development of significantly larger containerships than those in operation today will be limited by aspects such as: a) water depth in ports; b) limiting dimensions of canals and straits on the major world routes, and c) cargo handling facilities in container terminals, it is expected that the trend of increasing dimensions will continue for some years to come.

Fatigue cracks have been known to occur in welded ships for several decades, and with the introduction of higher tensile steels in hull structures the fatigue problem has become more imminent. Fatigue analysis procedures were developed to account for wave frequency loads[2;3]. Also, the phenomenon of springing response occurring when the wave encounter frequency coincides with the first flexural natural frequency of the vessel, was discovered especially for shallow-water inland vessels[4]. Transient dynamic response of ships (whipping) caused by wave slamming is normally associated with extreme loads[5;6], and is particularly relevant in harsh environments such as the North Atlantic. In recent years it has been shown that wave-induced vibrations due to whipping and springing can constitute a considerable part of the fatigue damage in hulls of large ocean going ships. The larger size of containerships implies an increased flexibility, and a larger natural period of the two node vertical vibration mode. As a result the importance of hydroelastic effects such as whipping and springing is increased. Based on full scale measurements on board of an iron ore carrier trading in the North Atlantic, Storhaug et al.[7] showed that the wave-induced vibrations caused 44% of the fatigue damage. For a containership of older design trading in the Pacific this contribution was approximately 50%[8]. The relative importance is, however, dependent on trade[9]. While methods are available for determining the linear wave frequency and high frequency stresses, the challenge is to understand the nonlinear hydrodynamic load mechanisms that can cause high frequency load effects, as well as the damping mechanisms.

Watanabe and Guedes Soares[10] performed a benchmark study by comparing predictions of the vertical wave-induced bending moment in a containership in regular waves of different steepness, by using different nonlinear time-domain computer codes. Most of the methods investigated were based on strip theory formulations applied either to a rigid body or a flexible hull. They showed that the results were consistent with the linear estimates in the lower wave height region. However, the agreement among the computed values became poor when the whipping vibration started to play a significant role. They recommended that experimental data should be used to decide whether nonlinear programs are reliable tools for predicting wave-induced load effects in ships. ISSC[6] presented a comparison between measured and calculated wave bending moments. In this comparison several nonlinear strip theory methods were used. Their general conclusion was that although the methods may give results with sufficient engineering accuracy, the calculated higher harmonics of the response did not comply very well with the measured values. This indicates that the modelling of the

nonlinear effects does not represent the real physics consistently. Further validation of the methods is therefore necessary. Storhaug et al.[7] compared four nonlinear hydroelastic codes with full scale measurements on an iron ore carrier trading in the North Atlantic. One of their conclusions was that the predicted wave-induced vibrations did not capture the measured trend and level for this *blunt* ship.

Second order blunt bow excitation is one of the four hypotheses of possible excitation sources described by Storhaug and Moan[11] to explain the significant vibrations observed from full scale measurements on bulk carriers. In head seas, a blunt bow reflects the incident wave in the opposite direction causing sum frequency effects that do not decay with depth. Storhaug[4] presented the results of an experimental investigation of wave-induced vibrations which increase the fatigue damage in ships.

Because of their slender bow, second order blunt bow excitation is expected to be less relevant in containerships. On the other hand, the unique hull form of these ships - with large, flat and overhanging sterns together with pronounced bow flare - coupled with high service speeds makes whipping an important issue. These high speeds also imply that a significant steady wave will be created by the vessel, which is another hypothesis of Storhaug and Moan[11].

In this paper we will present experimental results of fatigue damage obtained using a four segment flexible model of a containership of newer design. The sea states used in the investigation were representative for North Atlantic trade. The fatigue damage was determined using rainflow counting and the Palmgren-Miner linear cumulative damage rule. These results were used to investigate the importance of wave-induced vibrations for the fatigue damage. Moreover, the experimental results were applied to estimate how accurate current numerical methods are in predicting the total damage in general and the damage due to the wave-induced vibrations in particular. In this comparison the nonlinear hydroelastic strip theory computer code WINSIR[12] was used.

Experimental Setup

The model tests were performed in the towing tank at the Marine Technology Centre in Trondheim. The tank is 260m long, 10.5m wide and from 5.6m to 10m deep. The double flap wave maker is able to produce both regular and irregular waves. The model tested was based on a containership with a length between perpendiculars, L_{pp}, of 281m. It has a large, flat, overhanging stern, a pronounced bowflare and a large bulb. These features are considered to be representative for modern containerships.

The model was built to a scale of 1:45. In order to account for the global hydroelastic effect in the experiments, the model was made of four rigid segments connected by three rotational springs. The springs were located at cuts $0.02L_{pp}$ forward of the quarter lengths and the midships section. The forward quarter length, midships and aft quarter length sections will be denoted as QL-cut, MS-cut and 3QL-cut, respectively. The horizontal forces, which were converted to vertical bending moments as discussed below, were measured $0.036L_{pp}$ forward of these locations. These sections will be respectively denoted as QL-cut^m, MS-cut^m and 3QL-cut^m. All three springs had equal stiffness, tuned to give the correct Froude scaled natural frequency of the two node vertical vibration, 23.55rad/s (0.56Hz, full scale). The natural frequencies of the three and four node vertical vibration modes were approximately equal to 55rad/s and 86rad/s respectively.

We attempted to model one of the mass distributions from the loading manual of the vessel. However, due to the high mass of the springs it was not possible to obtain this mass distribution in the model. More detailed information about the experimental setup was given by Drummen[13].

The rigid body motions were measured using an optical system, while capacitive strips and wave probes measured the relative motion and the wave elevation. Force transducers, measuring the horizontal force, were mounted in the three cuts. The force transducers were placed above the neutral axis of the model. In this way, the horizontal force was a measure for the vertical bending moment, see Eq. 3. Full scale measurements, on the same containership for which the model tests were performed, presented by Storhaug and Moe[14] showed that the stress from the axial force (horizontal force at the neutral axis) had the same period as the wave frequency part of the vertical bending stress and that the two were approximately inphase. The axial force at midships contributed a stress of up to approximately 10% of that due to the vertical bending moment. This means that the midships wave frequency stresses presented in this paper can be up to 10% too high. The effect is expected to be somewhat larger in the quarter length cuts. This issue is investigated in more detail in the subsequent discussion.

The model was tested in irregular head waves, as this condition usually is the most severe condition with respect to the vertical response. The sea states were taken from the North Atlantic scatter diagram[15]. The chosen sea states are given in Table 1. These represent approximately 17% of the total number of sea states in the scatter diagram. Based on this, it was possible to determine the damage in 33 other sea states by means of interpolation. In this way 57% of the scatter diagram was represented in the experiments. The sea states outside this area in the scatter diagram make only a small contribution to the fatigue damage. This contribution was estimated by a linear analysis to be approximately 10%. The JONSWAP spectrum was used as target wave spectrum[15]. The spectral density function is:

$$S_\zeta(\omega) = \alpha g^2 \omega^{-5} exp\left[-\frac{5}{4}\left(\frac{\omega}{\omega_p}\right)^{-4}\right]\gamma^{exp\left[-0.5\left(\frac{\omega-\omega_p}{\sigma\omega_p}\right)^2\right]} \quad (1)$$

where

$$\alpha = \frac{5}{16}\frac{H_s^2\omega_p^4}{g^2}(1-0.287\ln\gamma)$$

$$\sigma = \begin{cases} 0.07 & \text{if} \quad \omega \le \omega_p \\ 0.09 & \text{if} \quad \omega > \omega_p \end{cases}$$

and ω is the wave frequency, ω_p is the peak frequency and g is the acceleration of gravity. The peakedness parameter, γ, was found by iteration using the significant wave height, H_s, and the average zero crossing period, T_z, from the scatter diagram, and the relations presented in DNV CN 30.5[15].

The forward speed was chosen constant in sea states with the same significant wave height, and was based on full scale measurements reported by Moe et al.[8]. The full scale forward speeds of the model in the investigated sea states are given in Table 1.

For each sea state, three runs were conducted in waves that were realisations of the same spectrum. The realisation periods were short enough to avoid repeating wave trains. The combination of the three runs resulted in a record length between 30 and 45 minutes full scale, depending on the chosen speed.

Fatigue Damage

The fatigue damage was calculated using the Miner-Palmgren linear cumulative damage rule:

$$D = \sum_{i=1}^{n} \frac{1}{\overline{a}_i} (\Delta\sigma_i)^{m_i} \tag{2}$$

where D is the accumulated fatigue damage, $\overline{a}_i$ and m_i are the parameters of the SN-curve, n is the total number of stress ranges and $\Delta\sigma_i$ is the stress range. The parameters $\overline{a}_i$ and m_i were taken from DNV CN 30.7[3], using a two slope SN-curve for welded joints in air or with cathodic protection. This means that:

$$\begin{aligned} \log \overline{a_i} &= 12.65 \text{ and } m_i = 3 \text{ for } \Delta\sigma_i \geq 76.5\text{MPa} \\ \log \overline{a_i} &= 16.42 \text{ and } m_i = 5 \text{ for } \Delta\sigma_i < 76.5\text{MPa}. \end{aligned}$$

By neglecting the axial force, the measured horizontal force, F_x, was converted into full scale stresses for a deck detail assuming a simple beam model:

$$\sigma = \frac{F_x h}{W} \cdot 1.025 \cdot \Lambda^4 \cdot K \tag{3}$$

where h is the vertical distance between the neutral axis and the force transducer and Λ represents the scale factor. K is the notch stress concentration factor, taken to be 2.0 for a typical hot spot of a fatigue sensitive deck detail and 1.025 is the ratio of the density of salt water and fresh water. Using the program Nauticus Hull[16], the section moduli at the deck, W, for the forward, midships and aft cuts were found to be $27.4m^3$, $30m^3$ and $30m^3$ respectively. The stress cycles were counted using WAFO, a Matlab toolbox for statistical analysis and simulation of random waves and random loads, developed at the Centre for Mathematical Sciences at Lund University in Sweden. The rainflow counting method used herein is based on the algorithm described by Rychlik[17].

The fatigue damage can be separated in three categories. The total damage denotes the damage due to the total stress history. Similarly, the wave frequency (WF) damage denotes the fatigue damage due to the wave frequency stresses. The latter was found by band pass filtering the stress signal to include only energy at frequencies in the wave frequency range. The full scale upper cut-off frequency was 2.5rad/s (0.4Hz). By high pass filtering the original signal using this frequency as a lower cut-off frequency, the high frequency (HF) part of the stress was obtained. The HF damage was found as the difference between the total damage and the WF damage. To determine the increase of the fatigue damage due to the HF stress by considering the HF stress only, is non-conservative due to the nonlinear dependence of the damage on the stress (Eq. 2). This is illustrated amongst others by Storhaug et al.[9] Wave-induced vibrations or simply vibrations is used in the following to denote the vibrations that cause the high frequency stress process.

Common practice in offshore engineering is to assume that the residual stresses, introduced during fabrication at welds, are close to the yield stress in tension. However, external loads on ships cause these residual stresses to be reduced over time. This implies that it could be possible that part of the stress cycle is in compression, implying that the effective stress range is smaller. There are, however, three other important contributions to the mean stress: a) still-water loads induced due to the weight distribution and buoyancy of the ship without forward speed; b) loads due to the steady flow resulting from the forward speed, and c) asymmetry in the dynamic wave loading. In still-water without forward speed, containerships mainly operate in hogging conditions. The steady flow due to the forward speed results in a vertical sagging bending moment in the hull[18]. The asymmetry in dynamic wave loading is of particular importance in containerships for which the difference between sagging and hogging bending moments is generally larger than for other ship types due to more pronounced nonlinearities. This difference introduces a non-zero (sagging) mean in the dynamic wave loading. In general, however, the latter two contributions are significantly smaller than that due to the weight distribution and the buoyancy of the ship. Moreover, for sea states important for fatigue, the dynamic loads will be smaller than the static loads. For these reasons it is expected that the complete stress cycle for a deck detail is in tension, which means that the full stress cycle should be considered effective. This statement will be quantified in the section presenting the fatigue damage obtained experimentally.

Experimental Results

General

This section deals with the experimental data and their analysis. The results are scaled and presented for the full scale vessel. The zero-level of the experimental responses was taken to be the model in static equilibrium in still-water, without any speed. Since damping is of particular importance for the high frequency fatigue damage, the damping ratio obtained in the model tests will be covered first. Subsequently, the standard deviations of the

measured stress histories are presented.

Damping Ratio

Decay tests were performed to determine the damping ratios in still-water without forward speed. The natural modes were excited by applying an impulsive force. This method should in general give vibration in all three flexible modes. The damping ratios were determined by means of the force transducer at midships, and were found to be approximately equal to 0.65%, 0.32% and 0.45% for the two, three and four node vibration, respectively. Decay tests were also performed with the model in air. For the two node mode, the natural frequency was found to be 32.2rad/s (model scale) and the damping ratio was estimated to be 0.2%. More details about the damping ratios and the methods of estimation were presented by Drummen[13].

In order to minimise the uncertainty in the comparison between experimental and numerical results, the damping ratio discussed above was used as input for the simulations. However, when the results from the model tests are used to make statements about the full scale vessel, it is important to relate the damping ratio of the model to that of the full scale vessel.

From full scale measurements on containerships, Drummen et al.[19] and Storhaug and Moe[14] found damping ratios of the two node flexural mode significantly higher than the value of 0.65% presented here. The damping ratio found by full scale measurements is influenced by the cargo system, container racks, etc. These influences on the damping ratio should be investigated. So further study is necessary, particularly because the methods to estimate damping under in-service conditions are prone to large uncertainties. In the subsequent discussion some results are presented showing the sensitivity of the high frequency damage to the damping ratio.

Stresses

The standard deviations of the measured stress histories (Std σ) are shown in Figs. 1-3. Due to differences between the requested and the measured wave, the peak periods given in the figures might not be exactly the same as those provided in Table 1. The peak periods are those found from the measured wave spectrum. The stresses given in these plots are calculated using Eq. 3 and thus *include a stress concentration factor of two.*

suggested location Figs. 1-3

The figures show, as expected, that the standard deviation of the WF stress reflects the shape of the response amplitude operator of the vertical bending moment. The latter has its peak around 15s for the lowest significant wave height and 13s for the highest. Accounting for vessel speed, this implies an encounter period of approximately 10s for all wave heights. The encounter frequency, ω_e, is related to the wave frequency, ω, by:

$$\omega_e = \omega + \omega^2 \frac{U}{g}. \tag{4}$$

The standard deviation of the HF stress shows a clear decreasing trend with increasing peak period. Whether the vibration is springing or whipping is not possible to decide based on these results. There is a small peak in the HF stress for the two highest wave heights around 13s to 14s. This could be related to whipping, since the relative motion has a peak at approximately this period.

Springing is considered as the steady-state resonant vibration of the two node flexural mode due to continuous wave loading. Linear springing is said to occur when n=1 in Eq. 5, nonlinear springing when n is larger than one.

$$n\omega_e = \omega_s \tag{5}$$

where ω_e is the encounter frequency and ω_s is the wet natural frequency of the two node vertical vibration mode. Springing could of course also be related to the three or four node flexible mode. Due the high natural frequencies of these modes, this is, however, not very likely to happen. Whipping is transient elastic vibration of the ship hull girder caused for example by slamming. Because of small damping, the decay of whipping-induced responses is slow. Springing and whipping may therefore be difficult to distinguish if slamming occurs frequently.

Furthermore, Figs. 1-3 show that the WF stress is close to the total one. This means that the effect of springing and whipping on the total standard deviation stress in these sea states is generally small. Depending on period and wave height, the increase of the WF stress due to vibration is up to 15% for all three sections. The overall trend in the stress shown in Figs. 1-3 is quite similar. The only obvious difference is the magnitude, which is largest at midships and smallest at the forward quarter length.

Less visible from Figs. 1-3 is the effect of nonlinearities on the standard deviation of the wave frequency stress. This feature will be illustrated by using the ratio, α, of the standard deviation of the stress histories, σ_1 and σ_2, in two sea states with the same peak period but different wave heights, $H_{s;1}$ and $H_{s;2}$ respectively, thus:

$$\alpha = \frac{\text{Std } \sigma_1}{\text{Std } \sigma_2}.$$

When the stresses are obtained using linear theory, the ratio is denoted as α_l. If the forward speed in both sea states are equal then:

$$\alpha_l = \frac{H_{s;1}}{H_{s;2}} \quad \text{where} \quad H_{s;1} > H_{s;2}$$

However, due to the reduction in speed with increasing wave height (see Table 1), α_l is somewhat less than the ratio of the two wave heights. Linear theory also predicts that α_l increases from bow to stern, although this increase is small. Since 16 sea states were investigated a number of α_l's can be calculated. In general, the α's found experimentally for the midships section were approximately the same as those found for the aft section, and both were generally close (within 5%) to the α_l's. For the forward cut, the α's were higher than those in the other two cuts, and up to 20% higher than the α_l's.

This comparison shows that, at least for the sea states considered here, the nonlinear effects on the wave frequency part of the vertical bending moments in the midships and the aft sections were quite small, compared to the effects in the forward cut. This conclusion is supported by Drummen et al.[18] who, for the same vessel, reported that the wave frequency part of the midships vertical bending moment showed almost no nonlinearities for a sea state with a significant wave height of 8m and a peak period of 12.6s, while modest nonlinearities were present in the vertical bending moment in the aft cut. The bending moment in the forward cut, on the other hand, showed considerable nonlinear effects in this sea state. Also Fonseca and Guedes Soares[20;21], who performed tests using a model the ITTC S-175 containership, concluded that nonlinearities affecting the vertical bending moment were more important in the bow area than at midships. The nonlinear behaviour in the bow area may be explained by the shape of the bow and the fact that it is subjected to the largest relative motions. When the ship sides are vertical, the vertical force is approximately linear with the relative motion between the hull and the waves. When there is a bow flare, the vertical force becomes nonlinear.

The α's found for the wave frequency stresses can also be compared with those obtained from experimental high frequency stresses. This showed that the α's for the HF stress were approximately 10% to 15% higher than the similar α's for the WF stress. This means that *the HF stress was more affected by nonlinearities than the WF stress.*

Fatigue Damage

As mentioned above, three runs were conducted for each sea state in Table 1. This resulted in a total time series of 30 to 45 minutes full scale for each sea state. The damage per sea state was calculated using rainflow counting and Eq. 2. Subsequently, this was converted into the half hour damage $D_{HH;kl}$, for a sea state with significant wave height k and peak period l. The results are presented in Figs. 4-6. The reason why the standard deviation of the HF stress in general shows a decreasing trend, while this is not the case for the HF damage, is due to the fact that the HF damage is found from the difference of the total damage and the WF damage, and not from the HF stress.

suggested location Figs. 4-6

The figures show that the WF damage is generally larger than the HF damage. It is also seen that the ratio of the HF and the WF damages tends to be larger for higher sea states. The reason for this is that the HF stress was more influenced by nonlinearities than the WF stress. Due to the power m_i in Eq. 2 this influence is however more obvious in Figs. 4-6 than in Figs. 1-3.

The results presented above represent the fatigue damage during 30 minutes in a particular sea state. By using the North Atlantic scatter diagram and assuming a total lifetime of 20 years of which the vessel will spend 2/3 of the time at sea and in head seas, it is possible to calculate the total time the vessel will be in a certain sea state during its lifetime. By combining this time with the half hour damage from Figs. 4-6 the lifetime damage, D_{kl}, for a sea state with significant wave height k and peak period l is easily found from:

$$D_{kl} = 2 \cdot D_{HH;kl} \cdot T \cdot p_{kl} \tag{6}$$

where p_{kl} is the probability of occurrence of a sea state with significant wave height k and peak period l, found from the scatter diagram. T denotes the total time at sea in hours. The factor 2 in the equation is introduced to convert half hour damage into damage per hour.

Figs. 7-9 show the contour plots of the lifetime fatigue damage. It is seen that the main wave and high frequency damage occur for sea states with a peak period of around 14s and a significant wave height between 5m and 7m. The "hot spot" area for fatigue damage in the scatter diagram is the same for both the wave and the high frequency damage. This is a result of the fact that the high frequency damage is not directly determined from the high frequency stresses, but from the difference between the total and the wave frequency damage. The figures furthermore show that the forward cut has its hot spot area closer to 7m than to 5m, in contrast to the midships and the aft cut. This is due to the nonlinear effect which is most pronounced in the bow segment. These figures also show that the fatigue damage varies gradually with the significant wave height and the peak period. This indicates that that using interpolation of the fatigue damage between different sea states is a reasonable approach.

suggested location Figs. 7-9

Figs. 7-9 present results for 16 sea states selected from the North Atlantic scatter diagram. These were extended to 49 sea states by using interpolation. The lifetime fatigue damage, D_L, can then be calculated from:

$$D_L = T \cdot \sum_k \sum_l p_{kl} \cdot 2 \cdot D_{HH;kl} \tag{7}$$

The results are given in Table 2. The presented damages are divided by the midships WF damage. The table shows that the HF damage represents around 40% of the total fatigue damage. This percentage is similar to the one found from approximately three years of full scale measurements on an iron ore carrier[8], even though the excitation sources differ considerably. The global vibration of blunt ships is generally dominated by springing, while this is whipping for slender ships such as containerships. Using one year of full scale measurements, Aalberts and Nieuwenhuijs[22] found a contribution of 25% for a small container vessel.

It is furthermore observed that the contribution of the HF damage to the total fatigue damage increases somewhat from bow to stern and is thus highest at the aft quarter length. The damage in the forward cut is negligible compared to the damage in the midships section, while the damage in the aft cut is about 25% of this value. The

large difference between the damages in the forward and aft cuts is related to the location of the cuts. This issue is investigated in the discussion.

The high frequency damage given in Table 2 includes the damage resulting from the two, three and four node flexural vibration. By increasing the upper cut-off frequency of the band pass filter from 2.5rad/s to 6rad/s, the WF stress will include the wave frequency stress as well as the stress caused by the two node vibrations, and the HF stress only includes the contribution of the three and four node vibration. Then, by following the same procedure as presented above, the three and four node vibrations were found to contribute 5% to the total damage in the forward part, less than 1% in the midships section and approximately 2% in the aft part.

Fig. 8 shows that the sea state with a significant wave height of 5m and a peak period of 13.4s contributes most to the fatigue damage of the hull. For this sea state, it will be shown that the mean stress effect can be disregarded and that the full stress cycle should be considered effective. For the loading condition used the still-water midships bending moment is equal to 2425MNm. This gives a stress at deck of approximately 81MPa, which is tension as the vessel operates in hogging in still-water. After inclusion of the stress concentration factor this becomes 162MPa. From the experimental data, the mean stress, due to both forward speed and asymmetries in the dynamic wave loading, was found to be approximately equal to 11MPa, which is sagging and includes the stress concentration factor. The mean hogging stress is thus 151MPa. Fig. 2 shows that the standard deviation of the stress was about 48MPa in this sea state. Even by neglecting possible tensile residual stresses the above facts imply that only 1% of the total number of stress ranges will, according to linear theory, be partly in compression. Thus it is clear that the full stress cycles should be considered effective.

Numerical Analysis and Comparison with Experimental Results

General

In this section numerical predictions of the stresses and fatigue damage will be presented and compared with the experimental ones. The simulations were performed with the nonlinear hybrid hydroelastic strip theory code presented by Wu and Moan[12]. In order to remove any statistical uncertainty between the numerical and the experimental results, the wave elevation measured by the wave probe in front of the towing carriage was used as input for the time domain simulations. The wave measured by this probe is the most relevant one for describing the wave condition in front of the test model. Using Airy wave theory, the measured wave was transformed to the location of the centre of gravity of the model. The measured mass distribution of the model was used as input for the simulations. As the stiffness of the model was not continuous, the stiffness distribution of the segmented model has been used. In order to account for the effect of the forward speed, the draft of the vessel was slightly modified to account for sinkage and trim. An overview of the steady responses of the model was given by Drummen et al.[18] Three global flexible modes were taken into account in the calculations. In order to minimise the uncertainty in the comparison between experimental and numerical results, the input for the numerical predictions can be summarised as follows:

- the measured time series of the wave elevation;
- the measured mass distribution;
- a segmented stiffness distribution;
- the measured dry structural damping ratio;
- a modified draft, to account for steady response;
- three global flexible modes.

The nonlinearities in the vertical motions and cross-sectional load effects in the computer code are introduced in the form of a nonlinear vertical excitation force. In this way the relationship between the ship motions or the load effects and the excitation force can remain linear, while the the excitation force is no longer linearly related to the incident wave. The total nonlinear excitation force, $f(t)$, consists of a linear part, $f_l(t)$, and a nonlinear modification part, $f_{nm}(t)$:

$$f(t) = f_l(t) + f_{nm}(t) \tag{8}$$

Similarly the response is decomposed. The linear part is evaluated by using 2D or 2.5D strip theory. The nonlinear modification part is obtained as the convolution of the linear impulse response function and the nonlinear modification force. The nonlinearities considered are the slamming impact force, the nonlinear incident wave force and the nonlinear hydrostatic restoring force. The numerical method does, however, not account for the quadratic velocity term in Bernoulli's equation for the fluid pressure. Furthermore, the code only calculates a first order velocity potential. It is thus not able to produce a second order pressure field which, under certain conditions, oscillates with the sum-frequency and does not decay with depth. These two features may cause nonlinear springing.

The damping used for the calculation of the impulse response function includes the internal structural damping and the linear potential hydrodynamic damping. The structural damping has to be given as input to the program. In this case 0.2% was used. It has been verified that a structural damping ratio of 0.2% leads to a total, i.e structural and hydrodynamical, damping of approximately 0.6%. The influences of viscous effects associated with relative motion[23] and forward speed on the damping ratio are, however, not or not fully accounted for by the numerical method. More details about the method are described in Wu and Moan[12;24] and Wu and Hermundstad[25].

Stresses

The standard deviation of the stresses resulting from the simulations are given in Figs. 10-12.

suggested location Figs. 10-12

These figures show a strong resemblance with Figs. 1-3. The standard deviation of the wave frequency stress shows the same trend as the experimental values, with a peak in general around 15s. The trend of the high frequency stress is also quite similar to the trend found experimentally. As described above, the total calculated nonlinear response is the sum of a linear part and a nonlinear modification part. For the HF stress, these two contributions are also shown in the figures. The linear part and the nonlinear modification part of the high frequency stress are denoted as 'HFl' and 'HFnm', respectively. The linear HF stress is solely due to linear springing. Slamming is only one feature of the nonlinear modification part of the HF stress, nonlinear springing (see Eq. 5) is another. It should be noted that, although the nonlinear effects accounted for in the numerical method may cause nonlinear springing, excitation sources could be missing, as discussed above.

To compare results from simulations (SIM) with experimental results (EXP), the ratio between the two is given in Figs. 13-15. The linear wave frequency stress is denoted as 'WFl'. The predicted WF stress is in general quite similar to the measured one. In the forward section, the WF stress is slightly over-predicted in the lower sea states, while it is under-predicted in the highest sea states. The WF stress at midship is generally over-predicted by around 5%. The linear predictions are somewhat better than those found by including nonlinearities, although the difference between the two is small. In the aft section the WF stress is also over-predicted, and the linear predictions are again in better agreement with the experiments than the nonlinear ones.

suggested location Figs. 13-15

For most of the sea states the HF stress is predicted with less accuracy than the WF stress. For almost all cases the numerical method over-predicts the HF stress, with a maximum ratio between predicted and measured values of 2.7. The ratio decreases with increasing significant wave height. The degree of over-prediction is quite similar in all three cuts. The figures also show that the HFl stress, for the lower two wave heights, is over-predicted. Use of a too small damping ratio could explain an over-estimation of numerical predictions. The structural damping ratio of 0.2% used in the simulations was found by decay tests in air, which are prone to some uncertainty. In order to see whether the uncertainty in the damping ratio can explain the over-prediction, the simulations were repeated using an increased structural damping ratio of 0.4% which is considered an upper limit for the structural damping ratio obtained from the decay tests. The value is, however, suitable for determining the sensitivity of the HF stress to the damping ratio. There could also be additional sources of damping contributing during the model tests which are not reflected by the numerical method, such as for instance damping due to stern slamming as mentioned at the end of this section, or the sources discussed above. Therefore a structural damping ratio of 1.0% was also investigated. The results are given in the discussion section below.

In order to get a better view of the differences between measurements and simulations, the simulated and the measured time series of the stresses for the sea state with 5m significant wave height and 13.4s peak period, are compared. Because the fatigue damage in the midships cut is largest, the comparison was only done for the this cut. Fig. 16 shows the comparison between wave frequency stresses, obtained by testing and theoretical predictions. The figure shows a good agreement between the two time series, similar to the agreement found for the time series of the heave and pitch motions which are not presented here.

suggested location Fig. 16

Fig. 17 shows the time series for the HF stress found from experiments and simulations for the same sea state. It also shows the time series of the linear part and the nonlinear modification part of the HF stress. For this sea state, the numerical method predicts a significant springing contribution, both linear and nonlinear, to the HF stress. This is not in agreement with the measurements and could imply that important damping mechanisms are not reflected in the method. According to Fig. 14, the standard deviation of the HF stress in this sea state was over-predicted by approximately 70%.

suggested location Fig. 17

Fig. 14 shows that a better prediction of the HF stress is achieved for the sea state with 9m significant wave height and a peak period of 12.8s. A comparison between the time series of the measured and simulated HF stresses in this sea state is given in Fig. 18. The figure shows that there is almost no linear contribution to the HF stress. The reason for this is that the speed was low, such that there was no wave energy with a frequency close to the natural frequency of the two node vertical vibration mode. By comparing the calculated HF stress with the measured one in Figs. 17 and 18, it is seen that the magnitude of the stress is reasonably well predicted. The same can be said for the time instant that the slamming event occurs. This agrees with the fact that the motion of the ship was predicted quite accurately. It is clear, however, that the numerical method does not capture all features.

When observing the experimental results more carefully, it was seen that the decay of the amplitudes of the HF stress after a slamming event stopped quite abruptly in some cases. This is believed to be caused by other slamming events, and is not reflected by the numerical method. One reason for this could be that the nonlinear modification part of the stress is based on the incident wave elevation, and does not include the effect of the radiated and the diffracted wave. This is particulary important

for the present tests, as the flat stern of the model was only slightly elevated above the water surface. Stern slamming could then easily be induced by, and damp, whipping events. This will also reduce the springing vibrations. Inclusion of the steady wave in the numerical method will have an effect on the HF stress as well. This feature is investigated in a simplified manner in the subsequent discussion.

It is noted that a large contribution to the HF stress is caused by bow flare slamming. This slamming force is predicted by using strip theory, while the actual flow is three dimensional. Based on results from a water entry study by Scolan and Korobkin[26] it was estimated that the 2D slamming force can be approximately 20% larger than the 3D force. More details about this estimate were presented by Drummen et al.[18]

suggested location Fig. 18

Fatigue Damage

Figs. 19-21 compare the half hour fatigue damage as found by simulations and experiments. For sea states with 3m and 5m significant wave height, the half hour wave frequency damage in the forward cut is predicted quite well. For the other sea states, the WF damage is under-predicted. The predicted WF damage for the midships section is generally on the conservative side and within 20% of the measured values. For the aft section, the WF damage found from simulations is also over-estimated. The maximum difference is 70%, although it is generally less than 50%.

The high frequency damage in the forward section is over-predicted for the lower sea states, while it is reasonably well predicted in the higher sea states. For the midships and the aft section, the HF damage is over-predicted for nearly all sea states. The maximum ratio between numerical and experimental values is close to 10.

suggested location Figs. 19-21

The numerically found half hour damages in the different sea states were combined in the same way as was done for the experimental results. The lifetime fatigue damage was calculated using Eq. 7. Results are presented in Table 3. These numerical results can be compared with the experimental ones in Table 2.

The WF damage in the forward cut is predicted quite accurately, this is however partly the result of a balance between over- and under-predictions of the damage in the sea states most important for fatigue, see Fig. 19. The predicted WF damage in the midships section is 17% higher than the experimental value. For the aft section, the WF damage is over-predicted by about 40%. Table 3 also shows that, for all three sections, the contribution of the HF damage to the total fatigue damage is approximately 10 percentage points higher than for the experimental results. The contribution of the HF damage to the total damage is seen to increase from bow to stern, which is in agreement with experimental results.

Table 3 shows the results from a nonlinear time domain analysis, Table 4 presents those from the linear analysis. As expected, predictions by linear theory are consistently lower than those from nonlinear simulations. Except for the forward cut, the WF damage is predicted very accurately by linear theory. The reason why the WF damage in the forward section is best predicted using nonlinear simulations is because the WF stresses in the sea states most important for fatigue are better predicted when nonlinearities are included, see Fig. 13. On the other hand, by looking at Figs. 14 and 15, it is seen that the linear WF stress is in better agreement with experiments than the nonlinear stress. This is at least partly related to the fact that strip theory over-estimates the vertical force in the bow area of the vessel. The nonlinearities affecting the vertical bending moments are most important in the bow area.

The HF damage in the midships and aft section is also better predicted by linear theory, yet this is related to the fact that the over-estimation in some sea states balances the under-prediction in others. Nonlinear simulations give too large values of the HF stress in almost all sea states, as discussed in the previous section.

Discussion

As mentioned above, the uncertainties that could affect the comparison between experimental and numerical results, were limited as much as possible. The damping ratio and stiffness distribution measured during the tests were therefore used as input for the calculations. There are, however, some uncertainties related to both measurements and the numerical analyses. Uncertainties in either damping ratio or stiffness only influence the high frequency fatigue damage, and do not affect the wave frequency damage. Table 5 illustrates the sensitivity of the lifetime HF damage to the damping ratio.

The base case refers to a structural damping ratio of 0.2%. A damping ratio 0.4% was investigated as it can be considered as an upper limit for the structural damping found from the decay tests in air. Structural damping is included in the numerical method. There could, however, be additional sources of damping during the model tests which are not reflected by the method. Furthermore, it was shown that the experimental damping ratio was significantly lower than that found from full scale measurements. For these two reasons, calculations were also done using a structural damping ratio of 1.0%.

Table 5 shows that the predicted HF damage using a damping ratio of 1.0% is in reasonable agreement with the experimental results. An increased damping reduces the ratio of the HF stresses in Figs. 13-15. The predictions of the standard deviation of the HF stresses in the 7m and 9m sea states become reasonable by this reduction. It does however not change the overall trends shown in the figures, meaning that the HF stress is still over-predicted by a factor two for the lowest sea states. Use of a damping ratio of 1.0% instead of 0.2% also reduces the stresses in

Fig. 17. However, it does not change the overall trends.

By decreasing the stiffness with 10%, the natural frequency of the two node flexural mode found from the calculations agrees better with experimental results[18]. Use of this lower stiffness leads to a difference of less than 5% compared with the base case.

The sensitivity of the lifetime HF damage, found from linear theory, to the damping ratio and stiffness is given in Table 6. It is noted that according to linear theory, the HF damage is only caused by linear springing. From Tables 5 and 6 it can be concluded that the uncertainties related to the measurements of the structural damping ratio and the stiffness do not lead to large uncertainties in the numerically determined lifetime fatigue damage. Moreover, this analysis shows that the large difference between the experimentally and numerically determined HF damages is not solely related to a too low damping ratio.

As described in the section on experimental setup, the physical cuts in the model were located $0.02L_{pp}$ forward of the quarter lengths and the midships section. The horizontal forces were, however, measured $0.016L_{pp}$ forward of the physical cuts. Tables 7 and 8 show a comparison between the fatigue damage calculated at the true midships and quarter length sections, and at cuts $0.036L_{pp}$ forward of these sections. As a result of this change in location, the midships WF and HF damage are increased by 5% and 15% respectively. The damages in the forward section are increased by a factor of approximately four and those in the aft cut are reduced by a factor two. However, the absolute values of the damages in these two cuts are small. It should be noted that the force, due to the hydrodynamic pressure acting on the whole rigid segment, was measured by the force transducers. The differences presented in Tables 7 and 8 can thus be considered as an upper limit. This was explained in more detail by Drummen[13].

The axial force of the model was not measured during the tests. According to Storhaug and Moe[14], this force is in-phase with the vertical bending moment and could, at midships, contribute a stress of 10% of that of the bending moment. This implies that the wave frequency stresses at midships, presented here, can be up to 10% too high. Tables 9 and 10 show the effect of a 10% reduction of the wave frequency stresses on the lifetime fatigue damage at midships. The high frequency stress was left unchanged. Similar results are presented for the quarter length cuts, although the relative effect due to the axial force might actually be larger at these locations. It is seen that the decrease in the WF damage is larger than that in the HF damage. If the results in Table 9 are used to update the experimental ones in Table 2, the contribution of the HF damage to the total damage at midships increases from 37% to 42%.

There was some discrepancy between the requested and the measured wave in the towing tank. In general, however, the measured significant wave height was well within 10% of the requested one. In some cases the wave was somewhat too high, in other cases too low, the effect of this on the lifetime fatigue damage is therefore very limited. The statistical uncertainty in the standard deviation of the total stress due to the fact that each sea state was only run for 30 to 45 minutes was estimated at approximately 10% using the numerical method. The uncertainty is slightly smaller for the wave frequency stress, and somewhat higher for the high frequency stress. It should be emphasised that both these uncertainties do not affect the comparison between the experimental and numerical results because identical time series were used. Other uncertainties regarding the model tests were discussed by Drummen et al.[18] and Drummen[13].

The numerical method did not account for the steady wave around the hull due to the forward speed of the model. The forward speed in sea states important for fatigue damage is generally quite high. The calculations were repeated while accounting for the measured steady wave in a simplified manner: the draft at the forward and aft perpendicular were increased by the height of the steady wave at these locations. The latter were determined from recordings of the forward and aft part of the model made by two video camera's during runs in still-water. For the sea states in which the vessel had a forward speed of 22kn, the used draft increase had a maximum height of 50% of that of the significant wave height. For the 20kn case this was only 20%, and for the other two cases less than 3%. The draft increase at the forward perpendicular was larger than that at the aft perpendicular. Tables 11 and 12 show the effect of the steady wave on the lifetime damage. It is seen that inclusion of the steady wave significantly reduces the HF fatigue damage, and increases the WF damage. The reduction of the HF lifetime damage by approximately 40% is mainly related to a decrease in the HF damage of up to 70% in sea states with a significant wave height of 3m, and approximately 50% in those with 5m significant wave height.

In the discussion above it was shown that simulations performed with a higher structural damping ratio will result in a reduced HF damage. The same was found to be true when accounting for the steady wave. The HF damage obtained from simulations done using a structural damping ratio of 1.0% and including the effect of the steady wave in a simplified manner will then be closer to the damage found from the experiments. The better agreement would however largely be based on an over-prediction of the damage for some sea states and an under-prediction for others, and does not imply that the physics are captured in an accurate manner.

As indicated above the experimental damping ratio was significantly lower than that found from full scale measurements. A higher damping ratio will reduce the contribution of the HF damage to the total damage. Therefore, when the results presented in this paper are extrapolated to the real vessel, this difference in damping ratio has to be accounted for. The results from Table 5 can be used to scale the fatigue damages obtained experimentally in Table 2, and to estimate the effect of a structural damping ratio of 1.0% instead of 0.2% on the contribution of the HF damage to the total damage. By, in Table 5, taking the ratio of the HF fatigue damage in the midships cut using a structural damping ratio of 1.0% and that using a damping ratio of 0.2%, and multiplying this with the HF fatigue damage found in Table 2, the modified HF damage

as estimated for the real vessel is found to be 0.362, i.e. 27% of the total damage.

Furthermore, model test results were extrapolated by assuming that the vessel spends 2/3 of its lifetime in long crested head seas. In reality the vessel in the North Atlantic will encounter mainly head seas going west and following seas going east. Since, in general, long crested head sea is the most severe direction with respect to vertical vibration, a more realistic heading profile will also decrease the contribution of the high frequency damage to the total damage, e.g. Storhaug and Moe[14]. Other effects influencing the extrapolation of model test results to the real vessel are presented by Drummen et al.[19]

Conclusions

This paper deals with an experimental and numerical study of wave-induced fatigue damage in a containership of newer design, advancing at constant forward speed in irregular head waves. The model tests showed that the damage due to wave induced vibrations made up approximately 40% of the total damage, and that this percentage slightly increased from bow to stern. The high frequency contribution could be slightly smaller for full scale due to a larger damping. The main contribution to the high frequency damage came from the two node mode of vibration, while the other modes contributed less than 5% of the damage. The damage in the forward cut was negligible compared to the damage in the midships section, while the damage in the aft cut was about 25% of this value.

The largest contribution to the fatigue damage occurred in sea states with a peak period of around 14s and a significant wave height of 5m for the midships section and the aft quarter length, and 7m for the forward quarter length. For the sea states investigated, experimental results indicated that the nonlinear effects on the wave frequency stress were mainly important in the forward cut, while they affected the high frequency stress in all three cuts.

The experimental results were compared with predictions by a nonlinear hydroelastic strip theory method. It was found that the predicted total fatigue *damage* for the midships section was approximately 50% higher than the damage determined experimentally. This is the result of an over-prediction of 15% in the wave frequency *damage* and of 120% in the high frequency *damage*. The over-prediction of the latter is partly related to the fact that the 3D effects were not accounted for in the 2D slamming force calculation, the 2D slamming force was estimated to be 20% larger than the 3D force. The effect of including 3D effects in this calculation should be investigated, but is expected to reduce the HF damage by approximately 10%. Another part of the over-prediction of the high frequency damage is attributed to a too large springing contribution, both linear and nonlinear, to the high frequency stress. Therefore more work needs to be done to improve the high frequency stress modelling. This includes amongst others identifying and quantifying the sources of damping of the vibrations, and verification of the excitation sources of the high frequency response.

Furthermore, the numerical method did not account for the steady wave around the hull due to forward speed. Using a simplified approach, in which we increased the draft at the forward and aft perpendicular by the height of the steady wave at these locations, we showed that including this wave in the calculations can reduce the high frequency damage by 40%. Also, the radiated and the diffracted waves are expected to influence the nonlinear high frequency stress and should thus be added to the wave used to determine the nonlinear modification part.

The wave frequency stress and damage at midships and at the aft quarter length were best predicted by linear theory, while the best prediction for the forward cut was done by including nonlinearities. This is at least partly related to the fact that strip theory over-estimates the vertical force in the bow area of the vessel, where the nonlinearities are most important.

Acknowledgements

The authors acknowledge the financial support from the Research Council of Norway through CeSOS. Moreover, the yard and the owner of the vessel are acknowledged for permitting use of the ship lines. DNV deserves thanks for providing all the necessary ship data. Parts of the contents of this paper were discussed with Prof. Odd M. Faltinsen, who offered valuable comments. The first author also appreciates the many insights of Dr. MingKang Wu regarding his computer code. Dr. Ole A. Hermundstad is thanked for providing his code Wavegen.

References

1. Payer HG, Brostella R (2006) The Panama Canal expansion and the Panamax vessels of the future. In: Transactions Society of Naval Architects and Marine Engineers, Fort Lauderdale, US

2. Almar-Næss A (1985) Fatigue Handbook : Offshore Steel Structures, Trondheim: Tapir

3. Det Norske Veritas (2003) Classification Note 30.7: Fatigue Assessment of Ship Structures, Oslo, Norway

4. Storhaug G (2007) Experimental investigation of wave induced vibrations increasing fatigue damage in ships, Ph.D. thesis, Dept. of Marine Technology, Norwegian University of Science and Technology, Trondheim, Norway

5. Jensen JJ (1980) Wave-induced ship hull vibrations: A review. The Shock and Vibration Digest 12: 19–25

6. ISSC (2000) Report of special task committee vi.1: Extreme hull girder loading. In: Proceedings 14th International Ship and Offshore Structures Congress, Japan, pp 263–320

7. Storhaug G, Vidic-Perunovic J, Rüdinger F, et al (2003) Springing/whipping response of a large ocean going vessel - a comparison between numerical simulations and full scale measurements. In: Proceedings

of Hydroelasticity in Marine Technology, Oxford, UK, pp 117-129

8. Moe E, Holtsmark G, Storhaug G (2005) Full scale measurements of the wave induced hull girder vibrations of an ore carrier trading in the North Atlantic. In: Transactions Royal Institution of Naval Architects, Conference on Design & Operation of Bulk Carriers, London, UK

9. Storhaug G, Moe E, Holtsmark G (2006) Measurements of wave induced hull girder vibrations of an ore carrier in different trades. In: Proceedings of the 25th International Conference on Offshore Mechanics and Artic Engineering, Hamburg, Germany

10. Watanabe I, Guedes Soares C (1999) Comparative study on the time-domain analysis of non-linear ship motions and loads. Marine Structures 12 (2):153–170

11. Storhaug G, Moan T (2006) Springing/whipping response of a large ocean-going vessel - investigated by an experimental method. In: Proceedings Hydroelasticity in Marine Technology, Wuxi, China

12. Wu MK, Moan T (2005) Efficient calculation of wave-induced ship responses considering structural dynamic effects. Applied Ocean Research 21 (2):81–96

13. Drummen I (2008) Experimental and numerical investigation of nonlinear wave-induced load effects in containerships considering hydroelasticity. Ph.D. thesis, Dept. of Marine Technology, Norwegian University of Science and Technology, Trondheim, Norway, in prep

14. Storhaug G, Moe E (2007) Measurements of wave induced vibrations onboard a large container vessel operating in harsh environment. In: Proceedings of the 10th International Symposium on Practical Design of Ships and Other Floating Structures, Houston, US, 2007, pp. 64–72

15. Det Norske Veritas (2000) Classification Note 30.5: Environmental Conditions and Environmental Loads, Oslo, Norway

16. Det Norske Veritas (2000) Nauticus Hull User Manual, Oslo, Norway

17. Rychlik I (1987) A new definition of the rainflow cycle counting method. International Journal of Fatigue 9 (2):119–121

18. Drummen I, Wu MK, Moan T, Experimental and numerical study of containership responses in severe head seas. submitted to Marine Structures

19. Drummen I, Storhaug G, Moe E, et al (2006) Experimental and full scale investigation of the importance of fatigue damage due to wave-induced vibration stress in a container vessel. In: Transactions Royal Institution of Naval Architects, Conference on Design & Operation of Container Ships, London, UK, pp 61-74

20. Fonseca N, Guedes Soares C (2004) Experimental investigation of the nonlinear effects on the statistics of vertical motions and loads of a containership in irregular waves. Journal of Ship Research 48 (2):148–167

21. Fonseca N, Guedes Soares C (2004) Experimental investigation of the nonlinear effects on the vertical motions and loads of a containership in regular waves. Journal of Ship Research 48 (2):118–147

22. Aalberts PJ, Nieuwenhuijs MW (2006) Full scale wave and whipping induced hull girder loads. In: Proceedings Hydroelasticity in Marine Technology, Wuxi, China, pp 65-78

23. Fonseca N, Guedes Soares C (2002) Comparison of numerical and experimental results of nonlinear wave-induced vertical ship motions and loads. Journal of Marine Science and Technology 6:193–204

24. Wu MK, Moan T (1996) Linear and nonlinear hydroelastic analysis of high-speed vessels. Journal of Ship Research 40 (2):149–163

25. Wu MK, Hermundstad OA (2002) Time-domain simulation of wave-induced nonlinear motions and loads and its applications in ship design. Marine Structures 15 (6):561–597

26. Scolan Y, Korobkin A (2001) Three-dimensional theory of water impact. Part 1. Inverse Wagner problem, Journal of Fluid Mechanics 440:293–326

Table 1. Test program. H_s, T_p, γ and U denote significant wave height, peak period, peakedness parameter and vessel speed respectively

Number	H_s [m]	T_p [s]	γ	U [kn]
1	3	10.6	1	22
2	3	13.4	1	22
3	3	16.3	1	22
4	3	19.1	1	22
5	5	10.4	1.5	20
6	5	13.4	1	20
7	5	16.3	1	20
8	5	19.1	1	20
9	7	9.5	5	16
10	7	13.4	1	16
11	7	16.3	1	16
12	7	19.2	1	16
13	9	9.5	5	12
14	9	12.8	2.3	12
15	9	16.3	1	12
16	9	19.1	1	12

Table 2. Normalised lifetime wave and high frequency fatigue damage based on measurements. All damages are divided by the measured midships wave frequency damage. Values in braces represent the percentage of total fatigue damage

	QL-cut^m	MS-cut^m	3QL-cut^m
WF	0.027 (64)	1.000 (63)	0.204 (53)
HF	0.015 (36)	0.577 (37)	0.180 (47)

Table 3. Normalised lifetime wave and high frequency fatigue damage found by nonlinear time domain simulations. All damages are divided by the measured midships wave frequency damage. Values in braces represent the percentage of total fatigue damage

	QL-cut^m	MS-cut^m	3QL-cut^m
WF	0.026 (55)	1.175 (48)	0.289 (38)
HF	0.021 (45)	1.253 (52)	0.465 (62)

Table 4. Normalised lifetime wave and high frequency fatigue damage found by linear theory. All damages are divided by the measured midships wave frequency damage. Values in braces represent the percentage of total fatigue damage

	QL-cut^m	MS-cut^m	3QL-cut^m
WF	0.015 (63)	0.996 (54)	0.199 (41)
HF	0.009 (37)	0.856 (46)	0.288 (59)

Table 5. Sensitivity of the lifetime high frequency fatigue damage to structural damping and stiffness, found by nonlinear time domain simulations. All damages are divided by the measured midships wave frequency damage. The base case refers to a structural damping ratio of 0.2%

	QL-cut^m	MS-cut^m	3QL-cut^m
Base case	0.021	1.253	0.465
Damping, 0.4%	0.018	1.082	0.402
Damping, 1.0%	0.015	0.787	0.296
Stiffness, -10%	0.021	1.295	0.489

Table 6. Sensitivity of the lifetime high frequency fatigue damage to structural damping and stiffness, found by linear theory. All damages are divided by the measured midships wave frequency damage. The base case refers to a structural damping ratio of 0.2%

	QL-cut^m	MS-cut^m	3QL-cut^m
Base case	0.009	0.856	0.288
Damping, 0.4%	0.008	0.754	0.253
Damping, 1.0%	0.006	0.559	0.186
Stiffness, -10%	0.01	0.953	0.325

Table 7. Uncertainties in the lifetime fatigue damage as a result of the difference between the location of the true midships and quarter length sections and the measurement sections. Results were found from nonlinear time domain simulations. All damages are divided by the measured midships wave frequency damage

	WF	HF
QL-cut^m	0.026	0.021
QL-cut	0.104	0.075
MS-cut^m	1.175	1.253
MS-cut	1.242	1.434
3QL-cut^m	0.289	0.465
3QL-cut	0.152	0.270

Table 8. Uncertainties in the lifetime fatigue damage as a result of the difference between the location of the true midships and quarter length sections and the measurement sections. Results were found from linear theory. All damages are divided by the measured midships wave frequency damage

	WF	HF
QL-cut^m	0.015	0.009
QL-cut	0.077	0.040
MS-cut^m	0.996	0.856
MS-cut	1.042	0.991
3QL-cut^m	0.199	0.288
3QL-cut	0.096	0.158

Table 9. Sensitivity of the lifetime fatigue damage to the fact that the axial force was included in the calculation of the vertical bending moments. Results were found by nonlinear time domain simulations, wave frequency stresses were multiplied with 0.9. All damages are divided by the measured midships wave frequency damage

	QL-cut^m	MS-cut^m	3QL-cut^m
WF base case	0.026	1.175	0.289
WF	0.017	0.852	0.206
HF base case	0.021	1.253	0.465
HF	0.017	1.118	0.418

Table 10. Sensitivity of the lifetime fatigue damage to the fact that the axial force was included in the calculation of the vertical bending moments. Results were found by linear theory, wave frequency stresses were multiplied with 0.9. All damages are divided by the measured midships wave frequency damage

	QL-cut^m	MS-cut^m	3QL-cut^m
WF base case	0.015	0.996	0.199
WF	0.010	0.722	0.141
HF base case	0.009	0.856	0.288
HF	0.007	0.767	0.260

Table 11. Sensitivity of the lifetime high frequency fatigue damage to the steady wave effect, found by nonlinear time domain simulations. All damages are divided by the measured midships wave frequency damage

	QL-cut^m	MS-cut^m	3QL-cut^m
WF base case	0.026	1.175	0.289
WF	0.031	1.242	0.326
HF base case	0.021	1.253	0.465
HF	0.015	0.786	0.318

Table 12. Sensitivity of the lifetime high frequency fatigue damage to the steady wave effect, found by linear theory. All damages are divided by the measured midships wave frequency damage

	QL-cut^m	MS-cut^m	3QL-cut^m
WF base case	0.015	0.996	0.199
WF	0.020	1.082	0.250
HF base case	0.009	0.856	0.288
HF	0.005	0.413	0.143

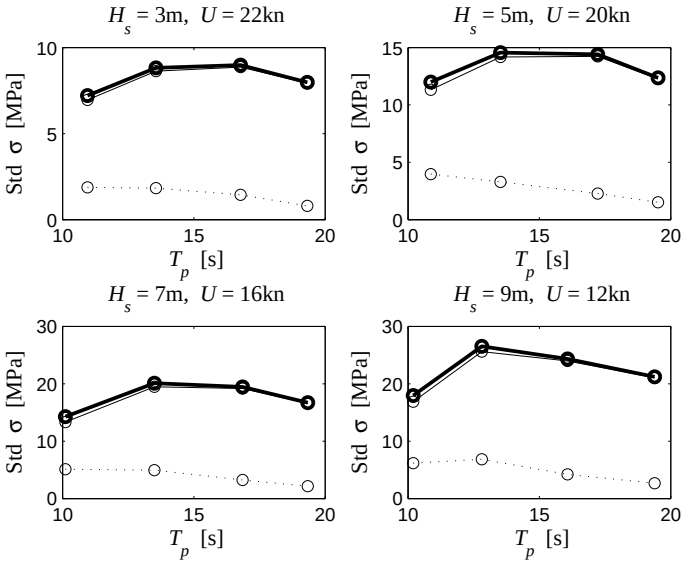

Fig. 1. Experimentally found standard deviation of the stress in the QL-cut^m. T(-o-), WF(-o-) and HF($\cdot \circ \cdot$)

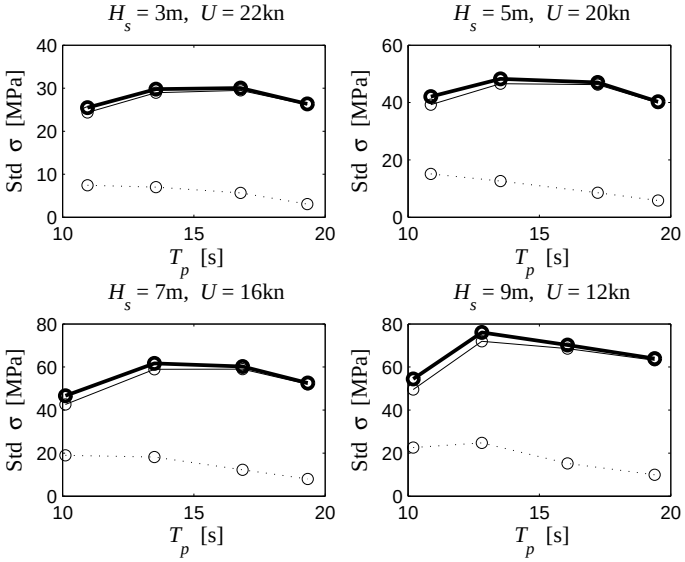

Fig. 2. Experimentally found standard deviation of the stress in the MS-cut^m. T(-o-), WF(-o-) and HF($\cdot \circ \cdot$)

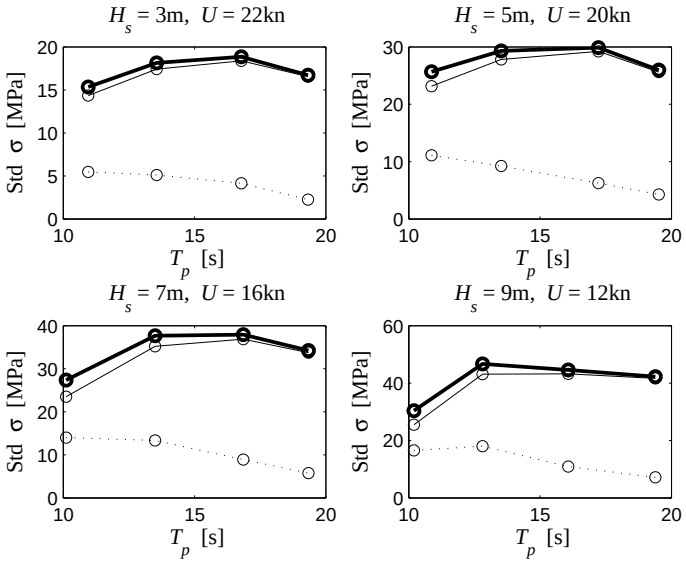

Fig. 3. Experimentally found standard deviation of the stress in the 3QL-cut^m. T(-o-), WF(-o-) and HF($\cdot \circ \cdot$)

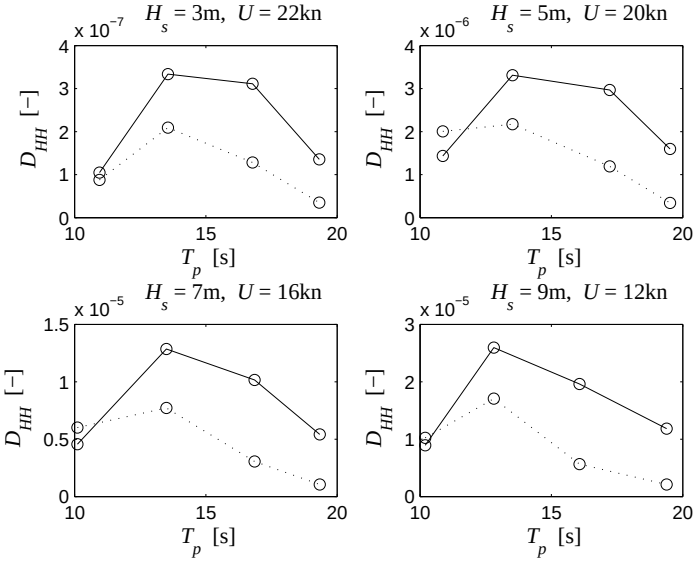

Fig. 4. Experimentally found half hour fatigue damage for the QL-cut^m. WF(-o-) and HF($\cdot \circ \cdot$)

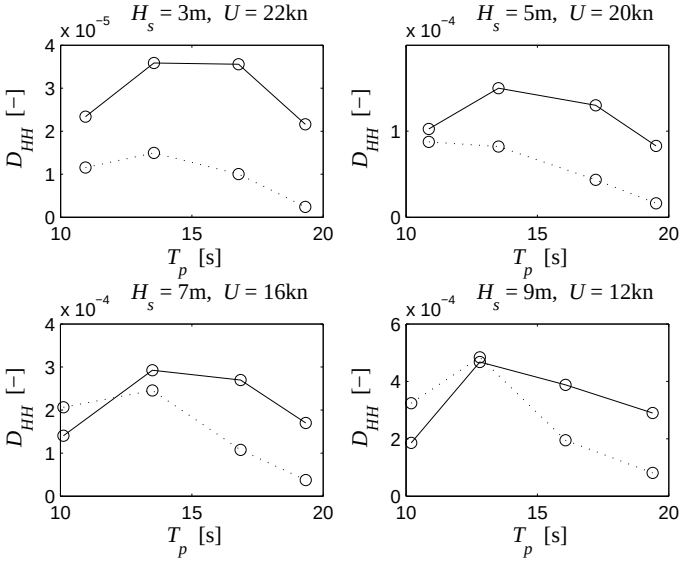

Fig. 5. Experimentally found half hour fatigue damage for the MS-cut^m. WF(-o-) and HF($\cdot \circ \cdot$)

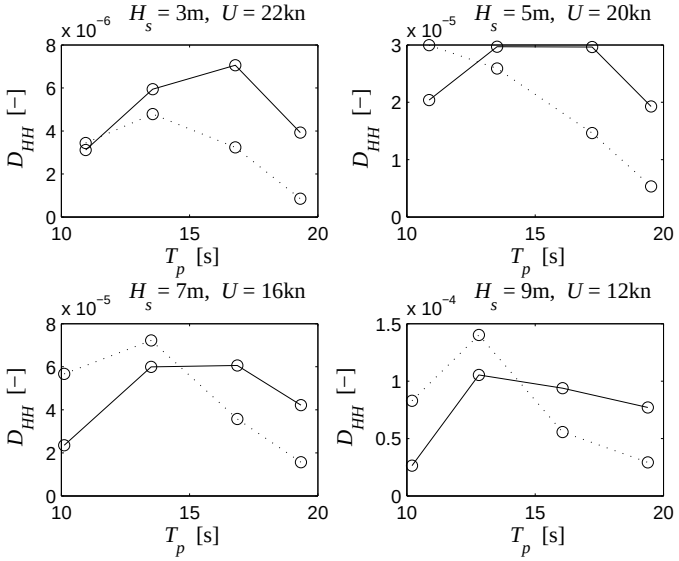

Fig. 6. Experimentally found half hour fatigue damage for the 3QL-cut^m. WF(-o-) and HF($\cdot \circ \cdot$)

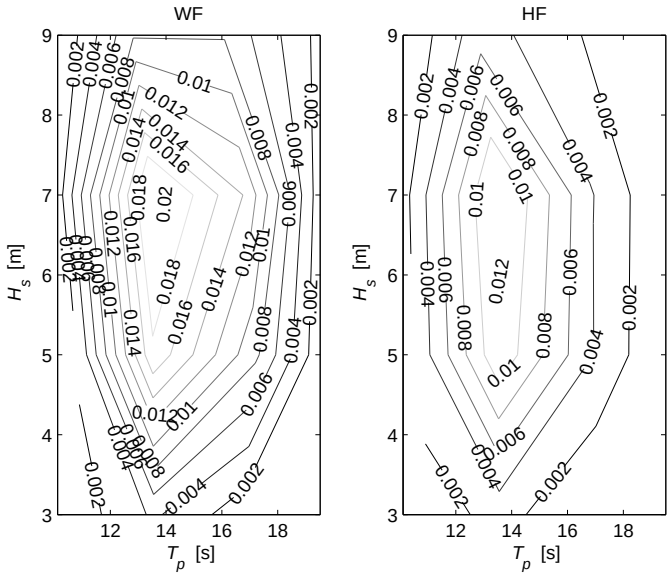

Fig. 7. Contour plot of lifetime fatigue damage for the QL-cut^m. The numbers in the figures denote the lifetime fatigue damage of the specific contour lines

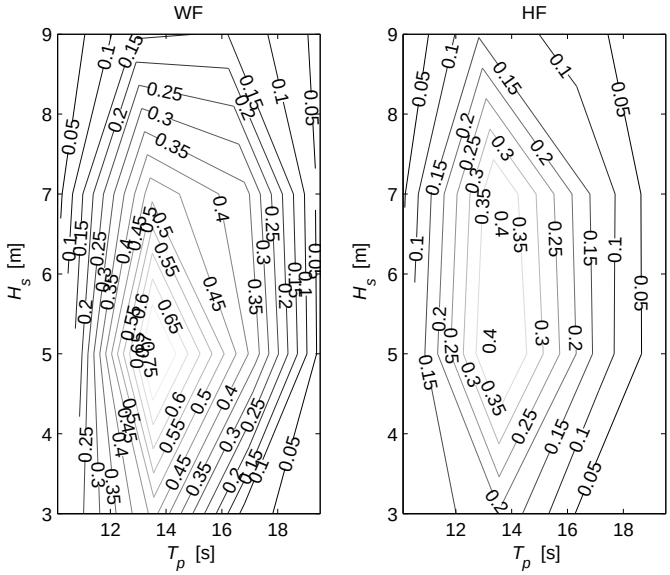

Fig. 8. Contour plot of lifetime fatigue damage for the MS-cut^m. The numbers in the figures denote the lifetime fatigue damage of the specific contour lines

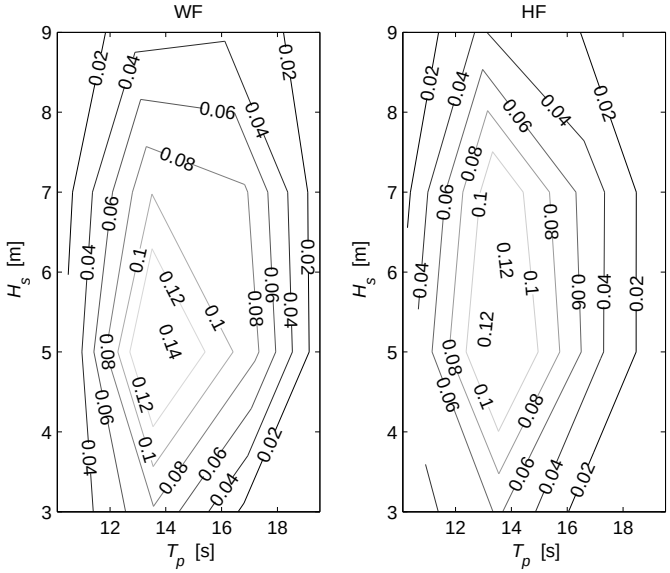

Fig. 9. Contour plot of lifetime fatigue damage for the 3QL-cut^m. The numbers in the figures denote the lifetime fatigue damage of the specific contour lines

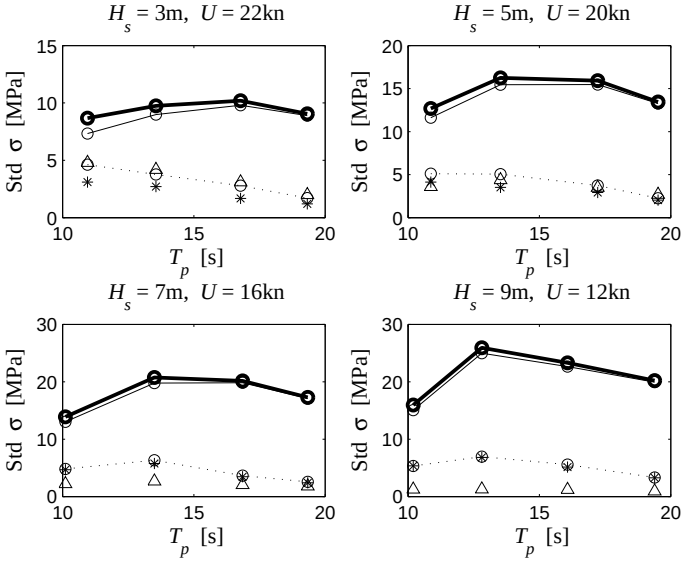

Fig. 10. Standard deviation of the stress in the QL-cut^m obtained numerically. T(⊸), WF(⊸), HF($\cdot \circ \cdot$), HFl(△) and HFnm($*$)

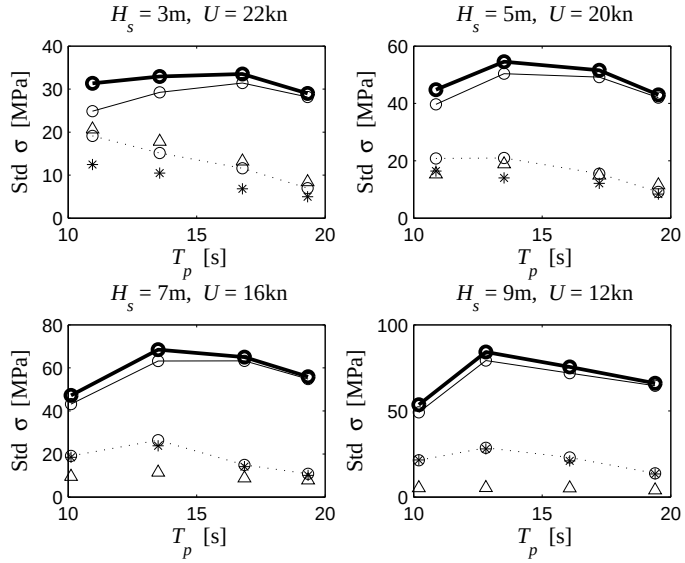

Fig. 11. Standard deviation of the stress in the MS-cut^m obtained numerically. T(⊸), WF(⊸), HF($\cdot \circ \cdot$), HFl(△) and HFnm($*$)

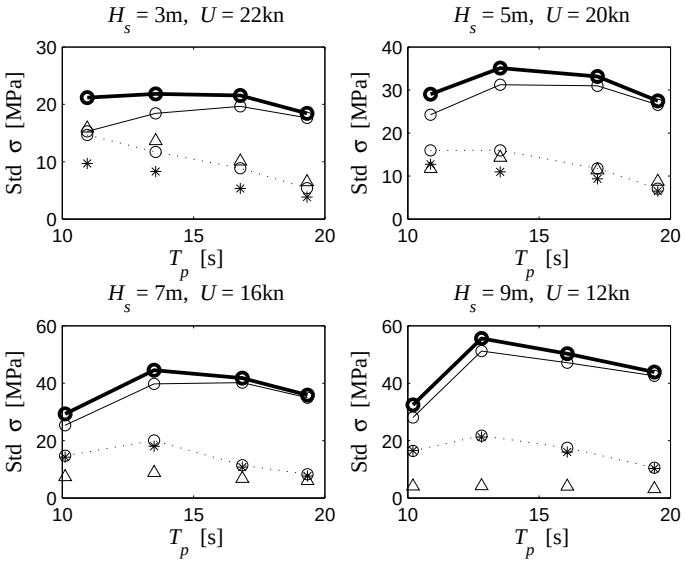

Fig. 12. Standard deviation of the stress in the 3QL-cut^m obtained numerically. T(⊸), WF(⊸), HF($\cdot \circ \cdot$), HFl(△) and HFnm($*$)

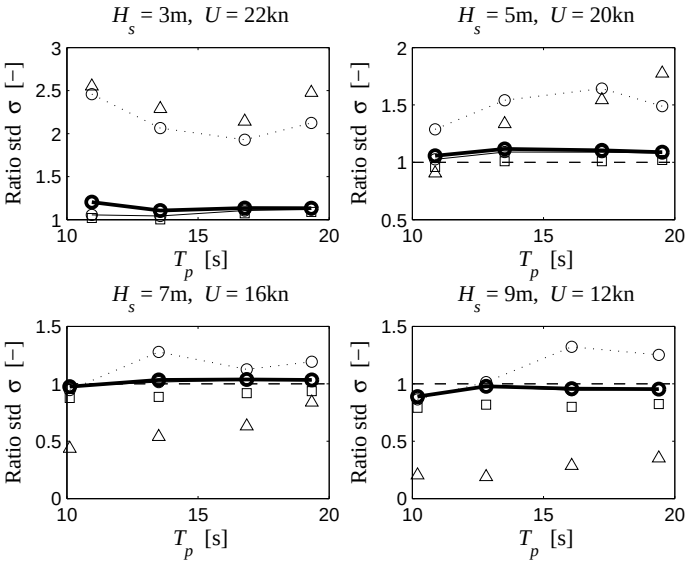

Fig. 13. Ratio of the standard deviation stress for the QL-cut^m. $\mathrm{T_{sim}/T_{exp}}$(—○—), $\mathrm{WF_{sim}/WF_{exp}}$(○—), $\mathrm{HF_{sim}/HF_{exp}}$(· ○ ·), $\mathrm{WFl_{sim}/WF_{exp}}$(□) and $\mathrm{HFl_{sim}/HF_{exp}}$(△)

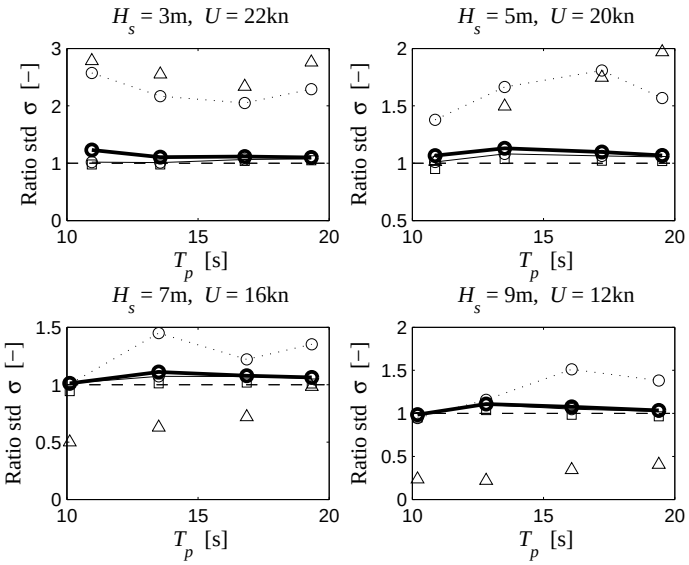

Fig. 14. Ratio of the standard deviation stress for the MS-cut^m. $\mathrm{T_{sim}/T_{exp}}$(—○—), $\mathrm{WF_{sim}/WF_{exp}}$(○—), $\mathrm{HF_{sim}/HF_{exp}}$(· ○ ·), $\mathrm{WFl_{sim}/WF_{exp}}$(□) and $\mathrm{HFl_{sim}/HF_{exp}}$(△)

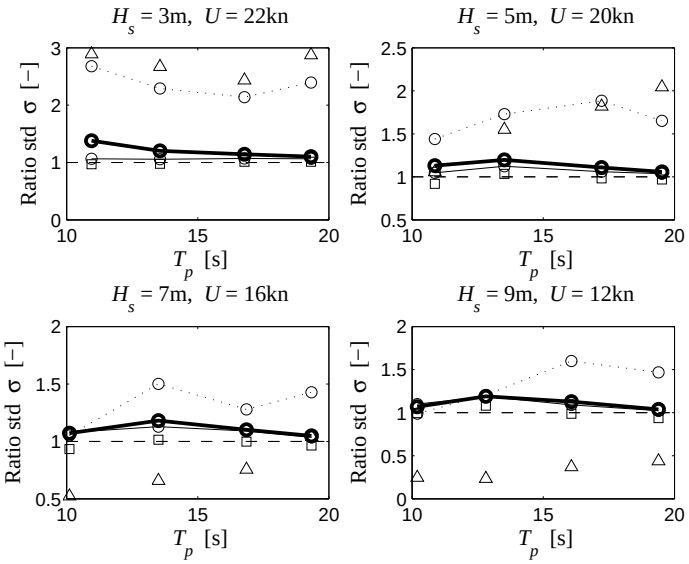

Fig. 15. Ratio of the standard deviation stress for the 3QL-cut^m. $\mathrm{T_{sim}/T_{exp}}$(—○—), $\mathrm{WF_{sim}/WF_{exp}}$(○—), $\mathrm{HF_{sim}/HF_{exp}}$(· ○ ·), $\mathrm{WFl_{sim}/WF_{exp}}$(□) and $\mathrm{HFl_{sim}/HF_{exp}}$(△)

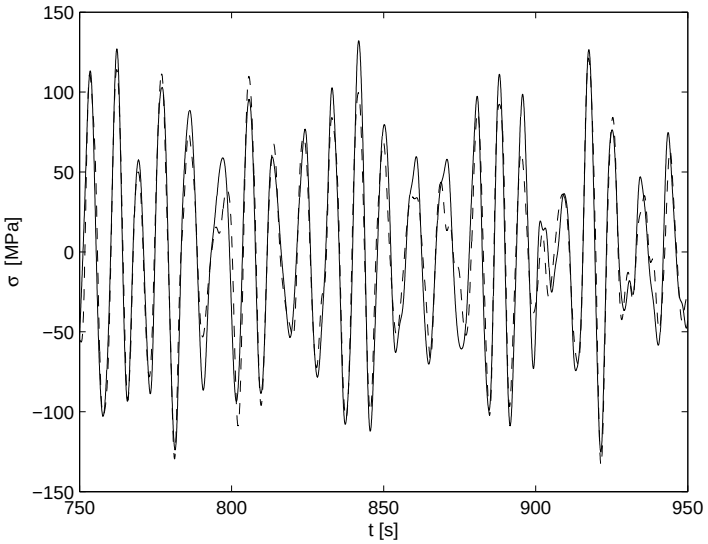

Fig. 16. Wave frequency stress in the MS-cut^m, H_s=5m, T_p=13.4s, U=20kn. EXP(—), SIM(- - -). Std σ_{exp} =47MPa, Std σ_{sim} =50MPa

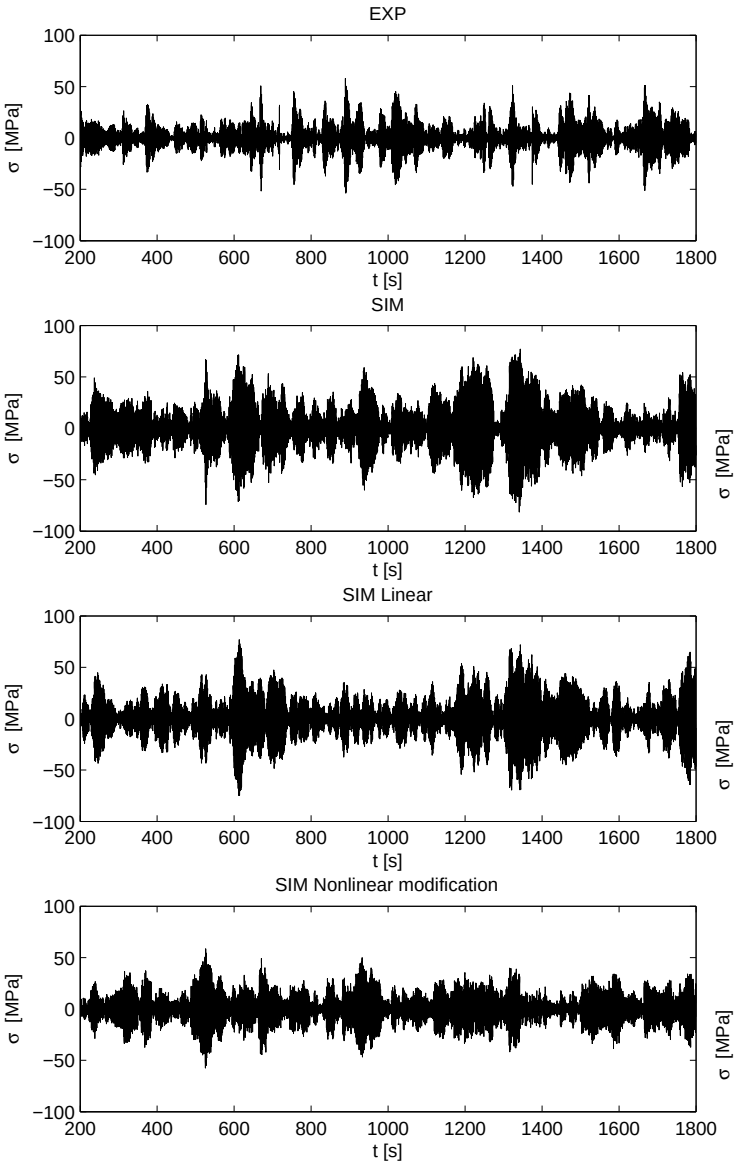

Fig. 17. High frequency stress in the MS-cut^m, H_s=5m, T_p=13.4s, U=20kn. The simulated high frequency stress is also given for the linear part and the nonlinear modification part. Std σ_{exp} =13MPa, Std σ_{sim} =21MPa

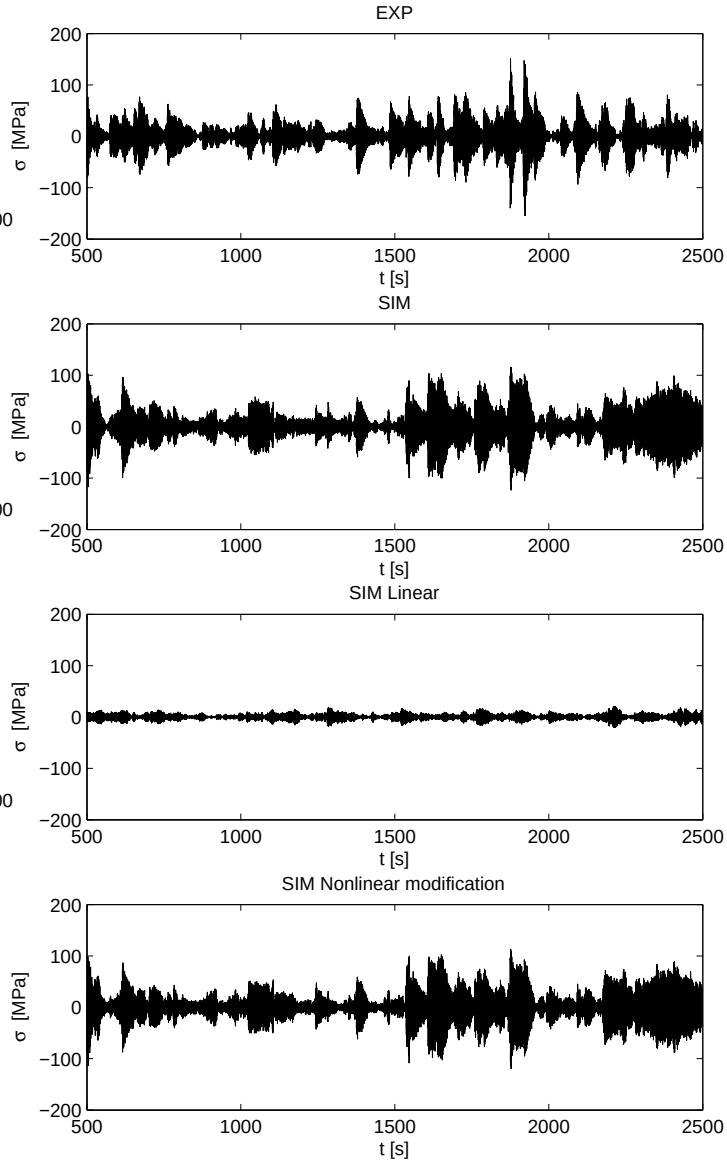

Fig. 18. High frequency stress in the MS-cut^m, H_s=9m, T_p=12.8s, U=12kn. The simulated high frequency stress is also given for the linear part and the nonlinear modification part. Std σ_{exp} =25MPa, Std σ_{sim} =29MPa

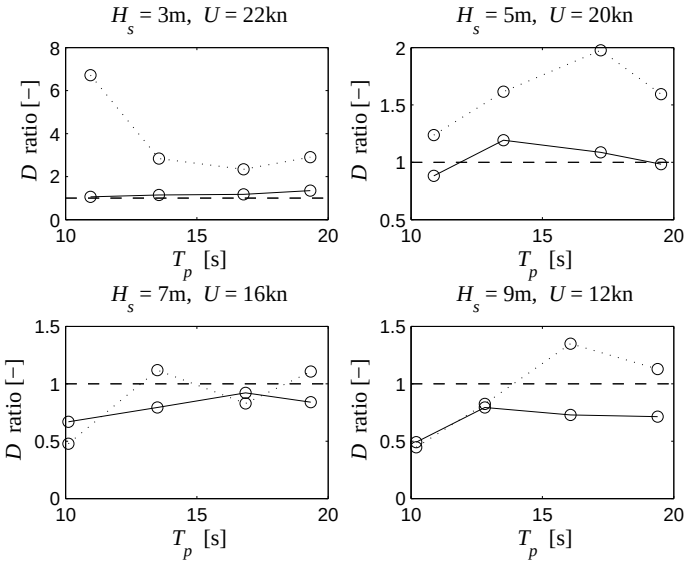

Fig. 19. Ratio half hour fatigue damage for the QL-cut^m. $\mathrm{WF_{sim}/WFexp}(\text{-}\circ\text{-})$ and $\mathrm{HF_{sim}/HFexp}(\cdot\circ\cdot)$

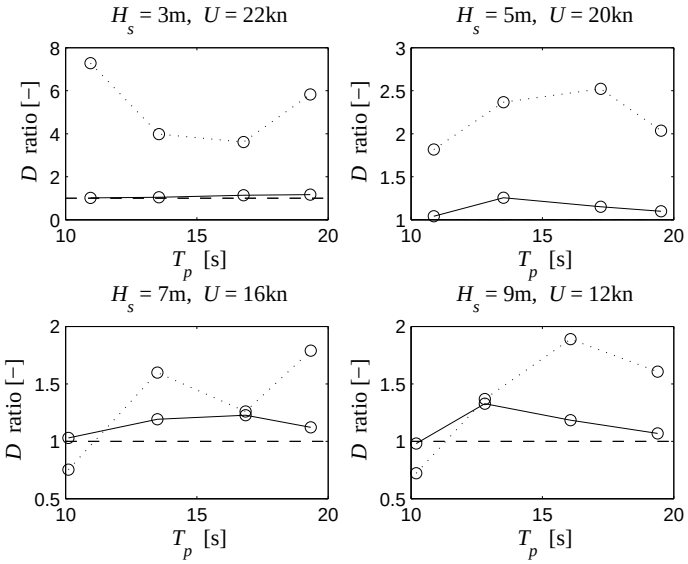

Fig. 20. Ratio half hour fatigue damage for the MS-cut^m. $\mathrm{WF_{sim}/WFexp}(\text{-}\circ\text{-})$ and $\mathrm{HF_{sim}/HFexp}(\cdot\circ\cdot)$

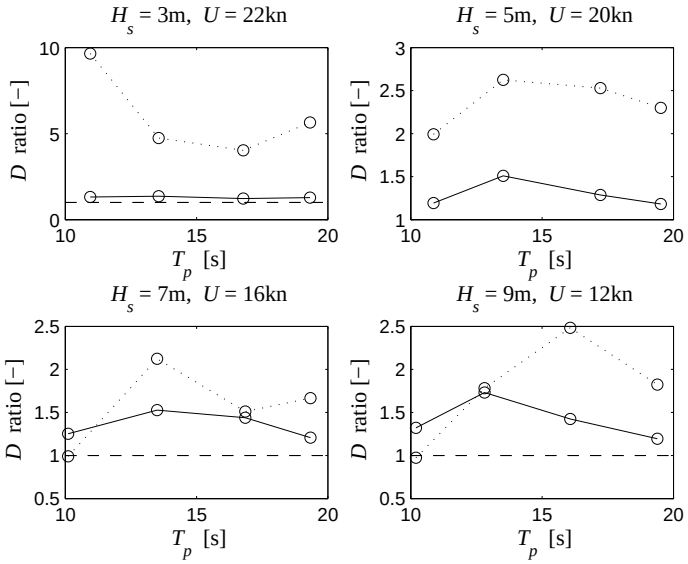

Fig. 21. Ratio half hour fatigue damage for the 3QL-cut^m. $\mathrm{WF_{sim}/WFexp}(\text{-}\circ\text{-})$ and $\mathrm{HF_{sim}/HFexp}(\cdot\circ\cdot)$

Paper 4

Experimental investigation of the application of response conditioned waves for long-term nonlinear analyses

Ingo Drummen and Torgeir Moan

Proceedings 10th International Symposium on Practical Design of Ships and Other Floating Structures. Houston, US, pp. 322-329, 2007

10th International Symposium on Practical Design of Ships and Other Floating Structures
Houston, Texas, United States of America
© 2007 American Bureau of Shipping

Experimental Investigation of the Application of Response Conditioned Waves for Long-Term Nonlinear Analyses

Ingo Drummen and Torgeir Moan

Centre for Ships and Ocean Structures
Norwegian University of Science and Technology
Trondheim, Norway

Abstract

Global load effects in novel ship designs are increasingly determined by direct load evaluation. The most common manner to establish design loads, in this way, is by means of a long-term analysis of the response. The coefficient of contribution method is an efficient approach for performing a long-term analysis. Combining it with response conditioning methods further improves the analysis efficiency. Although the response conditioning methods have been verified for particular cases, further verification is necessary before they can become established tools. In this paper, we present a comparison between the short-term probability distribution of the midships vertical hogging bending moment found experimentally using response conditioned waves and using random irregular waves. The comparison was performed for the sea state that contributes most to the midships vertical hogging bending moment with a return period of 10000 years, which was determined using the coefficient of contribution method. We found that the agreement between results from response conditioned waves and from random irregular waves was good as long as the hull was assumed to be rigid. For a flexible hull, results from response conditioned waves were approximately 15% lower than random irregular wave results in case severe slamming occurred.

Keywords

Response conditioned waves; Vertical bending moment; Experiments; Nonlinear; Long-term; Containership.

Introduction

For the strength assessment of ship structural members during design, it is necessary to estimate the maximum value of wave-induced loads during the ship's operating period. For ships of newer design, these maxima have to be found by direct load evaluation. The most common manner to establish design loads in this way is by means of a long-term description of the response. As the ship response in the most severe sea states is nonlinear, time domain simulations or model tests with long time series are required. The long-term analysis therefore becomes both time-consuming and expensive.

An efficient approach for predicting the nonlinear long-term extreme response is the coefficient of contribution method, described amongst others by Baarholm and Moan (2001), which identifies the most important sea states contributing to the extreme value. Although this method can strongly reduce the number of sea states considered, it is still rather time-consuming to find the short-term probability distributions in the selected sea states, especially since the values in the tail of the distribution are of main interest.

Based on the theory of the New Wave model (Tromans et al., 1991), Adegeest et al. (1998) proposed the most likely extreme response (MLER) method. Using the amplitude and phase information from the transfer function, this method conditions the incident wave profile to cause a predefined specific extreme response. Subsequently, time domain simulations or model tests can be carried out using the derived deterministic wave sequence as input. Pastoor (2002) extended this method, and described how it can be used for finding the nonlinear short-term probability distribution. He carried out model tests, in random irregular waves and some MLER waves, with a frigate and studied the midships vertical bending moment. Results from tests in response conditioned waves showed good agreement with those obtained using random irregular data.

The MLER method neglects the systematic association of large wave periods with large wave amplitudes. In order to incorporate this association, Dietz (2004) combined the idea of the MLER method with the idea of the most likely wave profile (Friis-Hansen and Nielsen, 1995) and developed the most likely response wave (MLRW). The most likely response wave is a special case of the conditional random response wave (CRRW), also developed by Dietz (2004). The CRRW profile includes a random background wave within the MLRW profile, and is therefore more capable of correctly capturing the contribution of transient effects like those of whipping. Both methods can be used for finding nonlinear short-term probability distributions. Assuming

a rigid hull girder, Dietz (2004) compared nonlinear probability distributions found using both the MLRW and the CRRW method with results from brute force simulations, and found good agreement. He furthermore showed that the effect of the random background wave is of increasing importance with increasing vessel speed. For a flexible hull girder, results from the CRRW method also corresponded well with brute force results. The same can be said for the sagging responses by application of the MLRW method. The hogging responses on the other hand compared less well with results from brute force simulations.

The fundamental assumption of the response conditioning techniques is that the nonlinear response is a correction of the linear response. For his comparison, Pastoor (2002) used a rigid model of a typical modern frigate with rather flat lines in the aft ship and a moderate bowflare. The latter was chosen to circumvent extreme slamming incidents. Dietz (2004) only made comparisons using one nonlinear time domain code. He recommended further analysis with other types of vessels and comparison with results from model tests. In general, ISSC (2006) recommended that response conditioning methods have to be verified with further numerical simulations and experiments before they can become established tools.

The purpose of this paper is to compare experimentally the short-term probability distribution found from random irregular waves and response conditioned waves, using both MLRWs and CRRWs. As a case study, the value of the midships vertical hogging bending moment with a mean return period of 10^4 years was investigated. The reason for focusing on such an event is to consider realistic physical events if design for an annual failure probability of 10^{-4} is aimed at. The results were obtained with a four segment flexible model of a container vessel of newer design. The unique hull form of these vessels - with large, flat and overhanging sterns together with pronounced bow flares - introduces nonlinear effects in ship motions and loads. In extreme conditions, a large part of these nonlinear effects is related to slamming incidents.

Experimental Setup

The model tests were performed in the towing tank at the Marine Technology Centre in Trondheim. The tank is 260m long, 10.5m wide and between 5.6m and 10m deep. The double flap wave maker is able to produce both regular and irregular waves. The model tested is based on a container vessel with a length overall of 294m. It has a large, flat, overhanging stern and pronounced bowflare. With these characteristics, it is considered as representative for modern container vessels. The main particulars are given in Table 1. The model was built using a scale of 1:45, resulting in a length between perpendiculars of 6.24m. The body plan of the vessel is shown in Fig. 1.

The model was made flexible in order to include the hydroelastic effect in the experiments. Based on Økland et al. (2003) it was decided that a four segment test model would be well suited for the experiments, as whipping was an important test aspect. This means that the model consisted of three elastic rotational springs and four rigid segments. The model was thus able to vibrate in the two node, three node and four node vertical vibration mode.

Table 1: Main particulars of the vessel

Main Particular	
Length overall	294.01m
Length between perpendiculars	280.98m
Beam	32.26m
Draft used in model tests	11.75m
Trim used in model tests	0.0m
Displacement (draft = 11.75m)	76656ton
Block coefficient	0.707
Natural freq. 2 node vibration	3.51rad/s

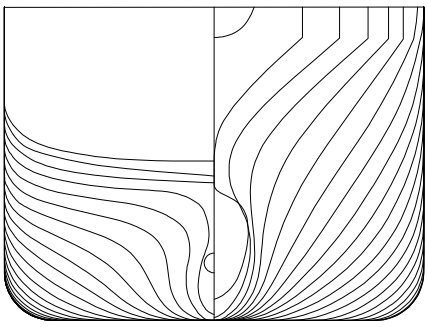

Fig. 1: Body Plan of the Vessel

A picture of the four segment model under the towing carriage is given in Fig. 2. The springs were located 0.13m (i.e. $0.02L_{pp}$) forward of the quarter lengths and the midships section. The location of the springs was chosen to represent the two node, three node, and four node vertical vibration in an optimal manner. All three springs had equal stiffness, which was tuned to give the correct Froude scaled natural frequency of the two node vertical vibration, 23.6rad/s. Furthermore, the springs were designed in order to operate within the elastic area during all tests. The four segments were made rigid by mounting an aluminum frame on each segment. The frame was designed as such that the natural frequency of the frame did not interfere with the frequencies of interest.

The rigid body motions were measured using an optical system, while capacitive strips and wave probes measured the relative motion and the wave elevation. Force transducers were mounted in the three cuts. The force transducers were placed above the neutral line of the model. In this way, the axial force was a measure for the bending moment. All sensors were sampled at 200Hz.

The model was tested in most likely response waves (MLRW), conditional random response waves (CRRW) and random irregular waves (RIW). The JONSWAP spectrum was used as the target wave spectrum. The test program is given in Table 2. In this table, *N* denotes the

number of investigated response levels for the specific sea state. The speed of the vessel in all sea states was taken as maneuvering speed, 5kn. The reasoning behind this test program will be given in a subsequent section.

Fig. 2: Model and Towing Carriage

Table 2: Test program. H_s, T_p, γ and N denote significant wave height, peak period, peakness parameter and the number of investigated response levels respectively. MLRW, CRRW and RIW respectively denote most likely response waves, conditional random response waves and random irregular waves

Type	H_s [m]	T_p [s]	γ [-]	N [-]
MLRW	18	16.16	3.93	4
MLRW	19	15.89	4.75	4
MLRW	20	15.81	5.00	3
MLRW	21	15.81	5.00	4
MLRW	22	15.81	5.00	3
CRRW	19	15.89	4.75	4
RIW	19	15.89	4.75	-

As the response conditioned waves are independent of the wave height (see e.g. Dietz et al., 2004), it is strictly speaking not necessary to run the most likely response waves for all sea states given in this table. In each sea state the response, used for conditioning of the wave profiles, was however varied somewhat in order to investigate its effect on the measured response.

A more thorough discussion of the experimental methods and of some details of the experimental use of response conditioned waves is given in Drummen (2008).

Theoretical Background

Most Likely and Conditional Random Response Waves

The most likely response wave profile is based on conditioning the response on both the response amplitude, M_c, and on the instantaneous frequency, ω_c. Similarly as for the most likely wave model by Friis-Hansen and Nielsen (1995), the MLRW method is based on Slepian model processes (e.g. Ditlevsen, 1985).

The most likely response wave profile, $\zeta_c(t)$, is established conditional on a given linear response amplitude and instantaneous frequency of the response $M(t)$ at time t_0:

$$\zeta_c(t) = \hat{\mathrm{E}}\left[\zeta(t) \mid M(t_0) = M_c, \Omega = \omega_c, \dot{M}(t_0) = 0\right] \quad (1)$$

where $\hat{\mathrm{E}}[\ ]$ is the conditional mean of the incident wave profile in the center of gravity of the ship, $\zeta(t)$. $\dot{M}(t)$ is the first derivative of the response $M(t)$ and $\Omega = \dot{\hat{M}}(t_0)/M(t_0)$, where $\dot{\hat{M}}(t)$ is the first derivative of the Hilbert transform of $M(t)$. The incident wave and the response are linked through the linear transfer function. If $\omega_c = m_1/m_0$, where m_n is the n^{th} order spectral moment of the response, the MLRW profile becomes identical to the MLER wave profile, developed by Adegeest et al. (1998). This expression is taken throughout this paper, and thus the MLRW is the same as the MLER wave. The most likely response wave with a random irregular background wave included, is referred to as the conditional random response wave (CRRW), and is found from Eq. 1 by omitting the conditional mean from the equation. The resulting equations describing both wave profiles were first derived by Dietz et al. (2004) and Dietz (2004), and were rewritten by Drummen et al. (2007) to more explicitly include the dependence on the specific transfer function.

By conditioning the wave profile on a certain linear response and subsequently using this wave profile in a nonlinear time domain code or during model tests, the nonlinear response is found. By applying this procedure over a range of linear responses for a particular sea state, one can find the short-term nonlinear probability distribution of the response in this sea state.

Coefficient of Contribution Method

Use of the MLRW or the CRRW method, for finding the short-term nonlinear probability distribution of the response in particular sea states, can be combined with the coefficient of contribution method. This method is an efficient way of finding the long-term response distribution. This combined approach was also suggested by Dietz (2004).

Baarholm and Moan (2001) demonstrated that a nonlinear long-term load analysis, for marine structures, can be performed by considering only a few short-term sea states, instead of determining responses for all sea states within the scatter diagram. The initial step is to perform a complete linear long-term analysis, and to find the response, r_D, with a return period of D years. This can be done very efficient in the frequency domain. As only one heading and one forward speed is considered in this paper, r_D is solved from:

$$Q_{LT}(r_D) = \sum_i \sum_j Q_R(R > r_D \mid i, j)\, p_{ij}\, \overline{w} = \frac{1}{N_D} \quad (2)$$

where N_D is the number of response cycles in D years. Q_R ($R > r_D \mid i, j$) is the short-term probability that the

response R is larger than r_D in a sea state with significant wave height i and peak period j, and p_{ij} is the probability of occurrence of this sea state, which is found from the scatter diagram. $\bar{w}$ is a weight function, which expresses the relative rate of peak responses within each sea state, and Q_{LT} (r_D) is the long-term probability that the response R is larger than r_D. The coefficients of contribution, $C_{R;ij}$, can then be written as:

$$C_{R;ij} = \frac{Q_R\left(R > r_D \mid i, j\right) p_{ij} \bar{w}}{Q_{LT}\left(r_D\right)} \tag{3}$$

In the linear analysis, the dominating area in the scatter diagram is located in the regions where the wave length is approximately equal to the ship length. When nonlinear effects are included, the dominating area does not necessarily coincide with the area found from the linear analysis. Multiple maxima may even occur due to large responses at other periods, e.g. due to slamming, which is generally occurs in slightly shorter and steeper waves. Therefore, Baarholm and Moan (2001) describe an iterative procedure for finding the coefficients of contribution when nonlinear effects are included. Using the sea states in the dominating area of the scatter diagram found using linear theory, nonlinear time domain simulations with response conditioned waves are performed in order to find Q_R ($R > r_{D;NL} \mid i, j$), and a long-term nonlinear response, $r_{D;NL}$, is derived:

$$Q_{LT}\left(r_{D;NL}\right) = \sum_i \sum_j Q_R\left(R > r_{D;NL} \mid i, j\right) p_{ij} \bar{w} = \frac{1}{N_D} \tag{4}$$

for all combinations of i and j for which $C_{R;ij} > \alpha$, where α is a threshold value. Using Eq. 3 the coefficients of contribution can then be updated. Based on the values of these along the edges of the area in the scatter diagram under consideration, more sea states are added. The iteration is stopped when the increase of $r_{D;NL}$ is below a certain value. Focusing then on the dominating area, the probability, $Q_{LT}(r)$, that the long-term value R will be larger than r may thus be approximated as:

$$Q_{LT}\left(r\right) = \sum_i \sum_j Q_R\left(R > r \mid i, j\right) p_{ij} \bar{w} \tag{5}$$

again, for all combinations of i and j for which $C_{R;ij} > \alpha$.

The iterative procedure described here starts with a linear analysis. Results are then refined using nonlinear time domain simulations to include nonlinear effects. Other approached exist, for example Winterstein et al. (1994) determine response moment influence coefficients. In order to include nonlinear effects, they, on the other hand, use a second order Volterra model to find the statistical moments, and a cubic model to relate these to the maximum response.

Case Study

The methods described above were used to find the nonlinear midships vertical hogging bending moment, with a mean return period of 10^4 years, for a containership trading in the North Atlantic. Therefore, the North Atlantic scatter diagram from DNV (2000) was extended, using the formulation provided by Bitner-Gregersen et al. (1995). We assumed that the vessel operates at a speed of 5kn in head sea conditions in all sea states. The transfer function of the midships vertical bending moment, for these conditions, was found using a strip theory method, (Wu and Moan, 2005).

The first step was to calculate the value of the midships vertical bending moment with a return period of 10^4 years from a linear long-term analysis. Using the MLRW method, it was then, possible to determine for each sea state the most likely wave profile giving this extreme response. This wave profile is independent of the significant wave height. Therefore, 15 different wave profiles were found, one for each zero crossing period, 3.5s, 4.5s ... 17.5s, in the scatter diagram. From these wave profiles, it was determined that the MLRWs in sea states with a zero crossing period equal to 3.5s would break. We assumed that waves with a wave height over wave length ratio of larger than 0.15 would break. This breaking criterion was applied to the highest wave in the MLRW profile. The MLRW profiles for which a ratio of less than 0.15 was found were tested in the towing tank to determine whether or not the waves would break. The fact that the MLRWs for the sea states with a zero crossing period equal to 3.5s would break means that in reality these sea states can never give the desired response. The sea states should therefore be excluded from the analysis. Subsequently, the linear long-term analysis was repeated, using a scatter diagram from which sea states with a zero crossing period of 3.5s were removed. This action resulted in a somewhat reduced extreme vertical bending moment. It was then again possible to determine the most likely waves underlying to the modified extreme response as well as the sea states for which these break. This procedure was repeated until the scatter diagram consisted only of sea states for which the most likely wave, underlying the linear response with a 10^4 years mean return period, did not break. It was determined experimentally that this was the case for a scatter diagram with zero crossing periods between 12.5s and 17.5s. Using this new scatter diagram, the linear response with a 10^4 years return period was found. The coefficients of contribution, for the most contributing sea states of the scatter diagram, are given in Table 3.

Table 3: Coefficients of contribution found from linear long-term analysis. H_s and T_z denote significant wave height and average zero crossing period, respectively

H_s [m]	T_z=12.5s	T_z=13.5s
17	5%	0%
18	13%	0%
19	21%	1%
20	19%	1%
21	14%	2%
22	8%	2%
23	5%	1%

These results were used as a basis for the iterative procedure described by Baarholm and Moan (2001). The iteration was performed using a nonlinear hydroelastic strip theory method, (Wu and Moan, 2005). Due to the nature of extreme waves, the focus in this paper is on the midships hogging vertical bending moment. Moreover, hogging is the dominant mode for container vessels, meaning that the extreme wave has a large peak at midships and two smaller troughs at the fore and aft perpendicular. The five most contributing sea states found from the iterative nonlinear long-term analysis were identical for both the rigid and the flexible hull, and had approximately equal contributions as those found from the linear long-term analysis, Table 3. This fact is probably related to the use of a scatter diagram with a minimum zero crossing period of 12.5s.

These five most contributing sea states were used in order to experimentally investigate the application of response conditioned waves for long-term nonlinear analyses, see also Table 2. Three or four response levels were investigated for each sea state. The responses on which the wave profiles were conditioned were chosen to vary around the linear midships vertical bending moment with a mean return period of 10^4 years. The results of this investigation are given in the next section.

Experimental Results

Comparison of Short-Term Probability Distributions

The comparison between the short-term probability distributions of the midships vertical hogging bending moment found experimentally from random irregular waves and response conditioned waves was done for the most contributing sea state. This sea state had a significant wave height of 19m and a zero crossing period of 12.5s, see Table 3. From Table 2, it can be seen that response conditioned waves were run at four different response levels for this sea state. The results, in the form of exceedance plots, are given in Figs. 3 and 4. Both figures present results obtained from random irregular waves, most likely response waves and conditional random response waves. Results from random irregular waves were obtained by running the model in the given sea state for a period of one day, full scale. Results from application of the MLRW method can be generated very fast, as it requires only one run per response level. However, for the sake of uncertainty each most likely response wave was run six times. The chosen response was the maximum midships vertical hogging bending moment near the constraint point in time, t_0. The value presented in the figures represents the average of these six responses for the particular response level. For the CRRW method, Dietz et al. (2004) recommend approximately 100 runs per response level. Using 100 runs per response level, it would roughly take one week of testing in order to find the short-term probability distribution for a single sea state, which is too long. As a compromise between the MLRW method and a full CRRW analysis, 10 CRRWs were run for each response level. The figures give the median value resulting from this. It should be noted that the actual wave height measured in the tank was lower than the requested wave height. Due to the nature of the response conditioned waves and the good repeatability (see the section on uncertainty), this however only influences the absolute value of the response and does not influence the comparison between the random irregular waves and the response conditioned waves.

Fig. 3 presents the short-term probability distribution function of the midships vertical hogging bending moment assuming a rigid hull. For this purpose, the response was low passed filtered at a circular frequency of 1.75rad/s. From the figure it can be seen that results from the response conditioned waves compare well with results from random irregular waves. The fact that the vertical bending moments found using the MLRW method are somewhat higher than those found from RIWs is believed to be the result of a larger influence of nonlinearities on the waves in the latter case. The response conditioned waves only propagated 30m in the tank, while this was approximately 130m for the random irregular waves. At the lower response levels, it seems that the results from MLRWs and CRRWs agree very well. It also seems, however, that the deviation between results from the two response conditioning methods increases with increasing response level. This effect is believed to be caused by the interaction between the most likely response wave and the random background wave for the conditional random response wave, which becomes more important with increasing wave height. The fact that, for a rigid hull with low forward speed, results from the response conditioned waves compare well with results from random irregular waves is in agreement with Dietz (2004), and basically implies that the nonlinear peaks of the vertical bending moment correlate well with the linear peaks.

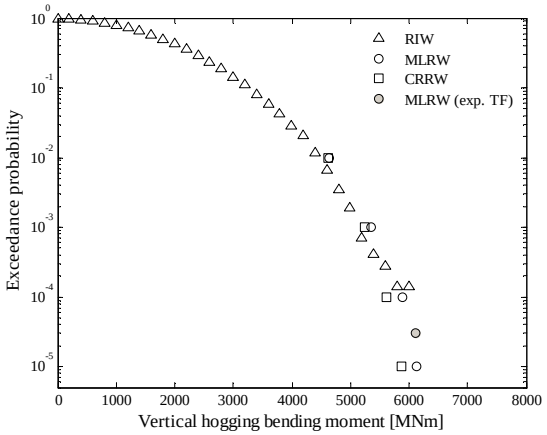

Fig. 3: Probability Distribution of the Midships Vertical Hogging Bending Moment, Rigid Hull.

Similar results for the flexible hull are given in Fig. 4. Here it seems that the vertical bending moment found using most likely response waves is approximately 15% lower than that found using random irregular waves. This result is in agreement with conclusions from Dietz (2004), who also found that the hogging vertical bending moment by application of the MLRW model is under-predicted compared to results from RIWs. Results from conditional random response waves compare

better with random irregular waves results, although the deviation between the two increases with increasing response level. This deviation could be the result of statistical uncertainties. It was determined numerically that the statistical uncertainty, due to the fact that only 10 CRRWs were run for each response level, leads to an error in the vertical bending moment of less than 5%. By taking this into account, and looking at the results from use of the bootstrap method to the RIW data, it seems that the described difference in vertical bending moments is not related to statistical uncertainties. Regarding this discussion, it should be noted that the most likely response wave profiles are deterministic, and therefore not subjected to statistical uncertainties. From the comparison presented in Fig. 4 it can thus be concluded that the vertical bending moments obtained based on the median CRRW results do not agree well with those found in RIWs in the case severe slamming occurred.

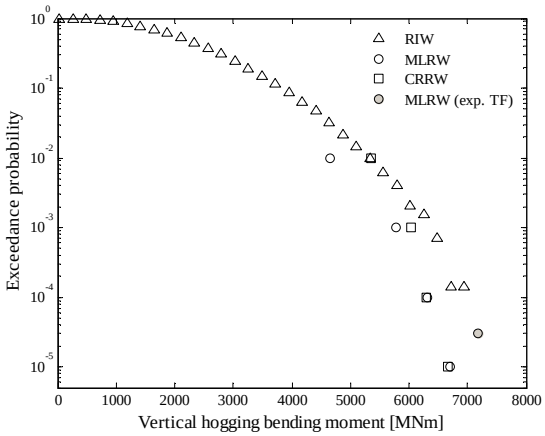

Fig. 4: Probability Distribution of the Midships Vertical Hogging Bending Moment, Flexible Hull.

As mentioned before, the transfer function, which is the basis of the response conditioned wave profiles, was found using a strip theory method. This transfer function was compared with the transfer function found in the experiments, see Figs. 5 and 6. In these figures, M^a, ζ^a and θ respectively denote the amplitude of the midships vertical bending moment, the wave amplitude and the phase difference between the wave at the center of gravity of the model and the response. ρ and g denote density of the water and acceleration of gravity respectively, and B and L represent the vessels' breadth and length between perpendiculars. The figures show that there is good agreement between calculated and measured results. The values for the two outermost frequencies are based on results from a single run, while the other values represent the average of six different runs at each frequency.

In order to investigate the effect of the small deviation between the calculated and the measured transfer functions, the profile of one of the most likely response waves was determined using the measured transfer function. The resulting midships vertical hogging bending moments are given in Figs. 3 and 4 and are denoted as 'MLRW (exp. TF)'. For the rigid hull it seems that the difference is of little influence. The influence is larger for the flexible hull, and it seems that the new results are in better agreement with results from random irregular waves. It is, however, believed that the good agreement is coincidental and does not change the conclusions described above.

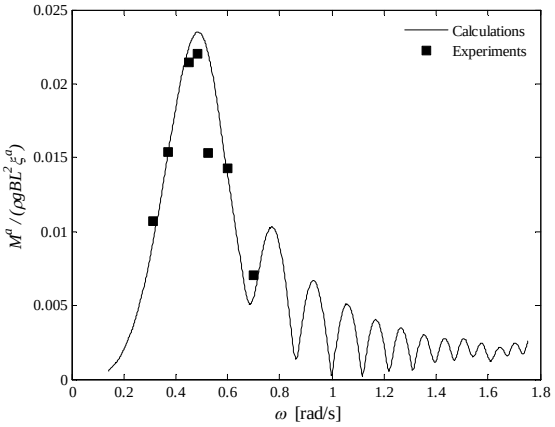

Fig. 5: Amplitude Information of the Midships Vertical Bending Moment Transfer Function, Head Sea, 5kn

For the response conditioned waves presented in this paper, the transformation of the target wave profile to the location of the wave maker was done using Airy wave theory. Alternatively, this transformation can be done using nonlinear techniques such as those described by e.g. Claus et al. (2004). This will increase the agreement between the target wave and the wave measured in the tank.

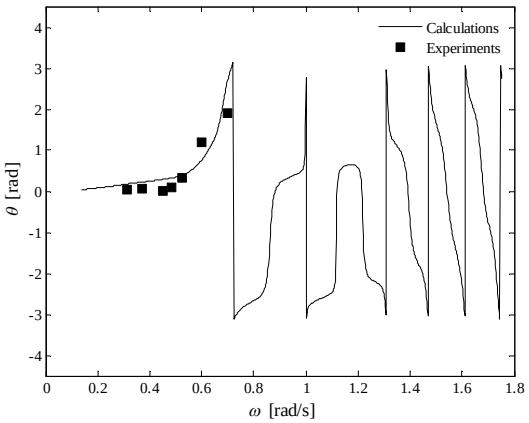

Fig. 6: Phase Information of the Midships Vertical Bending Moment Transfer Function, Head Sea, 5kn

Response with a Mean Return Period of 10000 Years

In general, results from the application of the CRRW method will be in better agreement with random irregular wave results than MLRW results are. On the other hand, even if only 10 CRRWs are used for each response level, the process becomes rather time consuming if more than one sea state needs to be investigated. One way to handle this problem is to refer to the simple MLRW method and characterize its uncertainty relative to a more accurate method by a

model uncertainty χ_m of the former. χ_m is defined as the ratio of the midships vertical hogging bending moment obtained by the CRRW method to that obtained by the MLRW method, (Dietz, 2004). The model uncertainty would generally be a random variable with a mean value and standard deviation. If it is deterministic it simply becomes a correction factor. The nice feature of the model uncertainty in the present case is that the response conditioned waves are independent of the significant wave height and very similar for the different peak periods considered. Hence, the model uncertainty found for one sea state can be applied to all other sea states. In this way a better prediction is found in a relatively fast manner. Results from random irregular waves are available in this paper. They represent an even more accurate estimate of the model uncertainty. Therefore, these results were used as a basis for establishing a correction factor.

Similar results as presented in Figs. 3 and 4 were also found for the other four sea states in Table 2. These results were combined with correction factors. Based on Fig. 4, a correction factor of 1.15 was used for the flexible hull for all exceedance probabilities. No correction was used for the vertical bending moment assuming a rigid hull. The rigid body vertical hogging bending moment with a mean return period of 10^4 years found from this analysis was roughly twice the ship rule value of the hogging bending moment for this vessel. This rule value was found from IACS (2006) and is based on an exceedance probability of 10^{-8}. It was furthermore found that hull flexibility increases the 1 in 10^4 years vertical hogging bending moment by approximately 20%. It should be noted however that these values are based on a vessel operating in head seas only, and can thus be considered an upper limit from this point of view. The coefficients of contribution for the five investigated sea states are given in Table 4. It seems that these few sea states are indeed sufficient for performing a long-term load analysis.

Table 4: Coefficients of contribution found from long-term analysis. T_z equals 12.5s for all cases

H_s [m]	Rigid hull	Flexible hull
18	8%	6%
19	36%	41%
20	27%	22%
21	17%	19%
22	12%	12%

Uncertainties

Using response conditioned waves experimentally in combination with a model with forward speed is a challenging task. The ship model should be at a certain location at a certain time, both determined by the response conditioned waves. Unless advanced methods are used to operate the wave maker as well as the towing carriage, uncertainties can be very large. At the Marine Technology Centre in Trondheim, these advanced facilities were available. In particular, the following two conditions could be fulfilled: a) the towing carriage could be positioned very accurately due to a digital positioning system; b) the towing carriage and the wave maker could be started simultaneously. It was furthermore verified that both the acceleration period and distance of the towing carriage, and the produced wave repeat very well. In order to obtain some information on the level of dispersion of the experimental data, some of the test runs were repeated. For the most likely response waves a coefficient of variation of less than 1% was found for the midships rigid body vertical hogging bending moment. For the flexible hull this value was less than approximately 2%. These values are based on five different most likely response waves, each of which was run six times. Only one conditional random response wave was run six times. This again led to a coefficient of variation of less than 1% for the rigid hull, and less than approximately 2% for the flexible hull.

These facts imply that the midships vertical bending moment found using response conditioned waves repeats very well. However, it does not necessarily mean that the actual wave measured in the tank agrees equally well with the requested wave. As mentioned above, the latter uncertainty only influences the absolute value of the vertical bending moment and does not affect the comparison between response conditioned waves and random irregular waves performed in the present study.

Discussion

Using a rigid model of a typical modern frigate, Pastoor (2002) concluded that, in case of weak nonlinear behavior of the vessel, results from response conditioned experiments show good agreement with random irregular wave results. In this paper, we showed that this also holds for the case of a strongly nonlinear behavior, as long as the hull is assumed rigid. For flexible hulls, Dietz (2004) showed numerically that, when a random background wave is included, results from response conditioned waves compare well with results from brute force simulations. We showed that in the case severe slamming occurred, vertical bending moments obtained based on median conditional random response wave results did not agree well with those found in random irregular waves

Conclusions

In this paper, we presented the results of an experimental investigation into the application of response conditioned waves for long-term nonlinear analyses. As a case study, the value of the midships vertical hogging bending moment with a return period of 10^4 years was investigated, using the coefficient of contribution method to identify the relevant sea states of interest.

The five most contributing sea states were used in order to experimentally find the midships vertical hogging bending moment with a return period of 10^4 years, assuming that the vessel operates in head seas at 5kn in

all sea states. The rigid body vertical hogging bending moment found from this analysis was roughly twice the 20 years ship rule value, and was increased by approximately 20% when hull flexibility was accounted for.

For the most contributing sea state, a comparison was made between the short-term probability distribution of the midships vertical hogging bending moment determined from random irregular waves and from response conditioned waves. This comparison showed that results from the response conditioning techniques agreed well with random irregular wave results as long as the hull was assumed rigid. For a flexible hull, results from response conditioned waves were approximately 15% lower than random irregular wave results in case severe slamming occurred. It should be emphasized however that this implied error is based on an event with a 10^4 years return period and would probably be less for an event with a 20 years return period.

Acknowledgement

The authors acknowledge financial support from the Research Council of Norway through CeSOS. Moreover, the yard and the owner of the vessel are acknowledged for approving use of the ship lines. DNV is thanked for providing all necessary ship data.

References

Adegeest, LJM, Braathen, A, and Løseth, RM (1998). "Use of Non-Linear Sea-Loads Simulations in Design of Ships," 7th Symposium on Practical Design of Ships and Other Floating Structures.

Baarholm, GS, and Moan, T (2001). "Estimation of Nonlinear Long-Term Extremes of the Vertical Bending Moment in Ships," 8th Symposium on Practical Design of Ships and Other Floating Structures.

Bitner-Gregersen, EM, Cramer, EH, and Løseth, R (1995). "Uncertainties of Load Characteristics and Fatigue Damage of Ship Structures," Marine Structures, Vol 8, pp 97-117

Claus, GF, Henning, J, Schmitter, CE, and Kühnlein, WL (2004). "Non-Linear Calculation of Tailored Wave Trains for Experimental Investigations of Extreme Structural Behavior," 23rd International Conference on Offshore Mechanics and Arctic Engineering.

Dietz, JS (2004). "Application of Conditional Waves a Critical Wave Episodes for Extreme Loads on Marine Structures," PhD thesis, Technical University of Denmark.

Dietz, JS, Friis-Hansen, P, and Jensen, JJ (2004). "Design Wave Episodes for Extreme Value Ship Response," 9th Symposium on Practical Design of Ships and Other Floating Structures.

Ditlevsen, O (1985). "Survey on Application of Slepian Model Processes in Structural Reliability," Proceedings of the 4th International Conference on Structural Reliability.

DNV (2000). "Classification Note 30.5: Environmental Conditions and Environmental Loads."

Drummen, I, Wu, MK, and Moan, T (2007). "Numerical Investigation of the Application of Response Conditioned Waves for Long-Term Nonlinear Analysis," in prep.

Drummen, I (2008). "Experimental and Numerical Investigation of Nonlinear Wave-Induced Load Effects in Containerships considering Hydroelasticity," PhD thesis, NTNU, in prep.

Friis-Hansen, P, and Nielsen, LP (1995). "On the New Wave Model for the Kinematics of Large Ocean Waves," 14th International Conference on Offshore Mechanics and Arctic Engineering.

IACS UR S.11 (2006). "Longitudinal Strength Standard."

ISSC (2006). "Report of Committee I.2: Loads," Proceedings 16th International Ship and Offshore Structures Congress, pp 85-173.

Pastoor, LW (2002). "On the Assessment of Nonlinear Ship Motions and Loads," PhD thesis, Delft University of Technology.

Tromans, PS, Anaturk, AR, and Hagemeijer, P (1991). "A New Model for the Kinematics of Large Ocean Waves - Application as a Design Wave," 1st International Offshore and Polar Engineering Conference.

Winterstein, SR, Ude, TC, and Marthinsen, T (1994). "Volterra Models of Ocean Structures: Extreme and Fatigue Reliability," Journal of Engineering Mechanics, Vol 120, No 6, pp 1369-1385

Økland, OD, Zhao, R, and Moan, T (2003). "Numerical Assessment of Segmented Test Model Approach for Measurements of Whipping Responses," 9th International Conference on Fast Sea Transportation.

Paper 5

Numerical and experimental investigation into the application of response conditioned waves for long-term nonlinear analyses

Ingo Drummen, MingKang Wu and Torgeir Moan

submitted to Marine Structures, under review

Numerical and experimental investigation into the application of response conditioned waves for long-term nonlinear analyses

Ingo Drummen [a,*] MingKang Wu [a,c] Torgeir Moan [a,b]

[a] *Centre for Ships and Ocean Structures*
Norwegian University of Science and Technology
NO-7491 Trondheim, Norway

[b] *Department of Marine Technology*
Norwegian University of Science and Technology
NO-7491 Trondheim, Norway

[c] *Norwegian Marine Technology Research Institute, POB 4125 Valentinlyst,*
NO-7450 Trondheim, Norway

Abstract

Response conditioned wave methods can be used to efficiently find the nonlinear short-term probability distributions of vessel responses. Several researchers have studied the accuracy and range of applicability of these methods. However, further investigations are necessary before they can become established tools. In this paper we compare the short-term probability distributions obtained numerically and experimentally from random irregular waves and response conditioned waves. The investigations were performed using a container vessel with a length between perpendiculars of 281m. Numerical simulations were done with a nonlinear hydroelastic time domain code. Experiments were carried out with a flexible model of the vessel in the towing tank at the Marine Technology Centre in Trondheim. The focus was on the probability distributions of the midships vertical hogging bending moments in the sea states contributing most to the hogging moments with a mean return period of 20 years and 10 000 years. We found that the response conditioned wave methods can very efficiently be used to accurately determine the nonlinear short-term probability distributions for rigid hulls, but either accuracy or efficiency is to a large effect lost for flexible hulls, when slamming induced whipping responses are accounted for.

Key words: Response conditioned waves, vertical bending moment, nonlinear, hydroelastic, experimental, strip theory, containership

Preprint submitted to Elsevier

1 Introduction

According to Airy wave theory, the most unfavourable wave condition for a vessel is not the wave of which all components have a peak at the same time instant, but the wave leading to a response for which this is the case. Using the ideas from Friis-Hansen and Nielsen [1], Taylor et al. [2] and Adegeest et al. [3], Dietz [4] developed the most likely response wave (MLRW). Using the amplitude and phase angle information from the transfer function, this method uses linear theory to condition the incident wave profile to cause a predefined specific response at a certain time instant. At this time all of the responses' components have a peak. The most likely response wave is a special case of the conditional random response wave (CRRW), also developed by Dietz [4]. The CRRW profile includes a random background wave within the MLRW profile, and is therefore more capable of correctly capturing the contribution of transient effects like those of whipping.

Using the conditioned wave sequence as input, time domain simulations or model tests can be carried out. Pastoor [5] showed that response conditioned wave methods can be used for predicting nonlinear short-term probability distributions of the midships vertical bending moments in an efficient manner. Assuming a rigid hull girder, Dietz [4] compared nonlinear probability distributions of the midships bending moments obtained using both the MLRW and the CRRW methods with results from brute force simulations, and found good agreement. He furthermore showed that the effect of the random background wave was of increasing importance for increasing vessel speed. For a flexible hull girder, bending moments obtained by the CRRW method also corresponded well with brute force results. The same can be said for the sagging moments by application of the MLRW method. The hogging moments on the other hand compared less well with results from brute force simulations. Dietz [4] stressed that he used only one time domain code and recommended further analysis with other types of vessels and comparison with results from model tests. Also, ISSC [6] recommended that response conditioning methods have to be verified with further numerical simulations and experiments before they can become established tools.

The fundamental assumption of wave conditioning techniques is that the nonlinear response is a correction of the linear response. It is therefore important to investigate their applicability under severe conditions, when nonlinear effects are significant. The purpose of this paper is to compare the short-term probability distributions obtained numerically and experimentally from

* Corresponding author: I. Drummen, currently employed at the Maritime Research Institute Netherlands, P.O. Box 28, 6700 AA Wageningen, The Netherlands. Tel.: +31 317 49 34 35, Fax: +31 317 49 32 45, *E-mail address*: i.drummen@marin.nl

random irregular and response conditioned waves. Both the MLRW and the CRRW methods were investigated. The studies were performed using a container vessel with a length between perpendiculars of 281m. The nonlinear hydroelastic hybrid time domain computer code developed by Wu and Moan [7] was used for the calculations. The focus was on the probability distributions of the midships vertical hogging bending moments in the sea states contributing most to the hogging moments with a mean return period of 20 years and 10 000 years. The experimental results were obtained by testing a four segment flexible model of the vessel in the towing tank at the Marine Technology Centre in Trondheim. In the experimental investigations only the probability distribution related to the 10 000 years return period was studied.

2 Theoretical background of response conditioned waves

According to linear theory the wave elevation may be seen as the superposition of sinusoidal wave components. Seen from a coordinate system moving with the forward speed of the ship, U, the wave elevation process, $\zeta(t)$, at the centre of gravity of the ship may be written as

$$\zeta(t) = \sum_{n=1}^{N} a^e_{\zeta;n}[V_n \cos(-\omega_{e;n}t) + W_n \sin(-\omega_{e;n}t)], \tag{1}$$

where N is the number of wave components, V_n and W_n are independent standard normal random variables, $\omega_{e;n}$ is the encounter frequency, ω_e, of the n^{th} component, and t represents time. The coefficients $a^e_{\zeta;n}$ are found from the encountered wave spectrum, $S^e_\zeta(\omega_e)$,

$$a^e_{\zeta;n} = \sqrt{S^e_\zeta(\omega_{e;n})\Delta\omega_{e;n}}, \tag{2}$$

where $\Delta\omega_{e;n}$ is the resolution of the discrete encounter frequency. The encountered wave spectrum is found from the wave spectrum, $S_\zeta(\omega)$, as follows

$$S^e_\zeta(\omega_e) = S_\zeta(\omega)\frac{d\omega}{d\omega_e}. \tag{3}$$

In head seas, the encounter frequency is related to the wave frequency, ω, by

$$\omega_e = \omega + \omega^2\frac{U}{g}, \tag{4}$$

where g is the acceleration of gravity. For linear responses the response spectrum, $S_M^e(\omega_e)$, can be obtained from

$$S_M^e(\omega_e) = [\Phi_M^e(\omega_e)]^2 S_\zeta^e(\omega_e). \tag{5}$$

Here $\Phi_M^e(\omega_e)$ is the response amplitude operator (RAO) of the response related to the wave at the centre of gravity of the vessel. The k^{th} spectral moment, m_k, of the response is given as

$$m_k = \int_0^\infty \omega_e^k S_M^e(\omega_e) d\omega_e. \tag{6}$$

The response of the ship, $M(t)$, in the time domain is found from

$$M(t) = \sum_{n=1}^{N} a_{M;n}^e [V_n \cos(-\omega_{e;n} t + \theta_{M;n}^e) + W_n \sin(-\omega_{e;n} t + \theta_{M;n}^e)], \tag{7}$$

where $\theta_{M;n}^e$ denotes the phase angle of the transfer function, of the n^{th} component. The coefficient $a_{M;n}^e$ is related to $a_{\zeta;n}^e$ through the RAO

$$a_{M;n}^e = \Phi_{M;n}^e a_{\zeta;n}^e = \sqrt{S_M^e(\omega_{e;n}) \Delta\omega_{e;n}}, \tag{8}$$

where $\Phi_{M;n}^e = \Phi_M^e(\omega_{e;n})$. Through the transfer function, $\Phi_M^e(\omega_e)$ and $\theta_M^e(\omega_e)$, $M(t)$ also depends on the spatial coordinate, x.

It is well known that narrow band processes tend to concentrate the upcrossings in clusters. The individual upcrossings can then not be assumed independent. It is therefore better to consider the envelope process, $R(t)$, of $M(t)$ instead of $M(t)$ itself. Cramér and Leadbetter [8] define the envelope process by

$$R(t) = \sqrt{M^2(t) + \hat{M}^2(t)}, \tag{9}$$

which is an envelope process of $M(t)$ since $R(t) \geq |M(t)|$ for all t, and $R(t) = |M(t)|$ for some t, [8]. Here $\hat{M}(t)$ is the Hilbert transform of $M(t)$,

$$\hat{M}(t) = \sum_{n=1}^{N} a_{M;n}^e [-V_n \sin(-\omega_{e;n} t + \theta_{M;n}^e) + W_n \cos(-\omega_{e;n} t + \theta_{M;n}^e)]. \tag{10}$$

The wave profile, $\zeta_c(t)$, conditional on a given linear response amplitude, M_c, at time $t = 0$ is then given by

$$\zeta_c(t) = [\zeta(t)|\mathbf{M}(0) = (M_c, 0), \dot{\mathbf{M}}(0) = (0, M_c\omega_M)], \tag{11}$$

with ω_M the instantaneous response frequency, and

$$\mathbf{M}(t) = \begin{bmatrix} M(t) \\ \hat{M}(t) \end{bmatrix}. \tag{12}$$

Considering Eqs. 7 and 10, Eq. 11 can be translated to the following four equations.

$$\sum_{n=1}^{N} a^e_{M;n}[V_{n;c}\cos(\theta^e_{M;n}) + W_{n;c}\sin(\theta^e_{M;n})] = M_c \tag{13}$$

$$\sum_{n=1}^{N} a^e_{M;n}\omega_{e;n}[V_{n;c}\sin(\theta^e_{M;n}) - W_{n;c}\cos(\theta^e_{M;n})] = 0 \tag{14}$$

$$\sum_{n=1}^{N} a^e_{M;n}[-V_{n;c}\sin(\theta^e_{M;n}) + W_{n;c}\cos(\theta_{M;n})] = 0 \tag{15}$$

$$\sum_{n=1}^{N} a^e_{M;n}\omega_{e;n}[V_{n;c}\cos(\theta^e_{M;n}) + W_{n;c}\sin(\theta^e_{M;n})] = M_c\omega_M \tag{16}$$

Where $V_{n;c}$ and $W_{n;c}$, respectively, denote the conditioned V_n and W_n for which the above equations are true. These were obtained by use of Slepian model processes, see e.g. Ditlevsen [9], Peter Friis Hansen and Nielsen [1], Dietz et al. [10] or Dietz [4], and are equal to

$$\begin{aligned} V_{n;c} = V_n - \frac{a^e_{M;n}}{m_2m_0 - m_1^2}[&(m_2 - \omega_{e;n}m_1)S_1\cos(\theta^e_{M;n}) + \\ &- M_c(m_2 - \omega_{e;n}m_1)\cos(\theta^e_{M;n}) + (\omega_{e;n}m_0 - m_1)S_2\sin(\theta^e_{M;n}) + \\ &+ (\omega_{e;n}m_1 - m_2)S_3\sin(\theta^e_{M;n}) + (\omega_{e;n}m_0 - m_1)S_4\cos(\theta^e_{M;n}) + \\ &- M_c\omega_M(\omega_{e;n}m_0 - m_1)\cos(\theta^e_{M;n})]; \end{aligned} \tag{17}$$

$$W_{n;c} = W_n - \frac{a^e_{M;n}}{m_2m_0 - m_1^2}[(m_2 - \omega_{e;n}m_1)S_1\sin(\theta^e_{M;n}) +$$

$$- M_c(m_2 - \omega_{e;n} m_1) \sin(\theta^e_{M;n}) - (\omega_{e;n} m_0 - m_1) S_2 \cos(\theta^e_{M;n}) +$$

$$- (\omega_{e;n} m_1 - m_2) S_3 \cos(\theta^e_{M;n}) + (\omega_{e;n} m_0 - m_1) S_4 \sin(\theta^e_{M;n}) +$$

$$- M_c \omega_M (\omega_{e;n} m_0 - m_1) \sin(\theta^e_{M;n})]. \tag{18}$$

Here S_1, S_2, S_3 and S_4 are

$$S_1 = \sum_{n=1}^{N} a^e_{M;n} [V_n \cos(\theta^e_{M;n}) + W_n \sin(\theta^e_{M;n})]; \tag{19}$$

$$S_2 = \sum_{n=1}^{N} a^e_{M;n} \omega_{e;n} [V_n \sin(\theta^e_{M;n}) - W_n \cos(\theta^e_{M;n})]; \tag{20}$$

$$S_3 = \sum_{n=1}^{N} a^e_{M;n} [-V_n \sin(\theta^e_{M;n}) + W_n \cos(\theta^e_{M;n})]; \tag{21}$$

$$S_4 = \sum_{n=1}^{N} a^e_{M;n} \omega_{e;n} [V_n \cos(\theta^e_{M;n}) + W_n \sin(\theta^e_{M;n})]. \tag{22}$$

Details of the above derivation were presented by Dietz et al. [10] and Dietz [4]. The correctness of Eqs. 17 and 18 is easily verified by substituting them in Eqs. 13∼16.

By substituting $V_{n;c}$ and $W_{n;c}$ in Eq. 1 the CRRW profile is obtained. The MLRW profile is found by substitution of the mean values of $V_{n;c}$ and $W_{n;c}$, $\bar{V}_{n;c}$ and $\bar{W}_{n;c}$ respectively, into Eq. 1,

$$\bar{V}_{n;c} = \frac{a^e_{M;n} M_c}{m_2 m_0 - m_1^2} [(m_2 - \omega_{e;n} m_1) + \omega_M (\omega_{e;n} m_0 - m_1)] \cos(\theta^e_{M;n}); \tag{23}$$

$$\bar{W}_{n;c} = \frac{a^e_{M;n} M_c}{m_2 m_0 - m_1^2} [(m_2 - \omega_{e;n} m_1) + \omega_M (\omega_{e;n} m_0 - m_1)] \sin(\theta^e_{M;n}). \tag{24}$$

From Eqs. 23 and 24 it is easily seen that under certain restrictions

$$\arctan\left(\frac{\bar{W}_{n;c}}{\bar{V}_{n;c}}\right) = \theta^e_{M;n}. \tag{25}$$

By substituting $\bar{V}_{n;c}$ and $\bar{W}_{n;c}$ in Eq. 7 it can then be verified that all components have a peak at t=0. Consequently the response is symmetric around this time instant. By a simple transformation the specified response can however

be made to occur at any other arbitrary time instant. Fukasawa et al. [11] used the idea that all response components have a peak at the same time instant in a more direct manner to derive the underlying design irregular wave. Their approach is similar to the MLRW method, but in their case the wave is not conditioned on a particular response.

In numerical methods the incident wave is often given in the centre of gravity of the vessel. In these cases $\zeta_c(t)$, as obtained above, can be used directly. For model tests on the other hand both the time of occurrence of the conditioned event and its location in the tank should be chosen. $\zeta_c(t)$ then has to be transformed from the target location to that of the wave maker.

If $\omega_M = \frac{m_1}{m_0}$ the MLRW profile is the same as the most likely extreme response (MLER) wave developed by Adegeest et al. [3]. This expression is used throughout this paper.

It should be noted that $a^e_{\zeta;n}$ is proportional to the significant wave height, H_s. The spectral moments on the other hand are proportional to H_s^2. This means that $\bar{V}_{n;c}$ and $\bar{W}_{n;c}$ are inversely proportional to H_s, and therefore that the MLRW profiles are independent of H_s. Furthermore, $\bar{V}_{n;c}$ and $\bar{W}_{n;c}$ are proportional to M_c. A change in M_c will thus only cause a change in the height of the conditioned wave, not in its shape.

Finally, it should be mentioned that, in order for the CRRW profile to be correct, it is important that the numerical integration in Eq. 6 is performed such that the following equations are true.

$$m_0 = \sum_{n=1}^{N} a^e_{M;n} \tag{26}$$

$$m_1 = \sum_{n=1}^{N} a^e_{M;n}\omega_{e;n} \tag{27}$$

$$m_2 = \sum_{n=1}^{N} a^e_{M;n}\omega^2_{e;n} \tag{28}$$

3 Case studies

3.1 General

In order to investigate the applicability of response conditioned waves, the short-term probability distribution of the midships vertical hogging bending

moment found in random irregular waves was compared with the one obtained using response conditioned waves. The investigations were done using a container vessel of newer design. The unique hull form of these vessels - large, flat and overhanging stern, and pronounced bow flare - can cause large ship motions relative to the water surface, which result in severe slamming impacts. The main particulars of the vessel and its conditions during the investigations are given in Table 1. The body plan is shown in Fig. 1.

Numerical and experimental investigations were carried out. In the former case, two sea states were studied, namely the ones most contributing to the midships hogging moments with a mean return period of 20 years and 10^4 years. Experimentally only the latter sea state was investigated. In all cases the vessel encountered head waves with 5kn forward speed. The parameters of the two sea states are presented in Table 2. The JONSWAP spectrum was used as wave spectrum. The sea state parameters were obtained by applying the coefficient of contribution method, [12], to the results of linear long-term analyses, [13]. The transfer function of the midships bending moment for a forward speed of 5kn used for these analyses was presented by Drummen and Moan [13].

Drummen and Moan [13] also described a procedure to reduce the scatter diagram used for the long-term analyses to only include sea states for which the most likely wave, underlying the linear response with the desired return period, does not break. For a mean return period of 20 years it was found that this is the case for a scatter diagram that includes sea states with a zero crossing period, T_z, of 9.5s and higher. For a mean return period of 10^4 years this was 12.5s and higher.

The reason for using the sea state most contributing to the hogging moment with a mean return period of 20 years is because this sea state is most relevant during the operational lifetime of the vessel. The reason that the sea state related to the response with a mean return period of 10^4 years was investigated is to consider realistic physical events if design for an annual failure probability of 10^{-4} is aimed at. Hogging is considered because it is the most relevant mode due to the nature of extreme waves (peaks are larger than troughs), and because it is the dominant mode for containerships. Moreover, the studies of Dietz [4] showed that the accuracy of the response conditioning methods was lower for hogging than for sagging moments.

3.2 Numerical analysis

The numerical simulations were performed with the nonlinear hydroelastic hybrid strip theory code presented by Wu and Moan [7]. The hybrid approach

is a combination of the conventional direct load evaluation for a rigid body and the modal superposition for a flexible hull. It still accounts for the dynamic effects in the lowest few global flexible modes, but to achieve improved computational efficiency omits to evaluate the quasi-static responses in the higher global flexible modes. The nonlinearities in the vertical motions and cross-sectional load effects are introduced in the form of a nonlinear vertical excitation force. In this way the relationship between the ship motions or the load effects and the excitation force can remain linear, while the excitation force is no longer linearly related to the incident wave. The total nonlinear excitation force consists of a linear part and a nonlinear modification part. The response is decomposed in the same manner. The linear part is evaluated using 2D or 2.5D strip theory. In this paper the former was used because of the low forward speed. The nonlinear modification part is obtained as the convolution of the linear impulse response function and the nonlinear modification force. The nonlinearities considered are due to the slamming impact force, the nonlinear incident wave force and the nonlinear hydrostatic restoring force. More details about the method were described by Wu and Moan [14; 7], Wu and Hermundstad [15] and Drummen [16]. For the calculation of the global structural dynamic effect only the first flexible vertical mode was taken into account. The number of wave components, N, was equal to 1599 for all simulations. The mass and stiffness distributions were chosen equal to those measured for the experimental model. Details about these distributions were presented by Drummen [16].

Figs. 2 and 3 show the probability distributions of the midships hogging moments for the sea state contributing most to the hogging moment with a mean return period of 20 years. Both figures present the distributions as obtained by numerical simulations in random irregular waves (RIW), most likely response waves (MLRW) and conditional random response waves (CRRW). For comparison the figures also show the Rayleigh distribution, based on the zeroth spectral moment, Eq. 6. The distributions denoted as 'RIW' were obtained by simulating the given sea state for a period of 240 hours. Results obtained by the MLRW method could be generated very fast, as this required only one run per exceedance probability. Eight exceedance probabilities were investigated, 10^{-1}, 10^{-2} ... 10^{-8}, which means that $\zeta_c(t)$ was obtained from Eq. 11 for eight different linear responses, M_c. The latter were found from the exceedance probabilities using the Rayleigh distribution. The wave profiles were conditioned to give the desired linear response after 150s. Each MLRW was simulated for 300s. The chosen nonlinear response, r_{NL}, was the maximum midships nonlinear vertical hogging bending moment in the time interval 148s $< t <$ 152s. In this way one r_{NL} was obtained for each M_c, thereby linking the linear and the nonlinear response. The probability that the nonlinear response,

R_{NL}, will be larger than r_{NL} was obtained from

$$P(R_{NL} > r_{NL}) = P(R_L > M_c) = \exp\left(-\frac{M_c^2}{2m_0}\right). \tag{29}$$

Note that this does not imply that $P(R_{NL} > r_{NL})$ follows the Rayleigh distribution, as r_{NL} will generally differ from M_c.

Also the CRRWs were conditioned to give the desired linear response after 150s, and the chosen nonlinear response was again the maximum midships nonlinear hogging moment in the time interval 148s $< t <$ 152s. Using these waves, two different sets of results were obtained. The first, denoted 'CRRW', was found using the approach described by Dietz [4] and Dietz et al. [10]. For the sea state corresponding to the mean return period of 20 years 50 different response levels, M_c, were investigated. For the sea state corresponding to the mean return period of 10^4 years this was 60. For each response, 100 simulations with CRRWs were performed. In this manner the conditional probability, $P(R_{NL} > r_{NL}|r_L = M_c)$, that R_{NL} will be larger than r_{NL} was obtained. The unconditional probability was found by unconditioning with respect to the linear response

$$P(R_{NL} > r_{NL}) = \int_0^\infty P(R_{NL} > r_{NL}|r_L = M_c) f_{R_L}(M_c) dM_c, \tag{30}$$

where $f_{R_L}(M_c)$ denotes the Rayleigh distribution. This method, however, requires a large number of runs. Experimental investigations by this method are not possible due to the efforts involved, as discussed by Drummen and Moan [13], and even numerical simulation times will be quite long. An overview of the simulated time for each method is given in Table 3.

As a compromise between the MLRW method and a full CRRW analysis, 26 simulations using CRRWs were performed for eight exceedance probabilities. For each exceedance probability the median of the 26 nonlinear moments was taken as the value presented in the figures. The probability that the nonlinear response, R_{NL}, will be larger than r_{NL} was again found from Eq. 29, where r_{NL} is now the median value as described here. This approach is denoted as 'CRRW (median)'.

Fig. 2 presents the results assuming a rigid hull girder. These results were found by low-pass filtering the response at a circular frequency of 1.75rad/s. The natural frequency of the lowest global flexible mode of the vessel was 3.5rad/s, [16]. Fig. 2 shows that moments obtained using response conditioned waves compare very well with those from random irregular waves. This is in agreement with results obtained by Dietz [4], and basically implies that the

nonlinear peaks of the vertical bending moment correlate well with the linear peaks. Similar results for the flexible hull are given in Fig. 3. The figure shows that the distribution obtained using the MLRW method deviates from the one obtained in RIWs, and that the former has a peculiar drop starting at an exceedance probability of 10^{-4}. This drop is explained as follows. The eight investigated MLRW profiles are scaled variations of the same wave, see Section 2. For low wave heights (high exceedance probabilities) there is almost no influence from slamming. As a result, the vertical bending moments for the flexible hull are approximately equal to those for the rigid hull. With increasing wave height (decreasing exceedance probability) slamming will start to occur around t=150s, increasing the maximum moment for the flexible hull compared to the rigid hull. As the wave height increases even further, slamming events will also occur at an earlier stage, so before t=150s. The whipping responses resulting from these slamming events will interfere with those from the slamming event around t=150s. As a result the maximum response at t=150s is decreased in this case. Since the results denoted as 'CRRW (median)' were based on 26 CRRWs, this method is less affected by the shape of one particular wave profile. The background wave introduces a randomness that prevents this from happening. For exceedance probabilities relevant for design, bending moments obtained from the CRRW (median) approach were 15% to 25% lower than those found in RIWs. Finally, Fig. 3 shows that the vertical bending moments obtained from a full CRRW analysis agree very well with those found in RIWs. But, as mentioned before, this method is computationally very expensive.

Similar probability distributions for the sea state most contributing to the vertical hogging moment with a mean return period of 10^4 years are shown in Figs. 4 and 5. The former figure again confirms the agreement between results from response conditioned and random irregular waves, for a rigid hull. Fig. 5 shows that there is a good agreement between the hogging moments obtained from a full CRRW analysis and those found in RIWs. Also in this case are bending moments found from the CRRW (median) approach 15% to 25% lower than those found in RIWs for exceedance probabilities relevant for design.

3.3 Experimental investigation

The model tests were performed in the towing tank at the Marine Technology Centre in Trondheim. The tank is 260m long, 10.5m wide and between 5.6m and 10m deep. The double flap wave maker is able to produce both regular and irregular waves. The model was built using a scale of 1:45, resulting in a length between perpendiculars of 6.24m. In order to account for the global hydroelastic effect in the experiments, the model was made of four rigid segments connected by three rotational springs. It could thus mimic the first three

global flexible vertical modes of the full scale vessel. A picture of the model is shown in Fig. 6.

As mentioned in Section 3.1, the short-term probability distributions of the midships vertical hogging bending moments were obtained for the sea state most contributing to the hogging moment with a mean return period of 10^4 years. Four exceedance probabilities were investigated, 10^{-2}, 10^{-3}, 10^{-4} and 10^{-5}. Details about the experimental setup and the test program were described by Drummen and Moan [13] and Drummen [16]. The latter reference also presents the challenges involved in using response conditioned waves experimentally in combination with a model with forward speed.

The experimental results are given in Figs. 7 and 8. It should be noted that the wave height measured by a wave probe 5m in front of the wave maker was lower than the wave height requested at this location. Due to the nature of the response conditioned waves and the good repeatability, [13], this however only influenced the absolute value of the response and did not influence the comparison between the random irregular and the response conditioned waves. The transformation, of the wave profile from the target location to that of the wave maker, described in Section 2 was done using Airy wave theory.

The short-term distribution for the response in random irregular waves was obtained by running the model in the given sea state for a period of one day, full scale. As mentioned above, the results by application of the MLRW method can be generated very fast, as this requires only one run per exceedance probability. However, for sake of uncertainty each most likely response wave was run six times. The value presented in the figures represents the average of the six responses obtained for each particular exceedance probability. The dispersion of the results was small, as indicated by Drummen and Moan [13]. As also mentioned above, a full experimental CRRW analysis was not possible. In this case 10 CRRWs were run for each response level, as a compromise between the MLRW method and a full CRRW analysis. The figures give the median value resulting from this. For both the MLRW and the CRRW (median) methods the nonlinear responses and their exceedance probabilities were obtained in the same way as described in the previous section.

Fig. 7 presents the short-term probability distribution of the midships vertical hogging bending moment assuming a rigid hull. The figure shows that the bending moments obtained in response conditioned waves compare well with those found in random irregular waves. Similar results for the flexible hull are presented in Fig. 8. Here it seems that the vertical bending moments obtained using MLRWs are approximately 15% lower than those found using RIWs. Results from CRRWs compare better with RIW results, although the deviation between the two increases with increasing response level.

3.4 Comparison between numerical analysis and experimental results

Figs. 4 and 7, and Figs. 5 and 8 show a considerable difference between the vertical bending moments obtained numerically and experimentally. For the rigid hull, the calculated hogging moments are approximately 30% higher than the corresponding measured ones at the exceedance probability level of 10^{-4}. For the flexible hull, this is about 100%. One important source for this difference is that, as described in the previous section, the wave height measured by a wave probe in front of the wave maker was lower than the wave height requested at this location. Another source are the nonlinear wave interactions in the towing tank. During its propagation from the wave maker to the model, the wave was affected by these nonlinear interactions. This was not accounted for in the numerical method since Airy wave theory was used. Thus part of the differences observed between Figs. 4 and 7, and Figs. 5 and 8 are related to incident waves which were not equal.

In order to better evaluate the accuracy of the numerical method, the calculations were repeated using the incident wave elevation which the model experienced in the tank as input. However, the wave elevation measured at the centre of gravity of the model during the tests was disturbed by the model. Therefore, the MLRWs were repeated without the model in the tank. In this way the wave elevation at the location of the centre of gravity of the model could be measured, without the model disturbing the flow field. This could be done since Drummen and Moan [13] concluded that the waves repeated very well in the towing tank at the Marine Technology Centre in Trondheim. The comparison between the experimentally and the numerically obtained vertical bending moments is shown in Figs. 9 and 10, and was done for the MLRW which led to a response with an exceedance probability of 10^{-4} in the sea state contributing most to the hogging moment with a mean return period 10^4 years. Experimentally, the wave profiles were conditioned to give the desired response at approximately t=600s. Sagging is positive in the figures.

Fig. 9 shows an almost perfect agreement between the measured and the calculated moments. The response of the vessel is not symmetric around the time instant used for conditioning. This is not inline with the remark made in Section 2, and is partly related to nonlinearities in the response, and partly to nonlinear wave interactions in the towing tank. The agreement is less around t=600s when the hull is considered flexible, Fig. 10. In this area the numerical method over-predicts the whipping response. The maximum hogging bending moment obtained using the numerical method is approximately 30% higher than the one found during the experiments, which is in line with the findings presented earlier by Drummen et al. [17]. The over-prediction is at least partly attributed to the fact that 3D effects are not accounted for in the 2D slamming force calculation. After t=620s measurements and calculations again agree

quite well.

4 Conclusions

In this paper we presented the results of a numerical and experimental investigation into the application of response conditioned waves for long-term nonlinear analyses. The studies were performed using a container vessel, with a length between perpendiculars of 281m. The calculations were done with a nonlinear hydroelastic hybrid strip theory method, and the model tests were carried out in the towing tank at the Marine Technology Centre in Trondheim. The probability distributions of the midships vertical hogging bending moments in the sea states contributing most to the hogging moment with a mean return period of 20 years and 10 000 years were investigated. These sea states were obtained by applying the coefficient of contribution method to the results of linear long-term analyses. For both sea states, a comparison was made between the short-term probability distributions determined numerically from random irregular waves (RIW) and from response conditioned waves. Experimentally only the sea state most contributing to the hogging moment with a mean return period 10 000 years was investigated. In all cases the vessel encountered head waves with 5kn forward speed. The comparisons showed that the most likely response wave (MLRW) method can very efficiently be used to accurately determine the nonlinear short-term probability distributions for rigid hulls.

When the hull girder is flexible, the MLRW method can no longer be used to accurately obtain the short-term probability distributions. It was also found that using the MLRW method in combination with a correction factor, as proposed by Dietz [4], can lead to unreliable results because the complete probability distribution obtained with this method is based on scaled variations of a single wave profile.

The vertical bending moments obtained numerically from a full conditional random response wave (CRRW) analysis agreed very well with those found in RIWs, even for the flexible hull. The simulated time was however long. For this paper approximately 17 days (417 hours) of simulated time was used. This time can be reduced by only performing simulations in the response range of interest, as well as by simulating only until several seconds after the conditioned event. It should, however, be noted that each single simulation using CRRWs requires a certain duration to eliminate the effects due to initial conditions. The required time for finding nonlinear short-term probability distributions from a full CRRW analysis will therefore in general be of the same order of magnitude as the time needed for a conventional analysis in RIWs, typically 100 hours to 150 hours according to Wu and Moan [18]. Ex-

perimental investigations with this duration are too long for most practical cases. A full CRRW analysis was therefore not done during the model tests.

As a compromise between the MLRW method and a full CRRW analysis, 26 numerical simulations using CRRWs were performed for eight response levels, and 10 CRRWs were run experimentally for four response levels. The nonlinear response was chosen as the median value of the 26 or 10 responses following from the analyses. Contrary to the MLRW method, this method depends on more than one wave profile and it requires considerably less time than a full CRRW analysis. It was found that vertical hogging bending moments obtained from this approach were 15% to 25% lower than those found in RIWs for exceedance probabilities relevant for design. It is therefore recommended not to use the MLRW method but the CRRW (median) method in combination with a correction factor, as an accurate and efficient approach for obtaining the nonlinear short-term probability distributions for flexible hulls.

A comparison between the time series of the measured and the calculated midships bending moments due to the same MLRW showed an almost perfect agreement when the hull was assumed rigid. For the flexible hull, the maximum hogging moment obtained using the numerical method was approximately 30% higher than the one found during the experiments. This is at least partly attributed to the fact that 3D effects are not accounted for in the 2D slamming force calculation.

Acknowledgements

The authors acknowledge the financial support from the Research Council of Norway through CeSOS. Moreover, the yard and the owner of the vessel are acknowledged for permitting use of the ship lines. DNV deserves thanks for providing all the necessary ship data. The first author would also like to thank Prof. Toichi Fukasawa for the discussions on the topic of response conditioned waves. Dr. Ole A. Hermundstad is thanked for providing his code Wavegen.

References

[1] Friis-Hansen P, Nielsen LP. On the new wave model for the kinematics of large ocean waves. In: Proceedings 14th International Conference on Offshore Mechanics and Arctic Engineering. Copenhagen, Denmark, 1995, p. 17–24.

[2] Taylor PH, Jonathan P, Harland LA. Time domain simulations of jack-up dynamics with the extremes of a Gaussian process. In: Proceedings 14th

International Conference on Offshore Mechanics and Arctic Engineering. Copenhagen, Denmark, 1995, p. 313–319.
[3] Adegeest L, Braathen A, Løseth R. Use of non-linear sea-loads simulations in design of ships. In: Proceedings 7th International Symposium on Practical Design of Ships and Other Floating Structures. The Hague, The Netherlands, 1998, p. 53–58.
[4] Dietz JS. Application of conditional waves as critical wave episodes for extreme loads on marine structures. Ph.D. thesis, Dept. Mechanical Engineering, Technical University of Denmark, Lyngby, Denmark, 2004.
[5] Pastoor LW. On the assessment of nonlinear ship motions and loads. Ph.D. thesis, Ship Hydromechanics Laboratory, Faculty of Design Engineering and Production, Delft University of Technology, Delft, The Netherlands, 2002.
[6] ISSC. Report of committee I.2: Loads. In: Proceedings 16th International Ship and Offshore Structures Congress. Southampton, UK, 2006, p. 85–173.
[7] Wu MK, Moan T. Efficient calculation of wave-induced ship responses considering structural dynamic effects. Applied Ocean Research 2005;21(2):81–96.
[8] Cramér H. Leadbetter M. Stationary and Related Stochastic Processes. Mineola, New York: Dover Publications, Inc., 1967.
[9] Ditlevsen O. Survey on applications of Slepian model processes in structural reliability. In: Proceedings 4th International Conference on Structural Safety and Reliability. Japan, 1985.
[10] Dietz JS, Friis-Hansen P, Jensen JJ. Design wave episodes for extreme value ship responses. In: Proceedings 9th International Symposium on Practical Design of Ships and Other Floating Structures. Luebeck-Travemuende, Germany, 2004.
[11] Fukasawa T, Kawabe H, Moan T. On extreme ship response in severe short-term sea state. In: Proceedings International Conference on Advancements in Marine Structures. UK, 2007.
[12] Baarholm GS, Moan T. Estimation of nonlinear long-term extremes of hull girder loads in ships. Marine Structures 2000;13(6):495–516.
[13] Drummen I, Moan T. Experimental investigation of the application of response conditioned waves for long-term nonlinear analyses. In: Proceedings 10th International Symposium on Practical Design of Ships and Other Floating Structures. Houston, US, 2007, p. 322–329.
[14] Wu MK, Moan T. Linear and nonlinear hydroelastic analysis of high-speed vessels. Journal of Ship Research 1996;40(2):149–163.
[15] Wu MK, Hermundstad OA. Time-domain simulation of wave-induced nonlinear motions and loads and its applications in ship design. Marine Structures 2002;15(6):561–597.
[16] Drummen I. Experimental and numerical investigation of nonlinear wave-induced load effects in containerships considering hydroelasticity. Ph.D. thesis, Dept. of Marine Technology, Norwegian University of Science and

Technology, Trondheim, Norway, 2008.
[17] Drummen I, Wu MK, Moan T. Experimental and numerical study of containership responses in severe head seas. submitted to Marine Structures.
[18] Wu MK, Moan T. Statistical analysis of wave-induced extreme nonlinear load effects using time-domain simulations. Applied Ocean Research 2006;28(6):386–397.

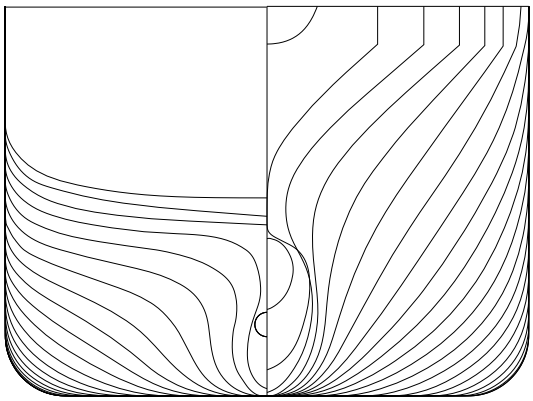

Fig. 1. Body plan of the vessel.

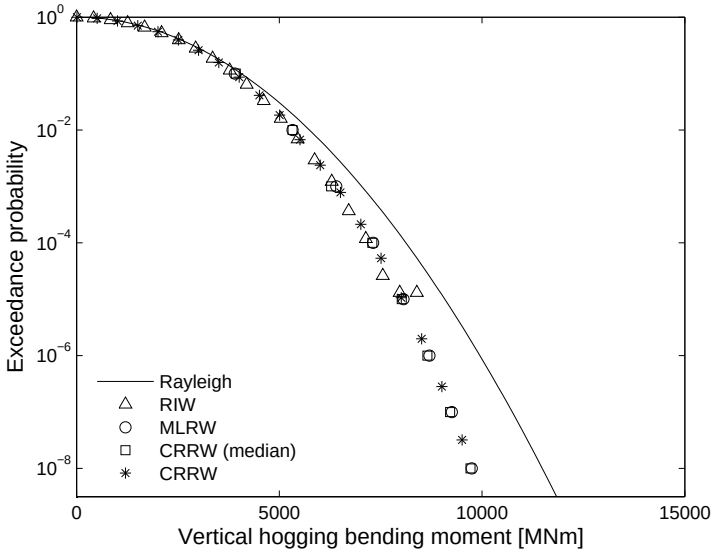

Fig. 2. Numerically obtained probability distribution of the midships vertical hogging bending moment for a rigid hull. H_s=15m, T_p=13.28s and γ=5. RIW, MLRW and CRRW respectively denote random irregular wave, most likely response wave and conditional random response wave.

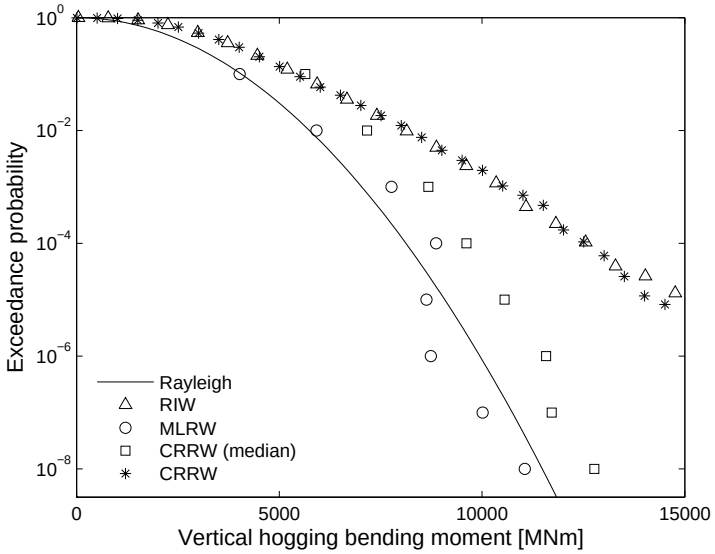

Fig. 3. Numerically obtained probability distribution of the midships vertical hogging bending moment for a flexible hull. H_s=15m, T_p=13.28s and γ=5. RIW, MLRW and CRRW respectively denote random irregular wave, most likely response wave and conditional random response wave.

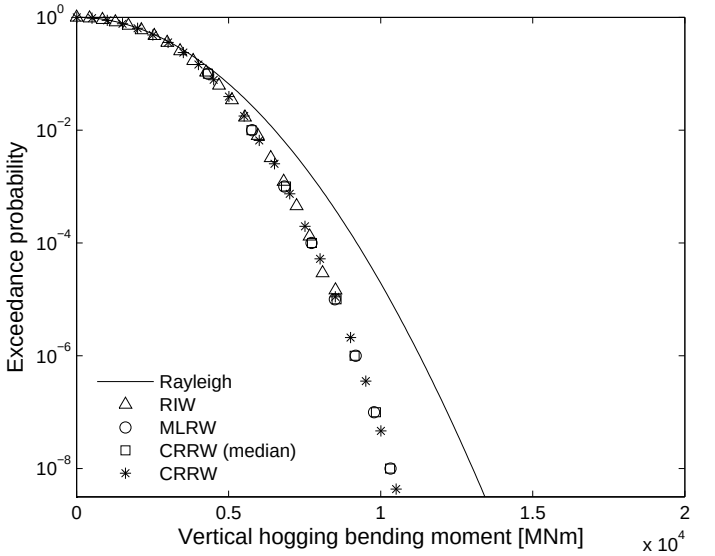

Fig. 4. Numerically obtained probability distribution of the midships vertical hogging bending moment for a rigid hull. H_s=19m, T_p=15.89s and γ=4.75. RIW, MLRW and CRRW respectively denote random irregular wave, most likely response wave and conditional random response wave.

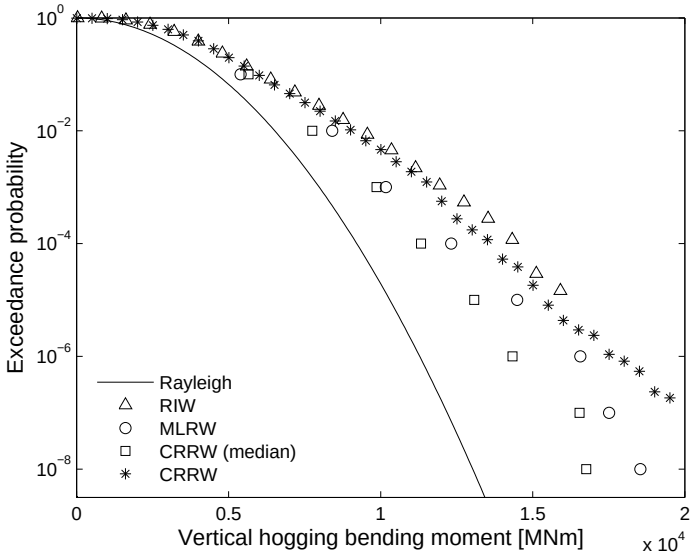

Fig. 5. Numerically obtained probability distribution of the midships vertical hogging bending moment for a flexible hull. H_s=19m, T_p=15.89s and γ=4.75. RIW, MLRW and CRRW respectively denote random irregular wave, most likely response wave and conditional random response wave.

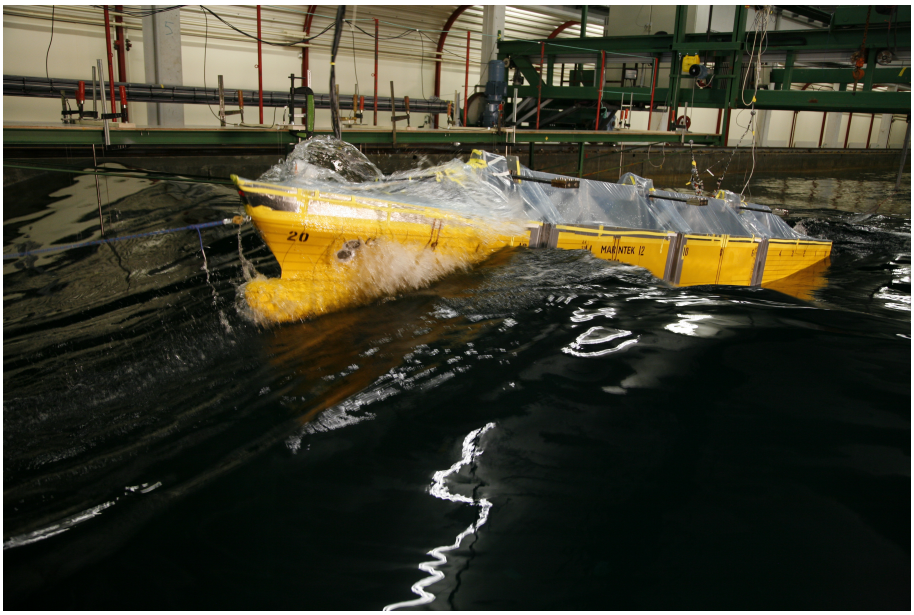

Fig. 6. Model and towing carriage.

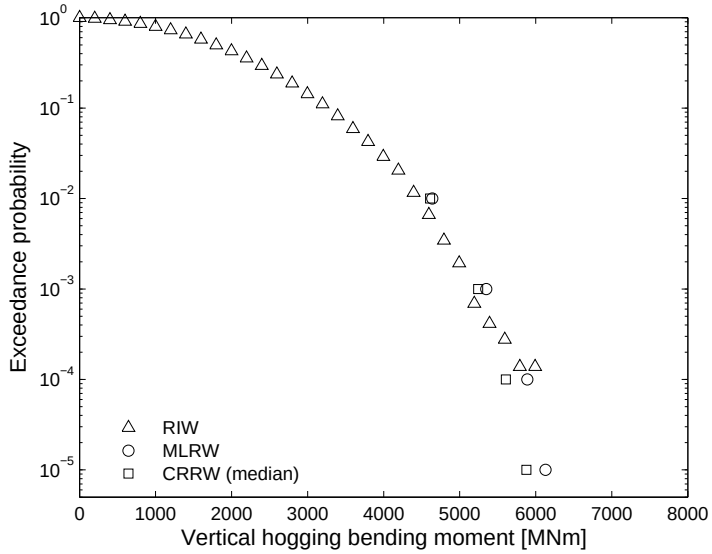

Fig. 7. Experimentally obtained probability distribution of the midships vertical hogging bending moment for a rigid hull. H_s=19m, T_p=15.89s and γ=4.75 (requested). RIW, MLRW and CRRW respectively denote random irregular wave, most likely response wave and conditional random response wave.

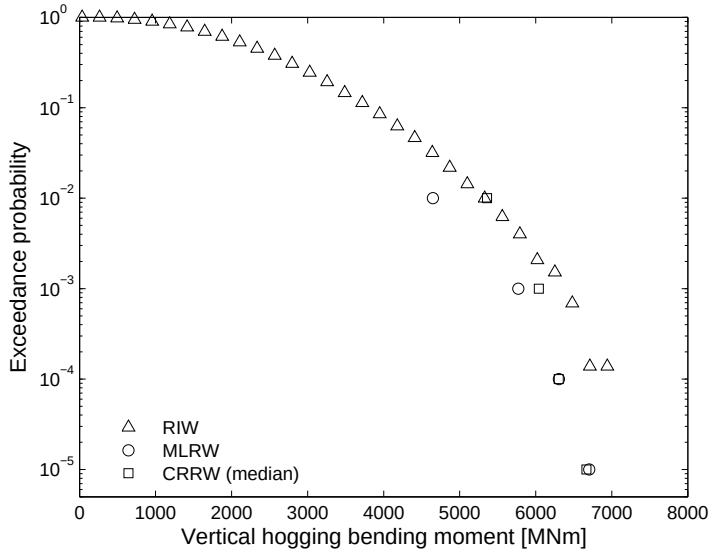

Fig. 8. Experimentally obtained probability distribution of the midships vertical hogging bending moment for a flexible hull. H_s=19m, T_p=15.89s and γ=4.75 (requested). RIW, MLRW and CRRW respectively denote random irregular wave, most likely response wave and conditional random response wave.

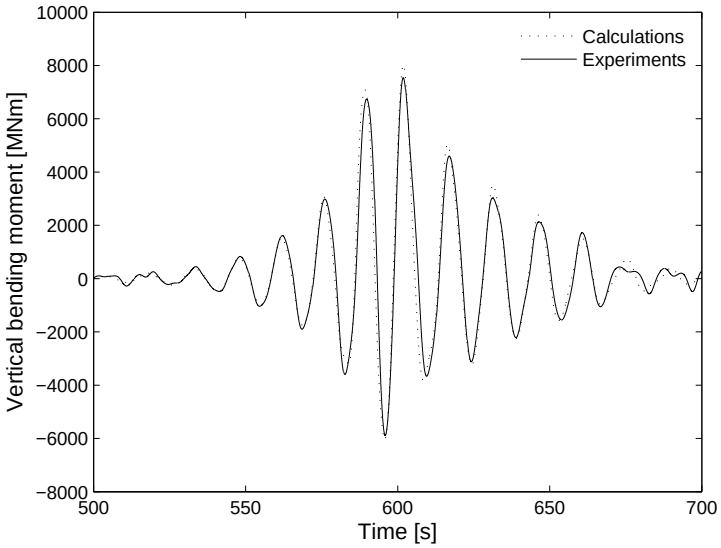

Fig. 9. Midships vertical bending moment in a most likely response wave, rigid hull.

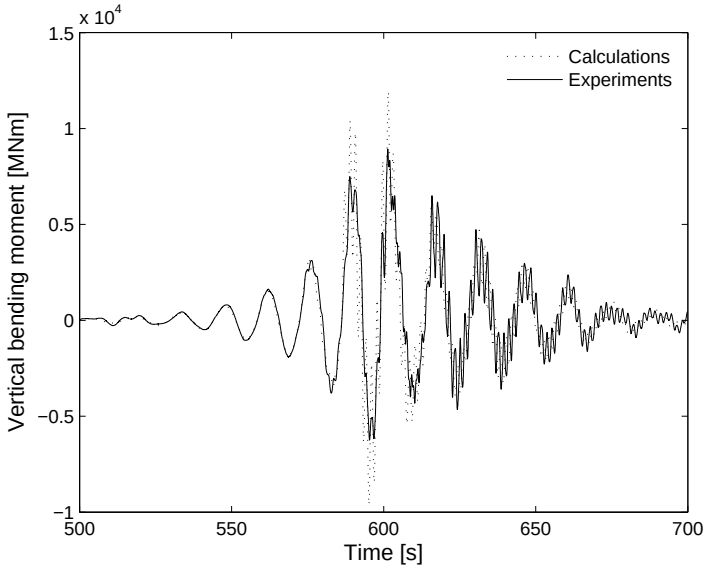

Fig. 10. Midships vertical bending moment in a most likely response wave, flexible hull.

Table 1
Main particulars of the vessel and its conditions during the investigations

Main particular	
Length overall	294.01m
Length between perpendiculars	280.98m
Beam	32.26m
Draft during investigations	11.75m
Trim during investigations	0.00m
Displacement during investigations	76656ton
Speed during investigations	5kn

Table 2
Parameters of the most contributing sea states. H_s, T_p and γ denote significant wave height, peak period and peakedness parameter respectively

	Mean return period	
	20 years	10^4 years
H_s	15m	19m
T_p	13.28s	15.89s
γ	5	4.75

Table 3
Numerically simulated time. RIW, MLRW and CRRW respectively denote random irregular wave, most likely response wave and conditional random response wave

Method	Time [s]
RIW	864000
MLRW	2400
CRRW (median)	62400
CRRW	1500000

Previous reports published at the
Institute of Marine Technology
(previously: Faculty of Marine Technology)
Norwegian University of Science and Technology

UR-79-01 Brigt Hatlestad, MK:	The finite element method used in a fatigue evaluation of fixed offshore platforms. (Dr.Ing. Thesis)
UR-79-02 Erik Pettersen, MK:	Analysis and design of cellular structures. (Dr.Ing. Thesis)
UR-79-03 Sverre Valsgård, MK:	Finite difference and finite element methods applied to nonlinear analysis of plated structures. (Dr.Ing. Thesis)
UR-79-04 Nils T. Nordsve, MK:	Finite element collapse analysis of structural members considering imperfections and stresses due to fabrication. (Dr.Ing. Thesis)
UR-79-05 Ivar J. Fylling, MK:	Analysis of towline forces in ocean towing systems. (Dr.Ing. Thesis)
UR-80-06 Nils Sandsmark, MM:	Analysis of Stationary and Transient Heat Conduction by the Use of the Finite Element Method. (Dr.Ing. Thesis)
UR-80-09 Sverre Haver, MK:	Analysis of uncertainties related to the stochastic modelling of ocean waves. (Dr.Ing. Thesis)
UR-85-46 Alf G. Engseth, MK:	Finite element collapse analysis of tubular steel offshore structures. (Dr.Ing. Thesis)
UR-86-47 Dengody Sheshappa, MP:	A Computer Design Model for Optimizing Fishing Vessel Designs Based on Techno-Economic Analysis. (Dr.Ing. Thesis)
UR-86-48 Vidar Aanesland, MH:	A Theoretical and Numerical Study of Ship Wave Resistance. (Dr.Ing. Thesis)
UR-86-49 Heinz-Joachim Wessel, MK:	Fracture Mechanics Analysis of Crack Growth in Plate Girders. (Dr.Ing. Thesis)
UR-86-50 Jon Taby, MK:	Ultimate and Post-ultimate Strength of Dented Tubular Members. (Dr.Ing. Thesis)

UR-86-51 Walter Lian, MH:	A Numerical Study of Two-Dimensional Separated Flow Past Bluff Bodies at Moderate KC-Numbers. (Dr.Ing. Thesis)
UR-86-52 Bjørn Sortland, MH:	Force Measurements in Oscillating Flow on Ship Sections and Circular Cylinders in a U-Tube Water Tank. (Dr.Ing. Thesis)
UR-86-53 Kurt Strand, MM:	A System Dynamic Approach to One-dimensional Fluid Flow. (Dr.Ing. Thesis)
UR-86-54 Arne Edvin Løken, MH:	Three Dimensional Second Order Hydrodynamic Effects on Ocean Structures in Waves. (Dr.Ing. Thesis)
UR-86-55 Sigurd Falch, MH:	A Numerical Study of Slamming of Two-Dimensional Bodies. (Dr.Ing. Thesis)
UR-87-56 Arne Braathen, MH:	Application of a Vortex Tracking Method to the Prediction of Roll Damping of a Two-Dimension Floating Body. (Dr.Ing. Thesis)
UR-87-57 Bernt Leira, MR:	Gaussian Vector Processes for Reliability Analysis involving Wave-Induced Load Effects. (Dr.Ing. Thesis)
UR-87-58 Magnus Småvik, MM:	Thermal Load and Process Characteristics in a Two-Stroke Diesel Engine with Thermal Barriers (in Norwegian). (Dr.Ing. Thesis)
MTA-88-59 Bernt Arild Bremdal, MP:	An Investigation of Marine Installation Processes - A Knowledge - Based Planning Approach. (Dr.Ing. Thesis)
MTA-88-60 Xu Jun, MK:	Non-linear Dynamic Analysis of Space-framed Offshore Structures. (Dr.Ing. Thesis)
MTA-89-61 Gang Miao, MH:	Hydrodynamic Forces and Dynamic Responses of Circular Cylinders in Wave Zones. (Dr.Ing. Thesis)
MTA-89-62 Martin Greenhow, MH:	Linear and Non-Linear Studies of Waves and Floating Bodies. Part I and Part II. (Dr.Techn. Thesis)
MTA-89-63 Chang Li, MH:	Force Coefficients of Spheres and Cubes in Oscillatory Flow with and without Current. (Dr.Ing. Thesis)

MTA-89-64 Hu Ying, MP:	A Study of Marketing and Design in Development of Marine Transport Systems. (Dr.Ing. Thesis)
MTA-89-65 Arild Jæger, MH:	Seakeeping, Dynamic Stability and Performance of a Wedge Shaped Planing Hull. (Dr.Ing. Thesis)
MTA-89-66 Chan Siu Hung, MM:	The dynamic characteristics of tilting-pad bearings.
MTA-89-67 Kim Wikstrøm, MP:	Analysis av projekteringen for ett offshore projekt. (Licenciat-avhandling)
MTA-89-68 Jiao Guoyang, MR:	Reliability Analysis of Crack Growth under Random Loading, considering Model Updating. (Dr.Ing. Thesis)
MTA-89-69 Arnt Olufsen, MK:	Uncertainty and Reliability Analysis of Fixed Offshore Structures. (Dr.Ing. Thesis)
MTA-89-70 Wu Yu-Lin, MR:	System Reliability Analyses of Offshore Structures using improved Truss and Beam Models. (Dr.Ing. Thesis)
MTA-90-71 Jan Roger Hoff, MH:	Three-dimensional Green function of a vessel with forward speed in waves. (Dr.Ing. Thesis)
MTA-90-72 Rong Zhao, MH:	Slow-Drift Motions of a Moored Two-Dimensional Body in Irregular Waves. (Dr.Ing. Thesis)
MTA-90-73 Atle Minsaas, MP:	Economical Risk Analysis. (Dr.Ing. Thesis)
MTA-90-74 Knut-Aril Farnes, MK:	Long-term Statistics of Response in Non-linear Marine Structures. (Dr.Ing. Thesis)
MTA-90-75 Torbjørn Sotberg, MK:	Application of Reliability Methods for Safety Assessment of Submarine Pipelines. (Dr.Ing. Thesis)
MTA-90-76 Zeuthen, Steffen, MP:	SEAMAID. A computational model of the design process in a constraint-based logic programming environment. An example from the offshore domain. (Dr.Ing. Thesis)
MTA-91-77 Haagensen, Sven, MM:	Fuel Dependant Cyclic Variability in a Spark Ignition Engine - An Optical Approach. (Dr.Ing. Thesis)

MTA-91-78 Løland, Geir, MH:	Current forces on and flow through fish farms. (Dr.Ing. Thesis)
MTA-91-79 Hoen, Christopher, MK:	System Identification of Structures Excited by Stochastic Load Processes. (Dr.Ing. Thesis)
MTA-91-80 Haugen, Stein, MK:	Probabilistic Evaluation of Frequency of Collision between Ships and Offshore Platforms. (Dr.Ing. Thesis)
MTA-91-81 Sødahl, Nils, MK:	Methods for Design and Analysis of Flexible Risers. (Dr.Ing. Thesis)
MTA-91-82 Ormberg, Harald, MK:	Non-linear Response Analysis of Floating Fish Farm Systems. (Dr.Ing. Thesis)
MTA-91-83 Marley, Mark J., MK:	Time Variant Reliability under Fatigue Degradation. (Dr.Ing. Thesis)
MTA-91-84 Krokstad, Jørgen R., MH:	Second-order Loads in Multidirectional Seas. (Dr.Ing. Thesis)
MTA-91-85 Molteberg, Gunnar A., MM:	The Application of System Identification Techniques to Performance Monitoring of Four Stroke Turbocharged Diesel Engines. (Dr.Ing. Thesis)
MTA-92-86 Mørch, Hans Jørgen Bjelke, MH:	Aspects of Hydrofoil Design: with Emphasis on Hydrofoil Interaction in Calm Water. (Dr.Ing. Thesis)
MTA-92-87 Chan Siu Hung, MM:	Nonlinear Analysis of Rotordynamic Instabilities in High-speed Turbomachinery. (Dr.Ing. Thesis)
MTA-92-88 Bessason, Bjarni, MK:	Assessment of Earthquake Loading and Response of Seismically Isolated Bridges. (Dr.Ing. Thesis)
MTA-92-89 Langli, Geir, MP:	Improving Operational Safety through exploitation of Design Knowledge - an investigation of offshore platform safety. (Dr.Ing. Thesis)
MTA-92-90 Sævik, Svein, MK:	On Stresses and Fatigue in Flexible Pipes. (Dr.Ing. Thesis)
MTA-92-91 Ask, Tor Ø., MM:	Ignition and Flame Growth in Lean Gas-Air Mixtures. An Experimental Study with a Schlieren System. (Dr.Ing. Thesis)

MTA-86-92 Hessen, Gunnar, MK:	Fracture Mechanics Analysis of Stiffened Tubular Members. (Dr.Ing. Thesis)
MTA-93-93 Steinebach, Christian, MM:	Knowledge Based Systems for Diagnosis of Rotating Machinery. (Dr.Ing. Thesis)
MTA-93-94 Dalane, Jan Inge, MK:	System Reliability in Design and Maintenance of Fixed Offshore Structures. (Dr.Ing. Thesis)
MTA-93-95 Steen, Sverre, MH:	Cobblestone Effect on SES. (Dr.Ing. Thesis)
MTA-93-96 Karunakaran, Daniel, MK:	Nonlinear Dynamic Response and Reliability Analysis of Drag-dominated Offshore Platforms. (Dr.Ing. Thesis)
MTA-93-97 Hagen, Arnulf, MP:	The Framework of a Design Process Language. (Dr.Ing. Thesis)
MTA-93-98 Nordrik, Rune, MM:	Investigation of Spark Ignition and Autoignition in Methane and Air Using Computational Fluid Dynamics and Chemical Reaction Kinetics. A Numerical Study of Ignition Processes in Internal Combustion Engines. (Dr.Ing. Thesis)
MTA-94-99 Passano, Elizabeth, MK:	Efficient Analysis of Nonlinear Slender Marine Structures. (Dr.Ing. Thesis)
MTA-94-100 Kvålsvold, Jan, MH:	Hydroelastic Modelling of Wetdeck Slamming on Multihull Vessels. (Dr.Ing. Thesis)
MTA-94-102 Bech, Sidsel M., MK:	Experimental and Numerical Determination of Stiffness and Strength of GRP/PVC Sandwich Structures. (Dr.Ing. Thesis)
MTA-95-103 Paulsen, Hallvard, MM:	A Study of Transient Jet and Spray using a Schlieren Method and Digital Image Processing. (Dr.Ing. Thesis)
MTA-95-104 Hovde, Geir Olav, MK:	Fatigue and Overload Reliability of Offshore Structural Systems, Considering the Effect of Inspection and Repair. (Dr.Ing. Thesis)
MTA-95-105 Wang, Xiaozhi, MK:	Reliability Analysis of Production Ships with Emphasis on Load Combination and Ultimate Strength. (Dr.Ing. Thesis)

MTA-95-106 Ulstein, Tore, MH:	Nonlinear Effects of a Flexible Stern Seal Bag on Cobblestone Oscillations of an SES. (Dr.Ing. Thesis)
MTA-95-107 Solaas, Frøydis, MH:	Analytical and Numerical Studies of Sloshing in Tanks. (Dr.Ing. Thesis)
MTA-95-108 Hellan, øyvind, MK:	Nonlinear Pushover and Cyclic Analyses in Ultimate Limit State Design and Reassessment of Tubular Steel Offshore Structures. (Dr.Ing. Thesis)
MTA-95-109 Hermundstad, Ole A., MK:	Theoretical and Experimental Hydroelastic Analysis of High Speed Vessels. (Dr.Ing. Thesis)
MTA-96-110 Bratland, Anne K., MH:	Wave-Current Interaction Effects on Large-Volume Bodies in Water of Finite Depth. (Dr.Ing. Thesis)
MTA-96-111 Herfjord, Kjell, MH:	A Study of Two-dimensional Separated Flow by a Combination of the Finite Element Method and Navier-Stokes Equations. (Dr.Ing. Thesis)
MTA-96-112 Æsøy, Vilmar, MM:	Hot Surface Assisted Compression Ignition in a Direct Injection Natural Gas Engine. (Dr.Ing. Thesis)
MTA-96-113 Eknes, Monika L., MK:	Escalation Scenarios Initiated by Gas Explosions on Offshore Installations. (Dr.Ing. Thesis)
MTA-96-114 Erikstad, Stein O., MP:	A Decision Support Model for Preliminary Ship Design. (Dr.Ing. Thesis)
MTA-96-115 Pedersen, Egil, MH:	A Nautical Study of Towed Marine Seismic Streamer Cable Configurations. (Dr.Ing. Thesis)
MTA-97-116 Moksnes, Paul O., MM:	Modelling Two-Phase Thermo-Fluid Systems Using Bond Graphs. (Dr.Ing. Thesis)
MTA-97-117 Halse, Karl H., MK:	On Vortex Shedding and Prediction of Vortex-Induced Vibrations of Circular Cylinders. (Dr.Ing. Thesis)
MTA-97-118 Igland, Ragnar T., MK:	Reliability Analysis of Pipelines during Laying, considering Ultimate Strength under Combined Loads. (Dr.Ing. Thesis)
MTA-97-119 Pedersen, Hans-P., MP:	Levendefiskteknologi for fiskefartøy. (Dr.Ing. Thesis)

MTA-98-120 Vikestad, Kyrre, MK:	Multi-Frequency Response of a Cylinder Subjected to Vortex Shedding and Support Motions. (Dr.Ing. Thesis)
MTA-98-121 Azadi, Mohammad R. E., MK:	Analysis of Static and Dynamic Pile-Soil-Jacket Behaviour. (Dr.Ing. Thesis)
MTA-98-122 Ulltang, Terje, MP:	A Communication Model for Product Information. (Dr.Ing. Thesis)
MTA-98-123 Torbergsen, Erik, MM:	Impeller/Diffuser Interaction Forces in Centrifugal Pumps. (Dr.Ing. Thesis)
MTA-98-124 Hansen, Edmond, MH:	A Discrete Element Model to Study Marginal Ice Zone Dynamics and the Behaviour of Vessels Moored in Broken Ice. (Dr.Ing. Thesis)
MTA-98-125 Videiro, Paulo M., MK:	Reliability Based Design of Marine Structures. (Dr.Ing. Thesis)
MTA-99-126 Mainçon, Philippe, MK:	Fatigue Reliability of Long Welds Application to Titanium Risers. (Dr.Ing. Thesis)
MTA-99-127 Haugen, Elin M., MH:	Hydroelastic Analysis of Slamming on Stiffened Plates with Application to Catamaran Wetdecks. (Dr.Ing. Thesis)
MTA-99-128 Langhelle, Nina K., MK:	Experimental Validation and Calibration of Nonlinear Finite Element Models for Use in Design of Aluminium Structures Exposed to Fire. (Dr.Ing. Thesis)
MTA-99-129 Berstad, Are J., MK:	Calculation of Fatigue Damage in Ship Structures. (Dr.Ing. Thesis)
MTA-99-130 Andersen, Trond M., MM:	Short Term Maintenance Planning. (Dr.Ing. Thesis)
MTA-99-131 Tveiten, Bård Wathne, MK:	Fatigue Assessment of Welded Aluminium Ship Details. (Dr.Ing. Thesis)
MTA-99-132 Søreide, Fredrik, MP:	Applications of underwater technology in deep water archaeology. Principles and practice. (Dr.Ing. Thesis)
MTA-99-133 Tønnessen, Rune, MH:	A Finite Element Method Applied to Unsteady Viscous Flow Around 2D Blunt Bodies With Sharp Corners. (Dr.Ing. Thesis)

MTA-99-134 Elvekrok, Dag R., MP:	Engineering Integration in Field Development Projects in the Norwegian Oil and Gas Industry. The Supplier Management of Norne. (Dr.Ing. Thesis)
MTA-99-135 Fagerholt, Kjetil, MP:	Optimeringsbaserte Metoder for Ruteplanlegging innen skipsfart. (Dr.Ing. Thesis)
MTA-99-136 Bysveen, Marie, MM:	Visualization in Two Directions on a Dynamic Combustion Rig for Studies of Fuel Quality. (Dr.Ing. Thesis)
MTA-2000-137 Storteig, Eskild, MM:	Dynamic characteristics and leakage performance of liquid annular seals in centrifugal pumps. (Dr.Ing. Thesis)
MTA-2000-138 Sagli, Gro, MK:	Model uncertainty and simplified estimates of long term extremes of hull girder loads in ships. (Dr.Ing. Thesis)
MTA-2000-139 Tronstad, Harald, MK:	Nonlinear analysis and design of cable net structures like fishing gear based on the finite element method. (Dr.Ing. Thesis)
MTA-2000-140 Kroneberg, André, MP:	Innovation in shipping by using scenarios. (Dr.Ing. Thesis)
MTA-2000-141 Haslum, Herbjørn Alf, MH:	Simplified methods applied to nonlinear motion of spar platforms. (Dr.Ing. Thesis)
MTA-2001-142 Samdal, Ole Johan, MM:	Modelling of Degradation Mechanisms and Stressor Interaction on Static Mechanical Equipment Residual Lifetime. (Dr.Ing. Thesis)
MTA-2001-143 Baarholm, Rolf Jarle, MH:	Theoretical and experimental studies of wave impact underneath decks of offshore platforms. (Dr.Ing. Thesis)
MTA-2001-144 Wang, Lihua, MK:	Probabilistic Analysis of Nonlinear Wave-induced Loads on Ships. (Dr.Ing. Thesis)
MTA-2001-145 Kristensen, Odd H. Holt, MK:	Ultimate Capacity of Aluminium Plates under Multiple Loads, Considering HAZ Properties. (Dr.Ing. Thesis)
MTA-2001-146 Greco, Marilena, MH:	A Two-Dimensional Study of Green-Water Loading. (Dr.Ing. Thesis)

MTA-2001-147 Heggelund, Svein E., MK:	Calculation of Global Design Loads and Load Effects in Large High Speed Catamarans. (Dr.Ing. Thesis)
MTA-2001-148 Babalola, Olusegun T., MK:	Fatigue Strength of Titanium Risers - Defect Sensitivity. (Dr.Ing. Thesis)
MTA-2001-149 Mohammed, Abuu K., MK:	Nonlinear Shell Finite Elements for Ultimate Strength and Collapse Analysis of Ship Structures. (Dr.Ing. Thesis)
MTA-2002-150 Holmedal, Lars E., MH:	Wave-current interactions in the vicinity of the sea bed. (Dr.Ing. Thesis)
MTA-2002-151 Rognebakke, Olav F., MH:	Sloshing in rectangular tanks and interaction with ship motions. (Dr.Ing. Thesis)
MTA-2002-152 Lader, Pål Furset, MH:	Geometry and Kinematics of Breaking Waves. (Dr.Ing. Thesis)
MTA-2002-153 Yang, Qinzheng, MH:	Wash and wave resistance of ships in finite water depth. (Dr.Ing. Thesis)
MTA-2002-154 Melhus, Øyvin, MM:	Utilization of VOC in Diesel Engines. Ignition and combustion of VOC released by crude oil tankers. (Dr.Ing. Thesis)
MTA-2002-155 Ronæss, Marit, MH:	Wave Induced Motions of Two Ships Advancing on Parallel Course. (Dr.Ing. Thesis)
MTA-2002-156 Økland, Ole D., MK:	Numerical and experimental investigation of whipping in twin hull vessels exposed to severe wet deck slamming. (Dr.Ing. Thesis)
MTA-2002-157 Ge, Chunhua, MK:	Global Hydroelastic Response of Catamarans due to Wet Deck Slamming. (Dr.Ing. Thesis)
MTA-2002-158 Byklum, Eirik, MK:	Nonlinear Shell Finite Elements for Ultimate Strength and Collapse Analysis of Ship Structures. (Dr.Ing. Thesis)
IMT-2003-1 Chen, Haibo, MK:	Probabilistic Evaluation of FPSO-Tanker Collision in Tandem Offloading Operation. (Dr.Ing. Thesis)
IMT-2003-2 Skaugset, Kjetil Bjørn, MK:	On the Suppression of Vortex Induced Vibrations of Circular Cylinders by Radial Water Jets. (Dr.Ing. Thesis)

IMT-2003-3 Chezhian, Muthu	Three-Dimensional Analysis of Slamming. (Dr.Ing. Thesis)
IMT-2003-4 Buhaug, Øyvind	Deposit Formation on Cylinder Liner Surfaces in Medium Speed Engines. (Dr.Ing. Thesis)
IMT-2003-5 Tregde, Vidar	Aspects of Ship Design: Optimization of Aft Hull with Inverse Geometry Design. (Dr.Ing. Thesis)
IMT-2003-6 Wist, Hanne Therese	Statistical Properties of Successive Ocean Wave Parameters. (Dr.Ing. Thesis)
IMT-2004-7 Ransau, Samuel	Numerical Methods for Flows with Evolving Interfaces. (Dr.Ing. Thesis)
IMT-2004-8 Soma, Torkel	Blue-Chip or Sub-Standard. A data interrogation approach of identity safety characteristics of shipping organization. (Dr.Ing. Thesis)
IMT-2004-9 Ersdal, Svein	An experimental study of hydrodynamic forces on cylinders and cables in near axial flow. (Dr.Ing. Thesis)
IMT-2005-10 Brodtkorb, Per Andreas	The Probability of Occurrence of Dangerous Wave Situations at Sea. (Dr.Ing. Thesis)
IMT-2005-11 Yttervik, Rune	Ocean current variability in relation to offshore engineering. (Dr.Ing. Thesis)
IMT-2005-12 Fredheim, Arne	Current Forces on Net-Structures. (Dr.Ing. Thesis)
IMT-2005-13 Heggernes, Kjetil	Flow around marine structures. (Dr.Ing. Thesis)
IMT-2005-14 Fouques, Sebastien	Lagrangian Modelling of Ocean Surface Waves and Synthetic Aperture Radar Wave Measurements. (Dr.Ing. Thesis)
IMT-2006-15 Holm, Håvard	Numerical calculation of viscous free surface flow around marine structures. (Dr.Ing. Thesis)
IMT-2006-16 Bjørheim, Lars G.	Failure Assessment of Long Through Thickness Fatigue Cracks in Ship Hulls. (Dr.Ing. Thesis)
IMT-2006-17 Hansson, Lisbeth	Safety Management for Prevention of Occupational Accidents. (Dr.Ing. Thesis)

IMT-2006-18 Zhu, Xinying	Application of the CIP Method to Strongly Nonlinear Wave-Body Interaction Problems. (Dr.Ing. Thesis)
IMT-2006-19 Reite, Karl Johan	Modelling and Control of Trawl Systems. (Dr.Ing. Thesis)
IMT-2006-20 Smogeli, Øyvind Notland	Control of Marine Propellers. From Normal to Extreme Conditions. (Dr.Ing. Thesis)
IMT-2007-21 Storhaug, Gaute	Experimental Investigation of Wave Induced Vibrations and Their Effect on the Fatigue Loading of Ships. (Dr.Ing. Thesis)
IMT-2007-22 Sun, Hui	A Boundary Element Method Applied to Strongly Nonlinear Wave-Body Interaction Problems. (PhD Thesis, CeSOS)
IMT-2007-23 Rustad, Anne Marthine	Modelling and Control of Top Tensioned Risers. (PhD Thesis, CeSOS)
IMT-2007-24 Johansen, Vegar	Modelling flexible slender system for real-time simulations and control applications.
IMT-2007-25 Wroldsen, Anders Sunde	Modelling and control of tensegrity structures. (PhD Thesis, CeSOS)
IMT-2007-26 Aronsen, Kristoffer Høye	An experimental investigation of in-line and combined in-line and cross flow vortex induced vibrations. (Dr.avhandling, IMT)
IMT-2007-27 Zhen, Gao	Stochastic response analysis of mooring systems with emphasis on frequency-domain analysis of fatgue due to wide-band processes. (PhD-thesis CeSOS).
IMT-2007-28 Thorstensen, Tom Anders	Lifetime Profit Modelling of Ageing Systems Utilizing Information about Technical Condition. Dr.ing. thesis, IMT.
IMT-2008-29 Pákozdi, Csaba	A Smoothed Particle Hydrodynamics Study of Two-dimensional Nonlinear Sloshing in Rectangular Tanks. Dr.ing.thesis, IMT.
IMT-2008-30 Berntsen, Per Ivar B.	Structural Reliability Based Position Mooring. PhD-Thesis, IMT.
IMT-2008-31 Ye, Naiquan	Fatigues Assessment of Aluminium Welded Box stiffener Joints in ships. Dr.ing.-Thesis, IMT.

IMT-2008-32 Radan, Damir	Integrated Control of Marine Electrical Power Systems. PhD-Thesis, IMT.
IMT-2008-33 Norum, Viggo L.	Analysis of Ignituin and Combustion in Otto Lean-Burn Engines with Prechambers. Dr.ing. thesis, IMT.
IMT-2007-33 Thorhus, Runar	Alliances in Development of Short-sea ransport systems. Dr.ing.thesis, IMT.

Previous reports published at the
Institute of Marine Technology
(previously: Faculty of Marine Technology)
Norwegian University of Science and Technology

UR-79-01 Brigt Hatlestad, MK:	The finite element method used in a fatigue evaluation of fixed offshore platforms. (Dr.Ing. Thesis)
UR-79-02 Erik Pettersen, MK:	Analysis and design of cellular structures. (Dr.Ing. Thesis)
UR-79-03 Sverre Valsgård, MK:	Finite difference and finite element methods applied to nonlinear analysis of plated structures. (Dr.Ing. Thesis)
UR-79-04 Nils T. Nordsve, MK:	Finite element collapse analysis of structural members considering imperfections and stresses due to fabrication. (Dr.Ing. Thesis)
UR-79-05 Ivar J. Fylling, MK:	Analysis of towline forces in ocean towing systems. (Dr.Ing. Thesis)
UR-80-06 Nils Sandsmark, MM:	Analysis of Stationary and Transient Heat Conduction by the Use of the Finite Element Method. (Dr.Ing. Thesis)
UR-80-09 Sverre Haver, MK:	Analysis of uncertainties related to the stochastic modelling of ocean waves. (Dr.Ing. Thesis)
UR-85-46 Alf G. Engseth, MK:	Finite element collapse analysis of tubular steel offshore structures. (Dr.Ing. Thesis)
UR-86-47 Dengody Sheshappa, MP:	A Computer Design Model for Optimizing Fishing Vessel Designs Based on Techno-Economic Analysis. (Dr.Ing. Thesis)
UR-86-48 Vidar Aanesland, MH:	A Theoretical and Numerical Study of Ship Wave Resistance. (Dr.Ing. Thesis)
UR-86-49 Heinz-Joachim Wessel, MK:	Fracture Mechanics Analysis of Crack Growth in Plate Girders. (Dr.Ing. Thesis)
UR-86-50 Jon Taby, MK:	Ultimate and Post-ultimate Strength of Dented Tubular Members. (Dr.Ing. Thesis)

UR-86-51 Walter Lian, MH:	A Numerical Study of Two-Dimensional Separated Flow Past Bluff Bodies at Moderate KC-Numbers. (Dr.Ing. Thesis)
UR-86-52 Bjørn Sortland, MH:	Force Measurements in Oscillating Flow on Ship Sections and Circular Cylinders in a U-Tube Water Tank. (Dr.Ing. Thesis)
UR-86-53 Kurt Strand, MM:	A System Dynamic Approach to One-dimensional Fluid Flow. (Dr.Ing. Thesis)
UR-86-54 Arne Edvin Løken, MH:	Three Dimensional Second Order Hydrodynamic Effects on Ocean Structures in Waves. (Dr.Ing. Thesis)
UR-86-55 Sigurd Falch, MH:	A Numerical Study of Slamming of Two-Dimensional Bodies. (Dr.Ing. Thesis)
UR-87-56 Arne Braathen, MH:	Application of a Vortex Tracking Method to the Prediction of Roll Damping of a Two-Dimension Floating Body. (Dr.Ing. Thesis)
UR-87-57 Bernt Leira, MR:	Gaussian Vector Processes for Reliability Analysis involving Wave-Induced Load Effects. (Dr.Ing. Thesis)
UR-87-58 Magnus Småvik, MM:	Thermal Load and Process Characteristics in a Two-Stroke Diesel Engine with Thermal Barriers (in Norwegian). (Dr.Ing. Thesis)
MTA-88-59 Bernt Arild Bremdal, MP:	An Investigation of Marine Installation Processes - A Knowledge - Based Planning Approach. (Dr.Ing. Thesis)
MTA-88-60 Xu Jun, MK:	Non-linear Dynamic Analysis of Space-framed Offshore Structures. (Dr.Ing. Thesis)
MTA-89-61 Gang Miao, MH:	Hydrodynamic Forces and Dynamic Responses of Circular Cylinders in Wave Zones. (Dr.Ing. Thesis)
MTA-89-62 Martin Greenhow, MH:	Linear and Non-Linear Studies of Waves and Floating Bodies. Part I and Part II. (Dr.Techn. Thesis)
MTA-89-63 Chang Li, MH:	Force Coefficients of Spheres and Cubes in Oscillatory Flow with and without Current. (Dr.Ing. Thesis)

MTA-89-64 Hu Ying, MP:	A Study of Marketing and Design in Development of Marine Transport Systems. (Dr.Ing. Thesis)
MTA-89-65 Arild Jæger, MH:	Seakeeping, Dynamic Stability and Performance of a Wedge Shaped Planing Hull. (Dr.Ing. Thesis)
MTA-89-66 Chan Siu Hung, MM:	The dynamic characteristics of tilting-pad bearings.
MTA-89-67 Kim Wikstrøm, MP:	Analysis av projekteringen for ett offshore projekt. (Licenciat-avhandling)
MTA-89-68 Jiao Guoyang, MR:	Reliability Analysis of Crack Growth under Random Loading, considering Model Updating. (Dr.Ing. Thesis)
MTA-89-69 Arnt Olufsen, MK:	Uncertainty and Reliability Analysis of Fixed Offshore Structures. (Dr.Ing. Thesis)
MTA-89-70 Wu Yu-Lin, MR:	System Reliability Analyses of Offshore Structures using improved Truss and Beam Models. (Dr.Ing. Thesis)
MTA-90-71 Jan Roger Hoff, MH:	Three-dimensional Green function of a vessel with forward speed in waves. (Dr.Ing. Thesis)
MTA-90-72 Rong Zhao, MH:	Slow-Drift Motions of a Moored Two-Dimensional Body in Irregular Waves. (Dr.Ing. Thesis)
MTA-90-73 Atle Minsaas, MP:	Economical Risk Analysis. (Dr.Ing. Thesis)
MTA-90-74 Knut-Aril Farnes, MK:	Long-term Statistics of Response in Non-linear Marine Structures. (Dr.Ing. Thesis)
MTA-90-75 Torbjørn Sotberg, MK:	Application of Reliability Methods for Safety Assessment of Submarine Pipelines. (Dr.Ing. Thesis)
MTA-90-76 Zeuthen, Steffen, MP:	SEAMAID. A computational model of the design process in a constraint-based logic programming environment. An example from the offshore domain. (Dr.Ing. Thesis)
MTA-91-77 Haagensen, Sven, MM:	Fuel Dependant Cyclic Variability in a Spark Ignition Engine - An Optical Approach. (Dr.Ing. Thesis)

MTA-91-78 Løland, Geir, MH:	Current forces on and flow through fish farms. (Dr.Ing. Thesis)
MTA-91-79 Hoen, Christopher, MK:	System Identification of Structures Excited by Stochastic Load Processes. (Dr.Ing. Thesis)
MTA-91-80 Haugen, Stein, MK:	Probabilistic Evaluation of Frequency of Collision between Ships and Offshore Platforms. (Dr.Ing. Thesis)
MTA-91-81 Sødahl, Nils, MK:	Methods for Design and Analysis of Flexible Risers. (Dr.Ing. Thesis)
MTA-91-82 Ormberg, Harald, MK:	Non-linear Response Analysis of Floating Fish Farm Systems. (Dr.Ing. Thesis)
MTA-91-83 Marley, Mark J., MK:	Time Variant Reliability under Fatigue Degradation. (Dr.Ing. Thesis)
MTA-91-84 Krokstad, Jørgen R., MH:	Second-order Loads in Multidirectional Seas. (Dr.Ing. Thesis)
MTA-91-85 Molteberg, Gunnar A., MM:	The Application of System Identification Techniques to Performance Monitoring of Four Stroke Turbocharged Diesel Engines. (Dr.Ing. Thesis)
MTA-92-86 Mørch, Hans Jørgen Bjelke, MH:	Aspects of Hydrofoil Design: with Emphasis on Hydrofoil Interaction in Calm Water. (Dr.Ing. Thesis)
MTA-92-87 Chan Siu Hung, MM:	Nonlinear Analysis of Rotordynamic Instabilities in High-speed Turbomachinery. (Dr.Ing. Thesis)
MTA-92-88 Bessason, Bjarni, MK:	Assessment of Earthquake Loading and Response of Seismically Isolated Bridges. (Dr.Ing. Thesis)
MTA-92-89 Langli, Geir, MP:	Improving Operational Safety through exploitation of Design Knowledge - an investigation of offshore platform safety. (Dr.Ing. Thesis)
MTA-92-90 Sævik, Svein, MK:	On Stresses and Fatigue in Flexible Pipes. (Dr.Ing. Thesis)
MTA-92-91 Ask, Tor Ø., MM:	Ignition and Flame Growth in Lean Gas-Air Mixtures. An Experimental Study with a Schlieren System. (Dr.Ing. Thesis)

MTA-86-92 Hessen, Gunnar, MK:	Fracture Mechanics Analysis of Stiffened Tubular Members. (Dr.Ing. Thesis)
MTA-93-93 Steinebach, Christian, MM:	Knowledge Based Systems for Diagnosis of Rotating Machinery. (Dr.Ing. Thesis)
MTA-93-94 Dalane, Jan Inge, MK:	System Reliability in Design and Maintenance of Fixed Offshore Structures. (Dr.Ing. Thesis)
MTA-93-95 Steen, Sverre, MH:	Cobblestone Effect on SES. (Dr.Ing. Thesis)
MTA-93-96 Karunakaran, Daniel, MK:	Nonlinear Dynamic Response and Reliability Analysis of Drag-dominated Offshore Platforms. (Dr.Ing. Thesis)
MTA-93-97 Hagen, Arnulf, MP:	The Framework of a Design Process Language. (Dr.Ing. Thesis)
MTA-93-98 Nordrik, Rune, MM:	Investigation of Spark Ignition and Autoignition in Methane and Air Using Computational Fluid Dynamics and Chemical Reaction Kinetics. A Numerical Study of Ignition Processes in Internal Combustion Engines. (Dr.Ing. Thesis)
MTA-94-99 Passano, Elizabeth, MK:	Efficient Analysis of Nonlinear Slender Marine Structures. (Dr.Ing. Thesis)
MTA-94-100 Kvålsvold, Jan, MH:	Hydroelastic Modelling of Wetdeck Slamming on Multihull Vessels. (Dr.Ing. Thesis)
MTA-94-102 Bech, Sidsel M., MK:	Experimental and Numerical Determination of Stiffness and Strength of GRP/PVC Sandwich Structures. (Dr.Ing. Thesis)
MTA-95-103 Paulsen, Hallvard, MM:	A Study of Transient Jet and Spray using a Schlieren Method and Digital Image Processing. (Dr.Ing. Thesis)
MTA-95-104 Hovde, Geir Olav, MK:	Fatigue and Overload Reliability of Offshore Structural Systems, Considering the Effect of Inspection and Repair. (Dr.Ing. Thesis)
MTA-95-105 Wang, Xiaozhi, MK:	Reliability Analysis of Production Ships with Emphasis on Load Combination and Ultimate Strength. (Dr.Ing. Thesis)

MTA-95-106 Ulstein, Tore, MH:	Nonlinear Effects of a Flexible Stern Seal Bag on Cobblestone Oscillations of an SES. (Dr.Ing. Thesis)
MTA-95-107 Solaas, Frøydis, MH:	Analytical and Numerical Studies of Sloshing in Tanks. (Dr.Ing. Thesis)
MTA-95-108 Hellan, øyvind, MK:	Nonlinear Pushover and Cyclic Analyses in Ultimate Limit State Design and Reassessment of Tubular Steel Offshore Structures. (Dr.Ing. Thesis)
MTA-95-109 Hermundstad, Ole A., MK:	Theoretical and Experimental Hydroelastic Analysis of High Speed Vessels. (Dr.Ing. Thesis)
MTA-96-110 Bratland, Anne K., MH:	Wave-Current Interaction Effects on Large-Volume Bodies in Water of Finite Depth. (Dr.Ing. Thesis)
MTA-96-111 Herfjord, Kjell, MH:	A Study of Two-dimensional Separated Flow by a Combination of the Finite Element Method and Navier-Stokes Equations. (Dr.Ing. Thesis)
MTA-96-112 Æsøy, Vilmar, MM:	Hot Surface Assisted Compression Ignition in a Direct Injection Natural Gas Engine. (Dr.Ing. Thesis)
MTA-96-113 Eknes, Monika L., MK:	Escalation Scenarios Initiated by Gas Explosions on Offshore Installations. (Dr.Ing. Thesis)
MTA-96-114 Erikstad, Stein O., MP:	A Decision Support Model for Preliminary Ship Design. (Dr.Ing. Thesis)
MTA-96-115 Pedersen, Egil, MH:	A Nautical Study of Towed Marine Seismic Streamer Cable Configurations. (Dr.Ing. Thesis)
MTA-97-116 Moksnes, Paul O., MM:	Modelling Two-Phase Thermo-Fluid Systems Using Bond Graphs. (Dr.Ing. Thesis)
MTA-97-117 Halse, Karl H., MK:	On Vortex Shedding and Prediction of Vortex-Induced Vibrations of Circular Cylinders. (Dr.Ing. Thesis)
MTA-97-118 Igland, Ragnar T., MK:	Reliability Analysis of Pipelines during Laying, considering Ultimate Strength under Combined Loads. (Dr.Ing. Thesis)
MTA-97-119 Pedersen, Hans-P., MP:	Levendefiskteknologi for fiskefartøy. (Dr.Ing. Thesis)

MTA-98-120 Vikestad, Kyrre, MK:	Multi-Frequency Response of a Cylinder Subjected to Vortex Shedding and Support Motions. (Dr.Ing. Thesis)
MTA-98-121 Azadi, Mohammad R. E., MK:	Analysis of Static and Dynamic Pile-Soil-Jacket Behaviour. (Dr.Ing. Thesis)
MTA-98-122 Ulltang, Terje, MP:	A Communication Model for Product Information. (Dr.Ing. Thesis)
MTA-98-123 Torbergsen, Erik, MM:	Impeller/Diffuser Interaction Forces in Centrifugal Pumps. (Dr.Ing. Thesis)
MTA-98-124 Hansen, Edmond, MH:	A Discrete Element Model to Study Marginal Ice Zone Dynamics and the Behaviour of Vessels Moored in Broken Ice. (Dr.Ing. Thesis)
MTA-98-125 Videiro, Paulo M., MK:	Reliability Based Design of Marine Structures. (Dr.Ing. Thesis)
MTA-99-126 Mainçon, Philippe, MK:	Fatigue Reliability of Long Welds Application to Titanium Risers. (Dr.Ing. Thesis)
MTA-99-127 Haugen, Elin M., MH:	Hydroelastic Analysis of Slamming on Stiffened Plates with Application to Catamaran Wetdecks. (Dr.Ing. Thesis)
MTA-99-128 Langhelle, Nina K., MK:	Experimental Validation and Calibration of Nonlinear Finite Element Models for Use in Design of Aluminium Structures Exposed to Fire. (Dr.Ing. Thesis)
MTA-99-129 Berstad, Are J., MK:	Calculation of Fatigue Damage in Ship Structures. (Dr.Ing. Thesis)
MTA-99-130 Andersen, Trond M., MM:	Short Term Maintenance Planning. (Dr.Ing. Thesis)
MTA-99-131 Tveiten, Bård Wathne, MK:	Fatigue Assessment of Welded Aluminium Ship Details. (Dr.Ing. Thesis)
MTA-99-132 Søreide, Fredrik, MP:	Applications of underwater technology in deep water archaeology. Principles and practice. (Dr.Ing. Thesis)
MTA-99-133 Tønnessen, Rune, MH:	A Finite Element Method Applied to Unsteady Viscous Flow Around 2D Blunt Bodies With Sharp Corners. (Dr.Ing. Thesis)

MTA-99-134 Elvekrok, Dag R., MP:	Engineering Integration in Field Development Projects in the Norwegian Oil and Gas Industry. The Supplier Management of Norne. (Dr.Ing. Thesis)
MTA-99-135 Fagerholt, Kjetil, MP:	Optimeringsbaserte Metoder for Ruteplanlegging innen skipsfart. (Dr.Ing. Thesis)
MTA-99-136 Bysveen, Marie, MM:	Visualization in Two Directions on a Dynamic Combustion Rig for Studies of Fuel Quality. (Dr.Ing. Thesis)
MTA-2000-137 Storteig, Eskild, MM:	Dynamic characteristics and leakage performance of liquid annular seals in centrifugal pumps. (Dr.Ing. Thesis)
MTA-2000-138 Sagli, Gro, MK:	Model uncertainty and simplified estimates of long term extremes of hull girder loads in ships. (Dr.Ing. Thesis)
MTA-2000-139 Tronstad, Harald, MK:	Nonlinear analysis and design of cable net structures like fishing gear based on the finite element method. (Dr.Ing. Thesis)
MTA-2000-140 Kroneberg, André, MP:	Innovation in shipping by using scenarios. (Dr.Ing. Thesis)
MTA-2000-141 Haslum, Herbjørn Alf, MH:	Simplified methods applied to nonlinear motion of spar platforms. (Dr.Ing. Thesis)
MTA-2001-142 Samdal, Ole Johan, MM:	Modelling of Degradation Mechanisms and Stressor Interaction on Static Mechanical Equipment Residual Lifetime. (Dr.Ing. Thesis)
MTA-2001-143 Baarholm, Rolf Jarle, MH:	Theoretical and experimental studies of wave impact underneath decks of offshore platforms. (Dr.Ing. Thesis)
MTA-2001-144 Wang, Lihua, MK:	Probabilistic Analysis of Nonlinear Wave-induced Loads on Ships. (Dr.Ing. Thesis)
MTA-2001-145 Kristensen, Odd H. Holt, MK:	Ultimate Capacity of Aluminium Plates under Multiple Loads, Considering HAZ Properties. (Dr.Ing. Thesis)
MTA-2001-146 Greco, Marilena, MH:	A Two-Dimensional Study of Green-Water Loading. (Dr.Ing. Thesis)

MTA-2001-147 Heggelund, Svein E., MK:	Calculation of Global Design Loads and Load Effects in Large High Speed Catamarans. (Dr.Ing. Thesis)
MTA-2001-148 Babalola, Olusegun T., MK:	Fatigue Strength of Titanium Risers - Defect Sensitivity. (Dr.Ing. Thesis)
MTA-2001-149 Mohammed, Abuu K., MK:	Nonlinear Shell Finite Elements for Ultimate Strength and Collapse Analysis of Ship Structures. (Dr.Ing. Thesis)
MTA-2002-150 Holmedal, Lars E., MH:	Wave-current interactions in the vicinity of the sea bed. (Dr.Ing. Thesis)
MTA-2002-151 Rognebakke, Olav F., MH:	Sloshing in rectangular tanks and interaction with ship motions. (Dr.Ing. Thesis)
MTA-2002-152 Lader, Pål Furset, MH:	Geometry and Kinematics of Breaking Waves. (Dr.Ing. Thesis)
MTA-2002-153 Yang, Qinzheng, MH:	Wash and wave resistance of ships in finite water depth. (Dr.Ing. Thesis)
MTA-2002-154 Melhus, Øyvin, MM:	Utilization of VOC in Diesel Engines. Ignition and combustion of VOC released by crude oil tankers. (Dr.Ing. Thesis)
MTA-2002-155 Ronæss, Marit, MH:	Wave Induced Motions of Two Ships Advancing on Parallel Course. (Dr.Ing. Thesis)
MTA-2002-156 Økland, Ole D., MK:	Numerical and experimental investigation of whipping in twin hull vessels exposed to severe wet deck slamming. (Dr.Ing. Thesis)
MTA-2002-157 Ge, Chunhua, MK:	Global Hydroelastic Response of Catamarans due to Wet Deck Slamming. (Dr.Ing. Thesis)
MTA-2002-158 Byklum, Eirik, MK:	Nonlinear Shell Finite Elements for Ultimate Strength and Collapse Analysis of Ship Structures. (Dr.Ing. Thesis)
IMT-2003-1 Chen, Haibo, MK:	Probabilistic Evaluation of FPSO-Tanker Collision in Tandem Offloading Operation. (Dr.Ing. Thesis)
IMT-2003-2 Skaugset, Kjetil Bjørn, MK:	On the Suppression of Vortex Induced Vibrations of Circular Cylinders by Radial Water Jets. (Dr.Ing. Thesis)

IMT-2003-3 Chezhian, Muthu	Three-Dimensional Analysis of Slamming. (Dr.Ing. Thesis)
IMT-2003-4 Buhaug, Øyvind	Deposit Formation on Cylinder Liner Surfaces in Medium Speed Engines. (Dr.Ing. Thesis)
IMT-2003-5 Tregde, Vidar	Aspects of Ship Design: Optimization of Aft Hull with Inverse Geometry Design. (Dr.Ing. Thesis)
IMT-2003-6 Wist, Hanne Therese	Statistical Properties of Successive Ocean Wave Parameters. (Dr.Ing. Thesis)
IMT-2004-7 Ransau, Samuel	Numerical Methods for Flows with Evolving Interfaces. (Dr.Ing. Thesis)
IMT-2004-8 Soma, Torkel	Blue-Chip or Sub-Standard. A data interrogation approach of identity safety characteristics of shipping organization. (Dr.Ing. Thesis)
IMT-2004-9 Ersdal, Svein	An experimental study of hydrodynamic forces on cylinders and cables in near axial flow. (Dr.Ing. Thesis)
IMT-2005-10 Brodtkorb, Per Andreas	The Probability of Occurrence of Dangerous Wave Situations at Sea. (Dr.Ing. Thesis)
IMT-2005-11 Yttervik, Rune	Ocean current variability in relation to offshore engineering. (Dr.Ing. Thesis)
IMT-2005-12 Fredheim, Arne	Current Forces on Net-Structures. (Dr.Ing. Thesis)
IMT-2005-13 Heggernes, Kjetil	Flow around marine structures. (Dr.Ing. Thesis)
IMT-2005-14 Fouques, Sebastien	Lagrangian Modelling of Ocean Surface Waves and Synthetic Aperture Radar Wave Measurements. (Dr.Ing. Thesis)
IMT-2006-15 Holm, Håvard	Numerical calculation of viscous free surface flow around marine structures. (Dr.Ing. Thesis)
IMT-2006-16 Bjørheim, Lars G.	Failure Assessment of Long Through Thickness Fatigue Cracks in Ship Hulls. (Dr.Ing. Thesis)
IMT-2006-17 Hansson, Lisbeth	Safety Management for Prevention of Occupational Accidents. (Dr.Ing. Thesis)

IMT-2006-18 Zhu, Xinying	Application of the CIP Method to Strongly Nonlinear Wave-Body Interaction Problems. (Dr.Ing. Thesis)
IMT-2006-19 Reite, Karl Johan	Modelling and Control of Trawl Systems. (Dr.Ing. Thesis)
IMT-2006-20 Smogeli, Øyvind Notland	Control of Marine Propellers. From Normal to Extreme Conditions. (Dr.Ing. Thesis)
IMT-2007-21 Storhaug, Gaute	Experimental Investigation of Wave Induced Vibrations and Their Effect on the Fatigue Loading of Ships. (Dr.Ing. Thesis)
IMT-2007-22 Sun, Hui	A Boundary Element Method Applied to Strongly Nonlinear Wave-Body Interaction Problems. (PhD Thesis, CeSOS)
IMT-2007-23 Rustad, Anne Marthine	Modelling and Control of Top Tensioned Risers. (PhD Thesis, CeSOS)
IMT-2007-24 Johansen, Vegar	Modelling flexible slender system for real-time simulations and control applications.
IMT-2007-25 Wroldsen, Anders Sunde	Modelling and control of tensegrity structures. (PhD Thesis, CeSOS)
IMT-2007-26 Aronsen, Kristoffer Høye	An experimental investigation of in-line and combined in-line and cross flow vortex induced vibrations. (Dr.avhandling, IMT)
IMT-2007-27 Zhen, Gao	Stochastic response analysis of mooring systems with emphasis on frequency-domain analysis of fatgue due to wide-band processes. (PhD-thesis CeSOS).
IMT-2007-28 Thorstensen, Tom Anders	Lifetime Profit Modelling of Ageing Systems Utilizing Information about Technical Condition. Dr.ing. thesis, IMT.
IMT-2008-29 Pákozdi, Csaba	A Smoothed Particle Hydrodynamics Study of Two-dimensional Nonlinear Sloshing in Rectangular Tanks. Dr.ing.thesis, IMT.
IMT-2008-30 Berntsen, Per Ivar B.	Structural Reliability Based Position Mooring. PhD-Thesis, IMT.
IMT-2008-31 Ye, Naiquan	Fatigues Assessment of Aluminium Welded Box stiffener Joints in ships. Dr.ing.-Thesis, IMT.

IMT-2008-32 Radan, Damir	Integrated Control of Marine Electrical Power Systems. PhD-Thesis, IMT.
IMT-2008-33 Norum, Viggo L.	Analysis of Ignituin and Combustion in Otto Lean-Burn Engines with Prechambers. Dr.ing. thesis, IMT.
IMT-2007-33 Thorhus, Runar	Alliances in Development of Short-sea ransport systems. Dr.ing.thesis, IMT.